Stony Brook University

Development of Photo-Affinity based ROMP Polymers for Identifying Receptors on Cell Surface

A Dissertation Presented

by

Siyeon Lee

to

The Graduate School

in Partial Fulfillment of the

Requirements

for the Degree of

Doctor of Philosophy

in

Chemistry

Stony Brook University

May 2014

Stony Brook University

The Graduate School

Siyeon Lee

We, the dissertation committee for the above candidate for the

Doctor of Philosophy degree, hereby recommend

acceptance of this dissertation.

Nicole S. Sampson –Dissertation Advisor
Professor and Chair of Chemistry

Scott Laughlin – Chair Person of Defense
Assistant Professor of Chemistry

Iwao Ojima – Third member of Defense
Professor of Chemistry

Michael Hayman – Outside member of Defense

Professor of Molecular Genetics and Microbiology

This dissertation is accepted by the Graduate School

Charles Taber
Dean of the Graduate School

Abstract of the Dissertation

Development of Photo-Affinity based ROMP Polymers for Identifying Receptors on Cell Surface

by

Siyeon Lee

Doctor of Philosophy

in

Chemistry

Stony Brook University

2014

Chapter 1

Receptors on cell membrane surfaces play critical roles for the cell to communicate with the outside environment by forming protein complexes. Therefore, identifying protein partners in the complex is of major importance. We are developed ROMP (ring opening metasthesis polymerization) polymers as tools for identifying the partners. The polymers bear several functional groups such as ligands for binding to a known receptor, benzophenone group to covalently connect the partner proteins to the polymer, and alkyne for click reaction to attach biotins. With this functionalized polymer, possible protein partners can be purified and analyzed by peptide mass finger printing. To optimize the function of this polymer and the experimental procedure, the αvβ3-MMP2, was used as a model system.

Chapter 4

A new prodrug for selective cancer therapy that uses the increased activities of histone deacetylase (HDAC) and protease cathepsin L (CTSL) in cancer cells was synthesized. Puromycine coupled with acetylated lysine group is not cytotoxic because the free amine is masked. We optimized the synthesis and the purification of puromycine coupled with acetylated lysine group to obtain highly pure (<95 %) product for testing in vivo.

Chapter 5

Early diagnosis of metastasis and prevention of metastasis is a major obstacle in cancer treatment due to the lack of imaging probes specific to early stage cancer. MT1-MMP, a membrane anchored matrix metalloproteinase, is upregulated in invasive human breast cancers even in early stages. The PEX domain of MT1-MMP is required for migration of aggressive cancer cells.Peptides mimicking 8 amino acids of the outermost β-strand of the blades from the PEX domain of MT1-MMP successfully inhibited the migration of aggressive cancer cells. This peptide was coupled to 18F-FDG for PET imaging and testing of the conjugate in vitro and in vivo

Table of Contents

List of Figures

Chapter 2

Chapter 4

Chapter 5

List of Tables

List of Schemes

List of Appendix Contents

List of Abbreviations

Ac	acetyl
ADAM	A disintegrin and a metalloprotease
Ala,	A alanine
Arg,	R arginine
Asn,	N asparagine
Asp,	D aspartic acid
Ar	argon
ATRP	atom transfer radical polymerization
Bpa	4-benzoyl-L-phenylalanine
Boc	*t*-butyloxycarbonyl
BSA	bovin serum albumin
CCA	α-cyano-4-hydroxy cinnamic acid
CRISP	cysteine rich secretory protein
CRP	cationic radical polymerization
Cys, C	cysteine
DBU	1, 8-diazabicyclo[5.4.0]undec-7-ene
DIC	differential interference contrast
DIEA	*N*,*N*-diisopropylethylamine
DMF	*N*,*N*-dimethylformamide
DMSO	dimethyl sulfoxide
DTT	dithiothreitol
ECD	glutamic acid-cysteine-aspartic acid
EGF	epidermal growth factor
ESA	glutamic acid-serine-alanine
ESI-MS	electrospray ionization mass spectormetry
Et2O	diethyl ether
EtOAc	ethyl acetate

Fmoc	fluorenylmethoxycarbonyl
F.I.	fertilization index
F.R.	fertilization rate
Gln, Q	glutamine
Glu, E	glutamic acid
Gly, G	glycine
GPC	gel permeation chromatography
GPI	glycosylphosphatidylinositol
hr	hour
H_2	hydrogen
HBTU	*O*-benzotriazole-*N*,*N*,*N'*,*N'*-tetramethyluronium hexafluorophosphate
Ig	immunoglobulin
IgSF	immunoglobulin super-family
IP	immunoprecipitation
IVF	*in vitro* fertilization
KO	knockout
Leu, L	leucine
Lys, K	lysine
MALDI-TOF	matrix assisted laser desorption ionization-time of flight
Mes	2,4,6-trimethylphenyl
MMP	matrix metalloproteinase
M_n	number-average molecular weight
Mo	molybdenum
M_w	weight-average molecular weight
N_2	nitrogen gas
NB	norbornene
NHS	*N*-hydroxysuccinimide
NMR	nuclear magnetic resonance
PBS	phosphate-buffered saline
Pd/C	palladium on carbon
PDI	polydispersity index

PEG	polyethylene glycol
Phe, F	phenylalanine
PMA	phosphomolybdic acid
ppm	parts per million
PVP	polyvinylpyrrolidone
QCD	glutamine-cysteine-aspartic acid
RGD	arginine-glycine-aspartic acid
ROMP	ring opening metathesis polymerization
RP-HPLC	reversed phase-high performance liquid chromatography
RPM	rotation per minute
rt	room temperature
Ru	ruthenium
SDS-PAGE	sodium dodecyl sulfate-polyacrylamide gel electrophoresis
SVMP	snake venom metalloprotease
TCEP-HCl	tris(2-carboxyethyl) phosphine hydrochloride
TFA	trifluoroacetic acid
TIPS	triisopropylsilane
THF	tetrahydrofuran
TLC	thin layer chromatography
TM	transmembrane
UV	ultraviolet
WT	wild-type
Cbz, Z	benzyloxycarbonyl
ZP	zona pellucida

Chapter 1

1.2. Introduction

- 1.2.1. Mammalian fertilization
- 1.2.2. Proteins involved in sperm-oocyte interactions on sperm and egg surfaces
- 1.2.3. Integrin complexes exerting different functions
- 1.2.4. Designs of photoaffinity based ROMP polymers for identifying receptors on cell surface
- 1.2.5. Specific aims

1.6. Current methods to identify protein-protein interactions

1.7. Chemical labeling of biomolecules to study biological process

1.8. Cleavable linkers

1.9. Polymers mimicking multivalent interactions in biological system

- 1.5.1. Multivalent interactions adapted in biological system
- 1.5.2. Diverse scaffolds for mimicking multivalent ligand system
- 1.5.3. Linear scaffold polymerization
- 1.5.5. Living radical polymerizations

1.1. Introduction

1.1.1. Mammalian fertilization

Fertilization is the fusion of two different gametes, sperm and egg, resulting in the formation of a zygote. In mammalian fertilization, a precise set of molecular and cellular events has to occur in order to initiate the development of a new organism.[1] Before a sperm can fuse with an egg, it must pass through the female reproductive tract, penetrate the cumulus layer surrounding the ovulated egg and bind to the zona pellucida (ZP) in a species-specific manner.[2, 3] Sperm-ZP interaction is an important prerequisite step in sperm-egg fusion. The sperm-ZP interaction induces the sperm to undergo the exocytosis of the acrosome vesicle located on the head of the sperm. This process is also known as the acrosome reaction. The acrosome reaction, releases degradative enzymes such as hyaluronidase and acrosin which facilitates penetration of the ZP by the sperm.[4] Only sperm which have undergone the acrosome reaction are able to proceed to the next step and fuse with the egg plasma membrane.[5]

Sperm-egg binding and fusion triggers a series of signaling events known as egg activation.[6, 7] Egg activation leads to an increase in cytosolic Ca^{2+} concentration, cortical granule exocytosis, cell cycle resumption and recruitment of maternal mRNA. Cortical granule exocytosis is homologous to the acrosome reaction in sperm. This reaction causes a release in the contents of the cortical granules, which changes the chemical composition of the zona pellucida preventing the egg plasma membrane from fusing with further sperm and becoming polyspermic.[8] Finally, the zygote divides into identical totipotent cells that can differentiate into all the cell types in the body. Elucidation of the mechanisms by which the sperm initiates these events may be essential for understanding developmental processes. This could have a great

impact on stem cell technology and could lead to the development of novel therapeutics for the treatment of degenerative diseases and infertility.[1]

1.1.2. Proteins involved in sperm-oocyte interactions on sperm and egg surfaces

There are several proteins on the egg and the sperm that have been identified as key players in sperm-egg interactions. Once the sperm penetrates the ZP it can begin to bind and fuse with the plasma membrane of the egg. Sperm surface proteins ADAM (A Disintegrin and A Metalloprotease), cyritestin, CRISP1 (cysteine-rich secretory protein) and Izumo have all been found to be involved in sperm-egg binding. On the egg surface, tetraspanins (CD9), GPI-anchored proteins, and integrins are present for egg-sperm binding and fusion (Figure 1-1).

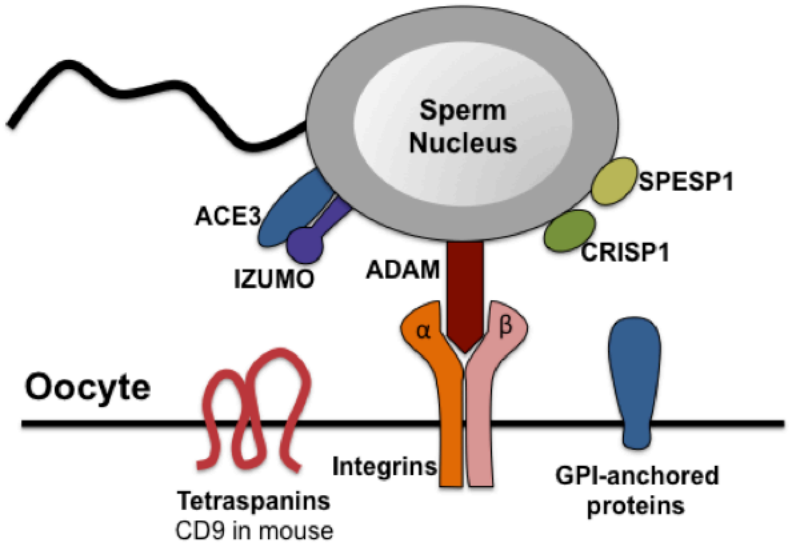

Figure 1-1. Molecules involved in sperm and oocyte binding and fusion.[1]

ADAM protein

Fertilinα, fertilinβ and cyritestin are members of the ADAM (A Disintegrin And Metalloprotease) family and are ADAM1, ADAM2 and ADAM3, respectively. This protein family involved in adhesion between a sperm and an egg. To date, 39 members of the ADAM family have been identified,[9, 10] and about half of them are present in reproductive tissues.[11]

ADAM proteins are similar in structure, and all contain a signal sequence domain, a prodomain, a metalloprotease domain, a disintegrin domain, a cysteine-rich domain, an EGF (epidermal growth factor)-like domain, a transmembrane domain and a cytoplasmic tail (Figure 1-2). ADAM proteins are structurally related to the snake venom metalloproteases (SVMPs).[12] The disintegrin domains of ADAM proteins have been of great interest as they are directly involved in cell adhesion.

Class II SVMP contains an RGD consensus sequence within a 13 amino acid stretch that is called the disintegrin loop, which binds to platelet integrins such as $\alpha_{IIb}\beta_3$ and $\alpha_v\beta_3$.[13] Class III SVMP and ADAM's disintegrin domain lack the RGD consensus sequence, but are still capable of binding to its corresponding integrin.[14, 15]

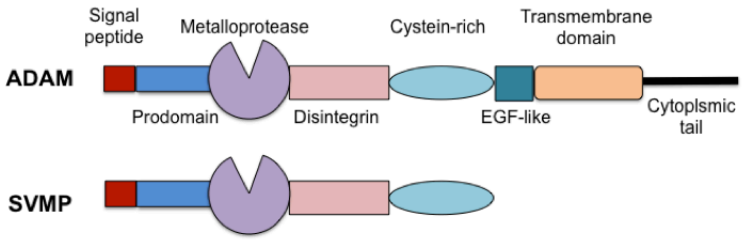

Figure 1-2. Domain organization of ADAMs and Snake venom metalloprotease

ADAM2 and ADAM3 are known to play roles in sperm-oocyte binding and fusion.[16, 17] Inhibition studies on fertilization with antibodies against ADAM2 and ADAM3[10, 18, 19] and recombinant forms of two ADAMs[15, 20-22] confirmed their role in sperm-oocyte binding and fusion. Synthetically prepared oligopeptides from the disintegrin loops[23-26] also showed inhibition of fertilization, which suggests that the disintegrin domain of ADAM protein participates in sperm-oocyte binding.[27]

The Disintegrin domains of ADAM2 and ADAM3 contain ECD[20, 25, 28, 29] and QCD[28, 29] tripeptide as a consensus sequence. It has been shown that these short peptides are a minimal sequence requirement for the binding to the oocyte (Table 1-1).[20, 29, 30]

SVMP-II disintegrins		
Kistrin		CKFSRAGKICRIP**RGD**-MPDDRCTGQSADC
Echistatin		CKFLKEGTICKRA**RGD**-DMDDYCNGKTCDC
Barbourin		CRFMKKGTVCRVAK**GD**-WNDDTCTGQSADC
SVMP-III disintegrins		
HR1B		CRFRTAGTECRAAES**ECD**IPESCTGQSADC
Jararhagin		CKFKSAGTECRASMS**ECD**PAEHCTGQSSEC
Atrolysin E		CKFTSAGNVCRPARS**ECD**IAESCTGQSADC
ADAM disintegrins		
	Species	Disintegrin Loop
ADAM1	Mouse	CTFKKKGSLCRPAEDV**CD**LPEYCDGSTQEC
	Mouse	CKLKRKGEVCRLAQD**ECD**VTEYCNGTSEVC
	Monkey	CLFMSQERVCRPSFD**ECD**LPEYCNGTSASC
	Guinea pig	CEFKTKGEVCRESTD**ECD**LPEYCNGSSGAC
ADAM2	Human	CLFMSKERMCRPSFE**ECD**LPEYCNGSSASC
	Cow	CAFIPKGHICRGSTD**ECD**LHEYCNGSSASC
	Rat	CNLKAKGELCRPANO**ECD**VTEYCNGTSEVC
	Rabbit	CTFKERGQSCRPPVG**ECD**LFEYCNGTSALC
	Mouse	CTIAERGRLCRKSKD**QCD**FPEFCNGETEGC
ADAM3	Rat	CRKSTD**QCD**FPEFC
	Human	CTIHERGHVCRKSVDM**CD**FPEYCNGTSEFC

	Monkey	CTIYARGHVCRKSIDM**CD**FPEYCNGTSEFC
ADAM4	Mouse	CKFAPTGTICRDKNGI**CD**LPEYCSGASEHC
ADAM5	Mouse	CTVKMNDVVCRKSVD**ECD**LLEYCNGKDPYC
ADAM6	Rat	CTYSPSGTLCRPIQNI**CD**LPEYCSGNNIGC
ADAM7	Monkey	CQIKKAGSICRPAED**ECD**FPEMCTGHSPAC
ADAM8	Mouse	CKVKPAGEVCRLSKDK**CD**LEEFCDGRKPTC
ADAM9	Mouse	CQFLPGGSMCRGKTS**ECD**VPEYCNGSSQFC
ADAM10	Rat	RDDSDCAKEGIC
	Human	RDDSDCAREGIC
ADAM11	Human	REAVN**ECD**IAFTC
ADAM12	Human	CQFLPGGSMCRDSSNS**CD**LPEFCNGSSQFC
ADAM14	*C.elegans*	CELRKAGDTCRSSKSP**CD**VAEQCDGKSGDC
ADAM15	Mouse	CKLHPAGWLC RPPTDD**CD**LPEF CPGDSSQC
	Human	CQLRPSGWQCRPTRGD**CD**LPEFCPGDSSQC
ADAM16	*X.laevis*	CKLLPKGTLCRMPKT**ECD**LAEYCDGASNHC
ADAM18	Rat	CELSAAGTPCRKVDP**ECD**FTEYCNGTSSDC
ADAM20	Human	CFKPSGTLCRQQVG**ECD**LPEWCNGTSHQC
ADAM21	Mouse	CKFMLLGELCRPKIN**ECD**LPEWCNGTSHQC
ADAM22	Mouse	CKFQPLGTVCREAVND**CD**IREICSGNSSQC
ADAM23	Human	CLFQPRGYECRDAVN**ECD**ITEYCTGDSGQC

Table 1-1. Comparison of disintegrin domains[14, 31]

Integrins on egg surface

Mouse eggs can express a limited number of integrin subunits such as β_1, β_3, β_5, α_1, α_2, α_3, α_5, α_6, α_8, α_9, and α_v, and there are at least 10 possible combinations that make a functional integrin.[32]

$\alpha_6\beta_1$ integrin has been widely studied and shown to be involved in sperm-egg binding. In mouse, polyclonal antibodies anti-α_6-mAb GoH3 and anti-β_1 reduced the sperm binding to ZP free eggs.[22, 26] However, inhibition was dependent on the type of IVF assay used. In cultured cells that do not express $\alpha_6\beta_1$ integrin, sperm binding to the cells was significantly reduced compared to cells that do express $\alpha_6\beta_1$ integrin.[26]

Previously, H. Chen from the Sampson group prepared an ADAM2 mimic oligopeptide labeled with ^{125}I and containing a benzophenone group (Bpa-RLAQD**ECD**VTEYA-NH_2, ^{125}I-

labeled on tyrosine). This oligopeptide was cross-linked with the oocyte plasma membrane under long wave UV light, and the peptide-integrin complex was then immunoprecipitated with an anti-α_6 antibody (GoH3) (Figure 1-3). Though informative, it was not clear from the experiment whether integrin $\alpha_6\beta_1$ is the only receptor that recognizes the ADAM2 mimic peptide.

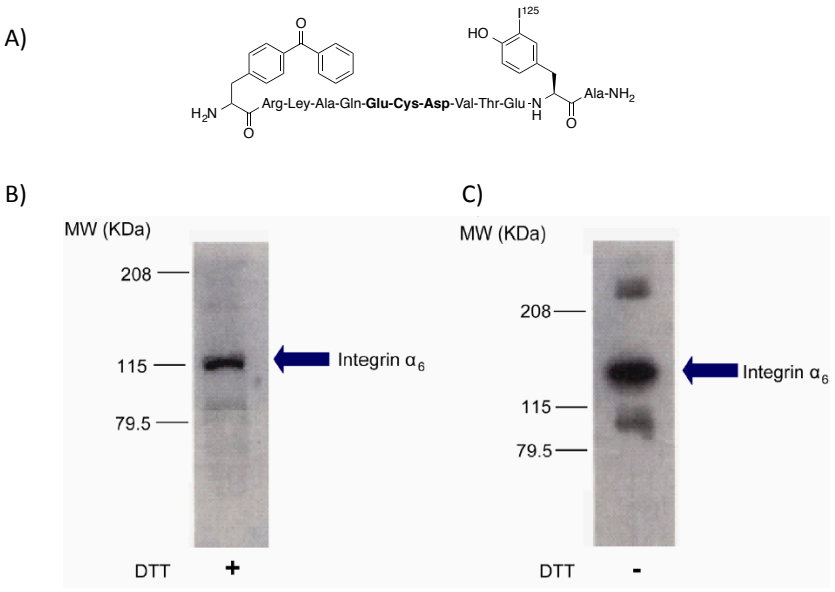

Figure 1-3. Autoradiograms of photoaffinity-labed oocyte proteins. A) Structure of ^{125}I-labeled ADAM2 mimic peptide. B) A 6% reducing SDS-PAGE gel of labeling reaction with DTT. C) A 6% non-reducing SDS-PAGE gel of labeling reaction.[27]

In a related study, Dr. Jaechul Lee from the Sampson research group synthesized a block copolymer that consists of 13 units of the ADAM2 mimic ligand monomer containing Bpa and a fluorophore (Figure 1-4A). The multivalent system was employed to enhance the binding efficiency. Even though the zona pellucida-free oocytes were labeled with the polymer (Figure 1-4C), the identification of the labeled oocyte was not successful.

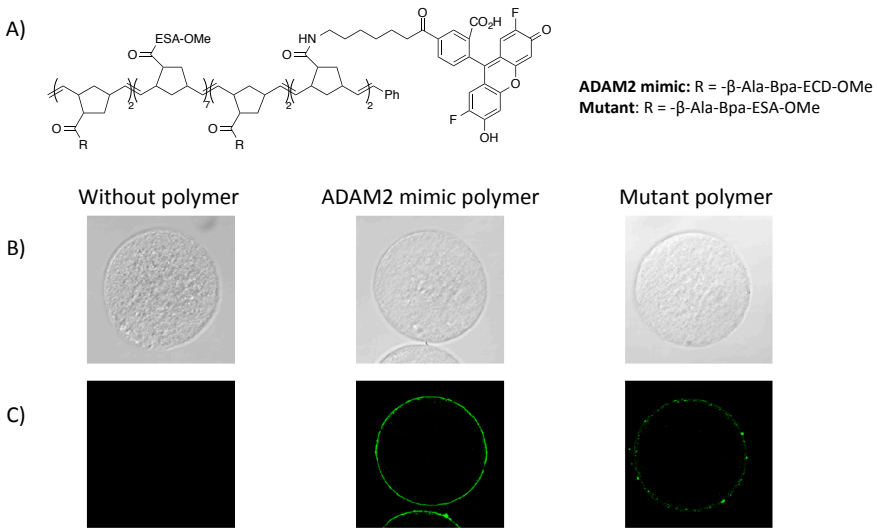

Figure 1-4. Photoaffinity labeling of zona pellucida-free oocytes performed by Jaechul Lee in the Sampson group.[8] A) Fluorophore-linked polymers. B) DIC images by confocal microscopy. C) Fluorescence images by confocal microscopy

Dr. Younjoo Lee from the Sampson research group resynthesized different lengths of the ADAM2 mimic polymers to optimize their binding affinity and the purification of the polymer-receptor complex. This inhibition efficiency of the mimic polymers was determined in an *in vitro* fertilization assay using 8- to 10-week-old virgin female mice (ICR or CD-1). Among various lengths of the polymers, $(NB\text{-}ECD)_{100}$, which contains 100 copies of the ECD peptide in a polymer (Figure 1-5) was found to be the most potent inhibitor of fertilization (Figure 1-6).

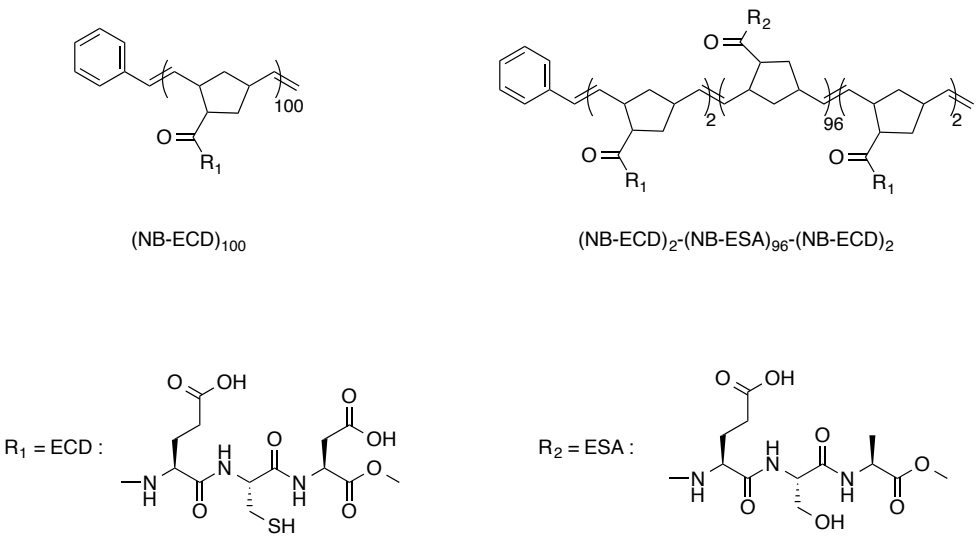

Figure 1-5. Structures of ECD polymers having the most potent inhibitory activity

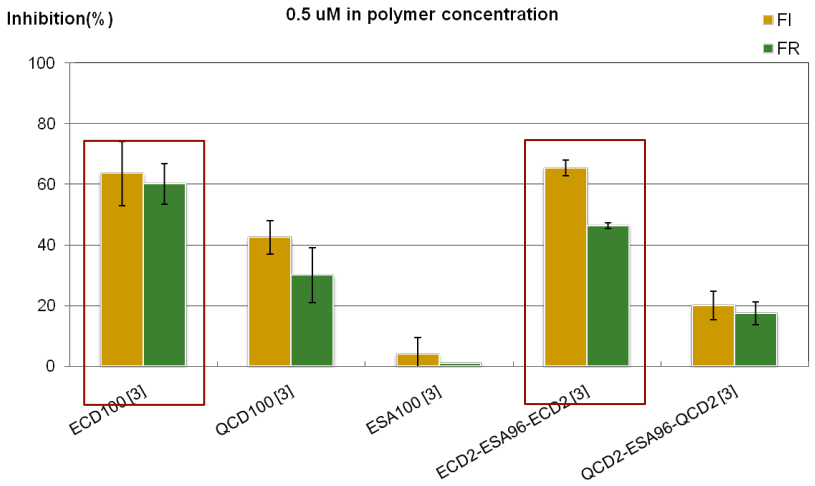

Figure 1-6. Inhibition of fertilization by homopolymer $(NB\text{-}ECD)_{100}$ and bivalent block copolymer $(NB\text{-}ECD)_2\text{-}(NB\text{-}ESA)_{96}\text{-}(NB\text{-}ECD)_2$ at 0.5 μM concentration.[33] Yellow bar: fertilization index (FI, mean number of fused sperm per oocyte); Green bar: fertilization rate (FR, percentage of oocytes fused with at least one sperm), [3]; polymers synthesized using Grubbs' catalyst 3rd generation.

In order to be certain that the inhibition was caused by the binding motif specifically, a mutant polymer containing ESA as the ligand instead of ECD was synthesized and tested by Younjoo Lee (Figure 1.6).

The ESA mutant polymer was unable to inhibit fertilization, which suggests that the inhibition caused by $(NB\text{-}ECD)_{100}$ is due to the specific interaction between the ECD peptide and its receptor.[34] Also, it was found that $(NB\text{-}ECD)_2\text{-}(NB\text{-}ESA)_{96}\text{-}(NB\text{-}ECD)_2$ (Figure 1-5) has the same inhibition potency as homopolymer $(NB\text{-}ECD)_{100}$ (Figure 1-6). Therefore, it was concluded that the mimic polymer interacts with the integrin in a bivalent fashion.[33]

There are discrepancies between chemical and genetic studies regarding integrins. Even though polymers bearing the ECD ligand showed inhibition of fertilization, one team reported that none of the integrins that are expressed on the egg surface is essential for fertilization.[35] In addition, kinetic studies conducted by a previous lab member Dr. Baessler, showed that even though there was a delay in sperm binding to β_1 KO eggs, the eggs could still be fertilized.[36] From this study, we could consider two possibilities, 1) there could be other receptors that recognize ADAM2, and 2) after ADAM2 binds to its receptor, $\alpha_6\beta_1$, it clusters other proteins to form a protein complex that is responsible for sperm-egg binding and fusion.

1.1.3. Integrin complexes exerting different functions

Integrins not only interact with neighboring cells and the ECM, but they also form a complex with other receptors to exert different functions (Table 1-2). Integrins can associate with matrix metalloproteinases (MMP) to control ECM degradation. $\alpha_v\beta_3$ cannot bind to native collagen found in the ECM, but the peptide fragments generated by MMP2 can be recognized by

$\alpha_v\beta_3$. This recognition suggests that a integrin-MMP complex may create its own ligand within the ECM during cell migration.[37]

The glycan phosphatidylinositol (GPI)-linked protein is another receptor that can interact with specific integrins. One of the most analyzed example of this type of association occurs between Urokinase-type plasminogen activator receptor (uPAR) and $\alpha_3\beta_1$. Upon ligand binding, the uPAR/$\alpha_3\beta_1$ interaction is enhanced, which results in up-regulation of urokinase-type plasminogen activator (uPA) in primary T lymphocyte[38] and ECM degradation.[39, 40] Also, it is known that integrins are co-receptors for uPAR signaling. uPAR/$\alpha_M\beta_2$ mediates leukocyte cell adhesion and recruitment during inflammatory responses without the involvement of uPA.[41, 42]

Testraspanins have been reported to play an important role in recycling integrins at the leading edge of the migrating cells.[43] Testraspanins are thought to assemble integrins and other molecules into complexes of a higher order.

Epidermal growth factor (EGF) and the platelet-derived growth factor (PDGF) receptors are also interaction partners of integrins, which may lead to making highly active growth factor receptors to sustain signaling.[44, 45] CD98, a large neutral amino acid transporter, was suggested to be involved in the regulation of integrin affinity. It has been reported that the α subunit of CD98 converts β_1 integrin to a high-affinity state. It is thought that CD98 and β_1 integrins may function together during T-cell-costimulation.[46] Antibodies to β_1 and β_2 integrins inhibit monocyte cell-cell fusion and aggregation functions induced by CD98 mAb.[46]

Membrane proteins Physically associated with integrins	Associated integrin	Function
Proteases		
MMP1	$\alpha_2\beta_1$	ECM degradation
MMP2	$\alpha_v\beta_3$	ECM degradation
Receptors		
uPAR	$\alpha_3\beta_1$, $\alpha_v\beta_3$, $\alpha_M\beta_2$, $\alpha_X\beta_2$	ECM degradation
CD16	$\alpha_M\beta_2$	IgG Fc receptor
CD14	$\alpha_M\beta_2$	Lipopolysaccharide-binding protein
EGF receptor	$\alpha_v\beta_3$, $\alpha_2\beta_1$	Tyrosine kinase growth factor receptor
PDGF receptor	$\alpha_v\beta_3$	Tyrosine kinase growth factor receptor
Insulin receptor	$\alpha_v\beta_3$	Tyrosine kinase growth factor receptor
P2Y	$\alpha_v\beta_3$	ATP receptor
CD47	$\alpha_v\beta_3$, $\alpha_{IIb}\beta_3$, $\alpha_2\beta1$	Receptor for thrombospondin and SIRRa
Transporters/channels		
CD98	Multiple β_1 integrins	Amino acid transporter
Kv1.3	β_1 integrins	Voltage-gated K^+ channel
Unknown function		
TM4SF	Multiple β_1 integrins	Unkown
CD147	$\alpha_3\beta_1$, $\alpha_6\beta_1$	Induction of MMPs

Table 1-2. Membrane proteins associated with integrins and their functions.[47]

1.1.4. Designs of photoaffinity based ROMP polymers for identifying receptors on cell surface.

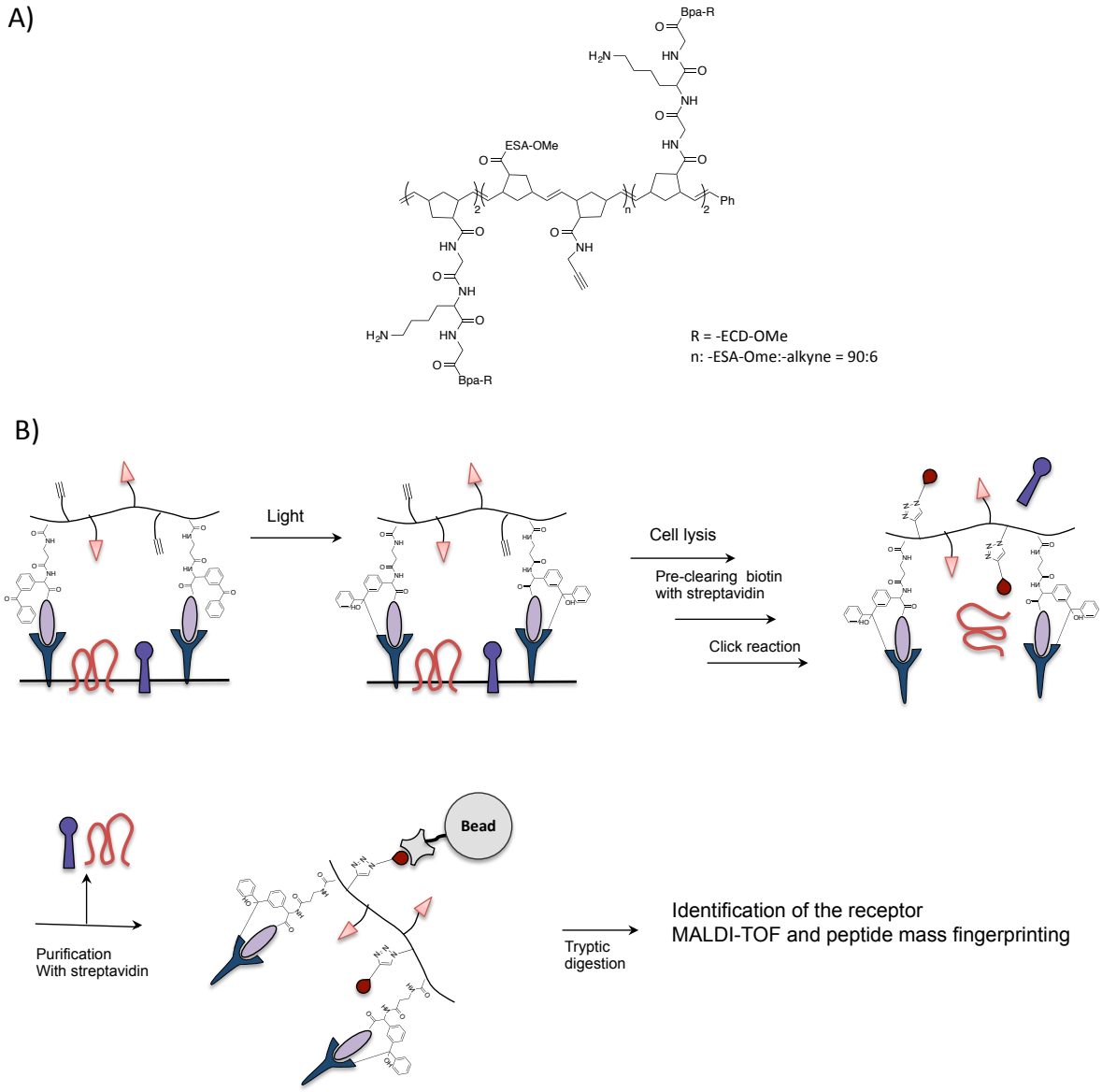

Figure 1-7. Schematic representation of a strategy to detect receptors on cell surface through photoaffinity based ROMP polymer. A) structure of ADAM2 mimic polymer containing Bpa for photoaffinity based receptor identification. B) Schematic representation of the photoaffinity labeling and identification of the receptors.

ADAM2 mimic polymers containing Bpa were prepared by Dr. Younjoo Lee to identify the possible receptor for ADAM2 (Figure 1-7A). Biotin was incorporated into the polymer backbone by click reaction in order to increase the efficiency of immunnoprecipitation (Figure 1-7B). The isolated polymer-receptor complexes were enzymatically digested, and the resulting peptide mixture was analyzed by LTQ Orbitrap XL ETD mass spectroscopy. However, no peak of oocyte transmembrane proteins was detected from the sample.

In order to successfully detect cell surface receptors using photoaffinity based ROMP polymers, optimization of the photoaffinity crosslinking, click reaction, and purification of polymer-receptor complexes is critical. Here, we employ a model system to optimize each step. We chose the mammalian cell culture system because mammalian cell cultures provide large quantities of protein compared to isolated eggs.

The $\alpha_v\beta_3$ integrin is expressed in various cell types such as platelets, endothelial cells, and tumor cells and plays a key role in numerous physiological processes such as angiogenesis, apoptosis, and bone resorption. $\alpha_v\beta_3$ integrin is known to bind to various RGD-containing proteins and numerous inhibitors showing specific inhibition to $\alpha_v\beta_3$ integrin have been investigated including cyclo(-RGDfV-) and linear RGDS peptide.[48, 49] Although the cyclo(-RGDfV-) inhibitor mentioned above showed a much higher IC_{50} value than the linear RGDS, we chose to base our model on the linear RGDS peptide as it will be most similar in structure to the ECD polymers designed by Younjoo Lee, its affinity should be enhanced in a multivalent polymer display.

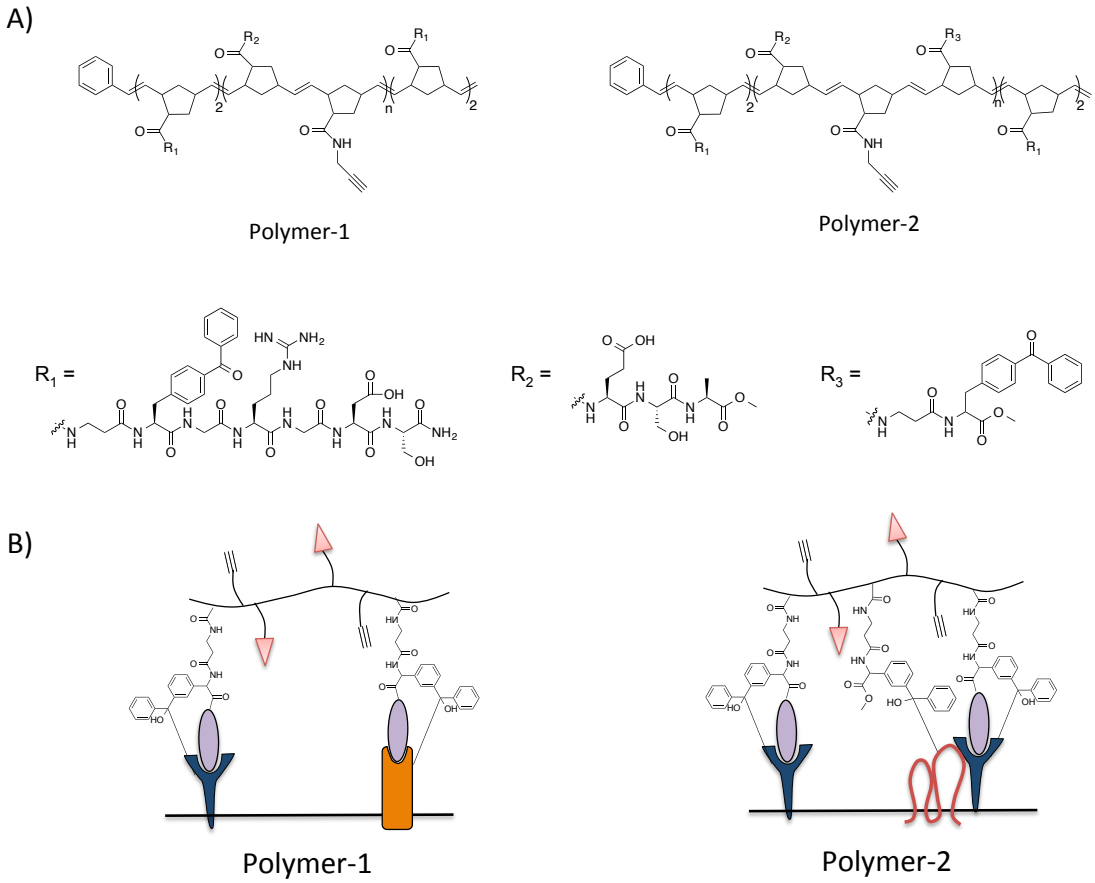

Figure 1-8. Structures of polymers for detection of receptors on cell surface. A) structures of the polymers, B) representation of the purposes of polymer-1 and polymer-2

To optimize experimental procedures, polymer-1 (Figure 1-8) was employed. U87-MG cells overexpressing $\alpha_v\beta_3$ integrin can be labeled with polymer-1 which contains Bpa adjacent to the RGDS peptide and be analyzed by MALDI-TOF mass spectrometry. Once each experimental condition is optimized, polymer-2 (Figure 1-8) will be used for detecting the binding partners of the known receptor. In polymer-2, the benzophenone moiety is moved into the spacer block. HT1080 cells can be used since the $\alpha_v\beta_3$ integrin on the cell surface forms a heterodimer with

MMP2 under phenazine methosulfate stimulation.[50] We will use randomly distributed NB-βAla-Bpa-OMe between the two ligands at the end of the polymer-2. If necessary, different positions of the NB-β-Ala-Bpa-OMe will be tested to capture the binding partenr

1.1.5. Specific aims

a. Optimization of experimental procedure for identifying receptor complex on the cell surface by using photaffinity based ROMP polymer

Protein-protein interactions play an important role in signal transduction and cell-cell interactions. Conventional methods used to predict protein-protein interactions often generate false positives and lack information on transient or weak interactions. To develop a tool to map protein-protein interactions on the cell surface, we develop a ROMP polymer bearing several functional groups: 1) known peptide ligand that interacts with its receptor, 2) benzophenone group for photoaffinity crosslinking of ligand to its receptor or adjacent proteins near the receptor, 3) alkynes for click reaction to attach biotin probe for purification of the polymer-protein complex. Combined with peptide mass fingerprinting technique, the candidate proteins extracted by the polymer can be analyzed and validated.

b. Development of cleavable biotin probe to improve sample purity after affinity purification

The strong affinity between biotin and streptavidin is frequently used to purify target proteins labeled with biotin probes. However, routine methods to elute biotinylated proteins from

streptavidin are harsh. Also, on-bead tryptic digestion generates unwanted peptide fragments from streptavidin or non-specifically bound proteins, which will increase the signal to noise ratio in the mass spectra. In order to avoid harsh elution conditions and increase the target protein recovery, several linkers have been invented to separate the biotin and the functional group. However, these linkers still posses their own drawbacks such as instability in biological fluid, limited application on certain protein samples and moderately harsh elution conditions that could still elute unwanted protein. To expand the choice of linker, which can be efficiently cleaved under mild conditions and be prepared with easy chemistry, we employed a cyclic acetal moiety as an acid sensitive linker.

1.2. Current methods to identify protein-protein interaction

The genome-sequencing project identified a dramatically increased number of proteins. Among the 500,000 different proteins encoded in the human genome, more than 10,000 proteins can be expressed by the cell at any given time, and 80% of them function by forming a complex with other proteins.[51] The interactions among membrane proteins are of special interest as they control various cellular processes some of which induce human diseases.[52] Therefore, developing techniques to map the interaction partners is pivotal.

Co-immunoprecipitation (co-IP)[51, 53]

One of the most commonly used techniques to identify a protein interaction partner is co-IP. This method uses a specific antibody against one of the target proteins. The antibody binds to its corresponding protein, the antigen, which is interacting with an unknown protein partner. The bound antibody can be immobilized with either protein G or protein A covalently attached to

sepharose or agarose beads. After removing excess unbound proteins, the complex, which includes the antibody, the bait and the unknown protein interaction partner, can be eluted by boiling the beads and the unknown protein identified by MS or immunoblot. Since co-IP does not include any artificial molecules such as affinity tags, this approach can be advantageous to study actual endogenous protein-protein interactions. To minimize false positive results, it is critical to use antibodies highly specific to its antigen. To improve the quality of the sample it is also crucial to thoroughly wash the immobilized protein complex before elution. However, these harsh washes may also cleave proteins which bind weakly to the antigen. Another disadvantage of co-IP is the loss of transient protein interactions, as co-IP is performed after lysing the cell.

Pull-down assay using affinity tags[51]

Generally, the bait proteins for pull down assays are prepared by linking an affinity tag to the bait protein or by expressing a fusion protein that contains the affinity tag at either the N- or C- terminus of the bait protein. Expression of the tagged protein in the cell is advantageous because the interactions occur at the same subcellular location. Therefore, it is highly possible to pull down physiological complexes. However, during cell lysis that is necessary for protein complex purification, there is a high chance for non-physiological targets to associate with the bait proteins increasing false positive results.

To minimize false positive results, tandem affinity purification (TAP)-tag method was invented.[54] The TAP method consists of two tags separated by a peptide that can be cleaved by tobacco etch virus (TEV) protease. This method decreases the amount of non-specifically bound proteins since the protease specifically releases the proteins with the tags. However, similar to co-IP, the TAP method may also cause a loss in transient or weakly interacting proteins during

stringent washes. As this method puts an artificial molecule on a protein, it may cause problems such as affinity changes and incorrect subcellular localization.

Chemical cross-linking[55]

Chemical cross-linking has been widely used to covalently connect the protein complex of interest. Covalent crosslinking with rapid reactivity of common functional groups is suitable to detect transient or weakly binding interactions. Typical crosslinkers target specific functional groups on proteins such as amines, sulfhydryls, carboxyls, carbonyls, or hydroxyls. Homobifunctional crosslinkers have identical reactive moieties on both ends to target the same residues on a given protein. Heterobifunctional crosslinkers have different reactive moieties on both ends to link different residues on separate proteins (Figure 1-9). In addition, a cleavable moiety can be inserted between two reactive groups when the linkage has to be reversed or broken.

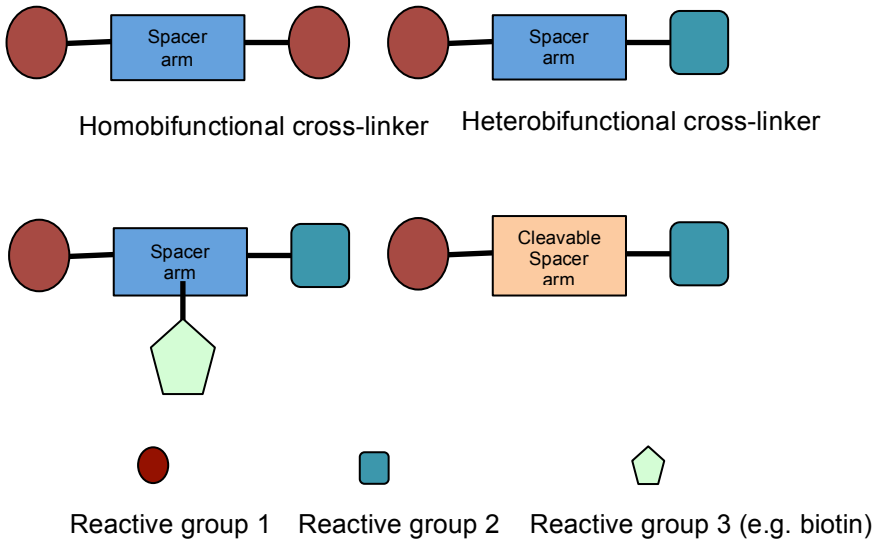

Figure 1-9 Representative structures of different types of cross-linkers[55]

Photoreactive crosslinkers are also commonly used to identify protein-protein interactions (Table 1-3). Unlike other crosslinkers that target specific functional groups on separate proteins, these crosslinkers can be connected with any neighboring C-C, C-H, N-H, or O-H bond by generating radicals under UV irradiation. Normally, photoreactive linkers are heterobifunctional and contain a reactive group on one end that is used to chemically label the protein of interest and a photoreactive group on the other end to crosslink proteins associated with the protein of interest. Proteins can also be metabolically engineered to have photoreactive moieties using unnatural amino acids such as L-photo-Leucine, L-photo-methionine, or L-photo-Isoleucine.[56]

Reactive groups	Target functional group
N-hydroxylsuccinimide, imidoester, carbodiimides	amine
Maleimides	sulfhydryl group
Photoreactive cross linkers Aryl azides at <280 nm Diazirines[57] at 360 nm Benzophenones[58] at ~350 nm Tris(2,2'-bipyridyl)ruthenium (II)[59]	**Neighboring covalent bond** C-H and N-H heteroatom-H or C-H C-C Histidine, tyrosine, or cysteine

Table 1-3. Typical reactive groups of crosslinkers and their targets.

The two-hybrid system[60]

The yeast two-hybrid system (Y2H) is another popular method for identifying protein-protein interactions. This system was first proposed by Fields and Song in 1989.[61] This system utilizes transcription factor Gal4, which is a modular protein consisting of a DNA binding domain (DBD)

and an activation domain (AD). This modular protein is still functional when DBD and AD are expressed separately but are in close proximity.[62] In this system, AD is referred to as the prey and the bait is DBD fused to the protein of interest. When the bait and the prey come in close proximity, Gal4 is activated promoting transcription of a reporter gene.

The most popular reporter genes are HIS3 and lacZ. HIS3, which allows positive selection of interactions, encodes imidazole glycerol-phosphate dehydratase (IGPD) which is used for histidine biosynthesis. In Y2H, 3-amino-1,2,4-trizole (3-AT) is added to the growth media in order to inhibit native IGPD activity leading to yeast growth restriction. Upon physical interaction between the bait and the prey, Gal4 is activated and transcribes HIS3 that encodes for IGPD. The protein-protein interaction allows the yeast to overcome the growth inhibitory activity of 3-AT. LacZ encodes the enzyme β-galactosidase (β-Gal) which cleaves X-Gal that is a colorless analogue of lactose. Once X-Gal is cleaved by β-Gal, it forms 5-bromo-4-chloro-indoxyl. Then, it spontaneously dimerizes and oxidizes to form a 5,5'-dibromo-4,4'-dichloro-indigo that generate a bright blue color, which indicates the interaction between the bait and the prey.

Y2H is an advantageous method since it detects interactions occurring *in vivo*, including transient and weak interactions which are commonly lost in other methods. The drawbacks of this system include detection of non-specific interactions due to the overexpression of the fusion protein, false results resulting from incorrectly folded proteins and the lack of post-translational modifications such as phosphorylation which is important for protein-protein interactions in mammalian cells. Also, since the interactions occur in the yeast nucleus, it is impossible to apply this method to hydrophobic integral membrane proteins. To overcome this problem, split-ubiquitin membrane-based Y2H has been developed.[63] The bait, protein of interest and DBD, are

fused with a C-terminal ubiquitin moiety (Cub, residues 35-76) and an N-terminal ubiquitin moiety (Nub, residues 1-34) respectively. Cub is expressed with the transcriptional factor. Upon the interaction between the bait and the prey, ubiquitin is reconstructed, and the transcriptional factor can be released by the action of ubiquitin specific protease allowing transcription of the reporter gene.

Peptide mass fingerprinting[64, 65]

Peptide mass fingerprinting (PTM) is a valuable technique for the analysis of proteins. This method is simple, sensitive and fast, making it very advantageous for protein analysis. The peptide masses from an unknown protein can be obtained by MALDI-TOF after tryptic digestion of the protein. The obtained peptide masses are then compared to the theoretical masses of proteins available on protein databases including NCBI and Swiss-Prot in order to identify the best match of proteins.

Other than PTM, tandem mass spectrometry (MS/MS) is also widely used to identify unknown proteins. MS/MS generates fragments (series of daughter ions) of a parent ion and provides sequence information regarding the parent ion (Figure 1-7). Subsequently, the sequence of ions and the parent masses are searched against a database. However, the accuracy of the suggested sequence by MS/MS could be diminished when translational modification is involved, which affects the matching and scoring process. Also, if the analyzed peptide sequence is shared among different proteins such as the same family, it is hard to identify specific proteins.

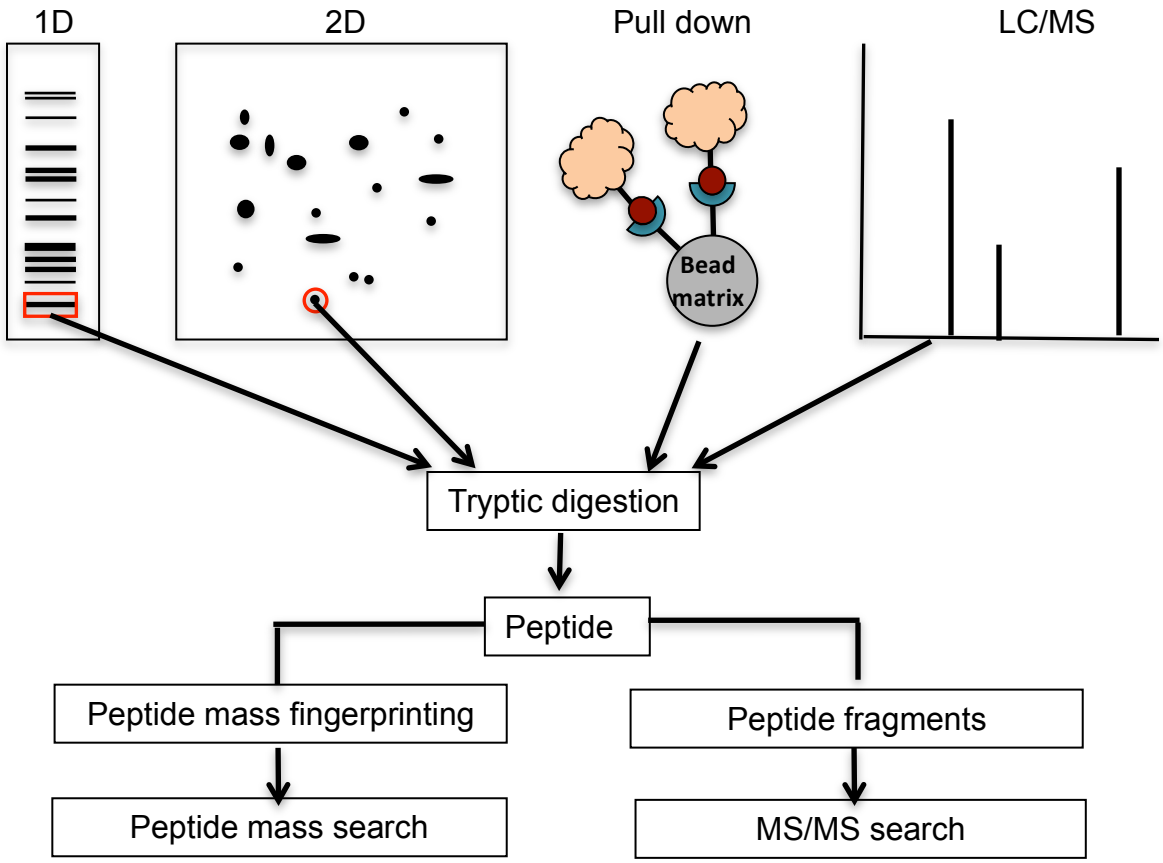

Figure 1-10. Procedures for identification of proteins by mass spectrometry.

The peptide mass matching process for PMF is based on probability. There are several protein search engines that are designed with their own algorithms such as MASCOT, Profound, and MS-fit. Among them the most popular protein search engine is MASCOT. MASCOT uses probability based on MOWSE scoring system. The total scores of the searched proteins are provided as the probability that the observed match is a random event. Mascot reports the threshold score that corresponds to a 5% significance level. A significant match is found only when the score of the matched protein is higher than the threshold score. The score is reported as $-10 \log_{10}(P)$, where P is the probability that the observed match is a random event. The threshold score is calculated as α value/number of database sequence where α is the probability of getting a

false positive match, and α is fixed as 0.05, though other numbers can also be used. The increased number of the sequences in the database directly affects the threshold. The theoretical peptides are generated according to the parameters such as the enzyme used for digestion of the protein, peptide mass tolerance, modification of the peptides, and taxonomy. Among them peptide mass tolerance mainly affects the score of the matched proteins. If the tolerance is too tight, MASCOT is unable to find a match. In contrast, if the tolerance is too generous, the match is no longer significant. Usually, tryptic digested peptides exist in modified forms and may be phosphorylated, oxidized on methionine residue, or alkylated on cysteine residues. Therefore, theoretical masses only including miscleavage might not be sufficient to get real matches. To take such modifications into account in the matching process, Mascot lets users choose fixed and variable modifications. Fixed modifications do not change the number of theoretical peptide masses to be compared with experimental masses. However, variable modifications increase the number of peptide masses to be tested in order to find the best match. For example, if oxidation on Met is selected and a peptide contains 3 Mets, it will compare the peptide mass containing 0, 1, 2 or 3 oxidized Met to the experimental data. It makes the search more complicated and results in reduced specificity. The limitations of PMF are that the majority of the sequence (>80%) of a protein has to be present in the database and that the number of peptides generated from the experiment has to be sufficiently high. Sometimes, very small proteins (<15 kDa) are problematic since they may generate small amount of tryptic digested peptides that is not enough to be detected. In addition, a mixture containing only 2-4 proteins can be identified in a single search.

1.3. Chemical labeling of biomolecules to study biological process

Bioorthogonal chemistry to label biomolecules

Elucidation of protein-protein interactions may reveal an unknown function of the protein and may be used to predict functional connections to different subcellular compartments. It is also important to understand details about biological processes such as the dynamic of protein synthesis, post-translational modifications, or lipid metabolism. Chemical labeling of biomolecules by using bioorthogonal chemistry has served as a valuable tool to study these biological processes.

Classically, protein modification has been achieved by using Cys or Lys residues to install small molecular probes such as biotin and fluorophores. Recently, Try and Trp have gained attention as alternative amino acid residues for protein modification since they are rarely present on protein surface, which allows controlled single site modification.[66] The N-terminus of a protein is also a target for protein modification. Francis and co-workers reported a transamination method, which involves condensation of the N-terminal amine with pyridoxal-5-phosphate and subsequent hydrolysis to produce a pyruvamide.[67] The resulting pyruamide can be further modified with hydrazide or aminooxy functionalized molecules. The modification efficiency depends on the amino acid placed on the N-terminus. Modifications using specific amino acid residue are limited if there are several target residues or no desired residues on the protein surface.

Another method frequently used for protein modification is native chemical ligation (NCL). The reaction mechanism involves rapid thioester equilibration and then irreversible *S*-*N* acyl transfer. The mostly explored applications of this type of reaction are expressed protein ligation

(EPL)[68] and protein trans splicing (PTS).[69] Such applications take advantage of self-splicing inteins to purify and modify proteins. The major concern of using this method is that natural thioesters are abundant, which can also react with the target protein.

The methods mentioned are limited in certain circumstances as pointed above. To overcome these limitations, bioorthogonal chemistry has emerged. Bioorthogonal chemistry, which was coined by Carolyn R. Bertozzi in 2003, is a method to selectively label biomolecules of interest by using reactions that do not interfere with biological processes.[70] Such reactions require fast reaction rate and are inactive towards diverse functionalities existing *in vivo*. Widely adopted bioorthogonal reactions include aldehyde/ketone-hydrazide/alkoxyamine pair, azide-alkyne or phosphine pair, and tetrazole-alkene pair. Among them, the azide-alkyne reaction has been widely applied in diverse systems.

Azide-alkyne 1,3-cycloaddition reactions

1,3-dipolar cycloaddition reaction was described by Huisgen in 1965.[71] Alkyne and azide functional groups are not present in biological system and the reaction produces triazole that is stable to further reaction conditions such as reduction, oxidation, and hydrolysis.[72, 73] However, the extreme conditions necessary to produce the triazole, high temperatures or pressure, is unsuitable for biological systems. However, Mendal and Sharpless[74] discovered that introducing Cu(I) as a catalyst can dramatically accelerate triazole formation between the azide and terminal alkyne. This Cu(I) catalyzed reaction is now called Cu(I)-catalyzed azide-alkyne 1,3-dipolar cycloaddition reaction (CuAAC) or simply the "click reaction"(Figure 1-11).

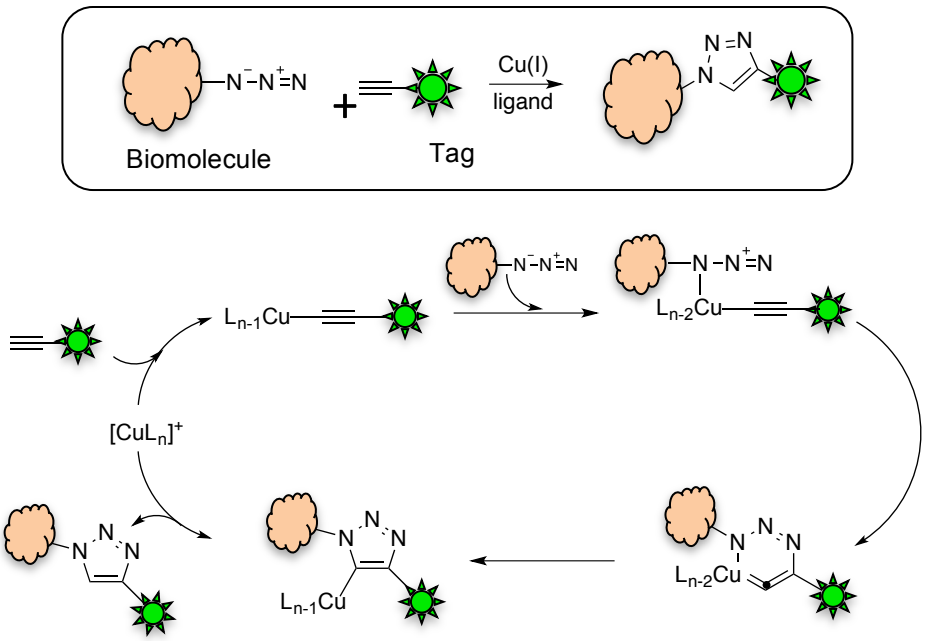

Figure 1-11. Copper-catalyzed azide-alkyne 1,3-dipolar cycloaddition for labeling biomolecule.[75]

Despite the fascinating advantages of CuAAC including fast reaction rate, excellent functional group tolerance, simplicity, and selectivity, the use of the Cu(I) catalyst impedes its use in cells due to toxicity.[76] To overcome cytotoxicity caused by Cu(I), copper free click reaction was introduced by Bertozzi and co-workers (2007). Instead of using a free metal catalyst to force the reaction, highly strained alkyne, cyclooctyne, was adopted. The driving force of the reaction is releasing the distortion energy of the twisted triple bond possess (*ca*. 8 kcal mol^{-1}).[77] However, the reaction rate with cyclooctyne without additional functional group on the ring was slower than a typical Staudinger ligation.[78] Derivatives of cyclooctyne such as difluorocyclooctyne (DIFO) and dibenzocyclooctyne (DIBO) improved the rate by 60-fold and have been proven to be a non-toxic and efficient reagents for live cell labeling (Figure 1-12).[79]

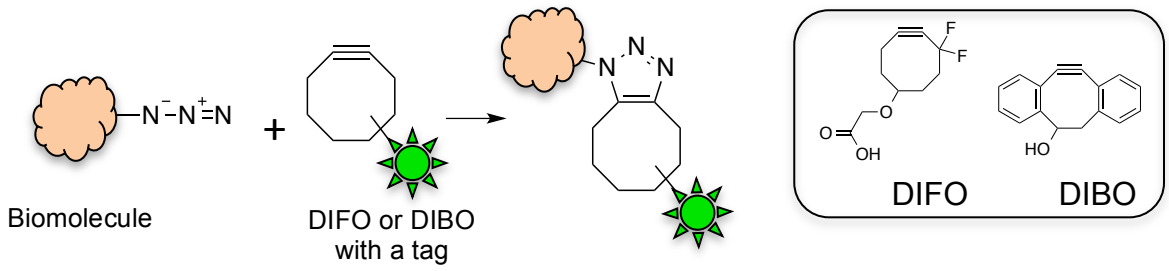

Figure 1-12. Strain-promoted azide-alkyne 1,3-dipolar cycloaddition used in biomolecule labeling.

1.4. Cleavable linkers

Despite the remarkable progress accelerated by bioorthogonal chemistry for the characterization of biological systems, it demands technical improvements particularly when the purpose of the labeling is to isolate and identify labeled proteins and to characterize the sites where the labeling event occurs.[80] To isolate the targeted proteins, affinity purification, typically by the biotin-streptavidin system, has been used. Although the biotin-streptavidin approach is an effective method to enrich the target biological molecules tagged with biotin, quantitative release of proteins from streptavidin is challenging due to the strong biotin-streptavidn binding (*K*d ~ 10^{-15} mol/L). Enrichment of biotinylated proteins from a complex mixture is efficiently achieved using a streptavidin-coated solid support such as an agarose resin. However, conventional methods to release biotinylated proteins from streptavidin bead matrices are harsh because of the strong binding interaction. For example, 2% SDS/6M urea,[81] boiling in 2% SDS or on-bead tryptic digestion are required to release the targeted protein. These non-selective conditions release the streptavidin monomer from the matrix. Similarly, digested peptides of streptavidin from on-bead trypsin treatment contaminate the protein to be analyzed. As a consequence of the

difficulty in isolating the desired protein from the matrix, the mass spectra required for target identification have increased noise. To avoid sample contamination originating from harsh elution conditions, a cleavable linker has been introduced between biotin and the effective molecule on the other end. A desired linker is the one that can be cleanly cleaved in mild conditions without releasing other contaminants and is stable enough to survive during labeling and separation.

Disulfides have been widely used as a cleavable linker due to their simple synthesis and rapid cleavage under mild reducing reagents such as dithiothreitol (DTT), β-mercaptoethanol, or tris(2-carboxyethyl)phosphine (TCEP). However, disadvantages of using this linker stem from the instability towards both electrophilic and nucleophilic polar reagents. electrophilic and nucleophilic polar reagents cause thiol exchange and leads to non-specific cleavage in physiological conditions. Gartner *et al*. developed a hindered disulfide linker for quantitative proteomic applications. The hindered disulfide is inert to thiol exchange or reduction by DTT under alkylating conditions (10 mM DTT/6M urea/buffer at room temperature for 60 min), but the elution condition includes 20% methanol, and it has to be incubated for 1 hour at 50 °C.[82]

Azo compounds are attractive as cleavable moieties since they undergo cleavage with sodium dithionite ($Na_2S_2O_4$), a mild and potentially bio-orthogonal reducing agent. Several different versions of azo-based biotin probes have been synthesized and analyzed. Verhelst *et al.* used a 4-(2'-hydroxy-phenylazo)-benzoic acid scaffold with biotin on one end and an activity-based probe for cathepsin attachment on the other end.[83] Elution with 25 mM dithionite at pH 7.4 for 15 minutes [84, 85]yielded 95% target protein coverage.[83, 86] In a comparative analysis of several azobenzene based biotin probes, Yang *et al.* showed that ortho-hydroxy-functionalization of the aromatic ring increased the efficiency of the cleavage.[87] This result is consistent with separately

investigated work from Wagner and coworkers (2010), which showed that a carboxylic acid group at the ortho position facilitates cleavage.[88]

Photocleavable and acid-sensitive linkers are also available for enrichment of biotinylated proteins. The most commonly used photocleavable linker is *ortho*-nitrobenzyl alcohol group. Its derivatives showed efficient cleavage under UV irradiation (λ = 300-365 nm)[89] which excites the nitro group leading to an intramolecular hydrogen abstraction in γ-position. Next, highly reactive azinic acid is formed and rearranged to a nitroso compound which can damage biological systems.[90] Recently, Szychowski *et al.* designed diphenyldialkoxysilane as a cleavable biotin probe, and it was efficiently cleaved by treatment with 5% formic acid (incubated at room temperature for 2 hours when the protein was bound to streptavidin agarose bead).[91] However, the low pH can denature the protein of interest and may cause non-specific cleavage of the protein.

1.5. Polymers mimicking multivalent interactions in biological system

1.5.1. Multivalent interactions adapted in biological system

Proteins on the cell surface are critical in transmitting external signals into the cell allowing the cell to adapt to external environmental changes. In addition, they participate in cell-cell interactions with neighboring cells, the ECM and pathogens. These events are often induced by the formation of multiple receptor-ligand binding interactions on the surface.[92] Multivalency is a term describing these multiple ligand and receptor interactions.

In nature, several examples of multivalent interactions are observed. Influenza virus uses multiple trimers of hemagglutinin to interact with multiple moieties of sialic acid on bronchial

epithelial cells.[93, 94] Experimental data obtained from microscopy, cross-linking, and X-ray crystallography have identified various multivalent cell-surface receptors from many structural classes including heptahelical GPCRs, methyl-accepting chemotaxis proteins, gated ion channels, receptor-protein tyrosine kinases and multichain immune recognition receptors.[95] There are two major benefits of adopting multivalency, (i) the strength of multiple ligand interactions, which is called avidity, is much greater than that of single ligand interaction, which results in a stronger interaction between the corresponding binding partners and (ii) the specificity of the interactions is greater in multivalent complexes. When biomolecules on the cell surface form heterogeneous complex, only a certain ratio of different types of ligands may bind to the heterogeneous complex on the cell.[96]

1.5.2. Diverse scaffolds for mimicking multivalent ligand system

Multivalent interactions control diverse cellular processes including cell surface recognition events. Therefore, understanding mechanistic principles of multivalent interactions on the cell surface could provide valuable information to develop therapeutic agents and biomaterials. Chemical synthesis of mimicking endogenous multivalent ligands can be achieved by several methods. Using synthetic ligands is advantageous not only because they can be used to understand the underlying mechanisms of naturally occurring multivalent interactions but also because the scaffold of structures, the identity of the ligands, the number of ligands, and the length of spacer can be tuned systematically.[92] Typical constructs providing scaffolds of multivalent ligands include liposomes, dendrimers, self-assembled monolayers and linear polymers (Figure 1-13).

Liposomes are artificial lipid bilayers and are ideal mimics of the cell surface membrane. The embedded ligands in the liposomes can interact with their targets in a similar manner as surface membrane ligands. There have been successful examples using liposomes as multivalent ligands.[97-99]

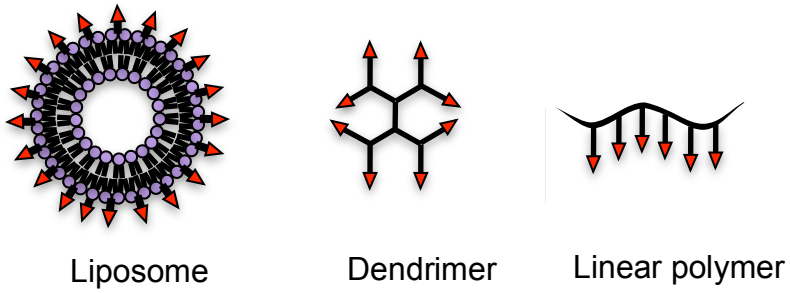

Figure 1-13. Commonly used scaffolds for multivalent interaction

Dendrimers are polymers which have multiple covalently attached branches spreading radially from its core. They have several advantages including precise nanometer size, high functionality and regular structural features. Densely-packed end-groups of dendrimers make them suitable for multivalent interactions. Many reports showed multivalent effects of dendrimers having amino acids or carbohydrate as their incorporated ligands.[100, 101] Since dendrimer polymers are a covalently connected system, concerns of formulation and stabilization of the system can be avoided unlike liposones.

Linear polymers have been widely used to prepare multivalent ligand systems of predetermined length and density. Many linear polymers bearing a broad range of carbohydrates or peptides have been applied as an inhibitor of specific receptors. There are three typical ways to prepare the linear polymers including ring opening metathesis polymerization (ROMP), atom transfer radical polymerization, and reversible addition fragmentation polymerization (RAFT).

1.5.3. Linear scaffold polymerization

Ring opening metathesis polymerization (ROMP)

ROMP has become a powerful method to prepare polymers with complex architectures and useful functions (Figure 1.14). ROMP is one of the "living polymerization" methods. Living polymerization defined by Swarzc in 1956, is a reaction proceeding without chain transfer or termination.[102, 103] In addition to Swarzc's original concept of living polymerization, there are four more essential criteria: (1) complete and rapid initiation (2) irreversible propagation (3) linear dependence of number-average molecular weight on degree of polymerization (4) narrow molecular weight distribution (PDI < 1.5).[104]

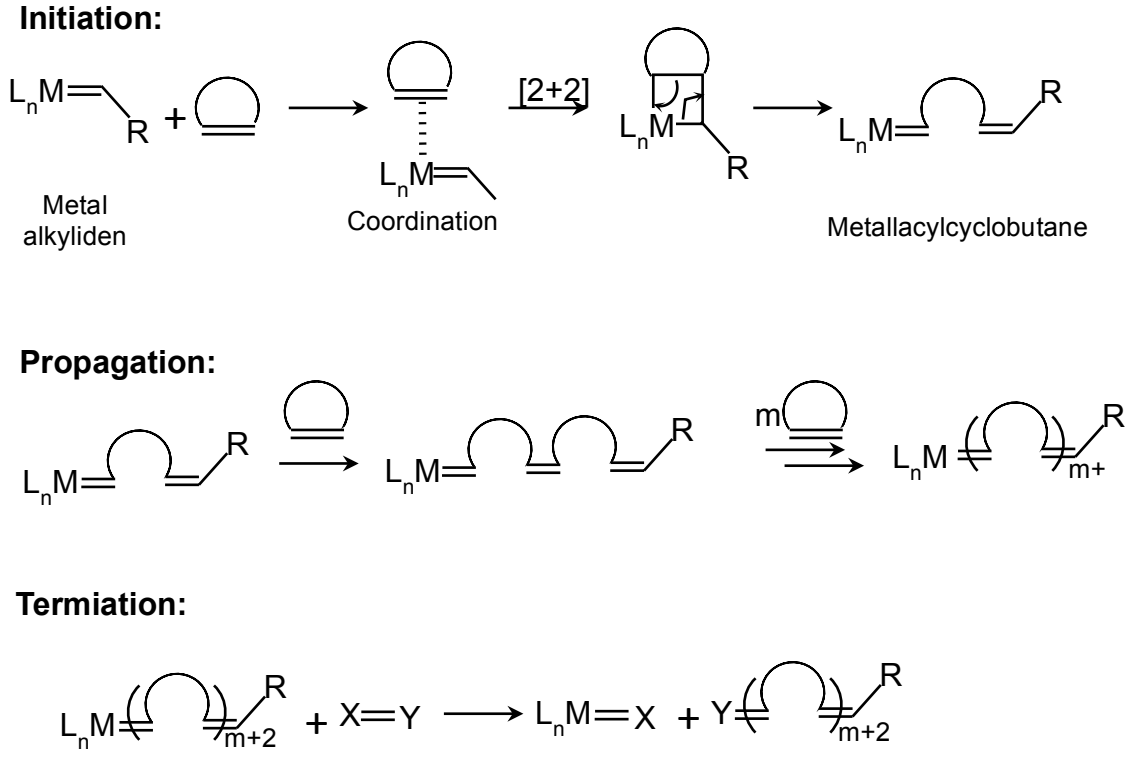

Figure 1-14. A general mechanism of ROMP polymerization

ROMP polymerization is based on olefin metathesis, a metal mediated carbon-carbon double bond exchange process.[105] ROMP converts cyclic olefins into linear polymers redistributing the double bond on a polymer backbone. A cyclic olefin coordinates with a transition metal catalyst leading to the formation of a metal alkylidene which undergoes a [2+2]-cycloaddition reaction to produce a highly strained metallacylobutane intermediate. This metal alkylidene is then able to propagate with an incoming olefin and form a polymer. Resulting intermediate undergoes cycloreversion to afford new metal alkylidene. The living polymer chain continuously propagates by repeating the analogue steps until it consumes all monomers, equilibrium is reached, or the reaction is terminated by the addition of a quencher (Figure 1-14). Ethyl vinyl ether is a standard and effective quencher in Ru catalyzed ROMP termination.

The driving force of ROMP, which counterbalances the entropy loss and carries the reaction forward, is the release of ring strain in the cyclic olefin monomer (negative $\Delta H°$) resulting in a decrease in entropy. Commonly used monomers such as cyclobutene, cyclopentene, *cis*-cyclooctene, and norbornene contain considerable amount of ring strains (> 5 kcal/mol), which are suitable for ROMP.[106] Norbornene derivatives are the most commonly used monomer since their ROMP reactivity is high and incorporation of substituents is convenient. Monomer concentration and reaction temperature are closely related to thermodynamics of ROMP. A critical temperature below which polymerization will not occur exists, and at this temperature the enthalpy contribution associated with the ring strain release cannot compensate the high entropic penalty. Generally, for a successful ROMP, the highest monomer concentration at the lowest temperature possible is the favorable polymerization condition.[104]

Catalysts for ROMP

Great advances in ROMP chemistry have been achieved using well-defined and functional group tolerant catalysts. Early catalyst systems were often heterogeneous, air sensitive and moisture sensitive. In addition, the active species were unclear, which made systematic analysis and optimization almost impossible. Transition metal complexes with organic ligands are preferable to perform controlled polymerization due to homogeneity of the reactions. It is possible to define and adjust catalytic activity by diverse ligand design.[107]

Titanium (Ti) was the first example of a well-defined catalysts mediating living ROMP. Ti catalysts generate polymers with low polydispersities (PDI<1.2), and the molecular weight ascends linearly as the monomer is consumed.[108] Tantalum (Ta) which has higher activity than Ti, polymerizes norbornene in a living fashion.[109] However, the Ti and Ta complexes are extremely Lewis acidic due to their high oxidation states. Because of this feature, these catalysts react rapidly with heteroatom-containing functional groups such as hydroxyl and amino groups, which limits their application in living ROMP.

Tungsten (W)-chloride-based catalysts successfully mediate ROMP, but the process is not living polymerization. On the other hand, the development of Lewis acid free initiators based on the general structure W(=CH-*t*-Bu)(CH_2-*t*-Bu)-Cl(OAr)(O($CHC(CH_3)_2$)$_2$ showed exceptional functional group tolerance.[110] However, the high activity of these catalysts stimulates secondary metathesis reactions. Schrock and coworker developed imido-alkoxy based catalysts with the general structure (Nar)$(OR)^2$W=CHR. These catalysts exhibited better initiation and higher activities,[111-113] but the extremely poor functional group tolerance limited their application.

Molybdenum (Mo)-based alkylidene complexes are structurally similar to W-based

alkylidenes though they exhibit improved functional group tolerances (ester, amide, imide, ketal, ether, cyano, trifluoromethyl, and primary halogen containing monomers), and are more stable towards decomposition and side reactions. In addition, by modifying the alkoxide ligand, the activity can be tuned. The high activities of the Mo-based catalysts with high functional group tolerances enable the preparation of biological polymers through the ROMP of *endo*-5-norbornen-2,3-dicarboximides obtained from the methyl esters of amino acids.[114, 115]

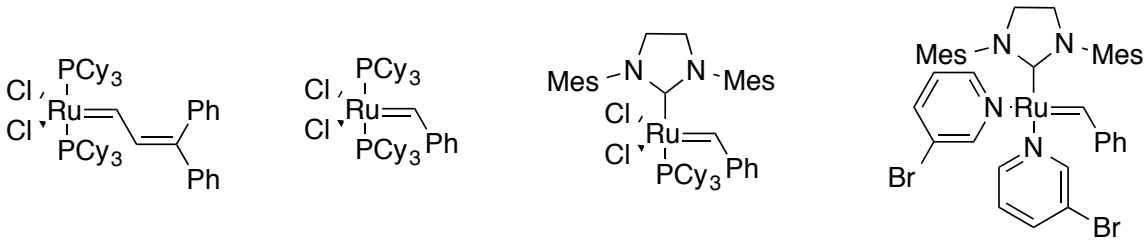

1 **2** **3** **4**

Figure 1-15. Ru-based catalysts for ROMP

Due to the low oxophilicity of ruthenium (Ru), its complexes are more stable to many polar functional groups than the complexes of Ti, Ta, W and Mo. Four generations of Ru complexes are commonly used in ROMP reactions (Figure 1.15). The first well-defined Ru complex, Catalyst 1, is stable in degassed and dry organic solvents, and no significant decomposition has been reported after exposure to water, various alcohols, or ethers. This Ru complex polymerized norbornene and cyclobutene monomers in a living fashion, but it did not show significant activity toward other olefins. To increase the activity, various bulky and electron rich phosphine ligands were tested. PCy_3 was found to be the most effective ligand for high activity of catalyst **1**. Ru complex containing PCy_3 showed stability toward organic and inorganic acids. However, the increased activity enlarged the difference between the rate of initiations, the rate of

propagations and chain transfer reactions, which results in high molecular weight and broad polydispersity (PDI>2). Ru-complex **2** was prepared via the treatment of $(PPh_3)_3RuCl_2$ with diazobenzylidene. It was able to polymerize norbornene and cyclobutene bearing diverse functional groups including hydroxyls, esters, amides, keto and amino groups. However, polymerization was not highly controlled due to slow initiation. Extensive studies on the mechanism of these Ru catalysts revealed that the dissociation of phosphine is a prerequisite before olefin coordination occurs. To maximize activity of the catalyst, stabilization of these coordinately unsaturated intermediates was also essential to avoid premature decomposition of catalyst. *N*-heterocyclic carbenes (NHCs) were introduced because they are less likely to be separated from the catalyst but can donate electron to the catalyst to stabilize the intermediates. Complex **3** possessed remarkable activities but again polymerization was uncontrollable and generated broad PDIs. Containing weakly coordinating pyridines, a new class of Ru based catalyst **4** exhibited extremely high activities and fast initiation rates resulting from the labile nature of pyridine ligands.[116] The PDIs of the polymers prepared using catalyst **4** were as low as 1.06.[104]

There is no universal catalyst that works for every monomer. Catalysts complexes have their own advantages and disadvantages. Therefore, one should choose the suitable catalyst according to the characteristic of the monomer. If necessary, diverse modifications of catalysts can be made.

1.5.4. Living radical polymerizations

Conventional radical polymerization is impossible to synthesize in a living

polymerization fashion owing to fast propagation rate and unavoidable radical termination reactions.[117] Controlled radical polymerizations (CRP) were developed over 10-15 years with new approaches that utilize the equilibria between growing radicals and dormant species. Atom transfer radical polymerization (ATRP) (Figure 1-16) is the most widely used CRP.[118, 119]

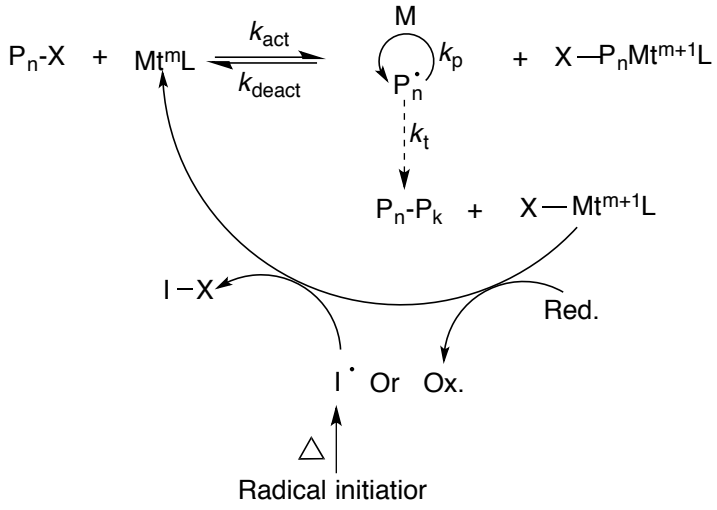

Figure 1-16. General mechanism of ATRP

The dormant species (P_nX) repeatedly reacts with transition metal complexes in their lower oxidation state, Mt^m/L (where Mt^m is a transition metal species with an oxidation state m, and ligand L). This leads to the formation of growing radicals ($P_n^{\cdot}$), and the deactivator (transition metal complexes in their higher oxidation state, $X\text{-}Mt^{m+1}/L$) reacts with the propagating radical in the reverse reaction to re-form dormant species and the activator (Figure 1-16). ATRP is a catalytic process and Cu^I has been the most popular transition metal for ATRP.[120] Biomolecules prepared by ATRP includes carbohydrates, proteins, nucleic acids or peptide nucleic acids. In addition, polymers with degradable and biodegradable moieties (aldehyde at low pH and

disulfide group labile in a reducing environment) were successfully prepared for tissue engineering and drug delivery.[120] Moreover, protected alkyne[121] and azido group monomers,[122] which are used for Cu(I) catalyzed Huisen 1,3-dipolar cycloaddition (click reaction) were able to polymerized by ATRP.

Reversible addition fragmentation chain transfer (RAFT) is also one of the versatile methods for providing living characteristic to radical polymerization with predetermined molecular weight (Figure 1.17).[123] RAFT polymerizations are tolerant of a broad range of reaction conditions including the preparation of water-soluble materials and functionalities.[124]

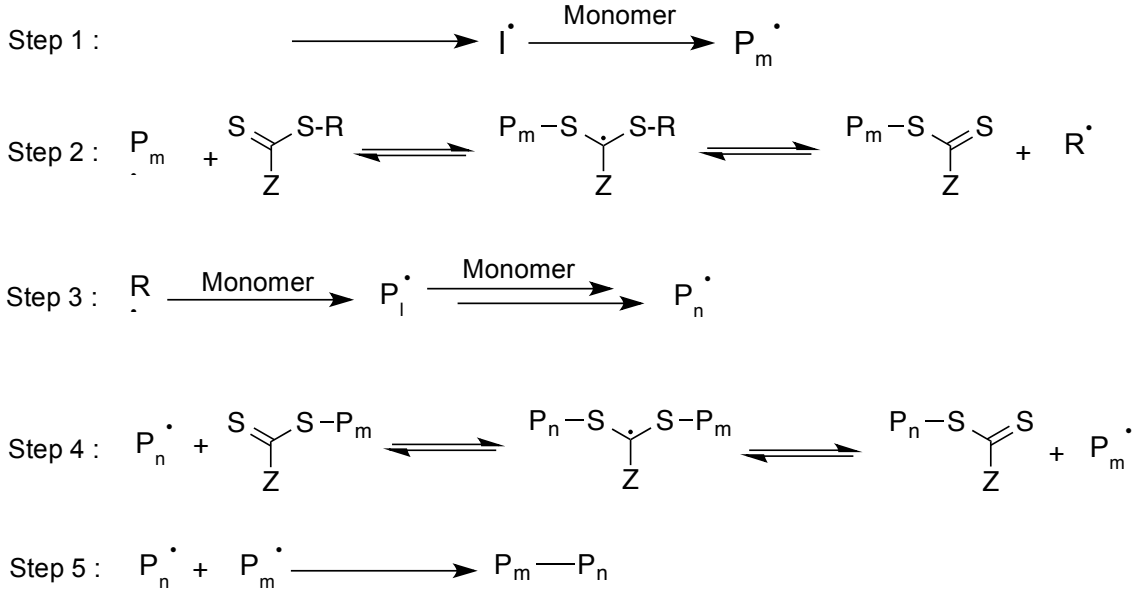

Figure 1-17. General mechanism of RAFT

The first step of RAFT is the generation of a radical. Radical initiators that can be decomposed thermally are most widely used for initiation owing to the commercial availability of such compounds. The oligomeric radicals generated from the initiation reacts with the RAFT agent producing (whatever R radical is from the picture. (step 2). Polymer chain is elongated by adding monomer. Existing growing radicals and the thiocarbonylthio group capped species (step 4) (Figure 1-17).

Functionalities in RAFT polymers can be introduced not only by the monomers but also by end-group functionalization and postpolymerization modifications. End group functionalizations are achieved by utilizing functional RAFT agents including functionalities such as hydroxyl, carboxylic acid, and allyl groups. Carboxylic acid is the most common functionality used for end group functionalization since it can be easily conjugated to peptides, proteins, or carbohydrates. Pyridyl disulfide (PDS) is widely applied for bioconjugation, which can make conjugation with thiol-containing biomolecules such as bovine serum albumin (BSA),[125, 126] peptides[127] and small interfering RNA.[128] Also, several azide-functional RAFT agents for application in click reactions have been reported.[129, 130] These functional groups mentioned above can also be incorporated using thiol reactive, activated ester, amine functionalized, and clickable monomers.[127]

Chapter 2. Results

1. Evaluation of photo-affinity based ROMP polymers as tools for identifying receptors on cell surfaces
    1.1. Synthesis of monomers, THPTA and coumarin azide
    1.2. Synthesis of photo-affinity based ROMP polymers
    1.3. Click reaction test and photoaffinity crosslinking efficiency of polymer
    1.4. Photoaffinity labeling of U87-MG cells using polymers and peptide mass fingerprinting
    1.5. Increasing affinity of ligand-receptor binding

2. Introduction of cyclic acetal as a cleavable linker for a biotin affinity probe
    2-1. Synthesis of cleavable biotin probes
    2-2. Preparation of biotinylated BSA and evaluation of the cleavable acetal probes
    2-3. Cleavage and capture in cell lysates
    2-4. Suppression of streptavidin monomer release
    2-5. Further labeling of the aldehyde tag on protein after cleavage

1. Evaluation of photo-affinity based ROMP polymer as tool for identifying receptors on cell surface

1-1. Synthesis of monomers

To prepare NB-E(OtBu)S(tBu)A-OMe (**3)** Cbz-based standard amino acid coupling procedures (Scheme 2-1) were performed in CH_2Cl_2 with 1-(3-dimethylaminopropyl)-3-ethylcarbodiimide hydrochloride (EDC•HCl), 1-hydroxybenzotriazol (HOBt) and N,N-diisopropylethylamine (DIEA) at room temperature. The Cbz protecting group was removed by treatment with 10% Pd/C under H_2 atmosphere. The resulting peptide was used without further purification for the next coupling reaction. Coupling and deprotection were monitored by thin layer chromatography (TLC).

After deptorection of Cbz group from Cbz-E(OtBu)S(tBu)A-OMe, the highly ring strained bicyclic molecule, 5-norbornene-*exo*-carboxylic acid, was coupled to the N-termini of synthesized peptides by standard amino acid coupling procedure to yield monomer **3** for ROMP. Synthesized monomer was purified by silica column chromatography and characterized via ^1H NMR spectroscopy and MS.

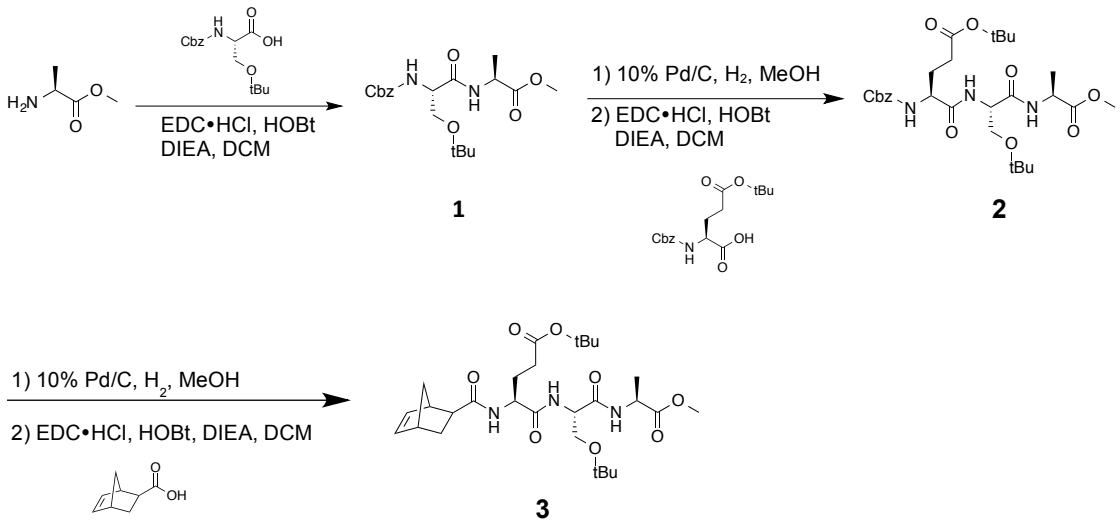

Scheme 2-1. Synthesis of NB-E(OtBu)S(tBu)A-OMe

Ligand monomer, NB-βAla-Bpa-GR(Pbf)GD(tBu)S(OtBu)-NH_2 (**4**) and NB-βAla-Bpa-ESA-NH_2 (**5**) were synthesized by Fmoc-based solid phase peptide synthesis on a Sieber amide resin to produce fully protected peptides that have an amide-protected C-terminus (Figure 2-1). A mixture of HOBt/TBTU/DIEA in DMF was used as a coupling reagent, and 20% piperidine in DMF was used to remove Fmoc protecting group from the growing peptide. Each coupling and deprotection step was monitored by Kaiser test. After cleaving the peptide from the resin using 2% TFA/DCM, the product was purified by silica column chromatography using 5%-10% MeOH/DCM.

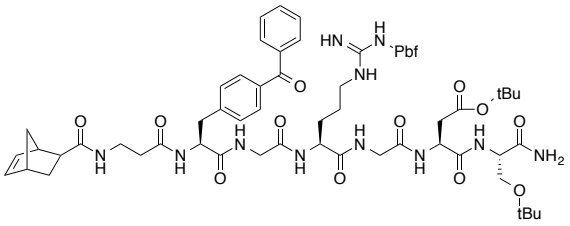

4

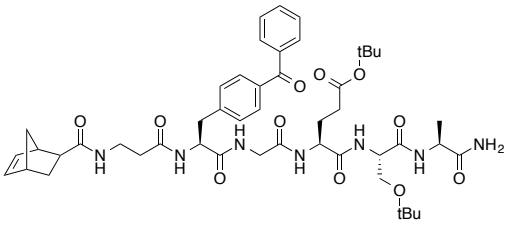

5

Figure 2-1. Structures of ligand monomers

NB-NHS (**6**) was generated by coupling 5-norbornene-*exo*-carboxylic acid to *N*-hydroxysuccinimide (Scheme 2-2).

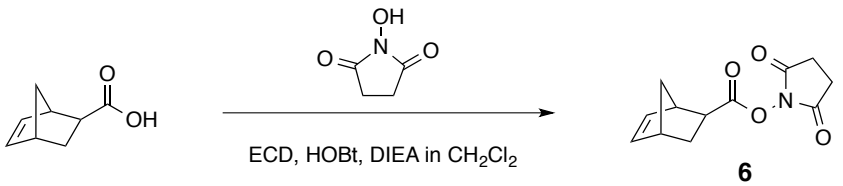

6

Scheme 2-2. Synthesis of norbornene carboxylic acid N-hydroxysuccinimide ester, NB-NHS, **6.**

1-2. Synthesis of photoaffinity based ROMP polymers

Tri-block copolymers were prepared by ROMP using fully protected peptides. The first monomer **4** or **5** was mixed with catalyst, $(H_2IMes)(3\text{-Br-pyr})_2Cl_2Ru{=}CHPh$, in DCM/$CH_3OH$ (3/1) in the presence of 3M LiCl. After confirming that the first monomer was consumed completely by TLC, monomers **3** and **6** dissolved in CH_2Cl_2/CH_3OH (3/1) were transferred to the reaction vessel. Once polymerization with the monomer, **3** and **6**, was completed, monomer **4** or **5** was added to the reaction. After quenching the reaction with ethylvinyl ether, side chain intact tri-block copolymers, **7a** and **7b**, were obtained (Scheme 2-3 A). To prepare random copolymer **8a** and **8b**, all the monomers **3**, **4**, **5**, and **6** were simultaneously mixed with the catalyst in DCM/MeOH (3/1) in the presence of 3M LiCl. After quenching the reaction with ethylvinyl ether, side chain intact polymers were obtained (Scheme 2-3 B).

(A) Synthesis of tri-block copolymer

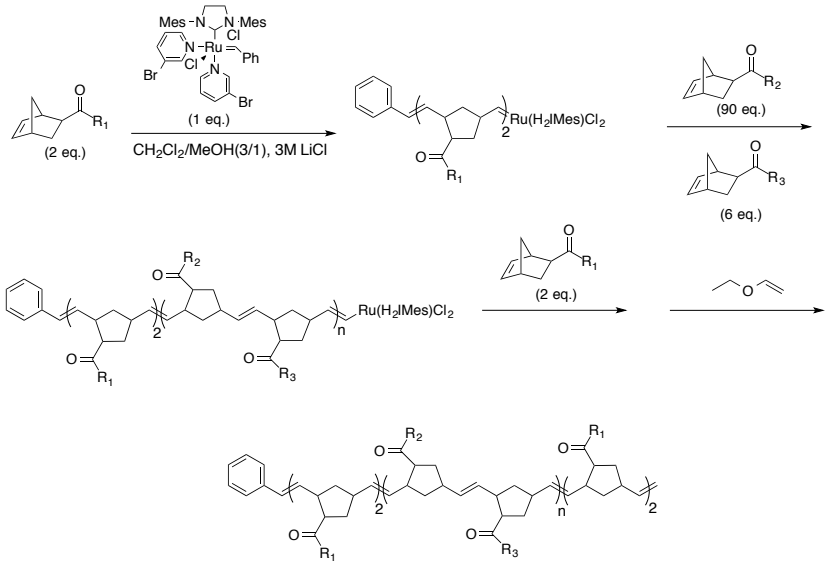

7 (n : R_2:R_3 = 90:6)

(B) Synthesis of random copolymer

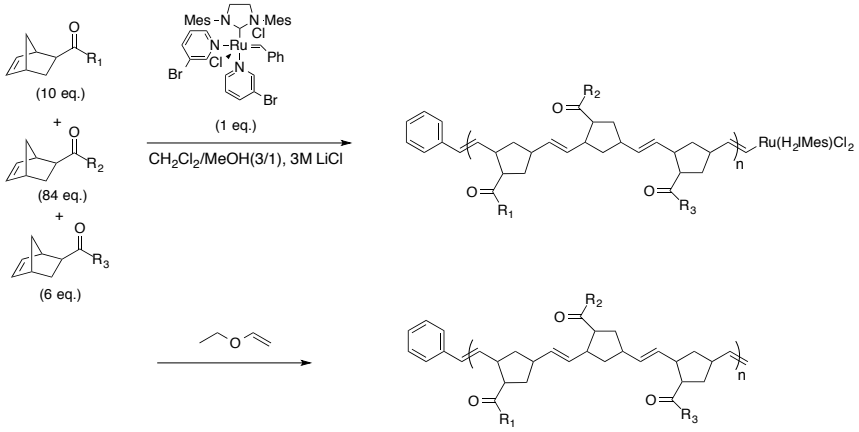

8 (n : R_1:R_2:R_3 = 10:84:6)

7a and **8a** : R_1=**4** and **7b and 8a**: R_1=**5**

R_1 = -βAla-Bpa-GR(Pbf)GD(OtBu)S(tBu)-$CONH_2$ (**4**) or -βAla-Bpa-E(OtBu)S(tBu)A-$CONH_2$ (**5**)
R_2 = -E(OtBu)S(tBu)A-$CONH_2$ (**3**)
R_3 = -NHS (**6**)

Scheme 2-3. Synthesis of tri-block and random copolymers

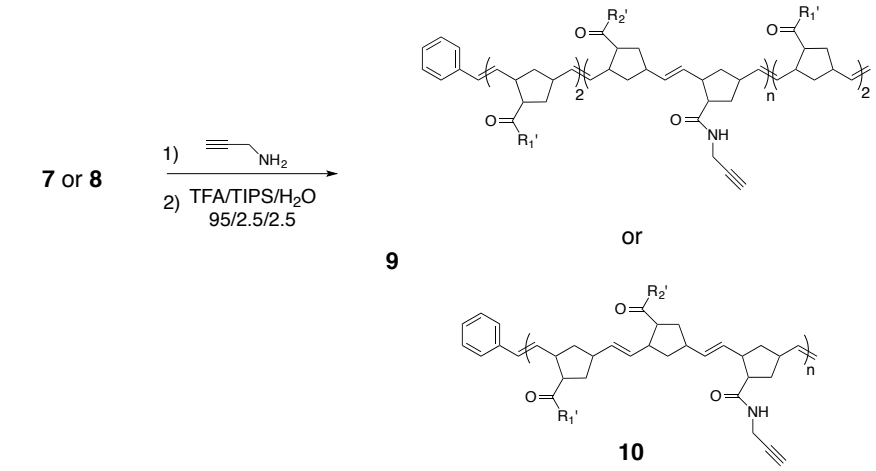

9a and **10a** : R_1' = **4'** and **9b** and **10b** : R_1' = **5'**

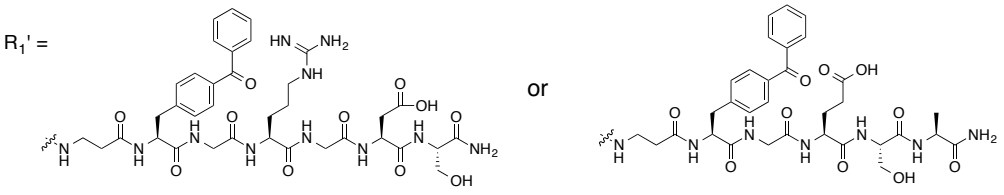

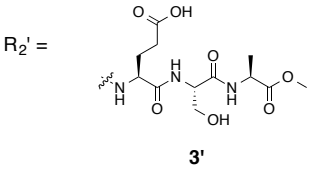

Scheme 2-4. Alkynylation and deprotection of polymers

The NHS activated carboxylic acids on polymers **7a**, **7b**, **8a**, and **8b** were replaced with propargyl amine in CH_2Cl_2 to produce the alkyne-tagged polymer (Scheme 2-4). The side chain protecting groups were removed with a cocktail of TFA/TIPS/H_2O (95/2.5/2.5) for 5 hr, and polymers **9a**, **9b**, **10a**, and **10b** were obtained (Scheme 2-4).

1-3. Click reaction test and photoaffinity crosslinking efficiency of polymer

THPTA (**14**) was synthesized using methods from Hong et al. (Scheme 2-5).[131] To obtain pure THPTA, recrystallization was performed using acetonitrile.

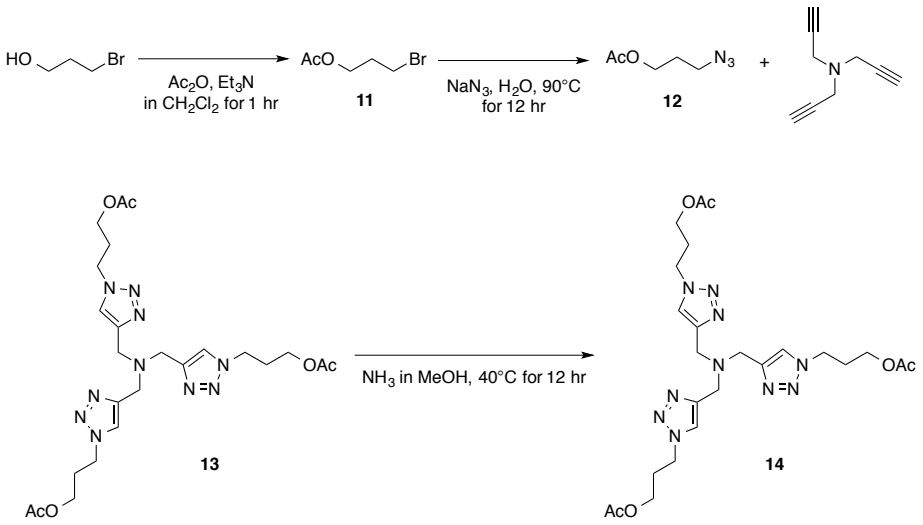

Scheme 2-5. Synthesis of click ligand THPTA

Coumarin azide was synthesized using methods from Sivakumar et al (Scheme 2-6).[132]

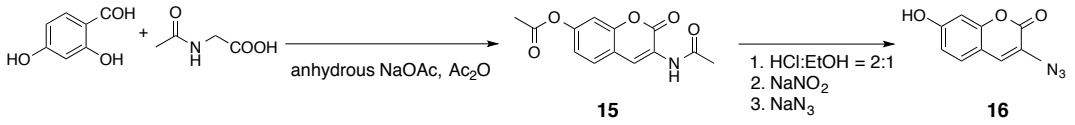

Scheme 2-6. Synthesis of coumarin azide

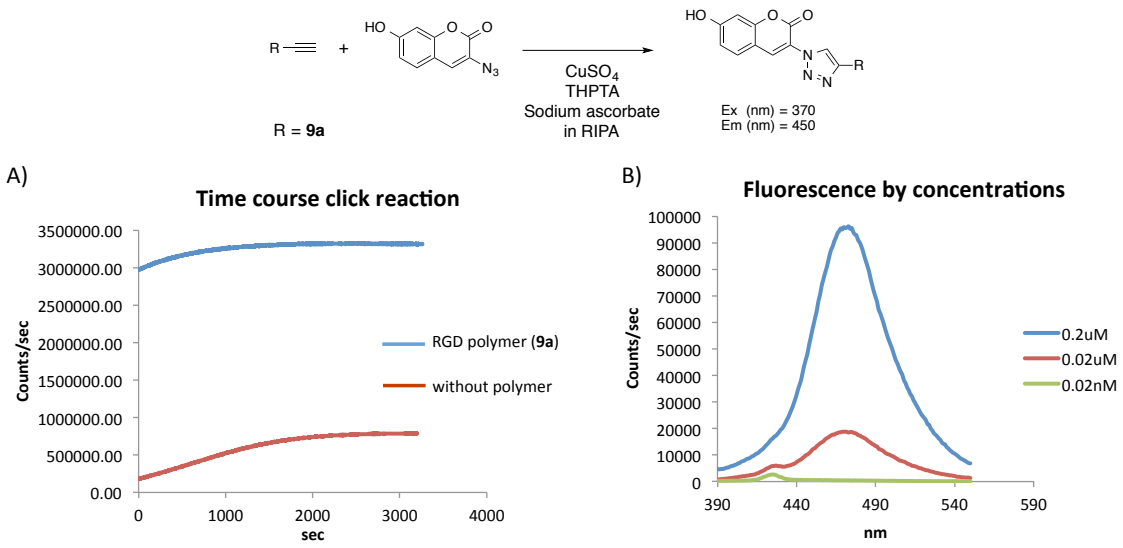

Figure 2-2. Click reaction test and the detection limit of coumarin azide-based fluorescence

To detect the presence of the alkyne on the polymers, coumarin azide was used since coumarin azide is known to fluoresce when it forms triazole.[133] As shown in figure 2-2A, the reaction reached the maximum in less than 20 minuts. Also, to test the detection limit of coumarin azide, click reaction was performed at various concentrations of **9a**. As shown in Figure 2-2B, the detection limit was observed to be between 20 pM and 20 nM.

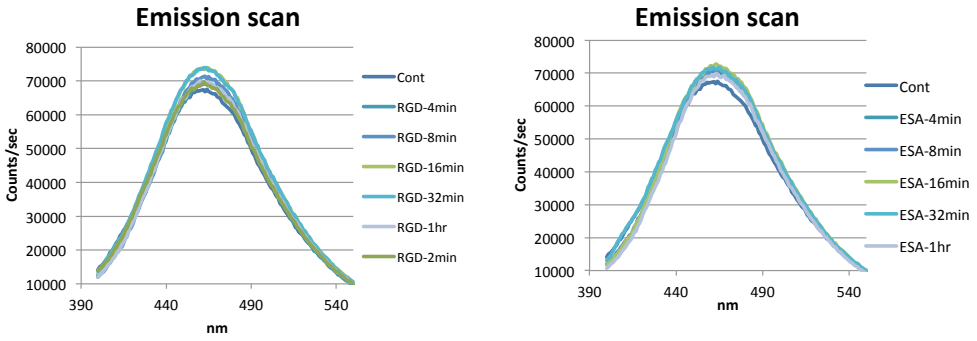

Figure 2-3. Time course of photocross linking to the receptors on the cell surface with polymer **9a** (A) and **9b** (B).

Coumarin azide was also used to test the photocrosslinking efficiency. The U87-MG cells were incubated with the polymer **9a** or **9b** in binding buffer for 2 hours at room temperature and irradiated under UV (λ = 350nm) on a 4 °C plate for a corresponding amount of time. After removing cells from UV irradiation at each time point, the cells were washed with PBS in order to remove any unreacted polymer and lysed in the presence of a protease inhibitor cocktail. Lysis was followed by a click reaction to generate the fluorescent triazole adduct which was used to determine the amount of proteins photo-crosslinked to the polymer. After quenching the click reaction with EDTA, the intensity of the fluorescence was checked. As shown in figure 2-3A, the negative control, which did not contain any polymer, also showed fluorescence. A small increase in fluorescence was observed for the sample from the cells treated with polymer **9a**. However, the difference was not significant. Also, the same phenomenon was observed in the sample from cells treated with **9b** (Figure 2-3B).

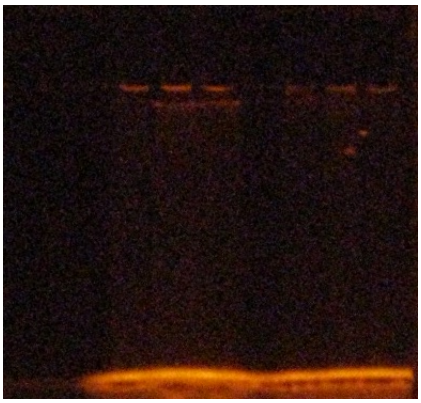

Figure 2-4. Separation of receptors labeled with polymer **9a** by SDS-PAGE. Lane 1, protein ladder; lane 2 and 5, controls that are prepared without polymer treatment, lane 3 and 6, protein sample treated with polymer **9a**; lane 4 and 7, protein sample treated with polymer **9b**.

As an alternative to visualize the proteins labeled with polymer **9a** or **9b**, the samples were separated by SDS-PAGE. The samples were prepared as described above and the resulting protein mixture was separated by SDS-PAGE, and the gel was exposed under UV (360 nm). Unfortunately, the protein did not separate well, and smear bands were detected through the lanes (Figure 2-4).

1-4. Photoaffinity labeling U87-MG cell using polymers and peptide mass fingerprinting

U87-MG cells were incubated with 10 μM of polymer **9a** or **9b** in binding buffer containing 1% polyvinylpyrrolidone (PVP) for 2 hours at 37 °C. Then, the cells were irradiated with long wave UV light at 4 °C for 15 minuts. To remove the unreacted polymer, the cells were washed with binding buffer containing 1% PVP and PBS. The cells were lysed with RIPA lysis buffer. The cell lysate was incubated with streptavidin-agarose beads for 1hours at 25°C to pre-clear the inherent biotinylated proteins. The biotin-PEG_{10}-azide was conjugated to the polymer bearing alkyne by click reaction. The click reaction was quenched by adding EDTA. To remove remaining click reaction reagents, the buffer was exchanged using a microconcentrator with a molecular weight cut off of 10 kDa. The cell lysate was then incubated with neutravidin agarose beads for 3 hours at room temperature. After removing the non-specifically bound proteins by washing the beads, on-bead tryptic digestion was performed. The resulting peptide mixtures were desalted by a pipette tip packed with C18 resin and loaded on a MALIDI plate with α-cyano-4-hydroxycinnamic acid (CHCA). After obtaining a MALDI spectrum, the peak list was generated. To rule out peaks from contaminates or non-specific binding to the neutravidin, the negative control was prepared without polymer treatment. Also, the polymer control that is treated with the polymer, **9b**, was used to eliminate peaks due to non-specific crosslinking by Bpa. The peaks were identified by a MASCOT search (www.matrixscience.com). To find the most prble protein candidate tagged, the search restrictions was used: 1) tryptic digestion missed cut = 1, 2) variable modification = carbamidomethyl and oxidation at Met, and 3) peptide mass tolerance = 50 ppm-100 ppm.

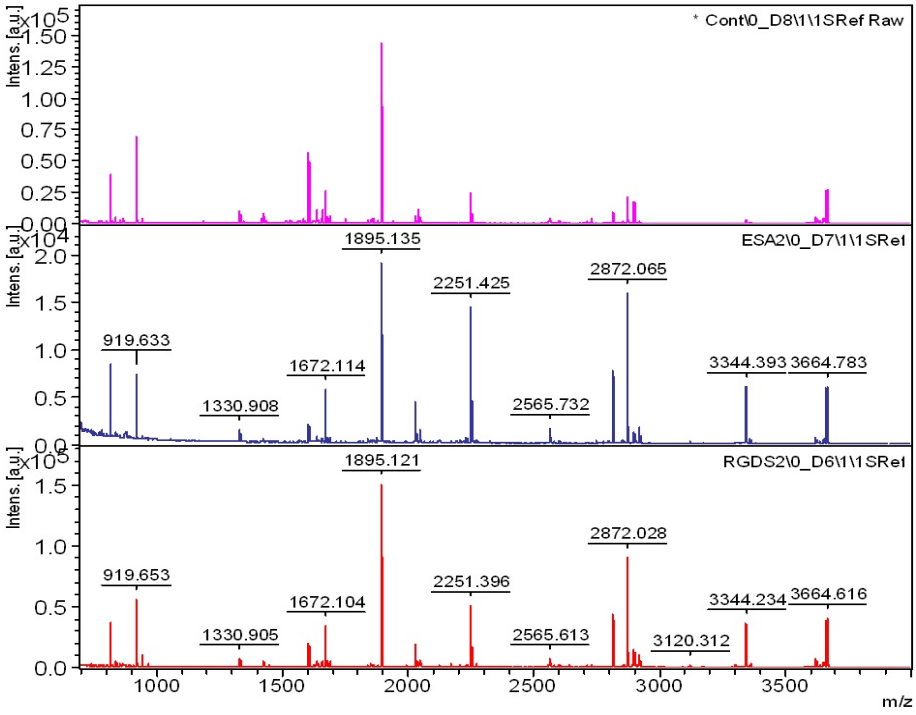

Figure 2-5. MALDI-TOF spectra of protein samples prepared through photoaffinity labeling by polymer **9a** and **9b**. A) Control obtained without polymer treatment, B) Protein sample treated with polymer **9b**, C) Protein sample treated with polymer **9a**.

Most of the major peaks were identified as contaminants as they were also present in the negative control and polymer control (Figure 2-5). In one of the batches of the experiment, we could extract integrin β_5 as a top hit with 27 ppm in peptide mass tolerance, but it was not identified in MASCOT using the same parameters. In another trial, we subtracted mass peaks of control from the peaks of the sample prepared with polymer **9a**. In this trial, integrin β_3 was ranked as 12 out of top 100 candidate proteins with 90 ppm in peptide mass tolerance. When changing the peptide tolerance to 100 ppm, the rank dropped to 37 out of 100 and no integrin was identified when the tolerance was 80 ppm. However, this search was not in the significant range as the score was 20 (the score higher than 56 was considered to be significant match). Also, the peaks of the sample treated with polymer **9b** was subtracted from the peaks of the sample prepared with polymer **9a**. This time, integrin β_5 was detected. When using only the peaks of the

sample prepared with polymer **9a** sample, integrin β_5 was ranked as 7 with 100ppm in peptide mass tolerance (Table 2-1).

Trial	Integrin	Rank	Peptide tolerance	Score
2nd	β_5	1	27 ppm	N/A
3rd RGD only	β_5	7	100 ppm	20
RGD-Control	β_3	12	90 ppm	20
RGD-ESA	β_5			

Table 2-1. MASCOT search results. RGD only; mass peaks from the sample prepared with polymer **9a** were used for MASCOT search, RGD-Control; mass peaks from control was subtracted from RGD only for M, RGD-ESA; mass peaks from ESA, which is mass peaks from the sample prepared with polymer **9b**, was subtracted from RGD only.

1-5. Photoaffinity labeling test of monomer 4

Photoaffinity efficiency is critical to obtain maximum amount of target receptors. Before directly applying the polymers to peptide mass fingerprinting, cell attachment assays with monomer **4** were performed to examine the photoaffinity labeling. U87-MG cells were incubated with calcein-AM for 30 minutes at 25°C. After washing the cells with binding buffer three times, the cells were incubated with monomer **4** for 2 hours at 37 °C. Meanwhile, a 96-well plate was coated with vitronectin for 1 hour at room temperature. After washing the plate with PBS three times, uncoated space was blocked with 1% BSA in PBS for 1 hour at 25 °C. The cells were divided into three different samples. Sample 1 served as control and was not treated with a monomer but was irradiated under long wave UV (λ = 360 nm).

Sample 2 was incubated with monomer **4** without irradiation with UV. Sample 3 was incubated with monomer **4** and irradiated under long wave UV. After incubation and UV irradiation, the cells were washed with binding buffer to remove any unreacted polymer. The cells were then added to the vitronectin-coated 96-well plate. The cells were allowed to adhere to the vitronectin for 2 hours at 37 °C. Non-adherent and loosely bound cells were gently washed off with PBS. The amount of cell adhered to vitronectin was measured by 96-well plate reader.

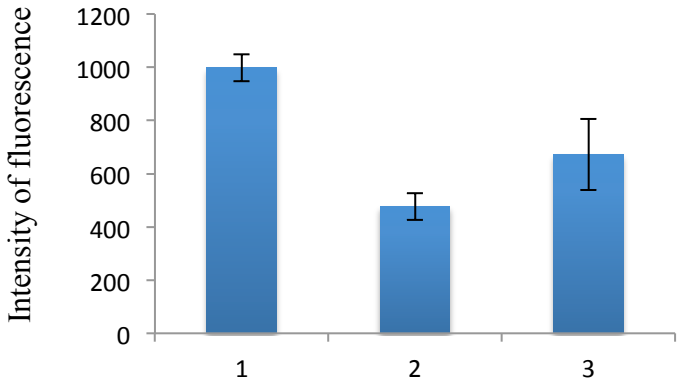

Figure 2-6. Cell attachment assay. Sample 1, control with no monomer treatment; sample 2, the cells treated with monomer **4** without UV irradiation; sample 3, the cells treated with monomer **4** with UV irradiation.

Monomer **4** showed inhibition in sample 2 even though the cells were washed after incubation with the monomer. Interestingly, the sample 3 that was treated with the polymer and irradiated under UV showed less inhibition then the sample 2 (Figure 2-12).

2. Introduction of cyclic acetal as a cleavable linker for biotin probe

The use of photoaffinity based ROMP polymers for the identification of receptors on cell surfaces involves purification of the polymer-receptor complexes using the biotin-strepavidin interaction. Strong binding affinity between biotin and streptavidin facilitates capture and enrichment of the targeted protein. However, the strong binding affinity involves harsh elution conditions such as 2% SDS/6M urea,[81] boiling in 2% SDS, or on-bead tryptic digestion. These non-selective conditions co-elute streptavidin monomer. Also, digested peptides of strepavidin from on-bead trypsin treatment contaminate the protein to be analyzed.

Recently, several biotin probes containing cleavable linkers have been developed to avoid such harsh elution conditions. Disulfide linkers have been widely used due to their rapid cleavage under mild reducing conditions. However, a disulfide linker is unstable to electrophilic and nucleophilic polar reagents, and thiol exchange with thiols in biological fluids can occur. Long-wave UV light can be used to release photocleavable linkers, but in some conditions, illumination of the sample is limited.[81, 134] There is also an acid labile linker from Pierce (proprietary structure) that is cleaved in 95% TFA. Another alternative is a dialkoxydiphenylsilane linker invented by Szychoswski et al. that is reported to be efficiently cleaved upon treatment with 10% formic acid for 0.5 h.[135 135] Also, other types of cleavable linkers have been developed such as enzymatically (TEV) cleavable linker,[84] diazobenzene-derived linkers that are cleaved with $Na_2S_2O_4$,[85, 87] and the linkers that are released in nucleophilic conditions including levulinoyl ester[136] and nitrobenzenesulfonamide.[137] Cleavable linkers used in chemical biology are reviewed well elsewhere (Gerog C. Rudolf et al, 2013, Geofrray Leriche et al).[138, 139]

Here, we exploited the cyclic acetal moiety as an acid-sensitive linker. Orthoesters, ketals, and acetals are accepted cleavable linkers for drug delivery in vivo.[140] In consideration of long term storage needs in

combination with the requirements for stability in physiological conditions and fast cleavage for target identification, we designed cyclic acetals as acid-cleavable linkers (Figure 2-13). They are readily prepared by simple chemistry from commercially available starting materials. In addition, the resulting aldehyde after hydrolysis of the acetal can serve as a chemical reporter via further modification of the purified protein. Here we introduce the synthesis and capture utility of cyclic acetal linkers in two model systems.

2-1. Synthesis of cleavable biotin probe.

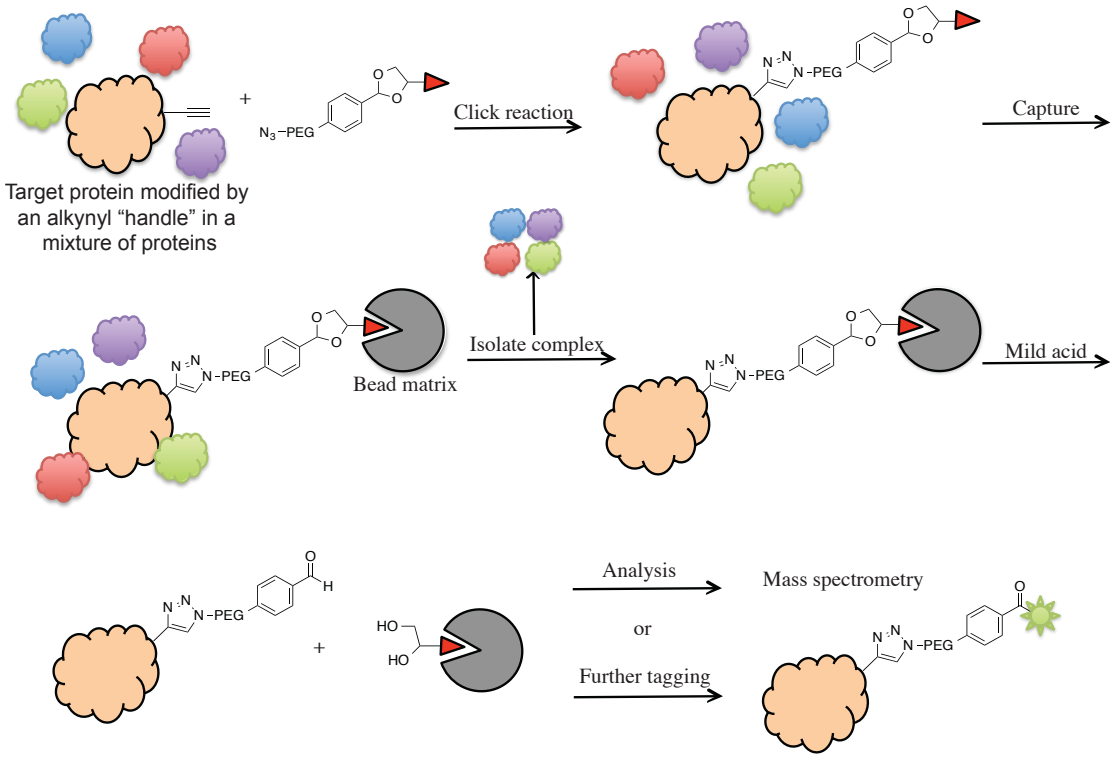

Figure 2-7. Schematic representation of target isolation using a cyclic acetal biotin probe.

To prepare the acetal-based cleavable biotin probe, azide-PEG_8-amine was coupled to dimethoxy acetal **17** using carbonyl diimidazole as a coupling reagent to generate acetal **18** (Scheme 2-7). A dimethoxy acetal was used to generate the cyclic acetals rather than forming the cyclic acetal directly from the aldehyde because the kinetics were more favorable. Basic alumina was employed for purification since the dimethoxy acetal is very sensitive to acid. In order to generate penta or hexa cyclic acetal, protected 3-amine-1,2-diol or serinol, respectively, was coupled to acetal **18**. The free amines in the diols were protected as their trifluoracetamides**, 19** or **20**. The cyclic acetal was formed using *p*-toluene sulfonic acid as a catalyst in THF/toluene to generate trifluoroacetamide **21**. THF was used to dissolve diol **19** or **20** and dry toluene was used to remove water by azeotrope formation to drive the equilibrium toward cyclic acetal formation. The reaction was monitored by thin layer chromatography. Trifluoroacetamide **21** was obtained in 64% - 72% yield. The trifluoroacetamide **21** was removed to generate free amine for the following coupling reaction to form **22**. Cyclic acetal **22** was purified on basic alumina in 82% yield. Finally, the amine was coupled to biotin activated with CDI to produce the final product **23a**, **23b or 23c** in 50% - 70% yield after gravity column chromatography (neutral alumina).

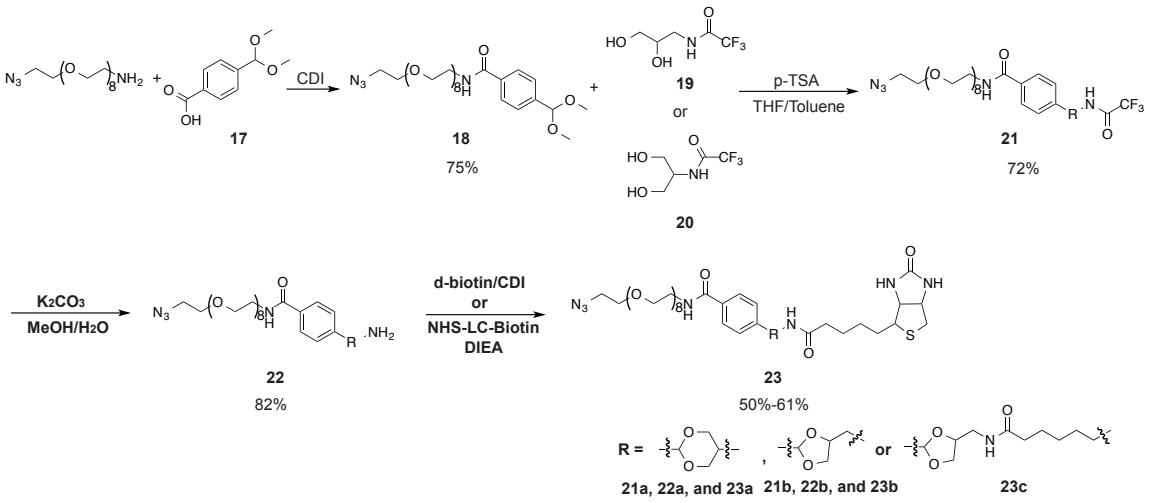

Scheme 2-7. Synthesis of cyclic acetal biotin probes.

2-2. Preparation of biotinylated BSA and evaluation of the cleavable acetal probes.

To examine the efficiency of capture with the acetal biotin probes, BSA was used as a model protein. BSA has one cysteine on the surface and an alkyne was installed on the thiol through N-alkynylmaleimide coupling. To facilitate complete coupling, 100 eq of N-alkynylamleimide was used. After 12 hours, the remaining N-alkynylmaleimide was removed by precipitation of BSA using cold acetone. The alkyne-functionalized BSA was subjected to azide-alkyne cycloaddition with each of the biotin probes (Scheme 2-8). After 1 hour, excess click reagents were removed using a microconcentrator with a molecular weight cut off of 3 kDa.

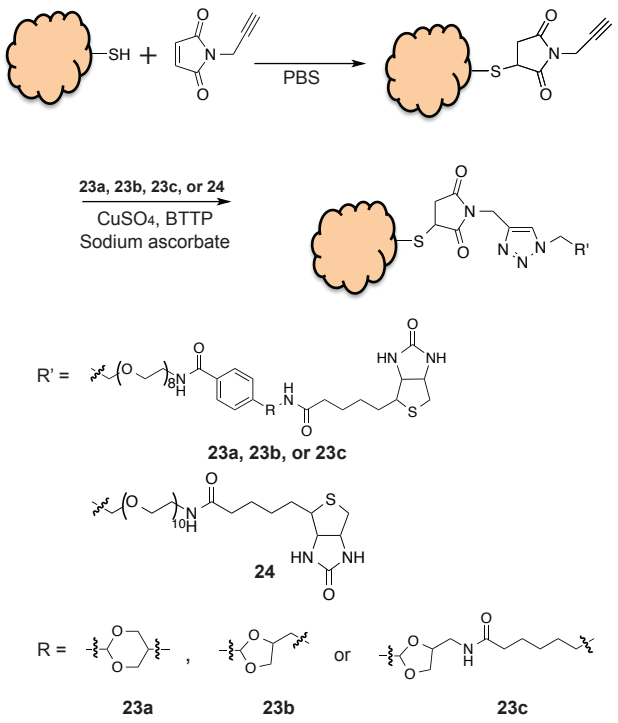

Scheme 2-8. Preparation of BSA or RNase A labeled with each biotin probe.

In order to find effective cleavage conditions, each of the biotinylated BSA conjugates was incubated in 1% TFA at 37 °C with gentle agitation and aliquots were removed at 30 minutes, 1 hour, and 2 hours. The quantity of biotin remaining on the BSA was detected by streptavidin blot. The acetal BSA-**23b** was

successfully cleaved in 30 minutes. On the other hand, non-acetal BSA-**24** and acetal BSA-**23a** were stable to the cleavage conditions (Figure 2-8A).

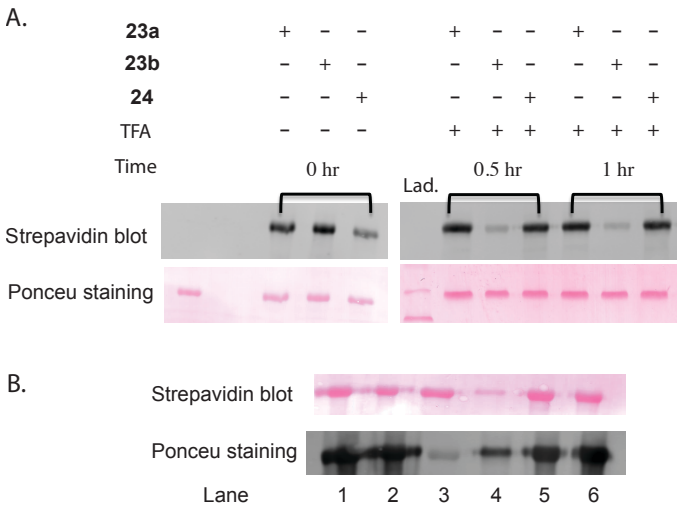

Figure 2-8. Evaluation of biotin probes **23a** and **23b** cleavage and comparison to non-cleavable biotin probe **24**. (A) BSA conjugated to each probe, **23a**, **23b**, or **24**, was incubated in 1% TFA at 37 °C in the absence streptavidin resin for the indicated time. (B) Test of BSA-**23b** linker cleavage. Lane 1, BSA-**23b** captured on streptavidin-ultralink beads; Lane 2, BSA-**24** captured on streptavidin-ultralink beads; lane 3, supernatant from BSA-**23b** incubated in 1% TFA at 37 °C for 1 hour; lane 4, supernatant from BSA-**24** incubated in 1% TFA at 37 °C for 1 hour; lane 5, streptavidin-ultralink beads with captured BSA-**23b** after TFA incubation; lane 6, streptavidin-ultralink beads with captured BSA-**24** after TFA incubation.

Acetal BSA-**23b** was further tested to evaluate the efficiency of cleavage when bound to streptavidin beads. BSA-**24** was used as a negative control to confirm that the elution of the streptavidin protein is not responsible for cleavage. The BSA conjugated to probe **23b** or **24** was captured on streptavidin agarose beads for 1 hour at room temperature, and the beads were washed sequentially with 1% SDS in PBS, 6M urea in 250 mM ammonium bicarbonate, 1 M NaCl in PBS to remove as much non-specifically bound protein as possible, and finally, washed two times with water. The loaded beads were incubated in 1% TFA at 37 °C with gentle agitation. After 1 hour, the supernatant was collected, the resin was washed with 0.1% SDS in PBS and PBS, and all eluate and wash fractions were combined. After washing, the beads were boiled to release BSA that was not eluted during the cleavage procedure. As shown in Figure 2-8B, BSA-**23b** was successfully released from the streptavidin resin under the cleavage conditions.

However, the cleavage of BSA-**23b** did not go to completion. In addition, a small amount of BSA-**24** was released under the cleavage conditions, although the probe linker remained intact as evidenced by the biotin signal in the streptavidin blot.

We repeated the capture/cleavage procedures with streptavidin-ultralink resin to compare cleavage of BSA-**23c** to BSA-**23b**. However, the cleavage efficiencies of BSA-**23b** and BSA-**23c** were similar (data not shown). We tried a capture medium, streptavidin-agarose beads to test whether different pore size affects the cleavage efficiency. As shown in Figure 2-9A, the probe with the extended linker, **23c**, was released more efficiently from the streptavidin-agarose bead complex than probe **23b** which has a shorter linker.

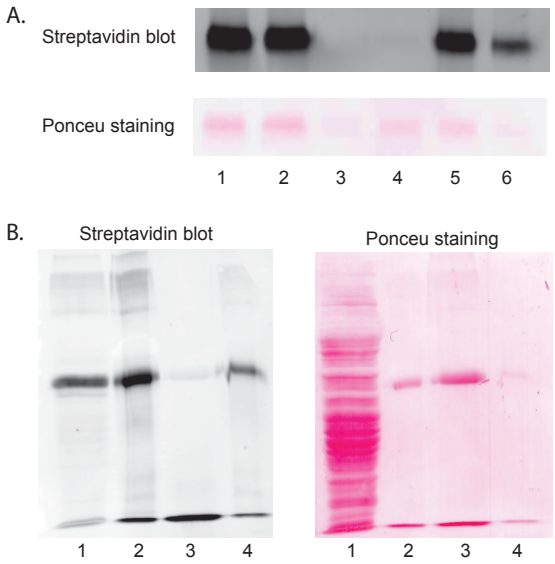

Figure 2-9. Comparison of BSA-**23b** and BSA-**23c** linker cleavage (A). Lane 1, BSA-**23b** captured on streptavidin-agarose beads; Lane 2, BSA-**23c** captured on streptavidin-agarose beads; lane 3, supernatant from BSA-**23b** incubated in 1% TFA at 37 °C for 1 hour; lane 4, supernatant from BSA-**23c** incubated in 1% TFA at 37 °C for 1 hour; lane 5, streptavidin-agarose beads with captured BSA-**23b** after TFA incubation; lane 6, streptavidin-agarose beads with captured BSA-**23c** after TFA incubation. (B) Capture and cleavage of BSA-**23c** in the presence of bacterial whole cell lysates; lane 1, cell lysate + BSA-**23c**; lane 2, BSA-**23c** captured on streptavidin-agarose beads from cell lysate; lane 3, supernatant from BSA-**23c** incubated in 1% TFA at 37 °C for 1 hour; lane 4, streptavidin-agarose beads with captured BSA-**23c** after TFA incubation.

2-3. Cleavage and capture in cell lysates.

Since the linker should be stable to physiological conditions and allow efficient capture from a complex mixture, the cleavage test was performed in the presence of bacterial cell lysates. Whole bacterial cell lysates (1 mg) mixed with BSA-**23c** (100 μg) was incubated with streptavidin beads. After washing as described above, the loaded beads were treated with 1% TFA at 37 °C with gentle agitation. After 1 hour, the supernatant was collected, the resin washed and protein eluted as described above for BSA-**23b**. The cyclic acetal linker **23c** remained intact in the cell lysate, and allowed successful capture of the BSA conjugate on the bead matrix. Subsequent release with mild acid treatment efficiently yielded the cleaved BSA with little protein remaining on the bead (Figure 2-9B).

To further establish the optimal cleavage conditions, we tested capture of another protein, RNase A that has a low molecular weight, 13.7 kDa. RNase A has two free cysteines that were used to conjugate an alkyne handle via maleimide chemistry as described above for BSA. The alkyne was further conjugated with cleavable biotin probe **23c** through azide-alkyne cycloaddition in the presence of Cu(I). RNase A-**23c** was captured from bacterial whole cell lysates and released as desired (Figure 2-10A). However, the eluted protein was contaminated with streptavidin monomer that was released from the bead matrix during the cleavage step (Figure 2-10A).

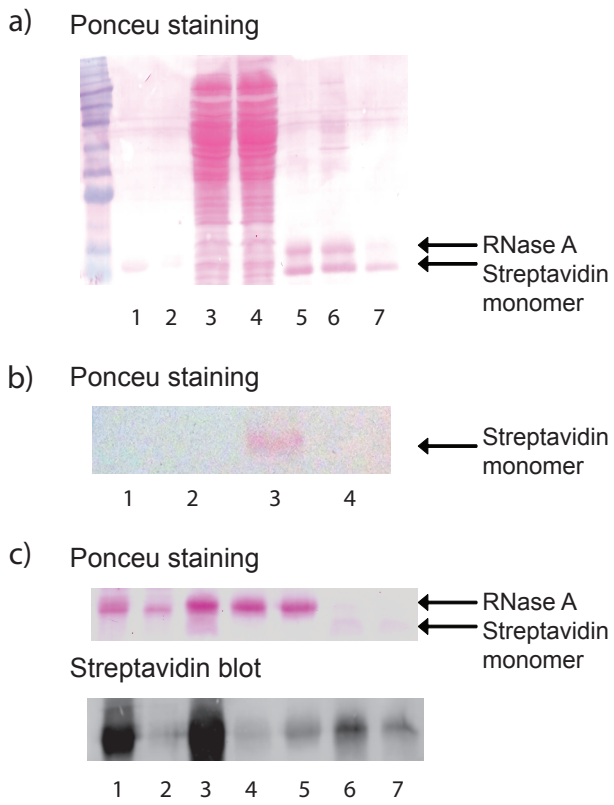

Figure 2-10. RNase A-**23c** capture and elution. (A) Capture of RNase A-**23c** in the presence of bacterial whole cell lysate and release; lane 1, RNase A-maleimide alkyne; lane 2, RNase A-**23c**; lane 3, cell lysate + RNase A-**23c**; lane 4, supernatant after RNase A-**23c** streptavidin capture; lane 5, RNase A-**23c** captured on streptavidin-agarose beads from cell lysate; lane 6, supernatant from RNase A-**23c** incubated in 1% TFA at 37 °C for 1 hour; lane 7, streptavidin-agarose beads with captured RNase A-**23c** after TFA incubation. (B) Test of streptavidin monomer release under cleavage conditions used for other cleavable linkers. Supernatant after treating streptavidin beads: lane 1, $Na_2S_2O_4$ for 1 hour at 25 °C; lane 2, 2% 2-mercaptoethanol for 1 h at 25 °C; lane 3, 5% formic acid for 2 hours at 25 °C; lane 4, 1M guanidine hydrochloride in 1% TFA at 37°C for 1 hour. (C) Effect of guanidine concentration on streptavidin monomer release from the beads. Lane 1, cell lysate + RNase A-**23c**; lane 2, supernatant after RNase A-**23c** streptavidin capture; lane 3, RNase A-**23c** captured on streptavidin-agarose beads from cell lysate; lane 4, supernatant from RNase A-**23c** incubated in 1M guanidine/1% TFA at 37 °C for 1 hour; lane 5, supernatant from RNase A-**23c** incubated in 3M guanidine/1% TFA at 37 °C for 1 hour; lane 6, streptavidin-agarose beads with captured RNase A-**23c** after 1M guanidine/TFA incubation; lane 7, streptavidin-agarose beads with captured RNase A-**23c** after 3M guanidine/TFA incubation.

2-4. Suppression of streptavidin monomer release.

When the amount of a targeted protein to be eluted is low, co-elution of the streptavidin monomer should be minimized in order to avoid signal suppression and elevated noise in the subsequent mass spectral analysis. We observed during the course of our investigations to improve cleavage efficiency that 1M guanidinium hydrochloride improved the efficiency of cleaved protein release and suppressed the release of streptavidin. Therefore, we analyzed the use of guanidinium hydrochloride during cleavage and compared its use to cleavage conditions for other cleavable biotin probes in order to determine whether the problem of streptavidin monomer release is widespread.

Streptavidin agarose beads were incubated separately under the following cleavage conditions: 5% $Na_2S_2O_4$ for 1 hour at 25°C, 2% of 2-mercaptoethanol for 1 hour at 25 °C, 5% formic acid for 2 hours at 25 °C, and 1M guanidinium hydrochloride in 1% TFA at 37 °C for 1 hour. As shown in Figure 4B, formic acid treatment also resulted in the release of streptavidin from agarose beads, whereas, reducing conditions did not. Gratifyingly, inclusion of 1 M guanidinium hydrocholoride in the 1% TFA cleavage mixture suppressed non-specific release of the streptavidin monomer (Figure 2-10A, lane 6 vs Figure 2-10B, lane 4).

Next we tested the effect of guanidine concentration on release and elution. Two different concentrations, 1 M or 3 M guanidinium hydrochloride, in combination with 1% TFA were tested. In both samples, suppression of streptavidin monomer release was observed. However, 3 M guanidinium hydrocholoride also releases some RNase A with the biotin probe still attached, indicating that the RNase A release is due to protein denaturation rather than

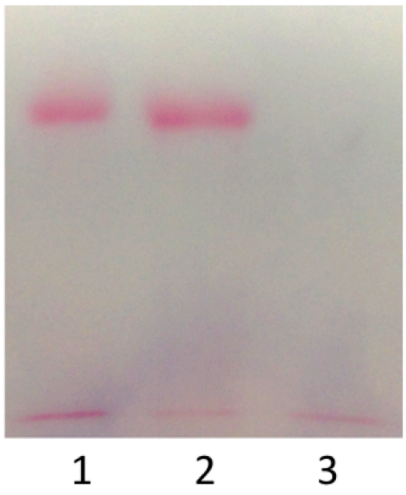

Figure 2-11. Cleavage of BSA-**23c** in the presence of 1M guanidine. Lane 1, BSA-**23c** captured on streptavidin-agarose beads; lane 2, supernatant from BSA-**7c** incubated in 1M guanidine/1% TFA at 37 °C for 1 hour; lane 3, streptavidin-agarose beads with captured BSA-**7c** after 1M guanidinium hydrochloride/1% TFA incubation.

acetal cleavage (Figure 2-10C). We tested cleavage efficiency with BSA since other proteins can be sensitive to 1M guanidinium hydrochloride. 1M guanidinium hydrochloride did not affect the release of BSA from the streptavidin resin (Figure 2-11). Therefore, 1 M guanidinium hydrochloride in 1% TFA is the preferred elution solvent for acetal linker release.

2-5. Further labeling of the aldehyde tag on protein after cleavage.

Aldehyde tags can be used to modify cell surface proteins specifically since the aldehyde functionality is not typically present in proteins.[141] Aldehydes readily react with a variety of aminooxy or hydrazide-functionalized molecules.[142, 143] Cleavage of the cyclic acetal linker **23** generates an aldehyde functionality on the tagged protein after purification.

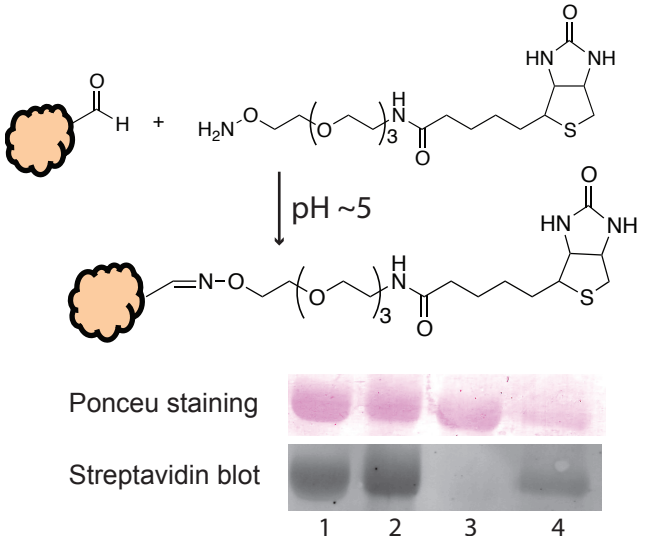

Figure 2-12. Further modification of the BSA aldehyde tag. Lane 1, BSA-**23c**; lane 2, BSA-**23c** captured on streptavidin-agarose beads; lane 3, supernatant from BSA-**23c** incubated in 1% TFA at 37 °C for 1 hour; lane 4, BSA-aldehyde after reaction with alkoxyamine-PEG-biotin at pH 5, 37 °C for 4 hours.

Therefore, we tested if the aldehyde is available for further modification of the protein. The cleaved BSA-**23c** was incubated with alkoxyamine-PEG-biotin for 4 hours, and the reaction mixture was directly analyzed by SDS-PAGE and streptavidin blot. After cleavage of the BSA-**23c** acetal, no BSA biotin signal remained (Figure 2-12, Lane 3). Upon reaction of the cleaved BSA with alkoxyamine-PEG-biotin, the biotin signal was restored (Figure 2-12, Lane 4).

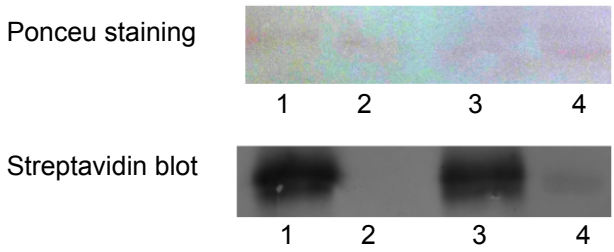

Figure 2-13. Further modification of the RNase aldehyde tag. Lane 1, RNase A-**23c** captured on streptavidin-agarose beads; lane 2, supernatant from RNase A-**23c** incubated in 1% TFA at 37 °C for 1 hour; lane 3, RNase A aldehyde after reaction with alkoxyamine-PEG-biotin at pH 5, 37 °C for 4 hours; lane 4, native RNase A subjected to the same alkoxyamine-PEG-biotin labeling reaction.

Likewise, RNase A-**23c** underwent the analogous reaction sequence (Figure 2-13). Therefore, the aldehyde funtionality generated through cleavage can be successfully conjugated with nucleophilic labeling reagents.

Chapter 3. Discussion

1. Synthesis of photoaffiniy-based ROMP polymers
    1.1. Synthesis of monomers for polymerization
    1.2. Synthesis of polymer
    1.3. Photoaffinity cross-linking efficiency test using coumarin azide
    1.4. Analysis of photoaffinity based labeled receptors by polymer **9a** or **9b** peptide mass fingerprinting (PMF)
    1.5. Enhancement of affinity of a polymer to its receptors by increasing the number of the ligands
2. Cyclic acetals as cleavable linkers for biotin probe
3. Summary

1. Synthesis of photoaffinity-based ROMP polymers

1-1. Synthesis of monomers for polymerization

RGD is a specific sequence present in some ECM proteins such as laminin,[144] fibronectin,[145] and vitronectin.[146] $\alpha_v\beta_3$ integrin is known to bind to vitronectin through an RGD peptide. Even though the RGD sequence is essential for the interaction with $\alpha_v\beta_3$ integrin, the binding affinity of this tripeptide to its receptor is low. However, addition of Ser at the N-terminus significantly enhanced the binding affinity to $\alpha_v\beta_3$ integrin.[49]

In designing a ligand monomer for identifying receptors that RGDS peptide binds to, Bpa (4-benzoyl phenylalanine) and β-Ala were introduced. Bpa is widely used for making a stable covalent bond between ligand and receptor. Under UV irradiation, it allows us to use the rigorous analytical tools such as electrophoresis and MS,[147] in examining the structure of protein receptor-ligand complexes. β-Ala is a spacer to give sufficient space between polymer backbone and the ligand. Gly is also added between the Bpa and the RGDS sequence to prevent interruption of the interaction between RGDS and the binding pocket on $\alpha_v\beta_3$ integrin. In order to establish that photocrosslinking specifically occurs after ligand-receptor interaction, the monomer containing ESA instead of RGDS was prepared. For ROMP, norbornene-*exo*-carboxylic acid was used. Due to the bridge and the double bond in the molecule, the cyclohexene ring is highly strained. During polymerization, relief of the high ring strain induces a significant reaction activity.

1-2. Synthesis of polymer

Tri-block copolymers **7a** and **7b** were prepared using fully protected peptides **4**, **5**, **6**, and NB-NHS. The polymerization was performed in the presence of 3 M LiCl to solubilize the growing chain of the polymer. NB-NHS and NB-ESA were randomly distributed between the ligands placed on the end side of the polymer. In order to measure molecular weights and polydiseprsity index (PDI), gel permeation chromatography (GPC) was performed using polystyrene as a standard. The molecular weights of the polymers **7a** were 60650 (Mn) and 65402 (Mw), and the PDI was 1.07. Active ester, NB-NHS in the polymer, was substituted with propargyl amine for click reaction. Random copolymers **8a** and **8b** were also prepared under the same reaction condition used for tri-block copolymer synthesis. The molecular weights of polymer **8a** were 42563 (Mn) and 53426 (Mw), and the PDI was 1.25. For polymer **8b**, molecular weights, 48281 (Mn) and 56002 (Mw) were observed, and the PDI was 1.16.

1-3. Photoaffinity cross-linking efficiency test using coumarin azide

Copper catalyzed 1,3-dipolar cycloaddition, widely known as a click reaction, has been a valuable tool for orthogonal coupling of small molecule to target proteins. Maintaining Cu(I) oxidation state is critical to obtain high yield of click reaction by using proper ligand in specific reaction condition. Among the ligands, THPTA has been investigated by Vu Hong et al.[148] and it showed tremendously reduced reaction time and reduced reactive oxygen species that are generated during the reaction.

Coumarin azide is a small molecule that is fluorescent once it forms triazole. Therefore, we used coumarin azide to test the click reaction on polymer **8a**, to monitor the reaction rate, and to

confirm the presence of alkyne on the polymer. The reaction rate was fast as expected. The maximum yield was reached in less than 20 min.

Benzophenone-based photoaffinity labeling of biomolecules has been widely used to profile the interaction partners of a specific ligand. Benzophenone forms a diradical under the long wave ultraviolet (UV) light (360 nm). One radical on oxygen abstracts a hydrogen from adjacent protein to from a hydroxyl group, generating a new radical on the protein. The other radical on the benzophenone reacts with the newly generated radical on the protein to form a carbon-carbon covalent bond. Photoaffinity labeling through benzophenone is highly specific and efficient, and the reactivity towards water is low. Therefore, Bpa was positioned at the N-terminus of ligand peptide GRGDS or ESA to crosslink a receptor the ligand binds to.

Although photoaffinity labeling takes place after ligand-receptor binding, there could be unwanted crosslinking through Bpa itself. We reasoned that the elongated UV irradiation time might increase the chance of photocross linking to random proteins. In order to find the irradiation time that balances maximum crosslinking to the target receptors by **7a** and minimum crosslinking to the random protein by **7b**, U87-MG cells were labeled with each polymer. The cells were removed from UV irradiation at each time point. The labeled cells were washed to remove the unreacted polymer, and the cells were lysed. To visualize the amount of the polymer crosslinked on the receptors, click reaction was performed using coumarin azide as a fluorophore. Since coumarin azide fluoresces upon triazole formation, further purification of the polymer-receptor complexes was not necessary. The fluorescence was read directly from the click reaction mixture. There was no significant difference between the samples treated with **9a** or **9b**. Also, the visualization of clicked sample was performed through SDS-PAGE. However, the

fluorescence was observed on the top of the gel, and smear bands through the lanes were detected.

Visualization of the photo-cross linked proteins with the polymer by coumarin azide failed. The detection limit of coumarine azide by fluorometer was between 20 pM and 20 nM. Maybe, the amount of the labeled receptors with the polymer was lower than the detection limit. A polymer has 4 units of ligand containing Bpa. Hence, if the photocrosslinking was reacted completely, one polymer could cross-linked with 4 receptors at maximum. Therefore, the size of the polymer-receptor might be too big to be separated by SDS-PAGE gel. In addition, since the molecular weight of the polymer is not uniform, it cannot be shown as a single band in the gel.

1-4. Analysis of photoaffinity labeled receptors by polymer **9a** or **9b** and peptide mass fingerprinting (PMF).

PMF has emerged as a valuable tool to identify proteins. PMF compares the experimentally obtained peptide masses that are generated by enzymatic digestion from an unknown protein to a database containing known sequences of protein or genome. The comparison is achieved by computer programs such as MASCOT. The programs provide parameters that can be adjusted according to the conditions used to generate the peptide masses experimentally. The parameters include taxonomy, enzyme used for peptide generation, number of missed cut allowed for cutting the protein, peptide tolerance, and various chemical modifications on peptide at a specific amino acid. According to the selected parameters, the program suggests the candidate proteins that are the best match. The program considers that peptide masses are from one protein. Therefore, it is important to prepare samples as pure as possible.

Validation of the method for identification of receptors on the cell surface with photoaffinity based ROMP polymers was performed using $\alpha_v\beta_3$ integrin overexpressed on U87-MG cell surface. 10^7 cells were labeled with polymer **9a** or **9b** under the long wave UV light to form a covalent bond to the receptors. After cell lysis, the biotin probe was incorporated into the polymer in the cell lysate via click reaction. Then, the biotin-tagged polymer-receptor complexes were captured by neutravidin immobilized on agarose beads. Tryptic digestion was performed directly with the beads on which the polymer-receptor complexes captured. Masses of the peptides that are generated by the tryptic digestion were obtained by MALDI-TOF.

The search engine for peptide mass fingerprinting assumes the peptide masses are produced from one protein. In the case of MASCOT, the maximum number of proteins that the program can distinguish from a sample is six. When the sample contains many peptide masses from contaminants, which are not matched with target protein, it affects the result of the search by lowering the score of the candidate proteins. Therefore, we prepared three samples to subtract the peptide masses from contaminants. Control sample without polymer treatment, the sample treated with **9a** (RGD sample,) and the sample treated with **9b** (ESA sample) were prepared. In this way, we subtracted the overlapped peaks common to the samples that were presumed to be generated by extra proteins.

In most of the cases, integrin α_v was not identified as a candidate protein. It might be because we lose the α_v during washing step if the covalent crosslinking is on the β subunit since α and β subunits are non-covalently interacting together. In various studies, the major binding site identified was β_3 subunit.[149-153] Photocrosslinking study using echistatin, which is a disintegrin from snake venoms and inhibitor of $\alpha_v\beta_3$ integrin showed that Bpa placed two peptides away

from the RGD crosslinked both α and β subunits, and Bpa positioned right next to RGD labeled β subunit (Table 3-1).[153] In our case, Bpa in the monomer **4** is positioned one peptide away from the RGD. Therefore, we assume that the monomer **4** might crosslink mainly β subunit. Even though we see integrins as a hit in the search, their score is low and they are not considered to be significant. In this case, the number of the peaks generated by the program with defined parameters was around 700 after subtraction of control peaks and only about 30 peptides are assigned to be the peptides from the integrin. The large number of non-matched peptides significantly reduced the score below the meaningful level. When the target protein is unknown, it is critical to have a significant score to be sure the match is reliable.

RGD-containing ligand	**Cross-linking site in $\alpha_v\beta_3$**
^{125}I-BH-Ahx-Cys-Lys(N$^{\varepsilon}$-Bpa)-Dmt-Arg-Gly-Asp-Cys-NH$_2$	α_v, β_3
^{125}I-[Arg^{35}, Lys^{45}(N$^{\varepsilon}$-Bpa)]echistatin	β_3[209-220]
[Bpa^{21}, Leu^{28}]echistatin	α_v, β_3
[Bpa^{23}, Leu^{28}]echistatin	β_3
[Bpa^{28}]echistatin	β_3[109-118]

Table 3-1. Cross-linking sites in $\alpha_v\beta_3$ integrin[149, 153]

Most of the impurities come from the non-specific binding to neutravidin agarose or the monomer of neuravidin. Therefore, it is critical to remove the impurities after incubation of the clicked cell lysate with neuravidin to increase the score. Also, the affinity of ligand binding in the polymer to its receptor through bivalent manner might not be high enough to pull out the sufficient amount of target receptors to be analyzed.

There are two ways to improve the detection of the target proteins: 1) increase of the number of ligands on a polymer, 2) use a biotin probe that can be cleaved after capturing receptor-protein complexes. The increased number of ligands can enhance the affinity of the ligand binding to its receptor, and also, the number of the receptors linked to the polymer will be increased. To avoid the generation of peptide masses from non-specific proteins on neutravidin-agarose matrix, a cleavable biotin probe can be employed. Since only the proteins linked with polymer will be released from the bead, the amount of contaminants can be minimized.

1-5. Norborbene does not affect $\alpha_v\beta_3$ binding to its receptors

Before mass analysis, a cell adhesion assay was performed to determine whether the monomer binds to the receptor and can block binding to the native ligand. Bpa forms a stable covalent bond between the ligand and receptor. Therefore, even though the cells were washed after UV irradiation, we expected that the monomer was still bound to the receptors on the cell surface, and therefore, sample 3 would show better inhibition than sample 2. Interestingly, the cells in sample 3 were attached to the vitronectin more than the cells in sample 2. We need to confirm that whether this phenomenon was caused by the technical method used or covalent crosslinking of the polymer to the integrin triggers other biological activity. During the process of UV irradiation, the internalization might happen, and the covalent attachment of monomer to the integrins could affect the integrin recycling or resynthesis rates.[154, 155]

2. Cyclic acetals as cleavable linkers for biotin probe

Affinity purification is commonly used to isolate target proteins. Streptavidin agarose beads are widely used for affinity purification of biotinylated proteins due to their strong binding affinity. However, existing methods to release biotinylated proteins from streptavidin bead matrices are harsh and often result in co-elution of high levels of contaminating proteins. For mass analysis of unknown proteins, it is important to minimize such contamination in a purified protein sample. Cleavable biotin probe has been employed to avoid co-elution of the contaminants. We chose cyclic acetals as a cleavable linker since a cyclic acetal is cleavable under mild acidic conditions.

BSA has one cysteine on the surface and an alkyne was installed on the thiol through N-alkynylmaleimide coupling. Click reaction was performed to incorporate cleavable biotin probes. BSA-**23b** was successfully released under mildly acidic conditions. However, the cleavage of BSA-**23b** did not go to completion. We reasoned that inefficient cleavage of **23b** was due to limited solvent access to the acetal because the short linker between acetal and biotin places the acetal in close proximity to the biotin binding pocket on the streptavidin. We investigated addition of various additives, e.g. SDS and guanidinium hydrochloride, to increase cleavage efficiency with limited success. Therefore, an extended linker with an additional seven atoms was introduced between the acetal and biotin by coupling NHS-LC-biotin with compound **22** (Scheme 1) to provide probe **23c**. Because the pore size of the bead can also affect solvent access to acetal and dissociation of the product aldehyde, we tried a different capture medium, streptavidin-agarose beads. The probe with the extended linker, **23c**, was released more efficiently from the streptavidin-agarose bead complex than probe **23b** which has a shorter linker. This result suggests that the combination of the extended linker and larger pore size are required

to favor cleavage and dissociation of the acetal moiety. Moreover, addition of guanidinium hydrochloride to the cleavage mixture suppresses release of monomeric streptavidin from the capture matrix under the acidic cleavage conditions. Lastly, cleavage of the cyclic acetal provides an aldehyde functionality on the captured protein, which conveniently can undergo further reaction to provide specific labeling of the captured protein. For example, a fluorophore or mass tag containing an aminooxy or a hydrazide functional group can be conjugated to the captured protein after cleavage.

3. Summary

ADAM proteins are known to interact with integrins. Especially, ADAM2 is known to interact with $\alpha_6\beta_1$ integrin. Moreover, it was confirmed that ADAM2 predominantly interacts with $\alpha_6\beta_1$ integrin by inhibition assay with ADAM2 mimic polymer. However, it is reported that none of the integrin on mouse oocyte is necessary for sperm-egg binding and fusion. We suggested that there might be another receptor or the ADAM2-integrin interaction might trigger protein complex formation with other protein on oocyte surface.

To develop a tool for identification of receptors on cell surface using photoaffinity-based ROMP polymer, we designed a polymer containing photoaffinity cross-linkable peptide. We used a model system to optimize each step including click reaction, photoafiinity crosslinking, and protein-polymer complex capture by biotin-streptavidin method. Photoaffinity cross-linkable peptide is composed of β-Ala, Bpa, and GRGDS. GRGDS is known as a binding partner of $\alpha_v\beta_3$ integrin, which is overexpressed on the surface of U87-MG cell.

The presence of alkyne on the polymer was tested using coumarin azide since the alkyne cannot be confirmed quantitatively by usual analytical methods such as NMR and IR. The chemical shifts of alkynes were overlapped with other chemical shifts from the monomers. In case of IR, the intensity of the peak was not strong enough to confirm that the peaks are from the alkyne. The click reaction was successful usuing the THPTA ligand for stabilizing Cu^{+}. We tried to test photoaffinity crosslinking efficiency by using coumarin azide based fluorescence. However, visualization of the degree of crosslinking by Bpa was failed. We proceeded to identification of the $\alpha_v\beta_3$ integrin by MALDI-TOF and peptide mass fingerprinting. Even though we detected β_3 and β_5 integrin, the signal to noise was not sufficient to definitively identify the receptors. The major obstacle of this method was contamination of the sample, which increases noise. In order to prepare a protein sample as clean as possible, we developed a cleavable biotin linker that has cyclic acetal moiety between biotin and azide. The acetal was efficiently cleaved in mild acidic condition, and guanidinium hydrochloride in the cleavage solution reduced the release of streptavidin monomer from the streptavidin-bead matrix. Therefore, we expect that the sample prepared using the cleavable biotin probe **7c** will provide the purer protein sample suitable for mass analysis. The application of cleavable biotin probe is not limited to protein purification. Once removed from the support, the target protein can be further characterized to determine its molecular or physical properties or tagged with an imaging label, e.g., fluorescent molecule or radioactive moiety.

As another approach to enhance the detection of targeted protein, we increased the number of ligand, GRGDS. According to cell attachment assay, the polymer **10a** inhibited the binding between $\alpha_v\beta_3$ integrin and its natural substrate, vitronectin. In order to confirm that the reduced number of cell attached to vitronectin is caused by inhibiting $\alpha_v\beta_3$ integrin with RGDS peptide

not by non-speicific interaction between random peptide and the integrin, the cell attachment assay with polymer **10b** has to be performed.

The amount of internalization of integrin-polymer complex can be measured with various concentrations of polymers by using cells that are biotinylated on their surface. After incubation with the polymers, the lysate can be separated into membrane and cytoplasmic fractions, and the amount of the biotin in cytoplasmic fraction can be measured by fluorescence tagged streptavidin. This experiment will provide the information if the internalization of the integrin-polymer complex affect the cell attachment assay results or change the amount of the integrin that will be pulled out by the polymer.

After optimizing the experimental conditions, polymer-2 will be tested to optimize the number of Bpa that will be present on the polymer randomly to detect protein complex on cell surface. For this purpose, HT1080 cell will be used since the formation of $\alpha_v\beta_3$ integrin/MMP2 heterodimer is activated by the treatment of phenazine methosulfate.

Chapter 4.

Selective anticancer agent targeting histone deacetylase and tumor-associated protease

1. Introduction

1.1. Chromatin remodeling

1.2. Histone deacetyl transferases (HDACs) in cancer

1.3. HDAC inhibitors

1.4. Cathepsin L in cancer

2. Results

3. Discussion

4. References

1. Introduction

Mutations that result in constitutive activation of oncogenes or the loss of the function of tumor-suppressor genes are essential tumorigenic processes. Abnormal gene expressions, usually downstream of oncogenes or tumor-suppressor genes, are also involved in tumor initiation and progression.[156, 157] In addition, epigenetic changes or mutations within gene promoter/enhancer regions can enhance aberrant expression of genes that control cellular differentiation, affect the cell cycle and initiate apoptosis. Moreover, tumor immune escape and angiogenesis, which are important for cancer progression, come from the abnormal expression of genes related to the initiation of the immune response and neovasculature induction.[158]

1.1. Chromatin remodeling

Epigenetic changes are mitotically and meiotically heritable changes in gene expression that are not caused by the primary DNA sequence changes. These changes involve alterations in CpG island methylation patterns, histone modifications, and dysregulation of DNA binding proteins.[159] Gene expressions regulated by epigenetic changes are considered crucial processes for the onset and progression of cancer.[160]

Chromatin remodeling plays a key role in epigenetic regulation of genes. Such remodeling is caused by the structural modification of nucleosomes. These modifications occur at the amino-terminal tails of histones and include acetylation, methylation, phosphorylation, poly-ADP ribosylation, ubiquitinylation, sumoylation, carboylation, and glycosylation.[161] Aberrant modifications of histone tails are closely related to carcinogenesis.[162]

1.2. Histone deacetyl transferases (HDACs) in cancer

The structure of chromatin is important in regulation of a gene expression. Its structural change allows DNA-binding transcription factors to access the naked target gene. The structural change in chromatin depends on the modifications of histones in nucleosomes.

Nucleosomes, which are the basic repeating unit of chromatin, consist of DNA wrapped around a histone octamer: an H3-H4 tetramer and two H2A-H2B dimers.[163] The linker histone H1 binds to the linker DNA segments and neutralizes it through positively charged carboxy-terminal domain for stabilization of the linker DNA. Histones are highly charged at NH_2-terminus, called histone "tail". The histone tails of H2 and H4 that protrude from the nucleosomes can be covalently modified at several locations. The modifications include acetylation, phosphorylation, and methylation.[164] Different modifications at different sites of histone tails can recruit proteins to alter chromatin structure and promote translation of particular genes.[164] Of such modifications, histone acetylation has been most extensively studied.

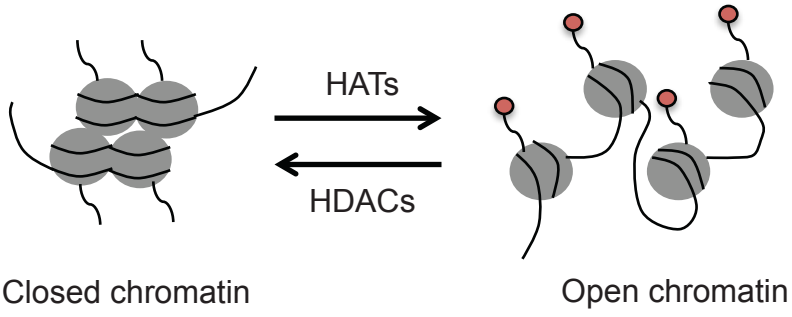

Figure 4-1. Chromatin structure and its conformational change

Acetylation by histone acetyltransferases (HATs) and deacetylation by histone deacetylases (HDACs) of the ε-NH_2 group on lysine in histone tails change the chromatin structure from an opened to closed conformation (Fig 4-1). Acetylation neutralizes positive charges on lysines within histone tails and decreases their affinity for DNA. As the affinity is lost, chromatin expands locally. Then, transcription factors can access the DNA and trigger gene expressions. HDACs remove those acetyl groups on lysines, increasing the positive charges of histone tail. This stimulates high-binding affinity between the histones and DNA backbone, preventing gene transcriptions.

HDACs are grouped into four classes according to their homology with yeast proteins: class I (HDAC1,2,3, and 8), class II (class IIa: HDAC4, 5, 6, 7, and 9, class IIb: HDAC6 and 10), class III (SIRT1, 2, 3, 4, 5, 6, and 7), and class IV (HDAC11).[165] Class I HDACs are ubiquitously expressed in all tissues. HDAC1 and HDAC2 participate in many cellular processes such as proliferation, cell cycle and apoptosis.[166] HDAC3 is involved in cell cycle processes and DNA damage response,[167] and HDAC8 is expressed in cells showing smooth muscle differentiation.[168] Different from class I HDACs, class II HDACs are expressed in a tissue-specific manner. They function as a transcriptional repressor in skeletal, cardiac, and smooth muscle, bone, immune and vascular systems, as well as in the brain.[169] Class III HDACs are widely expressed and have a broad range of biological functions including the regulation of oxidative stress, DNA repair, regulation of metabolism, and aging.[170, 171] The only member of class IV HDAC, HDAC11, has been less studied than other classes of HDAC. It has been reported that it is linked with oligodendrocyte development and the immune response.[172, 173]

One informative example showing the link between the altered level of HDACs and cancer is acute promyelocytic leukemia (APL). The retinoic acid (RA) receptor (RAR) is an important transcriptional factor for myeloid differentiation. In the absence of RA, RAR and its partner, retinoid X receptor (RXR), bind to retinoic-acid response elements (RAREs), and this complex contributes to the repression of transcription. Addition of RA releases the HDAC complex from RAR-RXR complex, leading to the association of RAR with HATs to initiate transcription.[174, 175] In APL, chromosomal translocations generate abnormal fusion proteins containing RAR and one of the following proteins: promyelocytic leukemia (PML) in more than 95% of cases or promyelocytic leukemia zinc finger (PLZF).[174, 176] These abnormal fusion proteins retain the ability to bind to RAREs and recruit HDACs to specific loci where target genes are present. However, these complexes are not responsive to RA.[177] Moreover, the fusion proteins oligomerize by means of self-association domains present in PML and PLZF, resulting in an increased stoichiometric association of HDAC-containing complexes and enhanced transcriptional repression.[178, 179]

In addition to abnormal recruitment of HDACs to specific loci by the fusion proteins, altered expression level of individual HDACs have been reported. HDAC1 is overexpressed in prostate,[180] gastric,[181] colon,[182] and breast[183] cancer. Overexpression of HDAC2 is detected in colorectal[182, 184], cervical[185], and gastric[186] cancer. Increased expression level of HDAC3 and HDAC6 are observed in colon tumors[182] and breast specimens,[187] respectively. Knockdown of individual HDACs by small interfering RNA (siRNA) in certain tumor cell lines suppresses tumor cell growth and survival,[182, 184, 185, 188] supporting the idea that altered expression level of HDACs might play critical role in tumor onset and progression.[189]

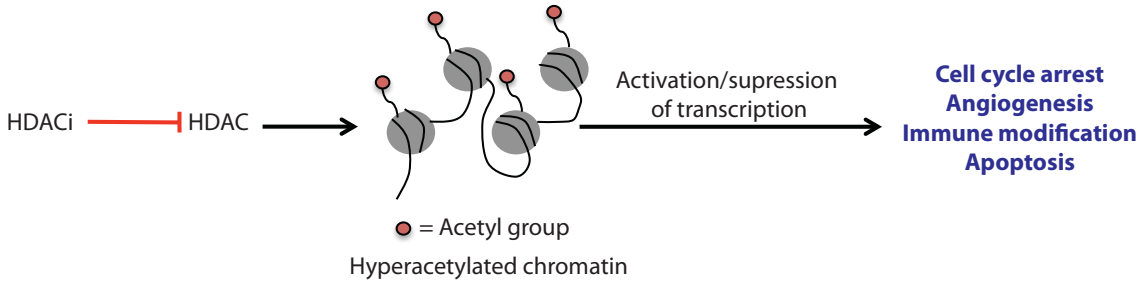

Figure 4-2. The effects of HDACi on tumor cells

1.3. HDAC inhibitors

A variety of structurally diverse HDAC inhibitors (HDACi) have been derived from both natural sources and synthetic routes. HDACi can be categorized based on their structures including hydroxamic acid derivatives, carboxylates, benzamides, electrophilic ketones and cyclic peptides.[190, 191] So far, most of HDACi work well against class 1, class 2 and class 4 HDACs. Only few have been reported to discriminate among HDACs such as depsipeptides that preferentially inhibit HDAC1/HDAC2[192] and MS-275 that is more active to HDAC1 than HDAC3.[193] At present, the lack of selectivity does not limit HDACi as an anticancer drug since there is no conclusive evidence that the individual HDAC has a defined role in cancer.[194]

HDACi have potential as anticancer drugs since they affect several cellular processes that are dysregulated in neoplastic cells. The key cellular processes that are induced by HDACi are induction of the differentiation programmes, inhibition of the cell cycle and apoptosis.[195, 196] Moreover, HDACi might play pivotal roles in activation of the host immune response[197-200] and inhibition of angiogenesis,[201] which results in tumor regression.

HDACi are capable of promoting cellular differentiation, which is closely associated with cell-cycle arrest at G1/S. Transcription of the cyclin-dependent kinase (CDK) inhibitor WAF1 (encoded by the CDKN1A) is induced by almost all HDACi.[202, 203] CDKN1A can inhibit cyclin E-CDK2 and cyclin A-CDK2, and the expressions of cyclin A and D are decreased by many HDACi, which results in hypophosphorylation of the retinoblastoma tumor-suppressor protein RB and inhibition of S-phase progression.[204, 205] Also, transcriptions of two genes encoding CPT synthase and thymidylate synthetase are also repressed by HDACi. The transcriptional repression of these two genes contributes to G1/S arrest.[206]

HDACi induce apoptosis of cancer cells via two functionally different pathways, the 'extrinsic' death receptor pathway and the 'intrinsic' mitochondrial pathway.[207] Although the initiation mechanism of apoptosis is different from two pathways, a number of the downstream components, for example the activation of caspase-3, is shared between the two pathways. Therefore, the biochemical and morphological characteristics such as phosphatidylserine exposure, effector caspase activation, and DNA fragmentation are similar.[208]

Overexpression of pro-survival Bcl-2 family proteins (Bcl-2 and Bcl-X_L) block HDACi-mediated apoptosis, indicating that HDACi play a role for intrinsic apoptotic pathways in regulating these components.[209, 210] How HDACi can initiate the intrinsic apoptotic cascade is not fully elucidated. There is evidence that HDACi may change the global gene transcription, leading to the altered balance of expression between pro-apoptotic and anti-apoptotic genes, and that newly established balance favors apoptotic process.[189] However, it is also possible that apoptosis activated by HDACi is associated with a specific protein or signaling pathway upstream of the mitochondria. Two proposed models for these specific processes are selective

activation or induction of BH3-only proteins[211] and regulation of ROS (reactive oxygen species) production/activity.[212]

HDACi can induce extrinsic death receptor pathways by triggering gene expressions of death receptors and their associated ligands and repress transcription of genes that are related to inhibition of death receptors, including FLIP, c-IAP2 and XIAP.[189, 213] Inhibition of the death receptors and/or their ligands via neutralizing antibodies and small interfering RNS (siRNA) allows the tumor cells to avoid HDACi-mediated apoptosis, which supports the idea that the death receptor pathway plays an important role in HDACi-mediated apoptosis. It is clear that HDACi can stimulate the extrinsic apoptotic pathway.[214, 215] However, whether the death receptors are necessary for the signaling pathways involved in HDACi-mediated apoptosis is controversial.

Until now, most of HDACi cannot selectively target HDAC isoforms, which causes diverse biological effects. The diverse biological effects result in adverse side effects during the treatment of the inhibitors.[216] Due to the reason, the cytotoxic profile has not been established, which makes the use of HDACi limited. For better understanding of how the inhibitor acts in cancer cells and which HDAC is involved in specific cancers, the isoform-selective inhibitors have to be developed.[217]

1.4. Cathepsin L in cancer

Proteases including matrix metalloproteases (MMPs) (the role of MMPs in cancer will be discussed in chapter 5), serine, cysteine, aspartic, and threonine proteases have gained attention as therapeutic targets due to their important roles at different stages in cancer. Among them, MMP proteases have been for many years a subject of major interest in the study of proteases

and cancer. However, cysteine cathepsin protease has recently emerged as an important enzyme for targeting cancers.

The lysosomal peptidase cathepsins have 11 members (cysteine cathepsin B, C, F, H, K, L, O, S, V, W, and X). They share a conserved active site comprised of cysteine, histidine and asparagine residues,[218] and they are active in the slightly acidic environment of lysosomes.[219] Most cathepsins degrade proteins in the lysosomes in the majority of cell types.[220] However, it has been recently discovered that cathepsins participate in other functions such as cardiac, brain, and skin development[221], as well as bone reabsorption[222]. In addition, it has been reported that the increased expression and/or activity of cathepsin K and S is involved in osteoporosis and rheumatoid arthritis.[223]

Increased expression, activation, and mislocation of several cathepsins have been observed in cancer progression of various human tumors.[224, 225] Among these cathepsins, the involvement of cathepsin B and L in malignant progression has been studied most intensively. Cathepsin B[226, 227] and L[228] have been shown to casually participate in migration and invasion of human osteosarcoma/globlastoma cells and human osteosarcoma cells, respectively. In particular, cathepsin L may play an important role in cancer cell migration and invasion. The increased extracellular activity of cathepsin L can reduce cell-cell interactions by cleaving E-cadherin and degrading the extracellular matrix (ECM),[229] which results in the release of growth factors at the metastatic site. In addition, the link between angiogenesis/apoptosis and cathepsin L has been investigated, but the results from the studies are controversial. The exact role of cathepsin L in these cellular processes remains to be elucidated.[230]

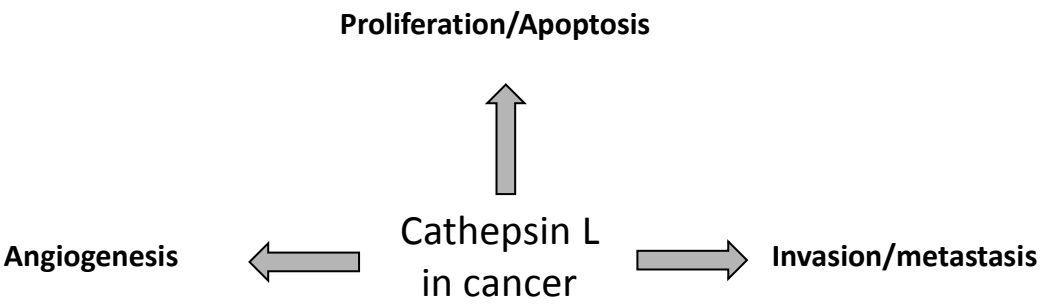

Figure 4-3. Schematic presentation of roles of cathepsin L in cancer

2. Specific aim

The reagents used in current chemotherapy often lack selectivity and target the molecules commonly existing in both tumor and normal cell, which causes adverse side effects. Therefore, it is urgent to develop an anticancer drug that specifically targets cancer cells, leaving healthy cells intact.

Based on the accumulated evidence indicating that the expression levels of HDACs and CTSL in certain tumors are increased, it was hypothesized by Dr. Ueki that the induced activities of both enzymes could be used as a selective modality to deliver anticancer drugs instead of directly inhibiting HDACs or CTSL, which is also used in certain types of normal cells.

A prodrug conjugated with ε-acetylated lysine is expected to be protected until it meets HDAC that will remove the acetyl group from the ε-acetylated lysine. Once the acetyl group has been removed, CTSL can cleave the amide bond linking lysine and the drug, resulting in release of active drug. Since releasing the active drug is completed by the dual actions of HDAC and CTSL, the activation of prodrug should be highly selective to tumor cells that highly express both HDAC and CTSL.

Puromycine has been chosen as a prodrug since its cytotoxicity can be masked by conjugating the ε-acetylated lysine. Therefore, we can test the hypothesis. The optimization of

synthesis and purification of the ε-acetylated lysine conjugated puromycine will be performed to produce a highly pure compound for biological experiments.

3. Results

The antibiotic puromycin is toxic to most types of cells, since it stops polypeptide chain growth and releases premature protein. The primary amine on puromycin is a key factor in its cytotoxicity. When masked with acetyl group by acetyltransferase, the puromycin activity is completely impaired. Based on this fact, puromycin was chosen for conversion into a prodrug. Boc-Lys-(Ac)-OH was coupled to puromycin in the expectation that promycin will stay inactive until an HDAC removes the acetyl group, and CTSL will successively cleave the amide bond between Lys and promicyn to generate free puromycin that kills the cells. Boc-Lys(Ac)-puromycin (Boc-KAc-Puro) was synthesized as a substrate for both HDAC and CTSL and was tested *in vitro* and *in vivo* to study whether HDAC and CTSL can act as a selective modality for delivering anticancer drugs to cancer cells.

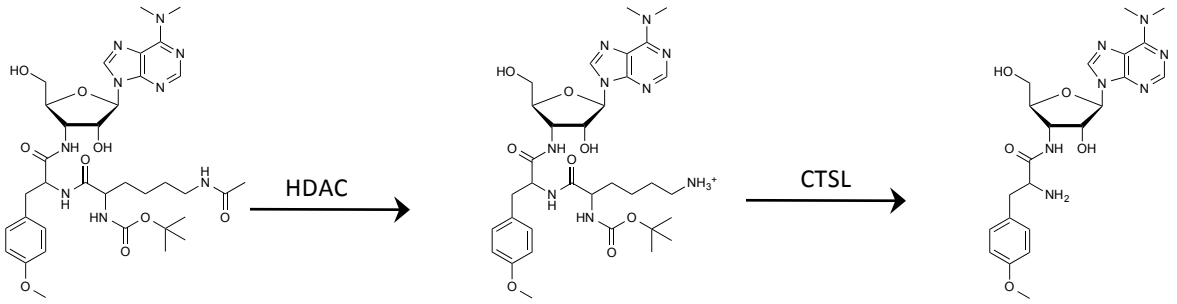

Scheme 4-1. The concept of converting pro-drug to active drug by HDAC and CTSL.

Synthesis of Boc-Lys(Ac)-Puromycin (Boc-KAc-Puro)

To a mixture of Boc-Lys(Ac)-OH, EDC·HCl and HOBt, commercially available puromycin·2HCl neutralized with 2 eq of DIPEA was added. The reaction was run for 12hr. After evaporating DMF, the product was redissolved in DCM, washed with usual workup, and purified by normal phase flash column chromatography. Even though the isolated product was a single spot on TLC plate, there were two different molecules when analyzed by LC/MS (reverse phase-C8 column).

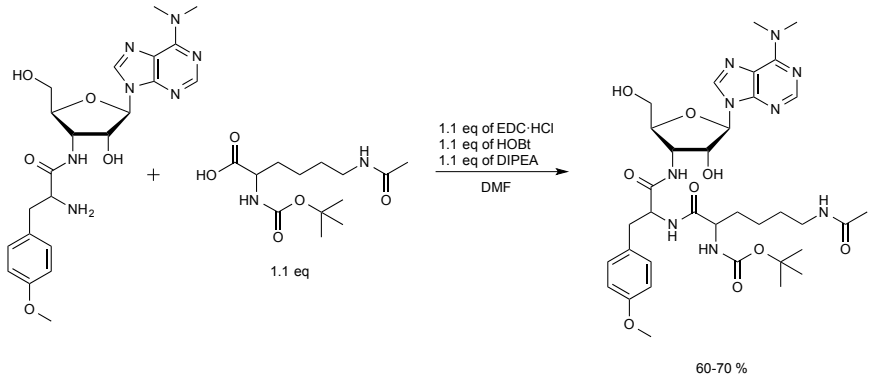

Scheme 4-2. Synthesis of Boc-KAc-Puro

The first peak eluted at 9.59 min was Boc-KAc-Puro, and the second peak at 12.49 min was the byproduct (Fig. 4-4). The molecular weight observed was 1012.19, which corresponds to the molecular weight of puromycin coupled with two Boc-Lys(Ac)-OH. This impurity was only obtained when the scale was increased (1g of puromycin as a starting material). To remove the impurity, recrystallization was performed using acetone/acetonitrile. However, it still contained 9% impurity and was not pure enough to test in vivo. When performing large scale, it is important to add activated carboxylic acid slowly to ensure proper cooling.

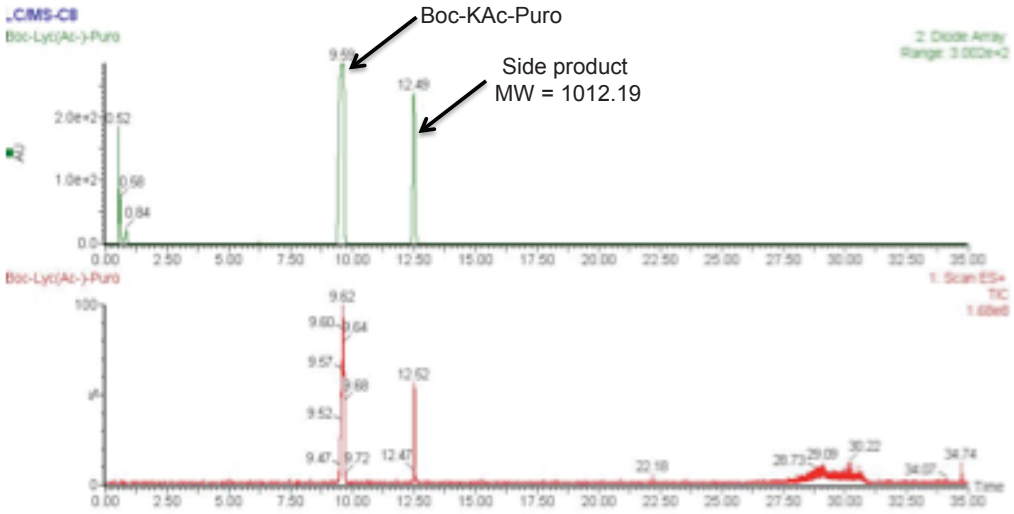

Figure 4-4. LC/MS analysis after purification by silica gel chromatography

Another impurity, different from the previous impurity, was observed. This was found to be the isomer of puromycine itself (Fig.4-5). The starting material from different commercial source contained a small amount of the isomer at the beginning. Therefore, the product was also obtained with another isomer.

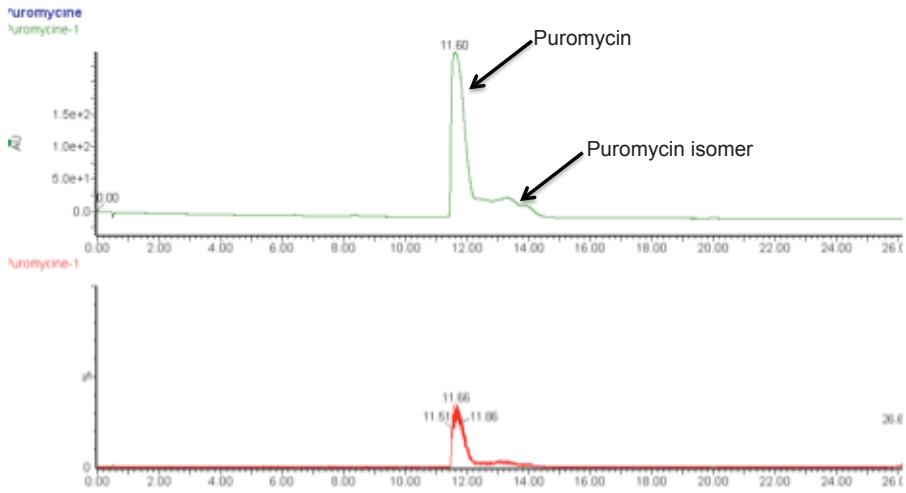

Figure 4-5. LC/MS analysis of puromycin directly from the bottle

Since the product and the isomer cannot be separated by silica gel column chromatography, we tried reverse phase column (C18) with the isomer mixture obtained by silica gel column chromatography, and the desired product was nicely separated from its isomer on C18 column (Fig.4-6a). The isomer was removed after the coupling reaction by chromatography since the desired product was separated from its isomebetter than puromycin isomers that are not conjugated with Boc-Lys(Ac)-OH were separated.

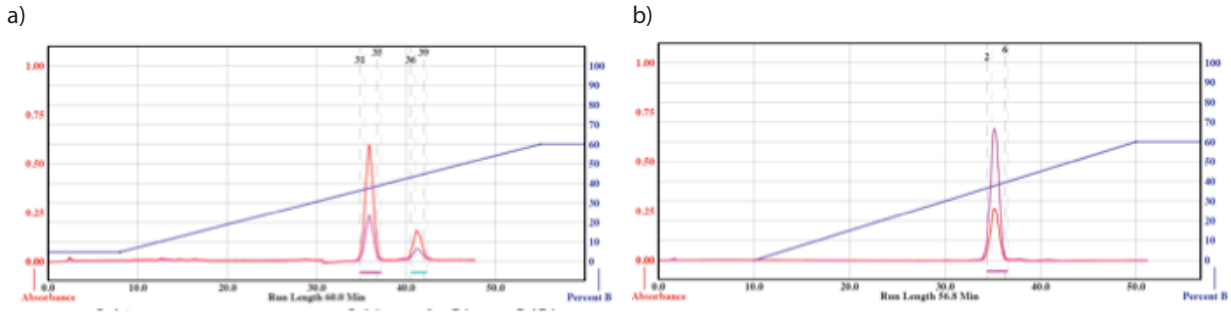

Figure 4-6. Reverse phase purification profile

Since Boc-KAc-Puro is not soluble in pure water, we tested water precipitation to see whether it can get rid of impurities in the reaction. After precipitation, the white solid was filtered and purified by C18 column. Water precipitation clearly removed most of the impurities from the mixture (Fig.4-6b). However, after precipitation, the resulting yield was low (~40%). We tested if the purification without precipitation would give the same separation on C18. The crude product dissolved in 10% ACN was loaded after evaporating solvent from the reaction mixture, and the separation was performed. The desired product was separable from other impurities. Since the product is not perfectly soluble in 10% ACN, ~300 mg of the crude was

purified at a time for better separation instead of overloading whole crude when large-scale reaction was performed. The purity of the product was checked by LC/HRMS, and it was ~98% pure (Fig 4-7).

Total ion count

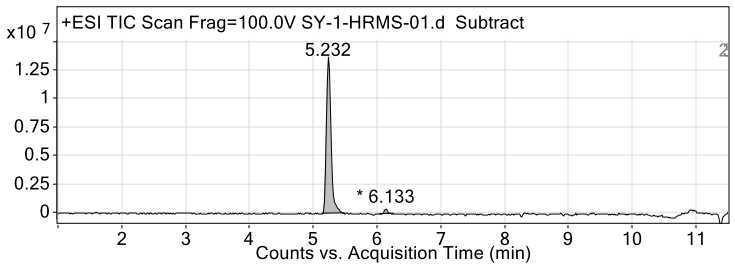

RT	Area	Area Sum %
5.232	74028291	97.83
6.133	1641828	2.17

UV trace

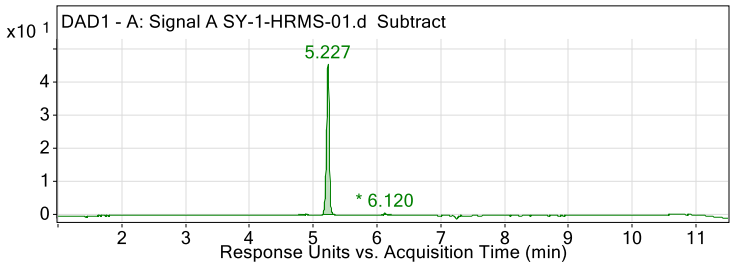

RT	Area	Area Sum %
4.883	0.96	0.7
5.227	133.91	98.21
6.12	1.49	1.09

Figure 4-7 LC/HRMS analysis of Boc-KAc-Puro

Characterization of anticancer properties of Boc-KAc-Puro in vitro[231]

(All work presented here was performed by Dr. Nobuhide Ueki)

Induced activity of HDAC and CTSL in various cancer cells

To confirm that increased HDAC and CTSL activity can be a specific target in cancer therapy, different types of cancer cells including colon cancer (Caco-2, COGA-10, HCA-7, HT29 and HCT116), pancreatic cancer (BXPC3 and MiaPaca-2), liver cancer (HepG2), cervical

cancer (HeLa), non-tumorigenic human colon epithelial cells (CCD841-Co), and normal mouse mammary epithelial cells (Eph4N) were tested. Enzyme activity was measured by standard HDAC assay using Boc-Lys(Ac) coupled with 7-amino-4-methylcoumarin (AMC). Briefly, HDAC removes the acetyl group on the substrate. Next, the cell is lysed in the presence of trypsin. During this step, trypsin recognizes and cleaves the amide bond between Lys and AMC only from deactlyated substrate, liberating AMC that fluoresces.

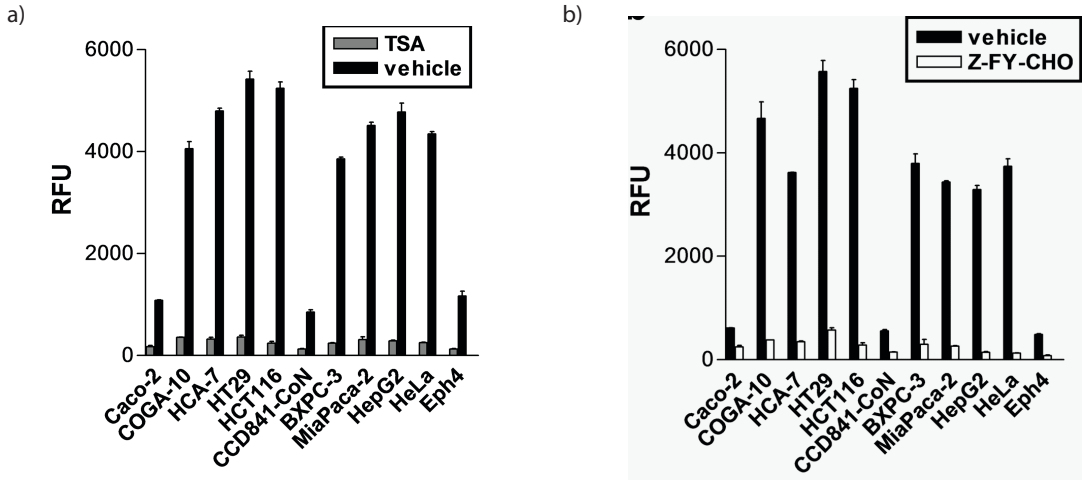

Figure 4-8 HDAC and CTSL activity in cancer cells.[231] (a) Comparative HDAC activity of the panel of cancer and normal cell lines was measured by a standard HDAC assay using substrate Boc-Lys(Ac)-AMC, either with vehicle control DMSO or HDACi TSA (1μM), (b) Comparative live-cell CTSL activity of the same cell lines as in using substrate Boc-Lys-AMC, either with control DMSO or CTSL inhibitor Z-FY-CHO (100 μM) (taken from the reference).

Clearly, activity of HDAC was markedly enhanced in malignant cell lines (fFg. 4-8a). When treated with HDAC-specific inhibitor trichostatin A (TSA), only a basal amount of activity was observed. It confirms that deacetylation of Boc-Lys(Ac)-AMC is directly related to HDAC activity. Next, CTSL activity was also measured. In this case, Boc-Lys-AMC was used as a

substrate. Also, increased activity of CTSL was observed. Similar to HDAC, CTSL-specific inhibitor Z-FY-CHO reduced the activity of CTLS (Fig.4-8b).

Design of an agent targeting HDAC and CTSL

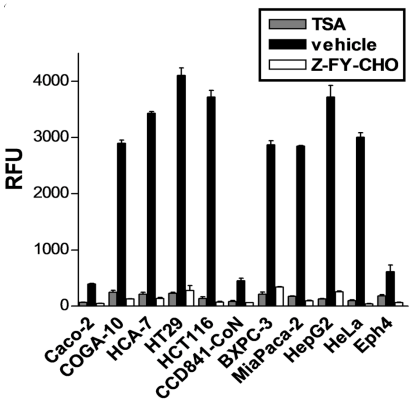

Figure 4-9 Comparative live-cell enzymatic activity of the same cell lines.[231] As in Fig. 4-8a using substrate Boc-Lys(Ac)-AMC, either with vehicle control DMSO, TSA (1 μM) or Z-FY-CHO (100 μM) (taken from the reference).

To test whether Boc-Lys(Ac)-AMC can be cleaved to Boc-Lys and AMC by endogenous HDAC and CTSL in the cells, enzyme activity assay without cell lysis and tryptic digestion was performed. In malignant cell lines expressing high levels of HDAC and CTSL, increased activity was observed. In contrast, the treatment of TSA or Z-FY-CHO significantly inhibited the observed effect, which confirms that Boc-Lys(Ac)-AMC was able to be processed by highly expressed HDAC and CTLS within the cell (Fig. 4-9).

Selectivity of Boc-KAc-Puro in vitro

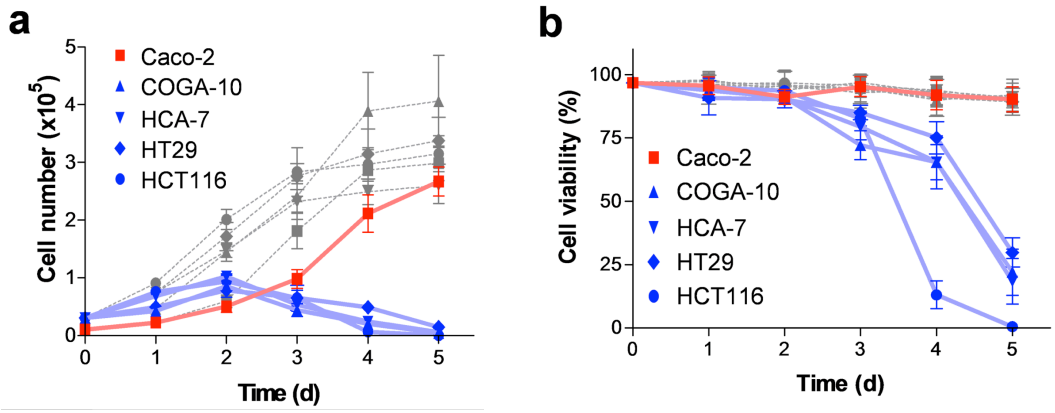

Figure 4-10 Anticancer properties of Boc-KAc-Puro in colon cancer cell lines.[231] (a) The colon cancer cell lines were grown for 5 days either with vehicle control DMSO (gray symbols) or 54 μM Boc-KAc-Puro (red and blue symbols), (b) The cell lines were grown as in (a) with vehicle control DMSO (gray symbols) or Boc-KAc-Puro (red and blue symbols) (taken from the reference).

With solid evidence supporting the hypothesis, Boc-Lys(Ac)-Puro (Boc-KAc-Puro) was tested with a panel of colon cancer cells. Antibiotic puromycin (Puro) was chosen as a cytotoxic drug because it kills most of the cells by terminating polypeptide growth. Each cell was treated with DMSO alone (vehicle) or 54 μM of Boc-KAc-Puro. The cell proliferation was measured by counting the number of cells at each time point. All the cell lines were confluent when treated with DMSO. In the presence of Boc-KAc-Puro, non-malignant Caco-1 was reached to confluency. On the other hand, massive cell death was observed only in the malignant cells (Fig.4-10a). Also, cell viability was measured by trypan blue exclusion. The malignant cells started to die on the second day of Boc-KAc-Puro treatment, and the cell survival was below 30% at day 5 (Fig.4-10b). These results indicate that Boc-KAc-Puro has selective anti-proliferative and cytotoxic effects on malignant cells, and that the release of puromycine specifically in malignant cells is mediated by the serial work of HDAC and CTSL.

Anticancer effect in vivo

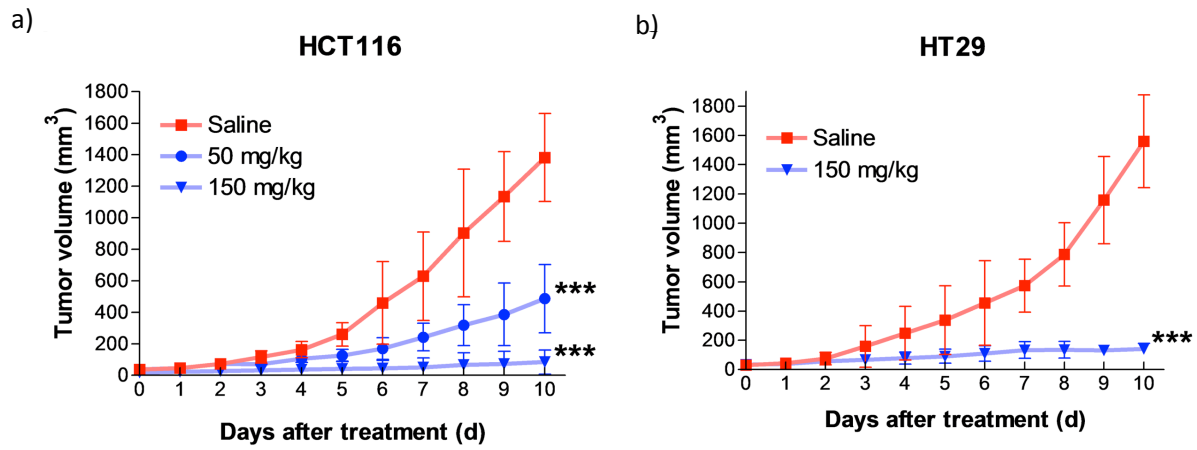

Figure 4-11 *In vivo* anticancer efficacy of Boc-KAc-puro.[231] (a) Tumor growth in HCT116 xenograft model. Animals were treated with acidified saline control or Boc-KAc-Puro (50 or 150 mg/kg), values are mean ± s,d, (n=5 mice per group). ***P<0.001 compared with the control group. P=0.000716 (50mg/kg), p=0.000349 (150mg/kg) at 10 days (two detailed Student's t-test), (b) Tumor growth in HT29 xenograft model as in a, values are mean ± s,d, (n=5 mice per group). ***P<0.001 compared with the control group. P=0.000514 (150mg/kg) at 10 days (two detailed Student's t-test) (taken from the reference).

To evaluate anticancer efficacy of Boc-KAc-Puro in vivo, mouse xenograft models bearing human colon cancer cell lines (HCT116 and HT 29) were used. Each cancer cell was injected subcutaneously into the lower flank of mice. When the tumor size had grown to 3 mm, Boc-KAc-Puro was treated intraperitoneally with 50 mg and 150 mg kg $^{-1}$ per dose for 10 days. With both cell models, HCT116 and HT 29, significantly small sizes of tumor were observed in mice treated with the prodrug. Also, 150 mg kg 10 of prodrug efficiently interfered with the growth of tumors without serious off-target systemic toxicity (Fig.4-10).

4. Discussion

Prodrug Boc-KAc-Puro was successfully synthesized and it was verified that puromycin, an anticancer drug, can be liberated specifically in malignant cancer cells by serial actions of enhanced HDAC and CTSL activity and it kills the cells *in vitro* and *in vivo*. Since enhanced activities of two enzymes are mandatory to release puromycin, releasing active drugs from prodrugs in target cells is expected to be more selective than inhibiting one active enzyme in cancer cells. This strategy is noteworthy since it does not have an adverse effect on normal cells. Also, since coupling of a small masking group on cytotoxic reagents is feasible, this strategy can be readily applied to other cytotoxic anticancer drugs to increase efficacy.

Other types of functional groups can be tested to enhance the hydrolysis of amide bond by CTSL such as fmoc (the work is in progress by Dr. Ueki). Also, puromycine can be replaced by other cytotoxic agents that can be masked by amide coupling.

The solubility of the Boc-KAc-Puro is not great in pure water. Therefore, the drug formulation has to be optimized. For clinical settings, administration route, dose, as well as detailed pharmacokinetics, pharmacodynamics, toxicology and drug resistance studies have to be established.[231]

Chapter 5

Novel cancer homing peptide for early cancer detection

1. Introduction
    1.1. Cancer metastasis and invasion
    1.2. Inhibition study on cell migration mediated by MT1-MMP-PEX-domain
    1.3. Positron Emission Tomography detecting cancer
2. Specific aim
3. Results
    3-1. Model study with dipeptide, AOAc-GY
    1.5. Full peptide, AOAc-GYPMP coupling to FDG
    1.6. ^{18}FDG coupling
    1.7. Cell migration assay
4. Discussion
5. References

1. Introduction

1.1. Proteases in metastasis and invasion

Currently, cancer is the second leading cause of death in America and is caused by "both external (tobacco, infectious organisms, chemicals, and radiation) and internal (inherited mutations, hormones, and immune conditions caused from metabolism) factors".[232] Although the genetic basis of tumorigenesis may vary between different types of cancer, most of the cancers share common physiological characteristics including self-sufficiency in growth signal, insensitivity to antigrowth signals, evasion of apoptosis, limitless replicative potential, sustained angiogenesis, and tissue invasion and metastasis.[156] Among these features, metastasis, a process by which cancerous cell disseminates to other organs distant from the primary tumor, is responsible for 90% of deaths from cancer.[233] Metastasis occurs at different rates and in organs specific to the type of cancer (Table 5-1).[234, 235] Uncovering the precise mechanism of cancer cell migration to distant organs at a molecular level is urgent to improve anticancer strategies given the deadly nature of the process.

	Metastasis site
Lung	Small-cell lung carcinomas (SCLD) to many organs and non-small-cell lung carcinomas (NSCLC) to the contra-lateral lung, brain, adrenal glands, liver, and bones
Skin	Skin, liver, brain, and lungs
Breast	Liver, brain, bone, and lungs
Colorectal	Liver and lungs
Ovarian	Local spread in the peritoneal cavity
Prostate	Bones
Sarcoma	Lungs

Table 5-1. Metastasis to specific organs by different tumor types[234, 235]

During the process of cancer invasion and metastasis, the degradation of natural barriers such as interstitial connective tissue and basement membranes is required.[236] The degradation of these barriers is processed by proteases such as matrix metalloproteinases,[237, 238] cysteine cathepins[218, 239], and serine proteases.[240] Theses proteases can promote cancer cell invasion and intravasation by several mechanisms. Individual proteases cleave the cell adhesion molecules such as epithelial (E)-cadherin. The cleavage results in the disruption of the cell-cell interactions, and the loosening of the cell contacts facilitates cancer cell migration.[239, 241] Protein degradation or turnover of proteins in the extracellular matrix (ECM) and basement membrane allows invasive cells to migrate into the surrounding tissue and vasculature. Also, proteases exert specialized processing roles that are critical for cell signaling, such as in the restricted cleavage of pro-domains and subsequent activation of growth factors and cytokines, which may significantly enhance chemoattraction, cell migration, and metastasis.[242] Theses two different functions act in collaboration to stimulate cancer cell spread and are tightly controlled in a cascade of protease interactions, allowing for control and amplification of proteolysis in invasion and metastasis.[243]

Among the all proteases, matrix metalloprotenases (MMPs) have been considered as a major contributor assisting tumor cells during metastasis because they can cleave virtually any component of ECM and basement membrane. Due to this important role in the progression of cancer to later stages, invasion and metastasis, MMPs have been serving as major drug targets in cancer therapy.

1.2. Matrix metalloproteinases (MMPs): structure and functions

Matrix metalloproteinases (MMPs) are a large family of calcium-dependent zinc-containing endopeptidases. There are 24 human MMPs, and they are divided into eight subgroups according to their distinct structure: five of the subgroups are secreted and three are membrane-type MMPs (MT-MMPs). MMPs share a common domain structure (Fig. 5-1); a signal peptide, a propeptide, a zinc containing catalytic domain, flexible hinge region between the catalytic domain and hemopexin (PEX) domain, and a PEX domain.[244]

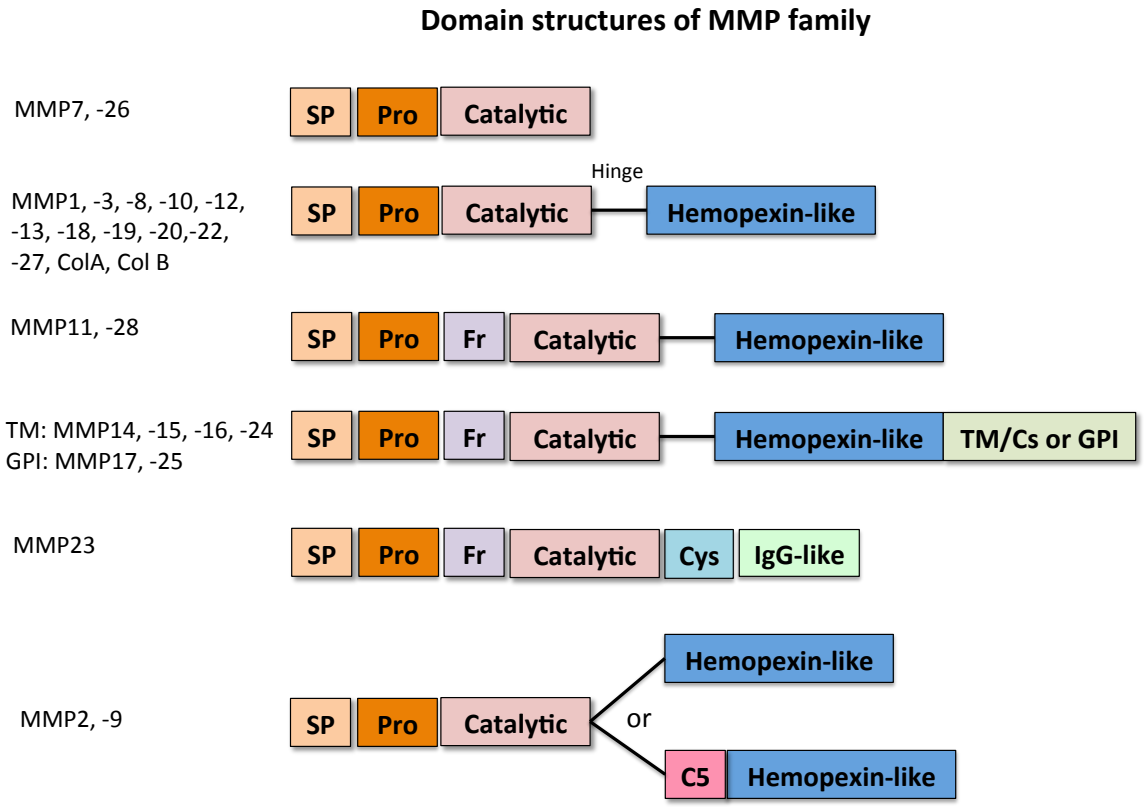

Figure 5-1. Domain structures of matrix metalloproteinases. The families are grouped based on their domain organization.[245, 246] SP: signal peptide, Pro: pro-domian, Fr: furin-cleavage site, TM: transmembrane, Cs: cytosolic, GPI: glycosylphosphatidylinositol, C5: type-V-collagen-like

The signal peptide directs MMPs to the secretory or plasma membrane insertion pathway. The zinc binding motif HEXXHXXGXXH in the catalytic domain and the cysteine motif PRCGXPD in the propeptide are highly conserved in all MMPs. Three histidines in the zinc binding motif hold a catalytically important Zn^{2+} ion. The cysteine residue from the conserved PRCGXPD motif coordinates with the catalytic zinc ion in the active site to prevent the cleavage of substrate when it is in the inactive form (Fig. 5-2).[244, 247] Other than five common domains of MMPs, MT-MMPs have an additional transmembrane domain of 20 amino acids and a cytoplasmic tail to anchor these enzymes on cell surface. [244, 247]

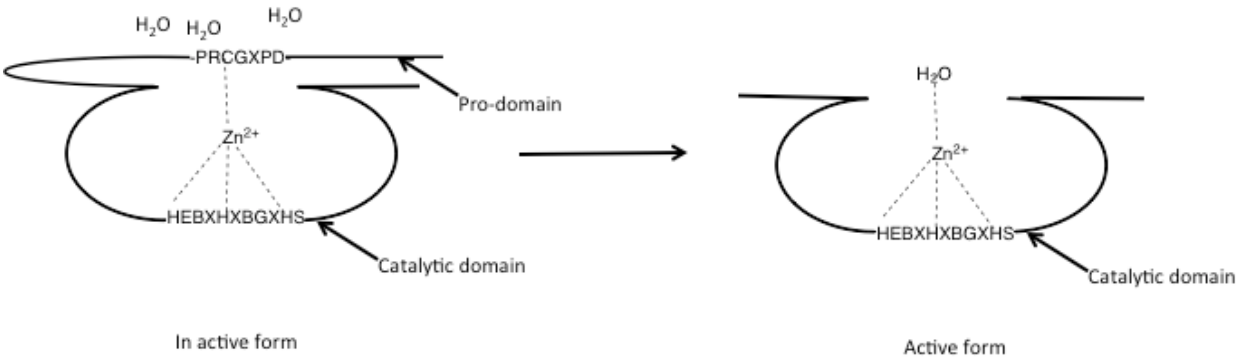

Figure 5-2. Schematic representation of "cysteine switch" during MMP activation[248]

Most human MMPs contain a PEX like domain consisting of ~210 amino acids except for MMP-7, -26 and MMP-23. The PEX domain exists in a propeller form with four blades arranged around a central axis. The first blade is linked to the fourth blade through a disulfide bond. Each blade is composed of four antiparallel β-sheets and one α-helix.[249]

MT1-MMP is the only membrane-anchored collagenases, and it participates in many physiological and pathological events including wound healing,[250] angiogenesis,[251] and cancer cell invasion and metastasis[252, 253]. Not only MT1-MMP cleaves collagens types I, II, and III, but also it degrades cell surface proteins such as glutaminsase,[254] CD44,[255] and syndecan 1[256]. In addition, MT1-MMP activates proMMP-2[252] and proMMP-13[257] and induces pericellular matrix proteolysis.

Homodimerization among MT1-MMP molecules through the PEX domain is important to activate proMMP2.[258, 259] After homodimerization of MT1-MMP, TIMP-2 binds to one of the catalytic domains of MT1-MMP.[260] In this process, TIMP-2 functions as a mediator to bind MMP-2 to MT1-MMP through hydrophobic interactions between the carboxyterminal domain of TIMP-2 and the PEX-like domain of MMP-2. This interaction anchors MMP-2 on MT1-MMP at the cell surface, and the other MT1-MMP activates the proMMP-2.[249, 261] Also, MT1-MMP forms heterodimer with CD44 through the PEX domain and cleaves CD44 to stimulate the migration and localization to the invadopodia.[262]

1.3. Inhibition study on cell migration mediated by MT1-MMP-PEX-domain[263]

Data mining using a DNA microarray showed that in most human cancers including breast cancer, MT1-MMP is upregulated (Fig. 5-3 A). To validate how relevant MT1-MMP is to breast cancer progression, breast cancer cells from human breast specimens were harvested and RT-PCR was performed to measure the expression level of MT1-MMP. MT1-MMP's expression level was significantly increased in the invasive stage of cancer (Fig. 5-3 C). Therefore, MT1-MMP is an indicator for invasive breast cancer.

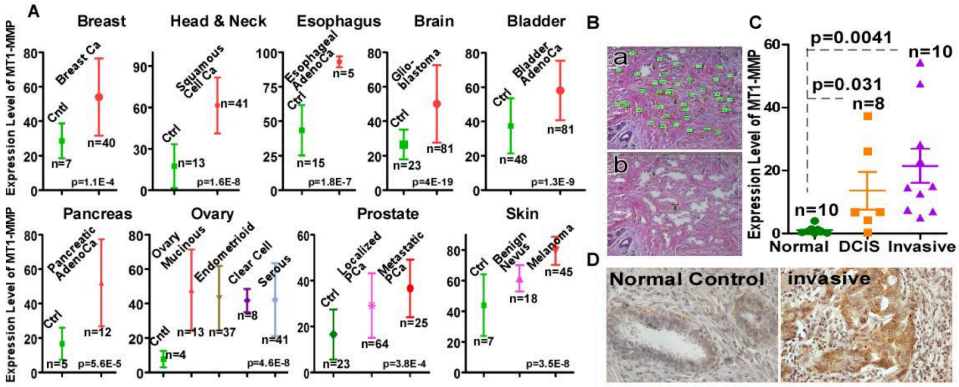

Figure 5-3. Enhanced expression of MT1-MMP in human cancers.[263] The data show that MT1-MMP expression is elevated in human cancers including human breast cancers and correlates with grade and stage. Method: A) Data mining of MT1-MMP expression in various human cancers vs corresponding normal adjacent tissues (Cntl) examined by DNA microarray (Ref: 8, 18-25) n=cases. B) Laser capture microdisection (LCM): The cancer cells in the section of human breast cancers and normal breast tissues were microscopically marked (a, before LCM) and laser captured to a microtube by LCM leaving empty spots in the section (b). C) Real time RT-PCR: The RNA was extracted from the cells harvested by LCM and amplified by real time RT-PCR (n=case number). D) Immunohistochemistry: Normal, DCIS and invasive breast cancer specimens were stained by anti-MT1-MMP antibody. The images show that MT1-MMP is upregulated in invasive breast cancers as compared to normal tissues.

To evaluate the expression level of MT1-MMP in more malignant cell lines, Du145 and MDA-MB-231 (prostate and breast cancer), versus less malignant cell lines, LNCaP and MCF-7 (prostate and breast cancer), mRNA levels were determined by RT-PCR. Almost no MT1-MMP mRNA was detected in the less malignant LNCaP and MCF-7 cells (Fig. 5-4A). Western blotting analysis showed an analogous result (Fig. 5-4B).

In a cell scattering experiment with type I collagen, MCF-7 and LNCaP cells formed aggregates in the gel (Fig. 5-4C-a,c). In contrast, a scattering growth pattern with elongated

morphology in Du145 and MDA-MB-231 (Fig. 5-4C-b, d) was observed. These two results indicate that MT1-MMP can be used as a biomarker to distinguish aggressive and indolent tumor cells.

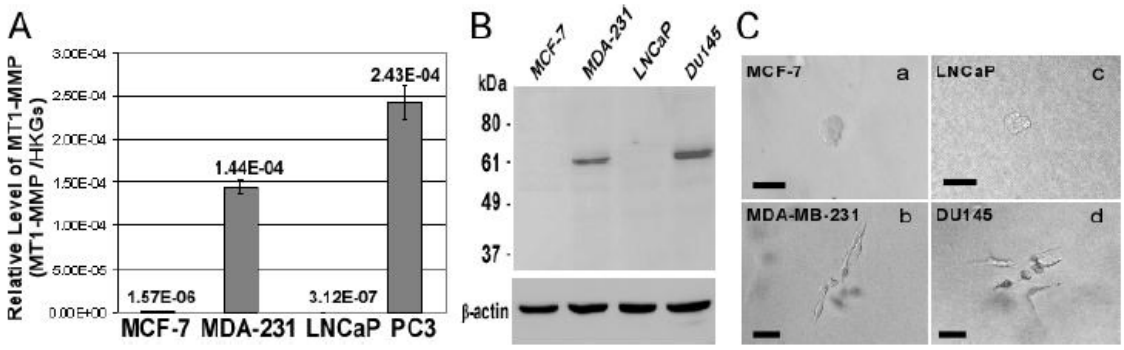

Figure 5-4. Characterization of four breast and prostate cancer cell lines.[263] (A) Expression levels of endogenous MT1-MMP in each cell line by real time RT-PCR. (B) Confirmation of MT1-MMP expression levels by western blotting. (C) Scattering patterns in 3D type I collagen.

The catalytic and PEX domains of MT1-MMP were suggested to play independent roles in ECM degradation and cell migration. When LNCap cells expressing MT1-GFP were treated with recombinant TIMP-2 or anti-PEX domain antibodies, the scattered growth patterns were abolished (Fig. 5-5A-c,d). In the FITC-labeled substrate (fibronectin) degradation-migration assay, anti-PEX antibody blocked MT1-MMP induced cell migration, but did not impair MT1-MMP catalytic activity (Fig. 5-5B). In contrast, TIPM-2 inhibited substrate degradation. These results indicate that both catalytic and PEX domains are necessary for LNCap cell scattering/invasion.

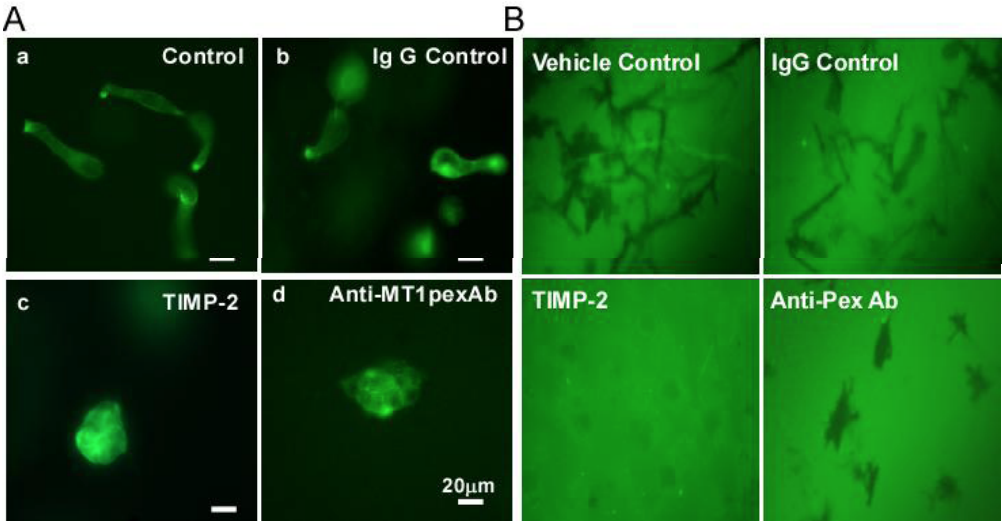

Figure 5-5. Domain requirement of MT1-MMP in cell scattering/invasion.[263] (A) Effect of TIMP-2 or anti-MT1-MMP hemopexin antibodies on MT1-MMP-induced LNCap cell scattering in 3D type I collagen. (B) Impaired MT1-MMP-induced cell migration, but not proteolytic activity.

It has been reported that the PEX domain of MT1-MMP is responsible for homodimerization between MT1-MMP and heterodimerization with CD44, which are important for cancer cell migration. To determine whether the outermost strands of four blades (IS4, IIS4, IIIS4, and IVS4) in PEX are involved in proMMP-2 activation and interaction with CD44, mutations of outermost strands in the four blades are generated by replacing blade strand sequences in MT1-MMP with the corresponding sequences from MMP-1, and gelatin zymography was carried out. The results (data not shown) showed the mutations of IS4 and IV4 completely disrupted the activation of MMP-2 by MT1-MMP, and the mutation of IS4 failed to induce cell migration by MT1-MMP.

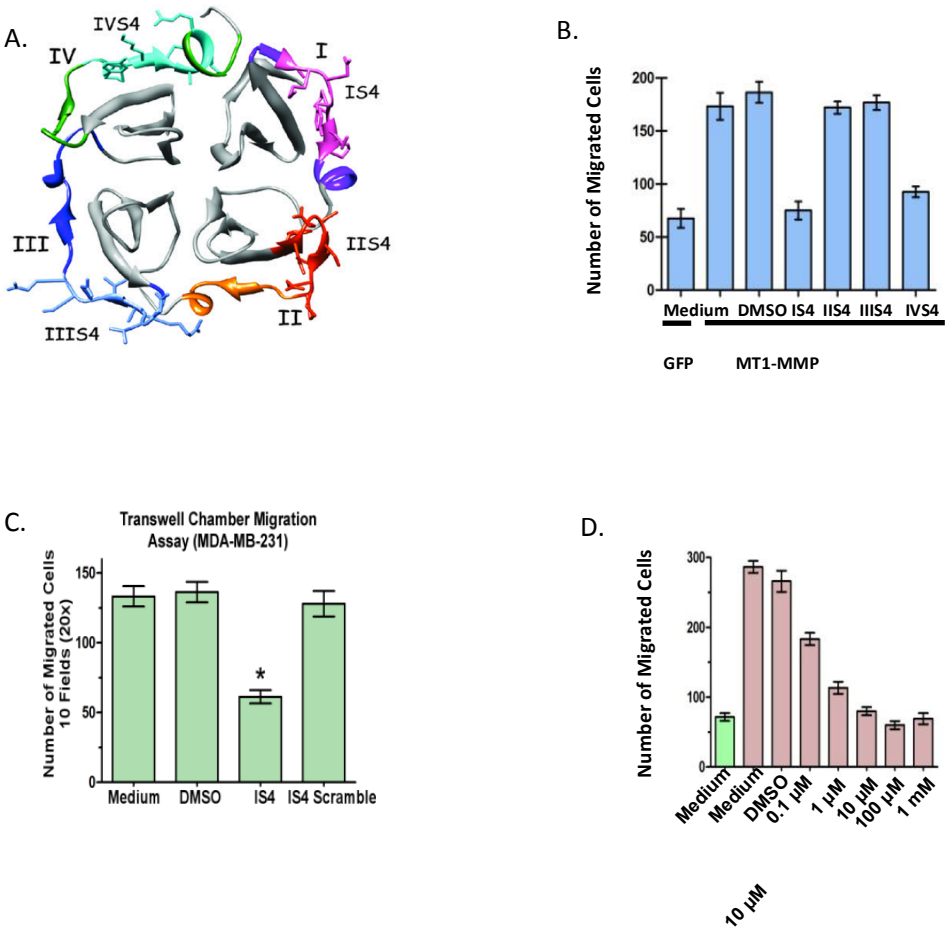

Figure 5-6. Peptide mimicking blade I and IV inhibit MT1-MMP induced cell migration. (A) Structure of the blades in PEX domain and sequence of 8 amino acids from each blade (B) cDNA transfected COS-1 cell migration assay with IS4-8, IIS4-8, IIIS-4-8, and IV4-8. (C) MDA-MB-231 expressing endogenous MT1-MMP with IS4-8 and scrambled peptide (D) Dose dependent inhibition of IS4-8 peptide

IS4-8	**Ac-VMDGYPMP-NH_2**
IS4-8 scrambled	**Ac-MVPDPMYG-NH_2**
IIS4-8	**Ac-FDEASLEP-NH_2**
IIIS4-8	**Ac-ELRAVDSE-NH_2**
IVS4-8	**Ac-GYPKSALR-NH_2**
IVS4-8 scrambled	**Ac-ALAIGAFA-NH_2**
IS4-5	**Ac-GYPMP-MH_2**

Table 5-2. Amino acid sequences of outermost blades of PEX domain

Since dimerization of MT1-MMP is crucial to induce cancer cell migration, the peptides containing 8 amino acids from the outermost β-strand of blades I, II, III, and IV were synthesized (Table 5-2) and tested as inhibitors of cell migration. The IS4-8 and IVS4-8 peptides reduced cell migration in COS-1 cell transfected with MT1-MMP cDNA (Fig. 5-6B). These peptides had no effect on MMP-9 or MT6-MMP cell signaling. Also, the 5 amino acids (IS4-5) from the C-terminal of IS4-8 and IVS4-8 were confirmed to be sufficient to inhibit MT1-MMP function (Fig. 5-6C).

A

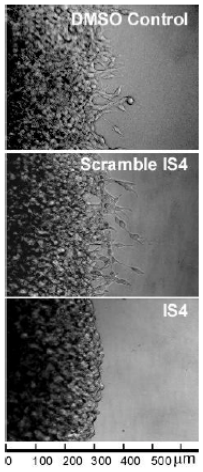

B

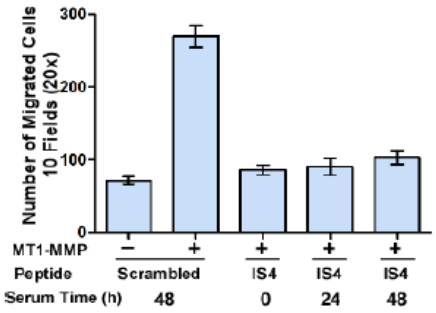

Figure 5-7. 3D invasion assay and the stability of IS4-8 in serum.[263] (A) MDA-MB-231 cells expressing endogenous MT1-MMP were examined in a 3D invasion assay in the presence of IS4-5 for 18 hrs. (B) COS-1 transfected with MT1-MMP were examined in a transwell chamber migration assay with the biotinylated IS4-8 preincubated in serum at different time periods.

Using a three-dimensional (3D) invasion assay[264], IS4-5 peptide (IC_{50} = 1.5 μM) effectively prevented human MDA-MB-231 breast cancer cell invasion (Fig 5-7A). In addition, biotinylated IS4-8 was stable in serum for 48 h. There was no significant reduction of inhibition in cell migration suggesting that acetylation or biotinylation and C-terminal amidation were not highly sensitive to serum peptidases or other proteases (Fig. 5-7B).

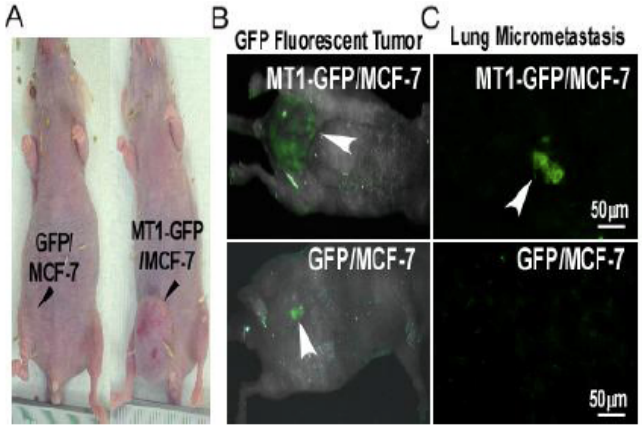

Figure 5-8. Imaging breast cancers in vivo using GFP as the indicator. (A), (B) Arrow heads indicate visible tumor masses at 13 weeks by eyes and by a Mestro in vivo imaging system. (C) Lung metastasis was detected in mice bearing MT1-GFP/MCF7 tumor, but not GFP/MCF-7 tumors.

To evaluate the role of MT1-MMP in cancer progression, hormone dependent MCF-7 breast cancer cells, which express a negligible amount of endogenous MT1-MMP, were stably transfected with MT1-GFP cDNA and injected into the mammary fad pad of female athymic nude mice (nu/nu) in the absence of estradiol pellets. After thirteen weeks from the initial injection, the mice bearing MT1-GFP/MCF-7 displayed lung metastases (Fig. 5-8), but no metastases were observed in the lungs of mice bearing GFP/MCF-7 tumors. These results emphasize the critical role of MT1-MMP in cancer dissemination.

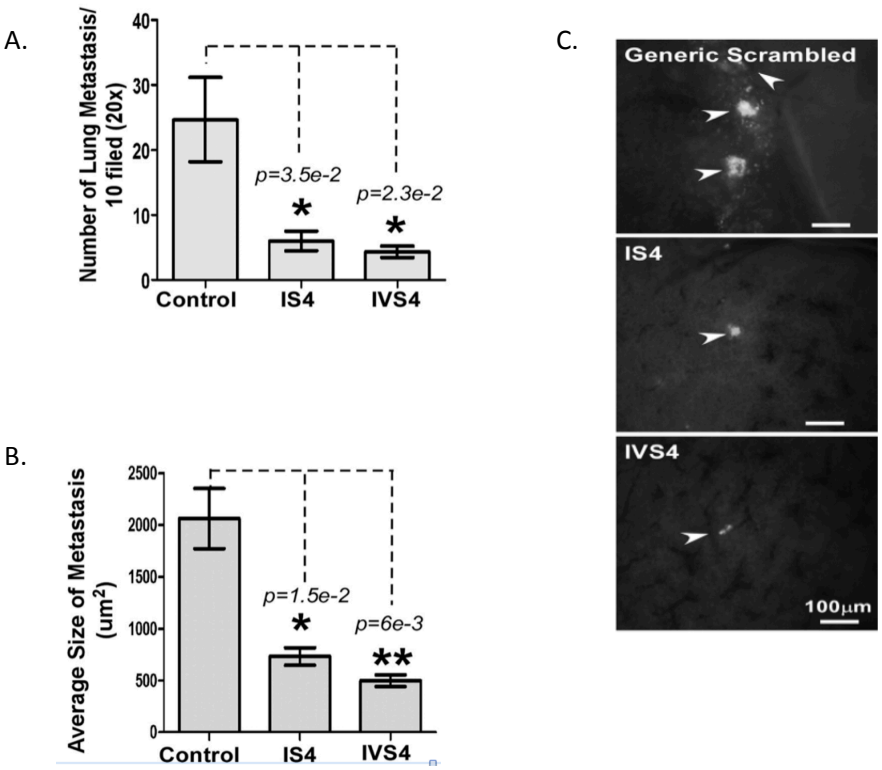

Figure 5-9. IS4-8 and IV4-8 interferes cancer cell metastasis

Then, in-vivo effects of the peptides were tested using MDA-MB-453 cancer cells expressing GFP cDNA. The tumor treated with a scrambled peptide displayed multiple large nodules (Fig. 9A). The degree of metastasis was notably reduced in IS4-8 and IVS4-8 peptides treated mice (Fig. 9B). Also, IS4 and IVS4 treated mice showed significantly smaller sizes of metastasis than the mice treated with scrambled peptide (Fig. 9C).

1.4. Positron Emission Tomography detecting cancer

Classical methods of detecting tumors such as X-ray and biopsy have been used for diagnosing and monitoring tumors. However, X-ray images are often indicators of late stage tumors. In the case of biopsy, sampling by needle is heterogeneous. The biopsy is often performed when the tumor is large enough to visualize, and thus, evaluation of the entire tumor is problematic. Therefore, a method, which is non-invasive and detects tumors at an early stage, is necessary. In this regard, molecular imaging has been developed and serves as a non-invasive tool to enhance the understanding, evaluation, and monitoring efficiency of cancer.[265, 266]

To visualize the physiological and biochemical events occurring in a body, molecular imaging techniques, such as MRI, positron emission tomography (PET), and single photon emission computed tomographic (SPECT) have been widely used. Among them, PET is a promising imaging tool in terms of sensitivity. It has approximately 10-fold higher sensitivity, better resolution and tracer quantification than SPECT.[265, 267] One of the advantages of PET imaging is that some of the positron-emitting radionuclides, O, N, and C, which are contained in biomolecules, can be used for PET. These low mass atoms can be incorporated into the biomolecules directly without disrupting their biological activity.

Radionuclide	Half-life,$t_{1/2}$(min)	Nuclear reaction	Target	Decay product
^{11}C	20.4	$^{14}N(p,\alpha)^{11}C$	$N_2(+O_2)$ $N_2(+H_2)$	^{11}B
^{13}N	9.97	$^{16}O(p,\alpha)^{13}N$	H_2O H_2O+EtOH	^{13}C
^{15}O	2.04	$^{15}N(d,n)^{15}O$	$N_2(+O_2)$	^{15}N
^{18}F	110	$^{20}Ne(d,\alpha)^{18}F$ $^{18}O(p,n)^{18}F$	$Ne(+F_2)$ $[^{18}O]H_2O$	^{18}O

Table 5-3. Commonly used short-lived radionuclides in PET[268]

In the body, the radionuclide used in PET decays by a process called positron emission. The emitted positron travels a short distance (0.5- 2.0 cm, depending on the isotope) until it encounters an electron in the surrounding tissue. The collision of a positron and an electron results in annihilation generating two gamma ray photons with the same energy of 511 keV, which migrate in approximately opposite directions (180°C) to each other.[268] A PET scanner camera detects the gamma ray photons to allow construction of an image of the location where the probe resides in the body.

$$^{11}C \longrightarrow {}^{11}B + \beta^{+} + \nu$$

Scheme 5-1. Positron emission decay equation of an ^{11}C isotope.[268]

Carbon is an attractive and important radioisotope due to its natural abundance in many types of molecules. Also, using carbon has a great advantage of retaining the same chemical and biological properties with unlabeled equivalents. ^{15}N and ^{13}O are also attractive choices for labeling since biologically active molecules often have many N and O atoms. However the main obstacle of using these isotopes is their short half-life time (Table 5-3). The short half-life of PET isotopes limits the total time of synthesis and purification of the target molecules.

In this regard, ^{18}F is considered to be a better choice as a radionuclide since it has short but manageable half-life (110 min), which is sufficient for performing multi-step syntheses for labeling[268]. ^{18}F is frequently used in the radiopharmaceutical sciences to label proteins or peptides for diagnostic imaging.[269] Large proteins or monoclonal antibodies showed clinical potential as a tumor targeting agent, but the applications are limited by poor tumor penetration due to their size and their immunogenicity. Peptides with a small radioactive tag can be used to overcome these limitations. Also, peptides have improved blood clearances.

In peptide labeling, prosthetic ^{18}F reagents target carboxylic acid, amine, or sulfhydryl functional groups within the peptide (Scheme 5-2). The primary amine at the N-terminus or on lysine residues is commonly used for conjugation with ^{18}F reagents. The most utilized methods for this type of conjugation are acylation reactions with active ester N-succinimidyl-4-[^{18}F]fluorobenzoate ([^{18}F]SFB)[270], formation of oximes between an aminooxy functional group on the amino acid and 4-[^{18}F]fluorobenzaldehyde ([^{18}F]FBA)[271], or photochemical conjugation reactions with 4-azidophenacyl[^{18}F]fluoride ([^{18}F]APF)[270].

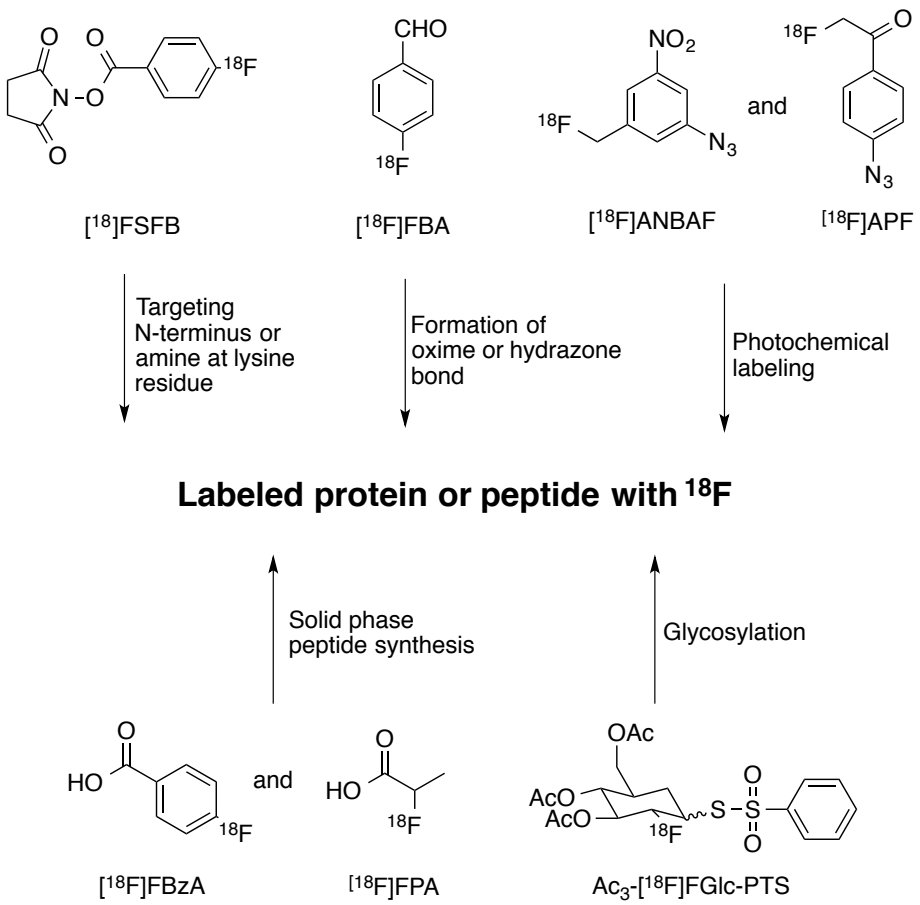

Scheme 5-2. Reagents for ^{18}F labeling to proteins and peptides[268]

Another useful amino acid functional group is a thiol (scheme 5-3). Since most proteins contain cysteine, it can be easily introduced into the proteins or peptides. Prosthetic [^{18}F]maleimide reagents can target a wide range of proteins or peptides. The free thiol forms a thioether bond with [^{18}F]maleimide reagents such as [^{18}F]FBAM, [^{18}F]FBABM, *N*-[2-(4-[^{18}F]flurobenzamido)ethyl]maleimide ([^{18}F]FBEM), or 1-[3-(2[^{18}F]fluoropuridin-3-yloxy)propyl]pyrrole-2,5dione ([^{18}F]FpyME].[268] However, these strategies need multiple step syntheses that have laborious purification steps and low yields for the final product.

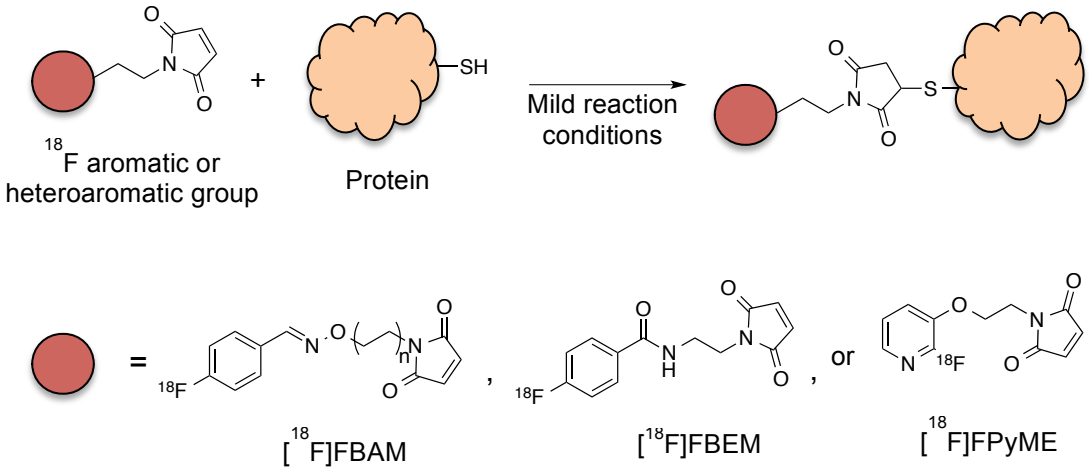

Scheme 5-3. ^{18}F reagents for maleimide coupling through thiol[268]

[^{18}F]fluoro-2-deoxy-D-glucose (^{18}F-FDG) has been used as an effective ^{18}F-glycosylating agent with amino acids to install a ^{18}F label (Scheme 5-4). This method is fascinating because it is a one-step synthesis and improves bioavailablility and blood brain barrier permeability (BBP)[272]. As a model study, Fmoc protected serine or threonine was coupled to the tetra-*O*-acetylated 2-deoxy-2-[^{18}F]fluoropyranoside in 25% and 12% radiochemical yield (RCY).

Method 1

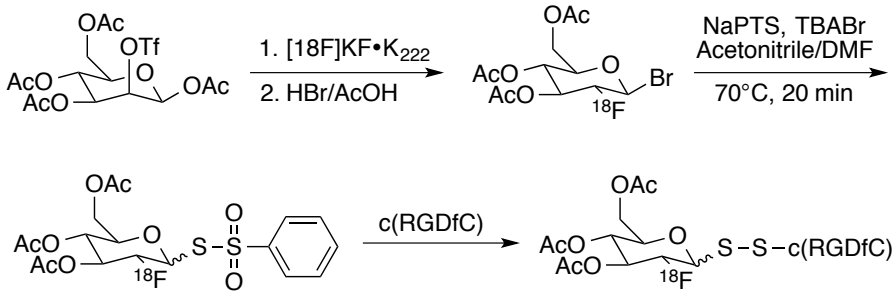

Method 2

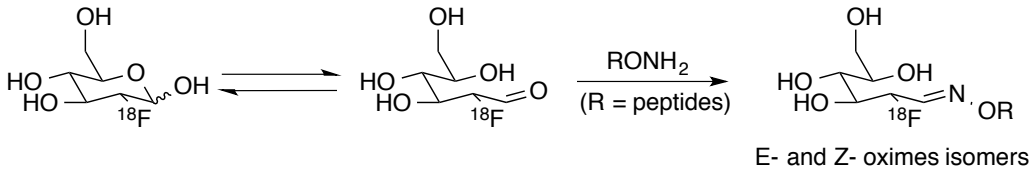

Scheme 5-4. Synthetic methods to prepare glycosylated proteins or peptides for ^{18}F labeling[268, 273]

Recently, 3,4,6-tri-*O*-acetyl-2-deoxy-2[^{18}F]fluoroglucopyranosyl phenylthiosulfonate (Ac_3-[^{18}F]FGlc-PTS) was developed to form disulfide bond with cysteine containing cyclic RGD peptide (peptide ligand for $\alpha_v\beta_3$) with 33% RCY after three steps and purification.[274] Also, ^{18}F-FDG has been used to label linear/cyclic RGD through oxime formation with an aminooxy-functionalized peptide. This method requires high temperature (100°C) to move the equilibrium in favor of the linear form of FDG with an aldehyde. Also, at pH 1.5-2.5, the maximum RCY was achieved.[273]

2. Specific aims

Cancer is treatable by surgery or local irradiation when detected at an early stage, but it becomes a major cause of death once it has developed to a metastatic stage.[275] However, it is hard to detect the early spread of tumors with current imaging technologies due to the lack of imaging probes specific to early stage cancer.

MMPs have been found to play important roles in tumor growth, angiogenesis, invasion, and metastasis and are highly up-regulated in invasive cancers. Accordingly, several classes of compounds have been developed to inhibit the catalytic activity of MMPs including peptidomimetic, tetracycline and bisphosphonate inhibitors. However, these inhibitors failed in clinical trial since they target multiple MMPs. MMPs have highly homologous catalytic sites leading to difficulty in designing specific inhibitors. The PEX domain of MT1-MMP could be an alternative drug target since the PEX domain of MT1-MMP is responsible for cancer cell invation.

Peptides mimicking 8 amino acids of the outermost β-strand of the blades from the PEX domain of MT1-MMP, GYPMP (IS4-5), have shown inhibitory activity specific to MT1-MMP mediated cell migration and invasion. Therefore, we hypothesize that targeting MT1-MMP with labeled peptide will specifically detect invasive tumors. We will prepare MT1-MMP peptide conjugated with ^{18}F-FDG and will test the peptide as a detection tool for cancer in an animal tumor model.

3. Results

The target of a molecular imaging probe to be used for primary screening of tumors should be stable and ubiquitously expressed in most types of tumors at an early stage. Membrane type 1-matrix metalloproteinase (MT1-MMP) meets these criteria and is localized to invadopodia at the leading edge of migrating cells, placing it in an ideal position to be detected.

Several studies attempted to develop molecular imaging probes for detection of MT1-MMP-expressing cancer cells. These probes include MT1-MMP cleavable peptides isolated from phage display peptide library and MT1-MMP monoclonal antibody.[276, 277] These approaches demonstrated a proof of principle for utilizing MT1-MMP as a biomarker for detection of cells expressing MT1-MMP. However, potential problem of host immune response using MT1-MMP antibodies and lack of tumor homing feature of MT1-MMP-cleavable peptide can hinder the process from the bench-to-bedside.

In a preliminary experiment, IS4-5 specifically inhibited MT1-MMP induced cell migration by inhibiting the dimerization of MT1-MMP. This result showed that IS4-5 is a potent molecular probe for detection of cancer cells highly expressing MT1-MMP. It is advantageous to use a short peptide as a probe since in general, short peptides have good tissue perfusion, fast clearance, minimal antigenicity in a body, and is relatively simple to synthesize, and can remain stable during strong chemical modifications that are sometimes necessary for radiolabeling reactions.[265]

A modification of the N-terminus of the peptide with biotin or an acetyl group had no effect on binding affinity (K_d = 101 nM) and the inhibitory activity, suggesting that functional molecules can be attached to the N-terminus as well. Based on this result, we hypothesized that

functionalization of IS4-5 with FDG will not affect its binding affinity (K_d = 101 nM) and inhibitory activities.

To conjugate FDG with IS4-5 for PET imaging, an aminooxy group can be installed on N-terminus of IS4-5 using (Boc-aminooxy)-acetic acid during the solid phase synthesis. Trifluoroacetic acid deprotection yields the free aminooxy group that is selectively conjugated with the FDG aldehyde. To increase half-life in serum, the C-terminus of IS4-5 can be amide-capped.

1.1. Model study with dipeptide, AOAc-GY

Using aminooxy acetyl (AOAc)-GY as a model, we tested the coupling efficiency. First, the stability of AOAc-GY was tested since the reaction runs in acidic condition (~ pH 2) and at high temperature (100 °C), which could hydrolyze the amide bonds. The reaction was quenched by the addition of water at 5 min, 10 min, 20 min, 30 min and 1 h. The resulting mixture was injected directly into a reverse-phase HPLC column. Based on the UV profile, no significant change occurred until 10 min into the reaction. At 20 min, a new peak started to appear right next to the starting material peak (data not shown), which suggests that the peptide was hydrolyzed. Therefore, we decided not to run the reaction more than 20 min.

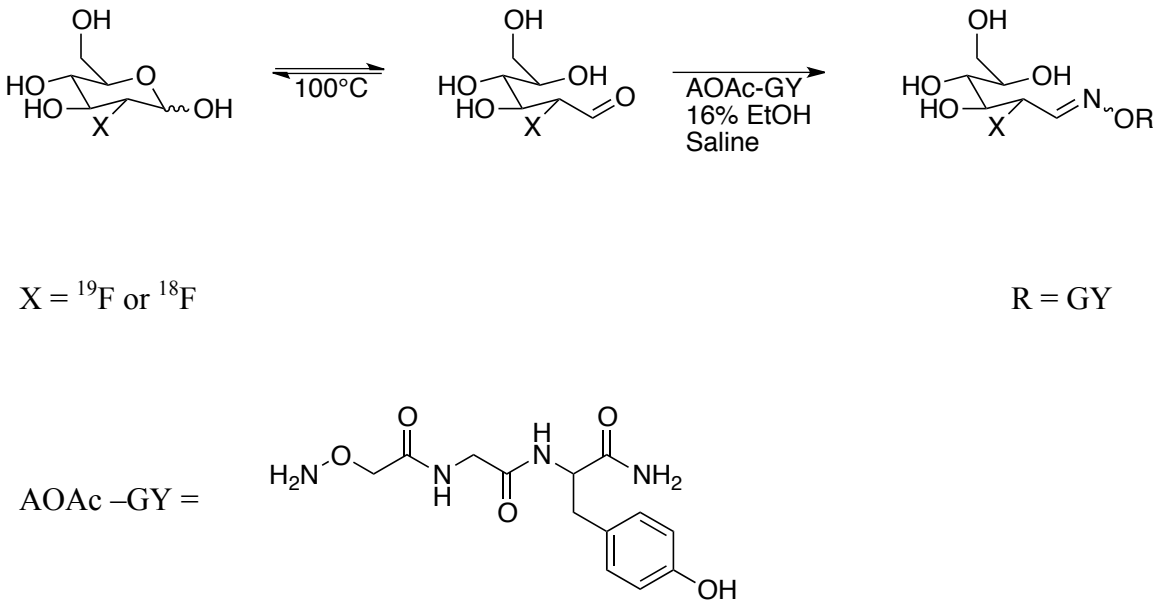

Scheme 5-5. Synthesis scheme for FDG coupling to model peptide

We tried the reaction in citrate buffer at pH 7 and pH 5.5 since ^{18}FDG solution is commercially available and provided as a solution with a pH ranging from 5.5~7. There was no reaction at pH 7, and a low reaction yield was obtained at pH 5.5. Therefore, we adjusted the pH to 2~2.5 by adding TFA. The yield increased as judged by HPLC monitoring of the reaction, and the separation of FDG-AOAc-GY from AOAc-GY was successful. The reaction did not go to completion because TFA evaporates at the high reaction temperature, and the pH increases.

After purification, the product reverted to the starting material during water removal. This reversion occurred because 0.1% TFA/ water as a solvent for HPLC purification was used.

During evaporation of the aqueous solution the pH decreased, resulting in hydrolysis of the oxmie bond. Hence, we changed the HPLC solvent to 0.1 N ammonium formate buffer, pH 7.

Since commercial ^{18}FDG solutions contain a large amount of glucose, we ran the model reaction with an excess of glucose and cold FDG to test if we could separate the glucose-conjugated dipeptide from the FDG-conjugated peptide. As shown in Fig. 10, the separation was also excellent.

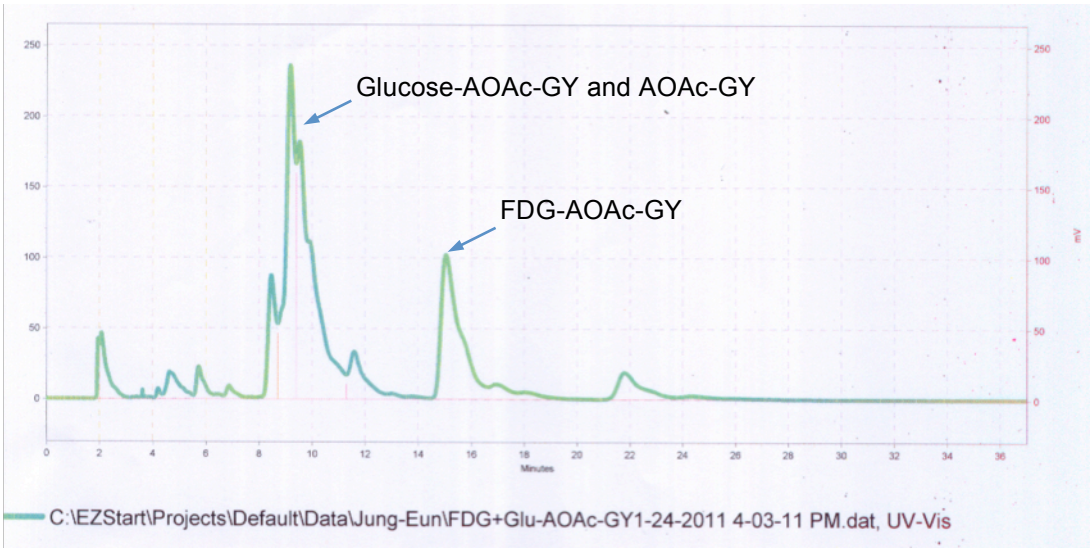

Figure 5-10. HPLC separation of FDG-AOAc-GY from glucose-AOAc-GY and AOAc-GY

1.2. Full peptide, AOAc-GYPMP coupling to FDG

Once the reaction conditions and time were optimized with the model peptide, we applied these conditions to synthesize the full-length peptide. Glucose-AOAc-GYPMP was successfully

separated from the desired product. However, the retention times of AOAc-GYPMP and FDG-AOAc-GYPMP were too close (solvent A: 0.1 ammonium formate, pH 7 and solvent B: acetonitrile) even with any gradient in contrast to the model reaction. We tested different types of buffers with different concentrations of salts, at different pHs, or with different columns of different pore sizes and several solvent gradients for each buffer system. However, the retention times were still too close. To obtain better separation and faster elution times, we used borate buffer at pH 9 since at this pH the diol on the sugar moiety generates borate ester reversibly and it allows the retention time to decrease.[278] Since only FDG-AOAc-GYPMP generates borate ester, better separation from AOAc-GYPMP was expected.

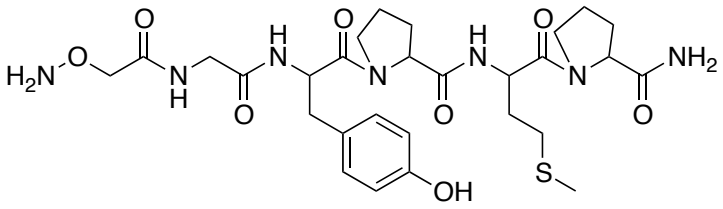

Figure 5-11. Structure of aminooxy-acetyl -GYPMP

As shown in Fig. 5-12, the separation and the retention times were improved. The order of elution of FDG-AOAc-GYPMP and AOAc-GYPMP was reversed since the borate ester increases peptide hydrophilicity.

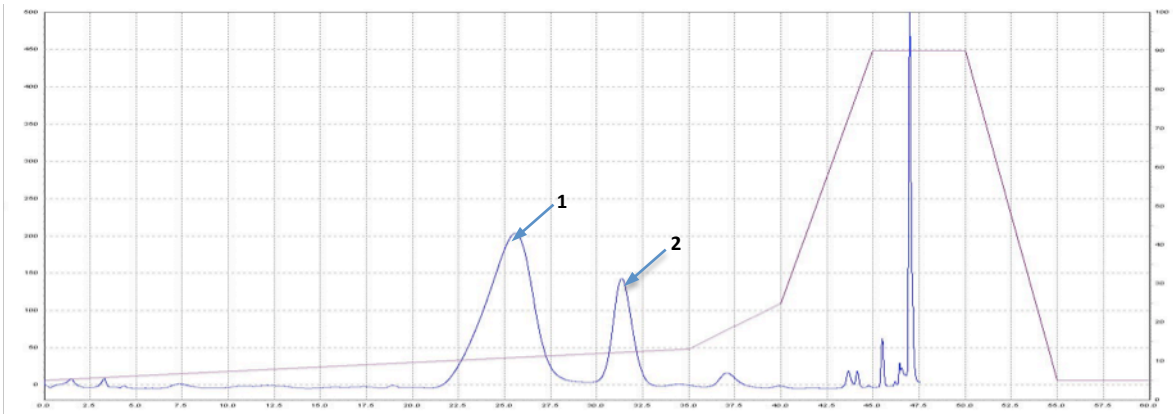

Figure 5-12. HPLC separation of FDG-AOAc-GYPMP (1) and AOAc-GYPMP (2)

To confirm whether the glucose-conjugated peptide is also separable from the product in this HPLC condition, the reaction was run in the presence of excess amount of glucose. The glucose-conjugated peptide was also successfully separated from the desired product, FDG conjugated peptide (Fig. 5-13).

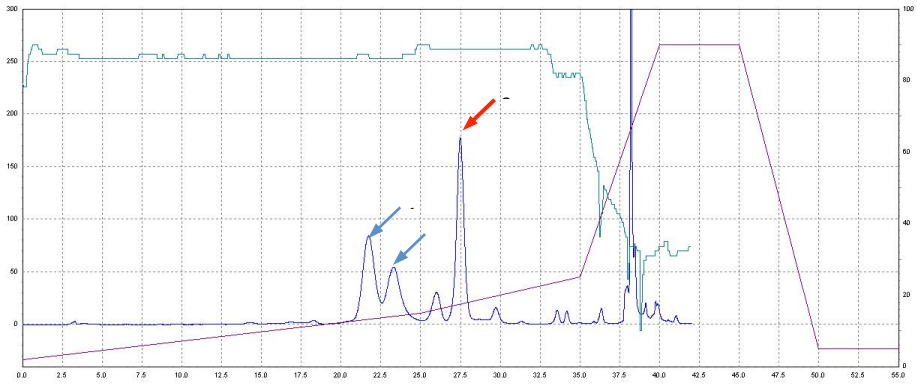

Figure 5-13. HPLC purification of Glucose and FDG conjugated peptides (Glucose-AOAc-GYPMP: peak 1; FDG-AOAc-GYPMP; peak 2, and AOAc-GYPMP; peak 3).

After HPLC purification, each peak was checked by LC/MS analysis. To remove borate ester after purification, the purified product was diluted with water, loaded onto a C18 Sep-Pak, washed with water, and eluted with absolute ethanol. However, after evaporating ethanol, we observed an oxidized product most likely oxidized methionine residue. Ethanol was substituted with ACN, and there was no oxidation after evaporation of the solvent. To remove insoluble particulate coming from the Sep-Pak, the resulting solution was clarified by filtration (0.4 μm). After evaporating ACN, the identity of the product was confirmed by LC/MS.

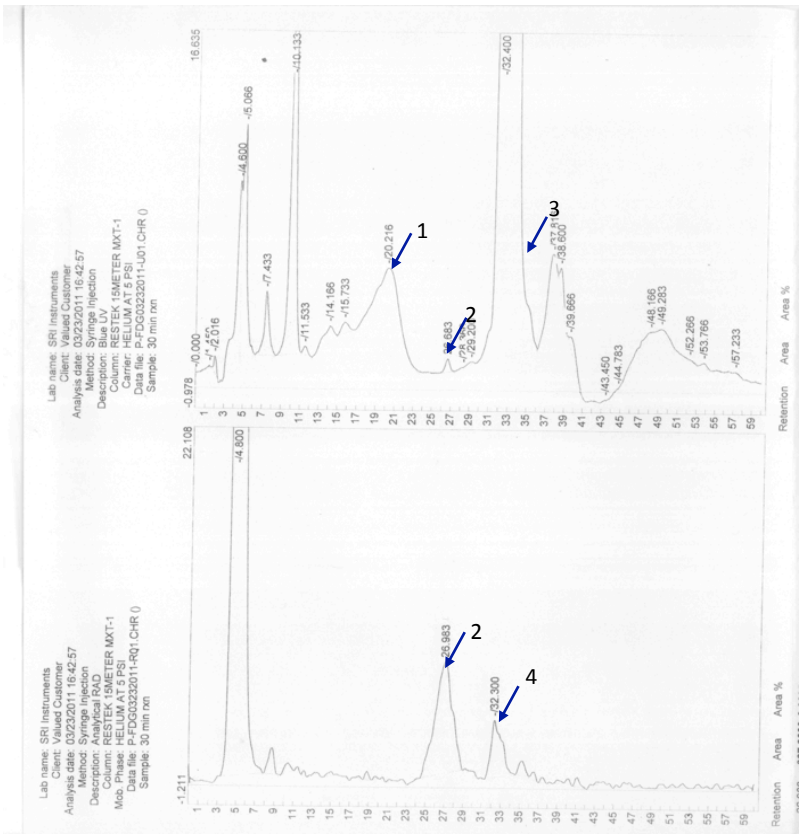

UV absorbance

1 : glucose-AOAC-GYPMP

2 : FDG-AOAc-GYPMP

3 : AOAc-GYPMP

Radioactive signal

2 : FDG-AOAc-GYPMP

4 : FDG-AOAc-GYPMP

Stereoisomer of 2

Figure 5-14. UV and radioactive HPLC traces of FDG-AOAc-GYPMP coupling reaction

3.3. ^{18}FDG coupling

To reduce the volume of reaction, ^{18}FDG solution formulated with citrate was purged with argon, and TFA was added to the reaction to decrease the pH. The reaction was performed in a sealed vial. The reaction was monitored by reversed TLC at each time point (the TLC was developed with 25% ACN/water). After 30 min, the reaction mixture was loaded onto a reverse – phase HPLC column; the radioactivity and UV signals were monitored. As shown in Fig. 5-14, we successfully separated FDG-peptide from glucose-peptide and the retention time of the desired product was 27 min. The activities of collected product and its isomer from HPLC purification were ~7.2 μCi and ~2.2 μCi respectively. After loading the product on a Sep-Pak, the radioactivity retained on the Sep-Pak was ~5.78 μCi. There was no radioactivity in the flow through. These data suggest that the product is efficiently trapped by Sep-Pak. The Sep-Pak was subsequently washed with water. After washing, the activity on Sep-Pak remained. There was no loss of the product during washing. Finally, the product was eluted using 100% EtOH and filtered with a syringe driven filter (Millipore) to remove Sep-Pak particles. The final activity of the product was ~4.68 μCi. ~0.70 μCi and 0.11 μCi were left on the filter and Sep-Pak respectively.

3-4. Cell migration assay

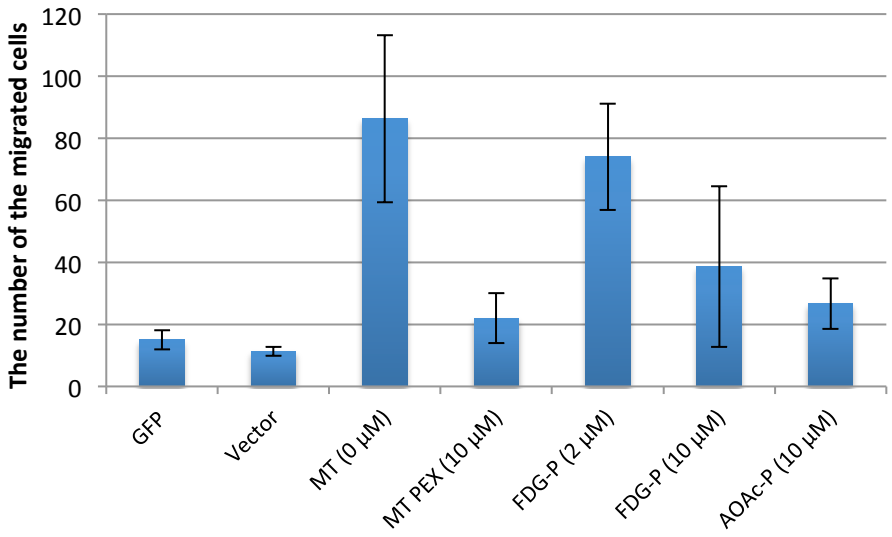

Figure 5-15. Cell migration assay: COS-1 cell transfected with MT1-MMP. GFP; the cells transfected with GFP by pQCXIP vector, Vector; empty vector (pQCXIP), MT; the cells expressing MT1-MMP by pQCXIP vector, MT PEX, the MT1-MMP expressing cells treated with the PEX domain of MT1-MMP, and FDG-P; the MT1-MMP expressing cells treated with FDG-GYPMP.

To confirm that the conjugation of FDG does not affect the binding affinity of the peptide for MT1-MMP, a cell migration assay was performed with FDG-AOAc-GYPMP and AOAc-GYPMP. COS-1 cells transfected with MT1-MMP were fused to GFP (MT1-GFP). The cells were incubated in a Boyden chamber for 18 hours and the number of migrated cells with or without the inhibitors were counted under the microscope. As a negative control, COS-1 cells expressing only GFP or containing empty vector were also tested. As a positive control, cells were treated with the whole PEX domain of MT1-MMP, which showed efficient inhibitory activity. FDG-AOAc-GYPMP (FDG-P) and AOAc-GYPMP (AOAc-P) inhibited cell migration

at 10 μM. However, the error bars were too large. Also, the number of the cells transfected MT1-GFP was low (Fig. 5-15).

4. Discussion

MT1-MMP levels are significantly elevated in the invasive stages of cancer. Considering the importance of detecting invasive cancer, targeting MT1-MMP is beneficial because it is highly expressed in invasive cancers. Blade I of the MT1-MMP's PEX domain is directly involved in homodimerization, and blade IV is the interface for forming heterodimers with other molecules.[263] Anti-PEX domain antibody blocks MT1-MMP induced cell migration. Further investigations with PEX domain mutations revealed that blade I and IV are required for MT1-MMP induced cell migration, but not for protease activity.

A short peptide comprised of five amino acids from blade I (IS4-5) also abolishes MT1-MMP induced cell migration. Modification of the N-terminal of the peptide with biotin or an acetyl group had no effect on the inhibitory activity, suggesting that other functional molecules can be attached to the N-terminus as well.

The number of steps in the synthesis of PET imaging probes has to be minimal due to the short half-life of radio nuclei and it also has to be easy to purify. In this aspect, FDG was chosen for incorporation of ^{18}F into the peptide since it can be conjugated in a single-step reaction. Procedures were optimized with cold ^{19}FDG before performing with ^{18}FDG. FDG was successfully coupled to IS4-5 peptide as the oxime even though the reaction did not go to completion due to the evaporation of TFA through heating during the reaction. Maintaining the pH at ~2 was the key to maximize the yield of the synthesis. Forming a reversible borate ester at

pH 9 with the sugar diol improved the retention time and the separation, which in turn shortened the purification time and improved the radioactive yield.

To confirm that attachment of an additional moiety at the N-terminus will not affect inhibitory activity, cell migration assays were performed. Inhibition was not impaired by modification of the N-terminus with FDG. However, the number of cells transfected with MT1-GFP without peptide treatment was too low. In summary, we showed the modification of peptide with FDG is a fast way to put a radioactive tag on it. These experiments were not pursued further because preliminary *in vivo* PET imaging studies performed by Yuwen Wu suggested the FDG-peptide probe needed to be optimized further for *in vivo* efficacy.

Chapter 6. Experimental methods

1. **Synthesis of the compounds for preparation of ROMP polymers**
2. **Synthesis of intermediates and final products towards a cleavable biotin probe**
3. **Preparation of FDG-AOAc-GYPMP**
4. **Cell migration assay**
5. **Photoaffinity labeling protocol**
6. **Cleavable biotin probe protocol**

1. Synthesis of compounds for preparation of ROMP polymers

Materials. Amino acids and coupling reagents used for the reaction were purchased from Advanced Chem Tech (Louisville, KY) or Novabiochem (Gibbstown, NJ). Solvents and chemicals were obtained from Fisher Sicentific, Inc. (Springfield, NJ) or Sigma-Alderich (Milwaukee, WI). $(H_2IMes)(PCy)_2Cl_2Ru{=}CHPh$ was purchased from Sigma-Aldrich (Milwaukee, WI). $(H_2IMes)(3\text{-Br-pyr})_2Cl_2Ru{=}CHPh$ was synthesized according to the literature. DCM, MeOH, THF, DMF, and Et_2O were dried and purified by pushstill (SG Water USA LLC, Naushua, NH). Air sensitive reactions were performed under an N_2 atmosphere in oven-dried glassware unless otherwise specified. Moisture and oxygen-sensitive reagents were handled in an N_2-filled drybox.

General methods. Analytical thin layer chromatography (TLC) was performed on precoated silica gel plates ($60F_{254}$). TLC spots were visualized by UV light and by staining with 10% phosphomolybdic acid (PMA) in ethanol. Usual workup for peptide coupling reactions was three washes of the DCM solution with 5% $NaHCO_3$ followed by three washes with 1N HCl. All compounds synthesized were purified by Combiflash personal flash chromatography system (Teledyne Isco, NE). NMR spectra were collected on Bruker instruments (400 or 500 MHz for ^1H and 100 or 125 MHz for ^{13}C). MS data were collected with AQUITY UPLC from Waters. ^1H-NMR spectra are reported as chemical shift in parts per million (multiplicity, coupling constant in Hz, integration).

General procedure for an amino acid coupling reaction in solution. C-terminal protected peptide (1 eq), Fmoc-protected amino acid (1.1 eq), HOBT (1.2 eq) and EDC (1.2 eq) were added to a round-bottomed flask. After addition of DCM (0.2 ~ 0.7 M) and DIEA (1.2 eq), the reaction mixture was stirred for 5-12 h at RT until the reaction was complete as analyzed by TLC. When the reaction was completed, DCM or EtOAc was added to dissolve the reaction mixture completely and the mixture was washed with 1N HCl and 5% $NaHCO_3$, three times each. The organic layer was dried over anhydrous Na_2SO_4. The solvent was evaporated and the residue was purified by Combiflash (normal phase).

General procedure for deprotection of the Fmoc group in solution. Fmoc groups of amino acids were deprotected as follows. Fmoc peptide (1 eq), octanethiol (10 eq) and DCM (0.5~0.1M) were added to a round-bottomed flask. After DBU (0.15 eq) was added, the reaction mixture was stirred for 15 h at rt. When the reaction was complete (by TLC monitoring), excess DCM was evaporated. The concentrated reaction mixture was purified by Combiflash (normal phase).

Synthesis of NB-E(OtBu)S(OtBu)A-OMe

Cbz-Ser(tBu)Ala-OMe, 1. H-Ala-OMe·HCl (1.0 g, 4.17 mmol), Cbz-Ser(tBu)-OH (4.59 mmol, 1.36 g), EDC·HCl (5.00 mmol, 959 mg), and HOBt·hydrate (5.00 mmol, 766 mg) were dissolved in 10 mL dry DCM and were cooled to 0 °C. DIEA (5.00 mmol, 885 μL) was added to the mixture, and the reaction was stirred for 4 h at rt. The usual workup and chromatography (acetone:DCM = 1:20) yielded Cbz-Ser(tBu)Ala-OMe (1.87 g, 90%) as a white powder. ^{1}H-NMR (500 MHz) δ 7.72 (d, J= 5.9 Hz, 1H),7.35 (m, 5H), 5.75 (d, J= 3.5 Hz, 1H), 5.14 (m, 2H),

4.83 (m, 1H), 4.27 (m, 1H), 3.83 (m, 1H), 3.76 (s, 3H), 3.44 (t, d= 8.3 Hz, 1H), 2.94 (dd, J=16.8, 4.4 Hz, 1H), 2.73 (dd, J= 17.0, 4.0 Hz, 1H), 1.44 (s, 9H), 1.24 (s, 9H) .

Cbz-Asp(OtBu)Ser(tBu)Ala-OMe, 2. Cbz-Ser(tBu)Ala-OMe (3.73 mmol, 1.79 g) was dissolved in 8 mL MeOH. 10% Pd/C (0.75 mmol, 80 mg) was added, and the reaction was stirred for 1 h at rt under H_2. After filtration of the catalyst through celite, the resulting amine product was used without further purification. H-Ser(tBu)Ala- OMe (3.73 mmol, 1. 29 g), Cbz-Asp(OtBu)-OH (4.10 mmol, 915 mg), EDC·HCl (4.48 mmol, 859 mg), and HOBt·hydrate (4.48 mmol, 686 mg) were dissolved in 10 mL dry DCM. DIEA (4.48 mmol, 579 µL) was added to the mixture, and the reaction was stirred for 5 h at rt. The usual workup and chromatography (MeOH:DCM = 1:50) yielded Cbz-Asp(OtBu)Ser(tBu)Ala-OMe (1.51 g, 74%) as a white powder. 1H-NMR (500 MHz) δ7.74 (d, J= 7.8 Hz, 1H), 7.34 (m, 5H), 6.82 (d, J= 4.6 Hz, 1H), 5.39 (d, H= 3.7 Hz, 1H), 5.13 (q, J=12.2 Hz, 2H), 4.83 (m, 1H), 4.43 (m, 1H), 4.30 (m, 1H), 3.81 (m, 1H), 3.76 (s, 3H), 3.38 (m, 1H), 2.93 (dd, J= 16.8, 4.6 Hz, 1H), 2.73 (dd, J= 16.8, 4.7 Hz, 1H), 1.44 (m,12H), 1.25 (s, 9H).

NB-Asp(OtBu)Ser(tBu)Ala-OMe, 3. Cbz-AlaSer(tBu)Asp(OtBu)-OMe (2.72 mmol, 1.5 g) was dissolved in 8 mL MeOH. 10% Pd/C (0.54 mmol, 60 mg) was added, and the reaction was stirred for 2 h at rt under H_2. After filtration of the catalyst with celite, the resulting amine product was used without further purification. H-AlaSer(tBu)Asp(OtBu)-OMe (2.72 mmol), 5-norbornene-exo-carboxylic acid (2.99 mmol, 413 mg), EDC·HCl (3.26 mmol, 625 mg), and HOBt·hydrate (3.26 mmol, 450 mg) were dissolved in 12 mL dry DCM. DIEA (3.26 mmol, 578 µL) was added to the mixture, and the reaction was stirred for 5 h at rt. The usual workup and chromatography (acetone:DCM = 1:11) yielded NB-Asp(OtBu)Ser(tBu)Ala-OMe (1.29 g, 88%) as a white powder. ^{1}H NMR (500 MHz) δ 7.70 (d, *J*= 8.0, 1H), 6.82 (t, *J*= 7.1, 1H), 6.21 (d, *J*=

6.2,1H), 6.15 (d, *J*= 2.8, 1H), 6.11 (m, 1H), 4.82 (m, 1H), 4.53 (dt, *J*= 12.9, 6.4, 1H), 4.44 (ddd, *J*= 10.8, 6.9, 3.5, 1H), 3.81 (dd, *J*= 8.6, 4.5, 1H), 3.75 (s, 3H), 3.40 (td, *J*= 8.3, 3.2, 1H), 2.93 (m, 3H), 2.73 (dd, *J*= 16.8, 4.8, 1H), 2.06 (dd, *J*= 7.2, 3.2, 1H), 1.92 (ddd, *J*=11.1, 7.4, 3.4, 1H), 1.70 (d, *J*= 8.3, 1H), 1.44 (m, 12H), 1.35 (m, 2H), 1.24 (s, 9H).

Solid phase peptide synthesis. Sieber amide resin (500 mg, 0.64 mmol) was swelled in DMF for 2 hr and washed with DMF three times. To remove the Fmoc group, 25% piperidine/DMF was added to the resin and the mixture was shaken for 10 min. This step was repeated three times. The resin was washed with DMF 6 times. To couple each amino acid, pre-mixed amino acid (3.2 mmol) with TBTU (3.2 mmol), HOBT hydrate (3.2 mmol), and DIEA (6.4 mmol) was added to the resin. The mixture was shaken for 2 h. The resin was washed with DMF 6 times. Each step was monitored by Kaiser test to check the presence of the primary amine. After coupling the last amino acid, 2.5 % TFA/DCM was added to the resin and it was agitated for 2 min. The solution was drained into the vial containing 2% pyridine in DCM. This step was repeated up to 10 times. The resin was washed with 3 × DCM and 3 × MeOH. The collected solution was evaporated, and the peptide was precipitated by adding water. The product was purified by column chromatography (5%-15% MeOH/DCM). This yielded NB-β-Ala-Bpa-GR(Pbf)GD(OtBu)S(OtBu)-CO-NH_2, **4** (yield: 40%-50%) as a yellowish solid (ESI mass spectrum:$[MH]^+$ calcd for $C_{65}H_{89}N_{11}O_{15}S$: 1296.63, found 1296.7) and NB-β-Ala-bpa-E(OtBu)S(OtBu)A-CO-NH_2, **5** (yield: 40-50%) as a white solid (ESI mass spectrum : $[MH]^+$ calcd for $C_{48}H_{65}N_7O_{11}$: 916.47, found 916.59).

Synthesis of NB-NHS, 6. *N*-hydroxysuccinimide (463 mg, 4.0 mmol), 5-norbornene-exocarboxylic acid (552 mg, 4.0 mmol), and EDC·HCl (694 mg, 3.6 mmol), were dissolved in 5 mL dry DCM. DIEA (709 μL, 4.0 mmol), was added to the mixture, and the reaction was stirred for 5 h at rt. The usual workup and chromatography (acetone:DCM = 2:10) yielded NB-NHS (672 mg, 79%) as a white powder. ^{1}H-NMR (500 MHz) δ 6.21 (dd, *J*= 5.5, 3.0 Hz, 1H), 3.28 (s, 1H), 3.01 (s, 1H), 2.84 (m, 4H), 2.51 (dd, *J*= 9.5, 5.0 Hz, 1H), 2.06 (dt, *J*=12.0, 4.0 Hz, 1H), 1.5 (m, 3H). MS (m/z) $[M]^+$ calcd for $C_{28}H_{45}N_3O_8$: 552.3, found: 552.3.

Synthesis of ROMP polymers. Peptide **4 or 5**, (5.8 mg, 4.5 μmol) was dissolved in 300 μL CH_2Cl_2/CH_3OH (3/1). To the reaction was oven-dried LiCl (51 mg, 1.1 mmol), $(H_2IMes)(PCy_3)Cl_2Ru$=CHPh (2.3 μmol, 2 mg) dissolved in 100 μL DCM/MeOH (3/1), and an additional 200 μL DCM/MeOH (3/1) at 0 °C under Ar. The reaction was stirred for 30 min at 25 °C under Ar. NB-Glu(OtBu)Ser(tBu)Ala-OMe, **3**, (111.7 mg, 202.5 μmol) and NB-NHS, **6**, (, 3.2 mg, 13.5 μmol) dissolved in 500 μL DCM/MeOH (3/1) was added to the reaction at 0 °C under Ar. The reaction was stirred for 1 h at rt under Ar. Peptide **4 or 5**, (5.8 mg, 4.5 μmol) was dissolved in 300 μL DCM/MeOH (3/1) was added to the reaction at 0 °C under Ar. The reaction was stirred for 2 h at rt under Ar. Ethylvinyl ether (1 mL) was added to quench the reaction, and the mixture was stirred for an additional 40 min. After removing the solvent by rotary evaporation, the residue was dissolved in DCM. The solution was washed three times with H_2O, dried with Na_2SO_4, concentrated by rotary evaporation, and precipitated with cold Et_2O (yield: 80-90%). The product **7a** or **7b** was isolated by centrifugation and dried. The protecting groups of amino acids on polymers were removed with TFA/TIPS/H_2O (95/2.5/2.5) for 5 h. The reaction mixture was concentrated with N_2 and was precipitated with cold Et_2O. The precipitate was collected by centrifugation. The deprotected polymer was re-dissolved in water and pH was

adjusted to ~8 using ammonium hydroxide. The resulting solution was diluted by water, the polymer **9a** and **9b** was precipitated with 1 N HCl. The precipitant was collected by centrifugation. The solid was washed with water three times and lyophilized (yield: 60-80%). The random copolymers, **8a**, **8b**, **10a** and **10b** were obtained by the same procedure as described above.

3-Azidopropyl acetate, 12. A mixture of Ac_2O (1.47 g, 1.35 mmol) and Et_3N (1.45 g, 14.4 mmol) was added to 3-bromo-propanol (2.00 g, 14.4 mmol) dissolved in DCM. The mixture was stirred at rt for 1 h. The DCM solution was washed with 2 × 5% $NaHCO_3$ and with 2 × brine. After drying with Na_2SO_4, the solvent was evaporated to yield compound **11** as colorless oil. Compound **11** was used without further purification. H_2O (40 mL) and NaN_3 (1.87g, 2.70 mmol) were mixed, and the mixture was stirred at 90 °C for 12 h. The product was extracted with DCM (3 × 40 mL). The organic layer was dried with Na_2SO_4. DCM was evaportated to yield **11** as a pale yellow oil (1.2 g, 60 % over two steps).

Tris(3-hydroxypropyltriazolylmethyl)amine, 14. To a solution of trispropargylamine (0.275 g, 2.09 mmol) and **12** (1.20 g, 8.38 mmol) in THF (40 mL) under N_2 was added CuOAc (5 mol%) and the resulting solution was heated to reflux overnight. The mixture was concentrated and dissolved in water (20 mL). 500 mg of Cuprisorb was added to the solution until the solution became colorless. The solution was filtered and concentrated. Product **13** was purified by Combiflash (0-5% MeOH/DCM) (0.46 g, 40%) as a pale yellow oil. The resulting compound was added to the solution of ammonia in MeOH (2M, 20 ml). The mixture was stirred for 12 hr, and solvent was evaporated under vacuum. The resulting pale yellow solid was dispersed in acetonitrile and sonicated for further break up of the solid. The fine solid was filtered and washed with acetonitrile. The solid was dried under vacuum to yield **14** (0.21 g, 40%): ^{1}H NMR

(500 MHz, DMSO-d_6) δ 8.03 (s, 3H), 4.68 (t, J = 4.95 Hz, 3H), 4.42 (t, J = 7.00 Hz, 6H), 3.63 (s, 6H), 3.40 (m, 6H), 1.97 (m, 6H); MS (m/z)) $[M]^+$ calcd for $C_{18}H_{30}N_{10}O_3$: 434.25, found: 434.5.

3-Azido-7-hydroxy-chromen-2-one (3-Azido-7-hydroxycoumarin), 16. A mixture of 2,4-dihydroxy benzaldehyde (2.76 g, 20.0 mmol), N-acetylglycine (2.34 g, 20.o mmol), anhydrous sodium acetate (4.9 g, 60.0 mmol) in acetic anhydride (100 mL) was stirred and heated reflux for 4 h. The mixture was poured onto ice to yield a yellow precipitate. After filtration, the yellow solid was washed with ice water before it was heated to reflux in a solution of conc. HCl and ethanol (2:1, 30 mL) for 1 h. Ice water then was added to dilute the solution. The solution was cooled in an ice bath and $NaNO_3$ (2.76 g, 40.0 mmol) was added. The mixture was stirred for 10 min and NaN_3 (3.9 g, 60 mmol) was added in portions. After stirring for another 15 min, the resulting solid was filtered off. The solid was washed with water and dried under vacuum to yield a brown solid. The product was used without further prufication. 40%): ^{1}H NMR (500 MHz, DMSO-d_6) δ 6.76 (d, J = 2.2 Hz, 1H), 6.82 (dd, J = 8.4 Hz, 1H), 7.49 (d, J = 8.5 Hz, aH), 7.61 (s, 1H); MS (m/z) $[M]^+$ calcd for $C_9H_5N_3O_3$: 203.03, found: 203.1.

2. Synthesis of intermediates and final products towards a cleavable biotin probe

General. Coupling reactions were performed under an Ar atmosphere using dry solvents. All commercially available reagents were purchased from Sigma-Aldrich and were used as received. NHS-LC-biotin and streptavidin agarose beads were purchased from Thermo Scientific. Spin ultrafilters (vivaspin 500) were purchased from GE Healthcare. ^{1}H and ^{13}C NMR spectra were recorded on Bruker instruments (400 or 500 MHz for ^{1}H and 100 or 125 MHz for ^{13}C). MS data were collected with an AQUITY UPLC from Waters.

Acetal 17.[279] To a solution of 4-carboxybenzaldehyde (2.00 g, 13.3 mmol) in dry MeOH (40 mL) was added ammonium chloride (4.00 g, 74.8 mmol). The mixture was heated under reflux for 20 h. The solvent was evaporated under reduced pressure and the product was recrystallized from boiling hexane (2.0 g, 77 %): ^{1}H NMR (500 MHz, CD_3OD) δ 7.81 (d, J = 8.4 Hz, 2H), 7.51 (d, J = 8.1 Hz, 2H), 5.43 (s, 1H), 3.68 –3.59 (m, 34H), 3.38 (m, 2H), 3.32 (s, 6H). ^{13}C NMR (126 MHz, $CDCl_3$) δ 171.94, 143.86, 130.21, 129.61, 126.98, 102.27, 52.70; MS (m/z) $[M]^-$ calcd for $C_{10}H_{12}O_4$: 196.2, found: 195.1.

Acetal 18. Carbonyldiimidazole (88.7 mg, 0.54 mmol) and **1** (107.4 mg, 0.54 mmol) were dissolved in DCM. The mixture was stirred for 30 min at rt. To the solution was added azido-PEG_8-amine (200 mg, 0.45 mmol). After 5 h, the solvent was evaporated under reduced pressure. Product **2** was obtained by gravity column chromatography (basic alumina, 0% - 5% MeOH/DCM) as an oil (210 mg, 75 %): ^{1}H NMR (500 MHz, $CDCl_3$) δ 7.87 – 7.75 (m, 2H), 7.51 (d, J = 8.1 Hz, 2H), 5.43 (s, 1H), 3.73 – 3.56 (m, 34H), 3.42 – 3.35 (m, 2H), 3.32 (s, 6H); ^{13}C NMR (126 MHz, $CDCl_3$) δ 167.17, 167.15, 141.31, 134.66, 127.04, 127.02, 126.88, 102.35, 70.68-69.77, 52.61, 50.66, 39.80; MS (m/z) $[M+H]^+$ calcd for $C_{28}H_{48}N_4O_{11}$: 617.33, found: 617.48.

Trifluoroacetamide 19. To a solution of 3-amino-1,2-propanediol (250 mg, 2.74 mmol) in THF, ethyl trifluoroacetate (2.33 g, 16.46 mmol) was added drop-wise. After 4 h, the solvent was evaporated. DCM was added to the oil and evaporated. This step was repeated two more times. Benzene was added and evaporated. This step was also repeated two more times. The resulting product was used without further purification to yield compound **19**: ^{1}H NMR (500 MHz, $CDCl_3$) δ = 3.3-3.6 (4H, m), 4.7-4.85 (1H, m); MS (m/z): $[M]^-$ calcd for $C_5H_8F_3NO_3$: 186.05, found: 185.98.

Trifluoroacetamide 20. Trifluoracetamide **20** was prepared from serinol (250 mg, 2.74 mmol) and ethyl trifluoroacetate (2.33 g, 16.46 mmol) as described for **19** to yield compound **20**: ^{1}H NMR (500 MHz, $CDCl_3$) δ = 3.45-3.55 (4H, m), 3.75-3.9 (1H, m), 4.75 (2H, t), 9 (1H, m); MS (m/z) : $[M]^-$ calcd for $C_5H_8F_3NO_3$: 186.05, found: 185.98.

Trifluoroacetamide 21. To a solution of **19** or **20** (191 mg, 1.022 mmol) in THF/toluene (3/7), **18** (20 mg, 0.34 mmol) and *p*-toluene sulfonic acid•H_2O (13 mg, 0.068 mmol) were added. The mixture was heated to 100 °C. The solvent was distilled to remove H_2O generated during the reaction and toluene added to maintain reaction volume as the reaction proceeded. After 4 h, the reaction was quenched with 50 μL of TEA. Product **21** was obtained by column chromatography (basic alumina, 0%-5% MeOH/DCM) as an oil: **21a** (from **20,** 180 mg, 72 %)**:** ^{1}H NMR (500 MHz, CD_3OD) δ 7.94 – 7.80 (m, 2H), 7.66 – 7.58 (m, 2H), 5.78 – 5.55 (m, 1H), 4.41 – 4.16 (m, 4H), 3.92 – 3.83 (m, 1H), 3.74 – 3.56 (m, 34H), 3.42 – 3.36 (m, 2H); MS (m/z): $[M+H]^+$ calcd for $C_{31}H_{48}F_3N_5O_{12}$: 740.36, found: 740.66**. 21b** (from **19,** 160 mg, 64 %)**:** ^{1}H NMR (500 MHz, CD_3OD) δ 7.88 (dt, *J* = 17.2, 7.8 Hz, 2H), 7.68 – 7.53 (m, 2H), 5.93 (d, *J* = 86.5 Hz,1H), 4.51 – 4.39 (m, 1H), 4.20 (ddd, *J* = 53.7, 8.5, 6.8 Hz, 1H), 4.01 – 3.76 (m, 1H), 3.73 – 3.59 (m, 34H), 3.59 – 3.50 (m, 2H), 3.38 (dd, *J* = 11.9, 6.6 Hz, 2H); MS (m/z): $[M+NH_4]^+$ calcd for $C_{31}H_{48}F_3N_5O_{12}$: 757.36, found: 757.55.

Amine 22. To a solution of **21a** or **21b** (160 mg, 0.22 mmol) in MeOH/H_2O (7/3) K_2CO_3 (209.35 mg, 1.5149 mmol) was added. The reaction was heated at reflux for 2 h. After evaporating all the solvent, the product was purified by gravity column chromatography (basic alumina, 2%-10% MeOH/DCM) to yield **22** as an oil. **22a** (from **21a**, 134 mg, 82 %): ^{1}H NMR (500 MHz, $CDCl_3$) δ 7.84 (dd, *J* = 11.2, 5.0 Hz, 2H), 7.60 – 7.51 (m, 2H), 5.58 – 5.26 (m, 1H), 4.39 – 3.95 (m, 4H), 3.64 (dd, *J* = 18.3, 3.7 Hz, 34H), 3.38 (d, *J* = 4.4 Hz, 2H), 3.33 – 3.13 (m,

1H): [M+H]+ calcd for $C_{29}H_{49}N_5O_{11}$: 644.34, found: 644.49. **22b** (from **21b,** 105 mg, 80 %): ^{1}H NMR (400 MHz, $CDCl_3$) δ = 7.82 (dt, *J* = 18.4, 9.2 Hz, 2H), 7.53 (dd, *J* = 16.4, 9.0 Hz, 2H), 6.05 –5.78 (m, 1H), 4.40 – 4.23 (m, 1H), 4.14 (ddd, *J* = 38.0, 16.3, 9.2 Hz, 1H), 3.92 – 3.72 (m, 1H), 3.70 – 3.55 (m, 34H), 3.37 (t, *J* = 4.9 Hz, 2H), 3.05 – 2.81 (m, 2H). MS (m/z): $[M+H]^+$ calcd for $C_{29}H_{49}N_5O_{11}$: 644.34, found: 644.57.

Amide 23. d-Biotin or NHS-LC-biotin (50.0 mg, 0.205 mmol) and carbonydiimidazole (33.0 mg, 0.205 mmol) were dissolved in dried DMF. The mixture was stirred for 30 min. To the mixture, **22** was added and the reaction was stirred for 12 h at rt. The product was purified by gravity column chromatography (neutral alumina, 3%-7% MeOH/DCM) to yield **7** as an oil. Compound **23a** (90 mg, 50 %): ^{1}H NMR (400 MHz, CD_3OD) δ 7.86 (t, *J* = 6.7 Hz, 2H), 7.61 (dd, *J* = 25.3, 8.3 Hz, 2H), 5.62 (dd, *J* = 65.0, 13.7 Hz, 1H), 4.66 – 44.09 (m, 5H), 3.82 (s, 1H), 3.65 (m, 35H), 3.43 – 3.35 (m, 2H), 3.29 –3.13 (m, 1H), 3.01 – 2.71 (m, 2H), 2.46 – 2.16 (m, 2H), 1.86 – 1.36 (m, 6H); MS (m/z) : $[M+H]^+$ calcd for $C_{39}H_{63}N_7O_{13}S$: 870.42, found: 870.38. Compound **23b** (100 mg, 67%): ^{1}H NMR (400 MHz, CD_3OD) δ 7.88 (t, *J* = 7.8 Hz, 2H), 7.60 (dd, *J* = 21.2, 8.3 Hz, 2H), 6.00 – 5.83 (d, 1H), 4.53 – 4.30 (m, 2H), 4.23 – 4.10 (m, 2H), 3.89 – 3.83 – 3.72 (m, 2H), 3.65 (m, 34H), 3.55 – 3.41 (m, 2H), 3.41 – 3.37 (m, 2H), 3.23 – 3.10 (m, 1H), 2.95 – 2.84 (m, 1H), 2.70 (d, *J* = 12.7 Hz, 1H), 2.35 – 2.17 (m, 2H), 1.85 – 1.35 (m, 6H); MS (m/z): [M+H]+ calcd for $C_{39}H_{63}N_7O_{13}S$: 870.42, found: 870.72. Compound **23c** (70 mg, 61%): ^{1}H NMR (500 MHz, MeOD) δ 7.89 (t, *J* = 7.6 Hz, 2H), 7.61 (dd, *J* = 25.3, 8.2 Hz, 2H), 5.93 (d, *J* = 81.6 Hz, 1H), 4.54 – 4.47 (m, 1H), 4.41 – 4.28 (m, 2H), 4.27-4.09 (m, 1H), 3.84 (ddd, *J* = 14.9, 8.3, 6.0 Hz, 1H), 3.74 – 3.58 (m, 34H), 3.46 (dddd, J = 22.8, 13.5, 11.9, 6.0 Hz, 4H), 3.26 – 3.13 (m, 3H), 2.99 – 2.91 (m, 1H), 2.73 (dd, *J* = 12.7, 4.5 Hz, 1H), 2.24 (ddd, J = 20.6, 14.2, 7.3 Hz, 4H), 1.72 – 1.31 (m, 12 H); HRMS (m/z): $[M+H]^+$ calcd for $C_{45}H_{74}N_8O_{14}S$: 982.5, found 983.505.

Biotin-PEG$_{10}$-N$_3$, 24. Biotin-NHS (0.31 mmol, 107 mg) and *O*-(2-Aminoethyl)-*O′*-(2-azidoethyl)nonaethylene glycol (0.21 mmol, 110 mg) were dissolved in 1 mL dry DMF. DIEA (0.31 mmol, 56 μL) was added to the mixture, and the reaction was stirred for 16 h at rt. After evaporation of solvent, the product was precipitated with Et_2O. Chromatography (MeOH:EtOAc/1:1) yielded product **24**: ^{1}H NMR (500 MHz, d_6-DMSO) δ 7.81 (t, *J*= 5.5, 1H), 6.40 (br s, 1H), 6.34 (br s, 1H), 4.30 (m, 1H), 4.12 (m, 1H), 3.60 (m, 2H), 3.53 (m, 38H), 3.39 (t, *J*= 5.1, 4H), 3.18 (q, *J*= 5.8, 2H), 3.09 (dd, *J*= 11.7, 7.3, 1H), 2.82 (dd, *J*= 12.4, 5.1, 1H), 2.58 (d, *J*= 12.4, 1H), 2.06 (t, *J*= 7.4, 2H), 1.62 (dd, *J*= 21.4, 7.9, 1H), 1.50 (dt, *J*= 14.4, 7.5, 3H), 1.30 (m, 2H); MS (m/z): $[M+H]^+$ calcd for $C_{32}H_{60}N_6O_{12}S$: 753.4, found: 753.4.

3. Synthesis of Boc-Lys(Ac)-Puromycin (Boc-KAc-Puro). A mixture of puromycin dihydrochloride (50 mg, 0.092 mmol), α-Boc-Lys(ε-Ac)-OH (31 mg, 0.11mmol), EDC·HCl (21 mg, 0.11 mmol), HOBt·H_2O (17 mg, 0.11 mmol), and DIEA (N,N-diisopropylethylamine) (18 μL, 0.11 mmol) was stirred in DMF (10 ml) at rt for 18 h. After concentrating the solution under reduced pressure, the residue was dissolved in DCM. The DCM solution was washed with H2O three times, dried over Na_2SO_4, and concentrated. The crude oil was purified by silica gel column chromatography using a linear gradient from 5 to 10 % MeOH in DCM and dried to yield α-Boc-Lys(ε-Ac)-Puromycin as a white solid (55 mg,75 % yield): mp: 182-183 °C; ^{1}H NMR (500 MHz, DMSO) δ 8.43 (s, 1H), 8.22 (s, 1H), 8.15 (d, *J* =7.7 Hz, 1H), 7.74 (d, *J* = 7.1 Hz, 2H, H-2'), 7.15 (d, *J* = 8.4 Hz, 2H), 6.86 (d, *J* = 8.3 Hz, 1H), 6.80 (d, *J* = 8.6 Hz, 2H), 6.03 (d, *J* = 4.6 Hz, 1H), 5.98 (d, *J* = 2.8 Hz, 1H), 5.18 (t, *J* = 5.4 Hz, 1H), 4.60 (dd, *J* = 13.6, 8.1 Hz, 1H), 4.52 – 4.39 (m, 2H, H-25), 3.98 – 3.76 (m, 2H), 3.70 (s, 3H), 3.69 –3.40 (m, 6H, H-34), 3.02 – 2.86 (m, 3H, H-3), 2.76 (dd, *J* = 13.7, 8.7 Hz, 1H), 1.77 (s, 3H), 1.52 – 1.38 (m, 2H), 1.38 – 1.32 (s, 9H), 1.33– 1.05 (m, 6H) ppm. ^{13}C NMR (101 MHz, DMSO) d 169.5, 158.4, 155.8,

154.8, 152.4, 150.2, 138.4, 138.3, 131.0, 129.8, 120.2, 114.0, 90.0, 78.8, 73.8, 61.5, 55.6, 55.3, 54.5, 51.0, 40 (underneath DMSO peak), 39.1, 38.2, 32.5, 29.5, 28.9, 23.7, 23.4; HRMS (*m/z*): $[M]^+$ calcd. for $C_{35}H_{51}N_9O_9$, 742.38; found, 742.3880

3. Preparation of FDG-AOAc-GYPMP

Coupling cold FDG to AOAc-GYPMP. To 200 μl of reaction solution (saline containing 4% TFA and 16% EtOH), FDG (2.0 mg, 4 eq) and AOAc-GYPMP (2.0 mg, 1 eq) was added. The mixture was stirred for 20 min at 100 °C using in a sealed vial. After quenching the reaction by adding 1ml of borate buffer (25 mM, pH9), the crude reaction mixture was injected onto a HPLC column (C18, 300Å, analytical column). After purification, the fraction containing the product was diluted with 10 mL of H_2O, loaded onto a C18 Sep-Pak, washed 10 mL of H_2O, and eluted with 2 mL of absolute ethanol. After evaporating ethanol, the identity of the product was confirmed by LC/MS (yield: 62%).

Coupling ^{18}FDG to AOAc-GYPMP. The solution containing ^{18}FGD was reduced by Ar purge. The resulting solid and AOAc-GYPMP were dissolved in 200 μL of reaction solution containing 5 μL of TFA. The mixture was stirred for 20 min at 100 °C using in a sealed vial. The purification step was the same procedure used for cold FDG coupling. The final product was used directly for biological experiments.

4. Cell migration assay

Transfection with plasmid DNA

1) COS-1 cells were plated on 3cm plates.
2) Each plasmid DNA (GFP, empty vector, and MT1-MMP) was incubated in 150 μL of 150 mM NaCl with 1 μL of 1 mg/mL of PEI in microcentrifuge tube.
3) The media was aspirated from the 3 cm plate
4) 850 μL of fresh media (DMEM) and the solution prepared above were added to the plate
5) The cells were incubated 16 h

Transwell Migration Assay

1) Set up chambers, such that each set is done in triplicate:
   a) Clean chambers by soaking in water
   b) Put 205 μL media in bottom of well
   c) Place polycarbonate membrane over the solution, shiny side down, avoid air bubbles
   d) Screw on the cap until it is firm; do not use excessive force
2) Prepare cells:
   a) Trypsinize the cells and neutralize with DMEM containing 10% FBS
   b) Collect the cells into 15 mL tubes
   c) Spin down at 1000 g for 5 min
   d) Aspirate most of the media and add fresh media
   e) Spin at 1000 g for 5 min and remove most of the media
   f) Resuspend in media and count the cells
   g) Adjust the cell concentration to 125,000 cells/mL
   h) Put 200 μL of cells in each chamber on top of the polycarbonate membrane
   i) Incubate 37 °C for 6-18 hr
3) Next day:

a) Prepare 2 Q-tips for each sample
b) Prepare 4% w/v paraformaldehyde (PFA) in PBS, and place in 12-well plates
c) Prepare crystal violet solution
d) Swab membrane with Q-tip to soak up the media
e) Add 200 μL of PBS to membrane and swab with new Q-tip
f) Repeat step d
g) Unscrew cap
h) Put membrane in 4% PFA/PBS, shiny side down
i) Fix the cells for at least 20 min
j) Prepare 6-well plates with PBS
k) Stain with crystal violet for 20 min exactly
l) Wash the membrane with PBS in 6-well plates
m) Place on glass slide and count the stained cells

Crystal violet: 11.72 mL of borate-buffered saline (0.17 M, pH 9.3)

7.82 mL H_2O

400 μL of EtOH (100%)

0.2 g of crystal violet

Borate buffered saline: 6.184 g of boric acid, 9.536 g of borax (sodium tetraborate), 4.384 g of NaCl, in 1 L of H_2O (adjust pH to 7.3 with 0.15 M NaOH).

5. Cell attachment assay protocol

1) Harvest cells and resuspend cells in DMEM at 1×10^6 cell/mL.
2) Incubate the cell with 2 μM of calcein AM for 30 min at 25 °C.
3) Spin down the cells at 1000 g for 10 min and remove the supernatant.

4) Add binding buffer and gently pipet up and down until the cells are separated individually. Spin down the cells at 1000 g for 10 min. Repeat step 6-7 two more times to remove remaining calcein-AM.
5) The cells stained with calcein-AM were incubated with each polymer for 2 h at 37 °C in the dark. Then, irradiate the cells with UV light (λ_{max} = 350 nm, under 4 cm) at 4 °C for 15 min.
6) Wash the cells following step 6-7.
7) Reconstitute the cells using binding buffer.
8) Meanwhile, coat 96-well plate with 10 μg of vitronectin in PBS containing 0.1 % BSA for 1.5 h.
9) Remove the vitronectin solution and gently wash the wells with PBS three times
10) Add 1% BSA/PBS (blocking solution) to block the wells.
11) Remove the blocking solution and add the cells treated with polymer.
12) Add 10^5 cells treated with polymer to vitronectin coated plate.
13) Allow the cells to adhere to vitronectin for 2 h at 37 °C in the dark.
14) Wash the non-adherent or loosely bond cells and add 150 μL of PBS.
15) Read the plate in a fluorescent plate reader at an excitation wavelength of 480 nm and an emission wavelength of 530 nm.

6. Photoaffinity labeling protocol

Preparation of cell

1) Detach U87-MG with trypsin-EDTA

2) Wash the cells with 1 × PBS, 1 × 10%FBS/DMEM, 1 × binding buffer
3) Resuspend the cells with binding buffer to give 1×10^6 cells/mL

Photoaffinity cross-linking

1) Incubate the cells in binding buffer (HEPES pH 7.4, 150 mM NaCl, 2 mM $MnCl_2$, 1mM $CaCl_2$, and 1 mM $MgCl_2$, 0.1 % polyvinylpyrrolidone) for 30 min for blocking.
2) Add appropriate concentration of the polymers and incubate for 2 hr at 37 °C.
3) Place the cells under UV lamp (14 watts, 4 cm above, λ_{max} = 350 nm, southern New England Ultraviolet Company, cat# PMR 3500) at 4°C and incubate for 15 min.
4) Collect the cells in a microcentrifuge tube.
5) Wash the cells with three times with PBS.
6) Lysis the cells with 500 μL of RIPA buffer by incubating the cells on ice for 1 hr and sonicate the lysate three times for 3 sec each.
7) Centrifuge the lysate at 15,000 g for 10 min.
8) Transfer the supernatant to a clean tube.

Pre-clearing

1) Wash Neutravidin agarose beads with 1mL of PBS three times
2) Add PBS to make a 50% slurry of bead.
3) Add 100 μL of the bead to the sample and incubate it for 1 h at 25 °C.
4) Centrifuge it at 1400 g for 3 min and transfer the supernatant to a clean tube.

Click reaction[148]

1) Add 10 μL of biotin-PEG_{10}-azide from 20 mM stock solution to 500 μL of pre-cleared cell lysates.
2) Add 7.5 μL of premixed $CuSO_4$ and THPTA (2.5 μL of $CuSO_4$ from 20 mM stock solution in water and 5 μL of THPTA from 50 mM stock solution in water).
3) Add 25 μL of aminoguanidine from 100 mM stock solution in water.
4) Add 25 μL of sodium ascorbate from 100 mM stock solution in water.
5) Mix well and incubate the reaction mixture for 1 h.
6) To quench the reaction, add 10 μL of 200mM EDTA.
7) Concentrate the samples using a microconcentrator (MWCO = 10 kDa) and replace the solvent with PBS.

Biotin-avidin affinity purification

1) Prepare Neutravidin beads as described above.
2) Add 100 μL of the beads and incubate it for 3 h at 25 °C.
3) Wash the beads with 0.2 % SDS/PBS for 10 min, 3 × 1 mL of PBS and 3 × 1 mL of H_2O. Now, hereafter referred to as loaded-beads.

On-bead tryptic digestion

1) 50 μL of a 6 M urea/PBS solution and 2.5 μL of a 200 mM TCEP solution in H_2O were added to the loaded beads
2) The tube was placed in a 65 °C heat-block for 15 min, then cooled to 35 °C.

3) 2.5 µL of a 400 mM iodoacetamide in water solution was added, and the mixture was incubated for 30 min at 35 °C.

4) The reaction was diluted with 95 µL PBS, centrifuged at 1 400 *g* for 2 min and the supernatant was removed.

5) 200 µL of a 2 M urea/PBS solution, 2 µL of 100 mM calcium chloride in water, and 4 µL of a stock trypsin solution (20 µg reconstitute in 40 µL of the trypsin buffer) were added to the beads. The reaction was incubated for 16 h at 37 °C. The mixture was centrifuged, and the supernatant collected.

6) The resulting solution was lyophilized

Desalting.10 µL of 0.1% TFA in H2O was added to the lyophilized tryptic digest.

A C18 zip-tip was washed with 0.1% TFA in ACN/ H_2O (1:1) twice, and was washed with 0.1% TFA in H_2O ten times. The tryptic digest solution was loaded on the zip-tip, and the solvent was expelled from the zip-tip. The sample loaded zip-tip was washed with 0.1% TFA in H_2O five times. The sample peptide in the zip-tip was eluted with 5 µL of 0.1% TFA in ACN five times. The eluted solutions were combined and lyophilized.

Mass analysis. 1.5 µL of 0.1% TFA in ACN/ H_2O (1:1) and 1.5 µL of saturated α–cyano-4-

hydroxycinnamic acid solution were added to the lyophilized sample. The whole sample solution was loaded onto a target plate by loading 1 μL each for MALDI-TOF spectroscopic analysis.

6. Cleavable biotin probe protocol

Alkyne functionalized bovine serum albumin. To a solution of bovine serum albumin (BSA) (20 μM) in PBS, N-(1-propynyl)-maleimide (120 μM) was added. The mixture was gently agitated for 12 h in the dark. The excess maleimide was removed using an ultrafiltration spin filter (MWCO = 3 kDa).

Chapter 4 Preparation of bovine serum albumin labeled with biotin probe. Alkyne functionalized BSA (50 μM) was mixed with biotin probe **7a** or **7b** (100 μM), BTTP (200 μM), $CuSO_4$ (100 μM), and sodium ascorbate (2.5 mM) for 1 h at rt. The reagents were removed using an ultrafiltration spin filter (MWCO = 3 kDa). The concentration of BSA was measured by Pierce Coomassie Plus protein assay, following the manufacturer's instructions.

Cleavage test. After coupling of BSA to probe, the mixture was incubated with streptavidin-ultralink resin or streptavidin-agarose resin for 1 h at rt. The beads loaded with biotinylated BSA were spun at 1000 g for 3 min. The pelleted beads were washed sequentially with 1% SDS in PBS, 6M urea in 250 mM ammonium bicarbonate, 1 M NaCl in PBS, and two times with H_2O. The beads were incubated in 1% TFA for 1 h at 37 °C. The supernatant was collected by pelleting the beads. The beads were washed sequentially with 0.1% SDS/PBS, and two times with PBS and the supernatant was combined with the washes. The combined solutions were concentrated using an ultrafiltration spin filter (MWCO = 3 kDa) at 7,000 g. After two more washes with PBS, the beads were boiled in sample loading buffer for 15 min.

Analysis of protein capture and release. Each protein sample was separated by 12% or 15% SDS-PAGE gel and transferred onto a PDVF membrane (Bio Rad). The membrane was blocked with 4% BSA/TBST for 1 h at rt. After washing the membrane with TBST three times, streptavidin conjugated with Alexa-488 (20 mg/mL) was added and the solution was gently agitated for 1 h at 25°C. The membrane was washed with TBST three times and was visualized using a Typhoon 9400 scanner (GE Healthcare).

References

1. Evans, J.P. and Florman, H.M. (2002). The state of the union: the cell biology of fertilization. *Nat Cell Biol 4 Suppl*, s57-63.
2. Yanagimachi, R. (1994). The physiology of reproduction. *New York: Raven Press*189-317.
3. Gratkin, R.B.L. (1977). Fertilization mechanisms in man and mammals. *New York: Plenum*.
4. Harvey M. Florman, C.A., Imrana G. Kazam, Chngqing Le, and Christine M.B. O'Toole. (1995). An intimate biochemistry: egg-regulated acrosome reactions of mammaliam sperm. *Adv Dev Biochem 5*, 147-186.
5. Vjugina, U. and Evans, J.P. (2008). New insights into the molecular basis of mammalian sperm-egg membrane interactions. *Front Biosci 13*, 462-76.
6. Runft, L.L., Jaffe, L.A., and Mehlmann, L.M. (2002). Egg activation at fertilization: Where it all begins. *Dev Biol 245*, 237-254.
7. Stricker, S.A. (1999). Comparative biology of calcium signaling during fertilization and egg activation in animals. *Dev Biol 211*, 157-76.
8. Lee, J. (2006). Probing ligand-receptor interactions in mammalian fertilization using ring oepning metathesis polymerization. *Ph.D. Thesis, Stony Brook University, Stony Brook*.
9. Wolfsberg, T.G. and White, J.M. (1996). ADAMs in fertilization and development. *Dev Biol 180*, 389-401.
10. Wolfsberg, T.G., Straight, P.D., Gerena, R.L., Huovila, A.P., Primakoff, P., Myles, D.G. and White, J.M. (1995). ADAM, a widely distributed and developmentally regulated gene family encoding membrane proteins with a disintegrin and metalloprotease domain. *Dev Biol 169*, 378-83.
11. Saunders, C.M., Larman, M.G., Parrington, J., Cox, L.J., Royse, J., Blayney, L.M., Swann, K. and Lai, F.A. (2002). PLC zeta: a sperm-specific trigger of Ca(2+) oscillations in eggs and embryo development. *Development 129*, 3533-44.
12. Gould, R.J., Polokoff, M.A., Friedman, P.A., Huang, T.F., Holt, J.C., Cook, J.J. and Niewiarowski, S. (1990). Disintegrins - a Family of Integrin Inhibitory Proteins from Viper Venoms. *Proc Soc Exp Biol Med 195*, 168-171.
13. Blobel, C.P. and White, J.M. (1992). Structure, function and evolutionary relationship of proteins containing a disintegrin domain. *Curr Opin Cell Biol 4*, 760-5.
14. Evans, J.P. (2001). Fertilin beta and other ADAMs as integrin ligands: insights into cell adhesion and fertilization. *Bioessays 23*, 628-39.
15. Eto, K., Huet, C., Tarui, T., Kupriyanov, S., Liu, H.Z., Puzon-McLaughlin, W., Zhang, X.P., Sheppard, D., Engvall, E. and Takada, Y. (2002). Functional classification of ADAMs based on a conserved motif for binding to integrin alpha 9beta 1: implications for sperm-egg binding and other cell interactions. *J Biol Chem 277*, 17804-10.
16. Evans, J.P. (1999). Sperm disintegrins, egg integrins, and other cell adhesion molecules of mammalian gamete plasma membrane interactions. *Front Biosci 4*, D114-31.
17. Cuasnicu, P.S., Ellerman, D.A., Cohen, D.J., Busso, D., Morgenfeld, M.M. and Da Ros, V.G. (2001). Molecular mechanisms involved in mammalian gamete fusion. *Arch Med Res 32*, 614-8.

18. Primakoff, P., Hyatt, H. and Tredick-Kline, J. (1987). Identification and purification of a sperm surface protein with a potential role in sperm-egg membrane fusion. *J Cell Biol 104*, 141-9.
19. Hardy, C.M., Clarke, H.G., Nixon, B., Grigg, J.A., Hinds, L.A. and Holland, M.K. (1997). Examination of the immunocontraceptive potential of recombinant rabbit fertilin subunits in rabbit. *Biol Reprod 57*, 879-86.
20. Bigler, D., Takahashi, Y., Chen, M.S., Almeida, E.A., Osbourne, L. and White, J.M. (2000). Sequence-specific interaction between the disintegrin domain of mouse ADAM 2 (fertilin beta) and murine eggs. Role of the alpha(6) integrin subunit. *J Biol Chem 275*, 11576-84.
21. Evans, J.P., Schultz, R.M. and Kopf, G.S. (1997). Characterization of the binding of recombinant mouse sperm fertilin alpha subunit to mouse eggs: evidence for function as a cell adhesion molecule in sperm-egg binding. *Dev Biol 187*, 94-106.
22. Evans, J.P., Kopf, G.S. and Schultz, R.M. (1997). Characterization of the binding of recombinant mouse sperm fertilin beta subunit to mouse eggs: evidence for adhesive activity via an egg beta1 integrin-mediated interaction. *Dev Biol 187*, 79-93.
23. Yuan, R., Primakoff, P. and Myles, D.G. (1997). A role for the disintegrin domain of cyritestin, a sperm surface protein belonging to the ADAM family, in mouse sperm-egg plasma membrane adhesion and fusion. *J Cell Biol 137*, 105-12.
24. Linder, B. and Heinlein, U.A. (1997). Decreased in vitro fertilization efficiencies in the presence of specific cyritestin peptides. *Dev Growth Differ 39*, 243-7.
25. Zhu, X., Bansal, N.P. and Evans, J.P. (2000). Identification of key functional amino acids of the mouse fertilin beta (ADAM2) disintegrin loop for cell-cell adhesion during fertilization. *J Biol Chem 275*, 7677-83.
26. Almeida, E.A., Huovila, A.P., Sutherland, A.E., Stephens, L.E., Calarco, P.G., Shaw, L.M., Mercurio, A.M., Sonnenberg, A., Primakoff, P., Myles, D.G. and White, J.M. (1995). Mouse egg integrin alpha 6 beta 1 functions as a sperm receptor. *Cell 81*, 1095-104.
27. Chen, H. and Sampson, N.S. (1999). Mediation of sperm-egg fusion: evidence that mouse egg alpha6beta1 integrin is the receptor for sperm fertilinbeta. *Chem Biol 6*, 1-10.
28. Takahashi, Y., Bigler, D., Ito, Y. and White, J.M. (2001). Sequence-specific interaction between the disintegrin domain of mouse ADAM 3 and murine eggs: role of beta1 integrin-associated proteins CD9, CD81, and CD98. *Mol Biol Cell 12*, 809-20.
29. Gupta, S., Li, H. and Sampson, N.S. (2000). Characterization of fertilin beta-disintegrin binding specificity in sperm-egg adhesion. *Bioorg Med Chem 8*, 723-9.
30. Myles, D.G., Kimmel, L.H., Blobel, C.P., White, J.M. and Primakoff, P. (1994). Identification of a binding site in the disintegrin domain of fertilin required for sperm-egg fusion. *Proc Natl Acad Sci U S A 91*, 4195-8.
31. Huovila, A.P., Turner, A.J., Pelto-Huikko, M., Karkkainen, I. and Ortiz, R.M. (2005). Shedding light on ADAM metalloproteinases. *Trends Biochem Sci 30*, 413-22.
32. Evans, J.P. (2002). The molecular basis of sperm-oocyte membrane interactions during mammalian fertilization. *Hum Reprod Update 8*, 297-311.
33. Lee, Y. (2008). Ph. D. Thesis, Stony Brook University
34. Baessler, K.A., Lee, Y., Roberts, K.S., Facompre, N. and Sampson, N.S. (2006). Multivalent fertilin beta oligopeptides: The dependence of fertilization inhibition on length and density. *Chem Biol 13*, 251-259.

35. He, Z.Y., Brakebusch, C., Fassler, R., Kreidberg, J.A., Primakoff, P. and Myles, D.G. (2003). None of the integrins known to be present on the mouse egg or to be ADAM receptors are essential for sperm-egg binding and fusion. *Dev Biol 254*, 226-37.
36. Sampson, N.S., Baessler, K.A. and Lee, Y.J. (2009). beta(1) Integrin Is an Adhesion Protein for Sperm Binding to Eggs. *ACS Chem Biol 4*, 357-366.
37. Xu, J., Rodriguez, D., Petitclerc, E., Kim, J.J., Hangai, M., Moon, Y.S., Davis, G.E. and Brooks, P.C. (2001). Proteolytic exposure of a cryptic site within collagen type IV is required for angiogenesis and tumor growth in vivo. *J Cell Biol 154*, 1069-79.
38. Bianchi, E., Ferrero, E., Fazioli, F., Mangili, F., Wang, J., Bender, J.R., Blasi, F. and Pardi, R. (1996). Integrin-dependent induction of functional urokinase receptors in primary T lymphocytes. *J Clin Invest 98*, 1133-41.
39. Tang, C.H. and Wei, Y. (2008). The urokinase receptor and integrins in cancer progression. *Cell Mol Life Sci 65*, 1916-32.
40. Chapman, H.A. and Wei, Y. (2001). Protease crosstalk with integrins: the urokinase receptor paradigm. *Thromb Haemost 86*, 124-9.
41. Bohuslav, J., Horejsi, V., Hansmann, C., Stockl, J., Weidle, U.H., Majdic, O., Bartke, I., Knapp, W. and Stockinger, H. (1995). Urokinase plasminogen activator receptor, beta 2-integrins, and Src-kinases within a single receptor complex of human monocytes. *J Exp Med 181*, 1381-90.
42. May, A.E., Kanse, S.M., Lund, L.R., Gisler, R.H., Imhof, B.A. and Preissner, K.T. (1998). Urokinase receptor (CD87) regulates leukocyte recruitment via beta 2 integrins in vivo. *J Exp Med 188*, 1029-37.
43. Berditchevski, F., Bazzoni, G. and Hemler, M.E. (1995). Specific association of CD63 with the VLA-3 and VLA-6 integrins. *J Biol Chem 270*, 17784-90.
44. Lin, T.H., Chen, Q., Howe, A. and Juliano, R.L. (1997). Cell anchorage permits efficient signal transduction between ras and its downstream kinases. *J Biol Chem 272*, 8849-52.
45. Renshaw, M.W., Ren, X.D. and Schwartz, M.A. (1997). Growth factor activation of MAP kinase requires cell adhesion. *EMBO J 16*, 5592-9.
46. McCormick, J.I. and Johnstone, R.M. (1995). Identification of the integrin alpha 3 beta 1 as a component of a partially purified A-system amino acid transporter from Ehrlich cell plasma membranes. *Biochem J 311 (Pt 3)*, 743-51.
47. Brown, E.J. (2002). Integrin-associated proteins. *Curr Opin Cell Biol 14*, 603-607.
48. Heckmann, D. and Kessler, H. (2007). Design and chemical synthesis of integrin ligands. *Methods Enzymol 426*, 463-503.
49. Verrier, S., Pallu, S., Bareille, R., Jonczyk, A., Meyer, J., Dard, M. and Amedee, J. (2002). Function of linear and cyclic RGD-containing peptides in osteoprogenitor cells adhesion process. *Biomaterials 23*, 585-96.
50. Yoon, S.O., Park, S.J., Yoon, S.Y., Yun, C.H. and Chung, A.S. (2002). Sustained production of H(2)O(2) activates pro-matrix metalloproteinase-2 through receptor tyrosine kinases/phosphatidylinositol 3-kinase/NF-kappa B pathway. *J Biol Chem 277*, 30271-82.
51. Berggard, T., Linse, S. and James, P. (2007). Methods for the detection and analysis of protein-protein interactions. *Proteomics 7*, 2833-42.
52. Gonzalez, M.W. and Kann, M.G. (2012). Chapter 4: Protein interactions and disease. *PLoS Comput Biol 8*, e1002819.

53. Bauer, A. and Kuster, B. (2003). Affinity purification-mass spectrometry. Powerful tools for the characterization of protein complexes. *Eur J Biochem 270*, 570-8.
54. Burckstummer, T., Bennett, K.L., Preradovic, A., Schutze, G., Hantschel, O., Superti-Furga, G. and Bauch, A. (2006). An efficient tandem affinity purification procedure for interaction proteomics in mammalian cells. *Nat Methods 3*, 1013-9.
55. Sinz, A. (2006). Chemical cross-linking and mass spectrometry to map three-dimensional protein structures and protein-protein interactions. *Mass Spectrom Rev 25*, 663-682.
56. Prescher, J.A. and Bertozzi, C.R. (2005). Chemistry in living systems. *Nat Chem Biol 1*, 13-21.
57. Brunner, J. (1993). New photolabeling and crosslinking methods. *Annu Rev Biochem 62*, 483-514.
58. Dorman, G. and Prestwich, G.D. (1994). Benzophenone photophores in biochemistry. *Biochemistry 33*, 5661-73.
59. Kodadek, T., Duroux-Richard, I. and Bonnafous, J.C. (2005). Techniques: Oxidative cross-linking as an emergent tool for the analysis of receptor-mediated signalling events. *Trends Pharmacol Sci 26*, 210-7.
60. Bruckner, A., Polge, C., Lentze, N., Auerbach, D. and Schlattner, U. (2009). Yeast two-hybrid, a powerful tool for systems biology. *Int J Mol Sci 10*, 2763-88.
61. Fields, S. and Song, O. (1989). A novel genetic system to detect protein-protein interactions. *Nature 340*, 245-6.
62. Keegan, L., Gill, G. and Ptashne, M. (1986). Separation of DNA binding from the transcription-activating function of a eukaryotic regulatory protein. *Science 231*, 699-704.
63. Gisler, S.M., Kittanakom, S., Fuster, D., Wong, V., Bertic, M., Radanovic, T., Hall, R.A., Murer, H., Biber, J., Markovich, D., Moe, O.W. and Stagljar, I. (2008). Monitoring protein-protein interactions between the mammalian integral membrane transporters and PDZ-interacting partners using a modified split-ubiquitin membrane yeast two-hybrid system. *Mol Cell Proteomics 7*, 1362-77.
64. Damodaran, S., Wood, T.D., Nagarajan, P. and Rabin, R.A. (2007). Evaluating peptide mass fingerprinting-based protein identification. *Genomics Proteomics Bioinformatics 5*, 152-7.
65. www.matrixscience.com.
66. Joshi, N.S., Whitaker, L.R. and Francis, M.B. (2004). A three-component Mannich-type reaction for selective tyrosine bioconjugation. *J Am Chem Soc 126*, 15942-3.
67. Scheck, R.A., Dedeo, M.T., Iavarone, A.T. and Francis, M.B. (2008). Optimization of a biomimetic transamination reaction. *J Am Chem Soc 130*, 11762-70.
68. Muir, T.W. (2003). Semisynthesis of proteins by expressed protein ligation. *Annu Rev Biochem 72*, 249-89.
69. Muralidharan, V. and Muir, T.W. (2006). Protein ligation: an enabling technology for the biophysical analysis of proteins. *Nat Methods 3*, 429-38.
70. Sletten, E.M. and Bertozzi, C.R. (2011). From mechanism to mouse: a tale of two bioorthogonal reactions. *ACC Chem Res 44*, 666-76.
71. Huisgen, R. (1963). 1,3-dipolar cycloadditions. *Angew Chem Int Ed Engl 2*, 565-632.
72. Lim, R.K.V. and Lin, Q. (2010). Bioorthogonal chemistry: a covalent strategy for the study of biological systems. *Sci China Chem 53*, 61-70.
73. Meldal, M. and Tornoe, C.W. (2008). Cu-catalyzed azide-alkyne cycloaddition. *Chem Rev 108*, 2952-3015.

74. Rostovtsev, V.V., Green, L.G., Fokin, V.V. and Sharpless, K.B. (2002). A stepwise huisgen cycloaddition process: copper(I)-catalyzed regioselective "ligation" of azides and terminal alkynes. *Angew Chem Int Ed Engl 41*, 2596-9.
75. Kolb, H.C., Finn, M.G. and Sharpless, K.B. (2001). Click Chemistry: Diverse Chemical Function from a Few Good Reactions. *Angew Chem Int Ed Engl 40*, 2004-2021.
76. Wolbers, F., ter Braak, P., Le Gac, S., Luttge, R., Andersson, H., Vermes, I. and van den Berg, A. (2006). Viability study of HL60 cells in contact with commonly used microchip materials. *Electrophoresis 27*, 5073-80.
77. R. B. Turner, A.D.J., P. Goebel and B. J. Mallon. (1973). Heats of hydrogenation. IX. Cyclic acetylenes and some miscellaneous olefins. *J Am Chem Soc 95*, 790-792.
78. Bach, R.D. (2009). Ring strain energy in the cyclooctyl system. The effect of strain energy on [3 + 2] cycloaddition reactions with azides. *J Am Chem Soc 131*, 5233-43.
79. Baskin, J.M., Prescher, J.A., Laughlin, S.T., Agard, N.J., Chang, P.V., Miller, I.A., Lo, A., Codelli, J.A. and Bertozzi, C.R. (2007). Copper-free click chemistry for dynamic in vivo imaging. *Proc Natl Acad Sci U S A 104*, 16793-7.
80. Rowland, M.M. and Best, M.D. (2010). Reeling in the catch: advancing cleavable linkers for proteomics. *Chem Biol 17*, 1166-8.
81. Rybak, J.N., Scheurer, S.B., Neri, D. and Elia, G. (2004). Purification of biotinylated proteins on streptavidin resin: A protocol for quantitative elution. *Proteomics 4*, 2296-2299.
82. Gartner, C.A., Elias, J.E., Bakalarski, C.E. and Gygi, S.P. (2007). Catch-and-release reagents for broadscale quantitative proteomics analyses. *J Proteome Res 6*, 1482-91.
83. Verhelst, S.H., Fonovic, M. and Bogyo, M. (2007). A mild chemically cleavable linker system for functional proteomic applications. *Angew Chem Int Ed Engl 46*, 1284-6.
84. Speers, A.E. and Cravatt, B.F. (2005). A tandem orthogonal proteolysis strategy for high-content chemical proteomics. *J. Am. Chem. Soc. 127*, 10018-9.
85. Leriche, G., Budin, G., Brino, L. and Wagner, A. (2010). Optimization of the Azobenzene Scaffold for Reductive Cleavage by Dithionite; Development of an Azobenzene Cleavable Linker for Proteomic Applications. *European Journal of Organic Chemistry*4360-4364.
86. Fonovic, M., Verhelst, S.H., Sorum, M.T. and Bogyo, M. (2007). Proteomics evaluation of chemically cleavable activity-based probes. *Mol Cell Proteomics 6*, 1761-70.
87. Yang, Y.Y., Grammel, M., Raghavan, A.S., Charron, G. and Hang, H.C. (2010). Comparative analysis of cleavable azobenzene-based affinity tags for bioorthogonal chemical proteomics. *Chem. Biol. 17*, 1212-22.
88. Geoffray Leriche, G.B., Laurent Brino, and Alain Wagner. (2010). Optimization of the Azobenzene Scaffold for Reductive Cleavage by Dithionite; Development of an Azobenzene Cleavable Linker for Proteomic Applications. *Eur J Org Chem*4360-4364.
89. Adams, S.R., Kao, J. P. Y., Tsien, R. Y. (1989). Biologically Useful Chelators That Take Up Ca2+ upon Illumination. *J Am Chem Soc 111*, 7957-7968.
90. Yu, H., Li, J., Wu, D., Qiu, Z. and Zhang, Y. (2010). Chemistry and biological applications of photo-labile organic molecules. *Chem Soc Rev 39*, 464-73.
91. Szychowski, J., Mahdavi, A., Hodas, J.J., Bagert, J.D., Ngo, J.T., Landgraf, P., Dieterich, D.C., Schuman, E.M. and Tirrell, D.A. (2010). Cleavable biotin probes for labeling of biomolecules via azide-alkyne cycloaddition. *J Am Chem Soc 132*, 18351-60.

92. Kiessling, L.L., Gestwicki, J.E. and Strong, L.E. (2000). Synthetic multivalent ligands in the exploration of cell-surface interactions. *Curr Opin Chem Biol 4*, 696-703.
93. Lees, W.J., Spaltenstein, A., Kingery-Wood, J.E. and Whitesides, G.M. (1994). Polyacrylamides bearing pendant alpha-sialoside groups strongly inhibit agglutination of erythrocytes by influenza A virus: multivalency and steric stabilization of particulate biological systems. *J Med Chem 37*, 3419-33.
94. Mammen, M., Dahmann, G. and Whitesides, G.M. (1995). Effective inhibitors of hemagglutination by influenza virus synthesized from polymers having active ester groups. Insight into mechanism of inhibition. *J Med Chem 38*, 4179-90.
95. Kiessling, L.L., Gestwicki, J.E. and Strong, L.E. (2006). Synthetic multivalent ligands as probes of signal transduction. *Angew Chem Int Ed Engl 45*, 2348-68.
96. Mathai Mammen, S.-K.C., and George M. Whitesides. (1998). Polyvalent Interactions in Biological SystemsL Implications for Design and Use of Multivalent Ligands and Inhibitors. *Angew Chem Int Ed Engl*2754.
97. Bruehl, R.E., Dasgupta, F., Katsumoto, T.R., Tan, J.H., Bertozzi, C.R., Spevak, W., Ahn, D.J., Rosen, S.D. and Nagy, J.O. (2001). Polymerized liposome assemblies: bifunctional macromolecular selectin inhibitors mimicking physiological selectin ligands. *Biochemistry 40*, 5964-74.
98. Gabizon, A., Horowitz, A.T., Goren, D., Tzemach, D., Mandelbaum-Shavit, F., Qazen, M.M. and Zalipsky, S. (1999). Targeting folate receptor with folate linked to extremities of poly(ethylene glycol)-grafted liposomes: in vitro studies. *Bioconjug Chem 10*, 289-98.
99. Gupta, S. and Sampson, N.S. (2001). Dimyristoylated peptides incorporated into liposomes are polyvalent fertilin beta mimics. *Org Lett 3*, 3333-5.
100. Reuter, J.D., Myc, A., Hayes, M.M., Gan, Z., Roy, R., Qin, D., Yin, R., Piehler, L.T., Esfand, R., Tomalia, D.A. and Baker, J.R., Jr. (1999). Inhibition of viral adhesion and infection by sialic-acid-conjugated dendritic polymers. *Bioconjug Chem 10*, 271-8.
101. Thompson, J.P. and Schengrund, C.L. (1998). Inhibition of the adherence of cholera toxin and the heat-labile enterotoxin of Escherichia coli to cell-surface GM1 by oligosaccharide-derivatized dendrimers. *Biochem Pharmacol 56*, 591-7.
102. M., S. (1956). 'Living' polymers. *Nature 178*, 1168-1169.
103. Darling TR, D.T., Fryd M, Gridnec AA, Haddleton DM, Ittel SD, et al. (2000). Living polymerization: rationale for uniform terminology. *Polym Chem 38*, 1706-1708.
104. Christopher W. Bielawski, R.H.G. (2007). Living ring-opening metathesis polymerization. *Prog Polym Sci 32*, 1-29.
105. Calderon N., O.E., Judy WA. . (1976). Mechanistic aspects of olefin metathesis. *Angew Chem Int Ed Engl 15*, 401-409.
106. Benson SW, C.F., Golden DM, Haugen GR, O'Neal HE, Rodgers AS, et al. (1969). Additivity rules for the estimation of thermochemical properties. *Chem Rev 9*, 279-324.
107. Sutthira Sutthasupa, M.s.a.F.S. (2010). Recent advances in ring-opening metathesis polymerization, and application to synthesis of functional materials. *Polym J 42*, 905-915.
108. Gillion, L.R.G., R.H. (1986). titanacyclobutanes derived from strained, cyclic olefins: the living polymerization of norbornene. *J Am Chem Soc 108*, 733-742.
109. Wallace, K.C.S., R. R. (1987). Ring-opening polymerization of norbornene by a tantalum catalyst: a living polymerization. *Macromolecules 20*, 1169-1172.

110. Ivin KJ, K.J., Osborn JA. (1992). Proton NMR study of the kinetics of metathesis polymerization of 5- and 5, 6-methoxycarboxyl derivatives of bicyclo[2.2.1]hept-2-ene, initiated by cyclopentylidenediboromobis(neopentyloxy)tungsten [cyclopentylidenedibromobis(neopentyloxy)tunsten]. *Makromol Chem 193*, 1695-1707.
111. Schaverien CJ, D.J., Schrock RR. . (1986). Multiple metal-carbon bonds. 43. Well-charaterized, highly active, Lewis acid free olefin metathesis catalysts. *J Am Chem Soc 108*, 2771-2771.
112. Schrock RR, D.R., Feldman J, Schaverien CJ, Dewan JC, Liu AH. (1988). Preparation and reactivity of several alkylidene complexes of the type W(CHR')(N-2,6-C6H3-iso-Pr2)(OR)2 and related tungstacyclobutane complexes. Controlling metathesis activity through the choice of alkoxide ligand. *J Am Chem Soc 110*, 1423-1435.
113. RR, S. (1990). Living ring-opening metathesis polymerization catalyzed by well-characterized transition-metal alkylidene complexes. *ACC Chem Res 23*, 158-165.
114. Coles MP, G.V., Mazzariol L, North M, Teasdale WG, Williams CM et al. (1994). Amino acid derived homochiral polymers via ring-opening metathesis polymerisation. *J Chem Soc Chem Commun*2505-2506.
115. Biagini SCG, C.M., Gibson VC, Giles MR, Marshall EL, North M. (1998). Living ring-opening metathesis polymerisation of amino ester functionalised norbornenes. *Polymer 39*, 1007-1014.
116. Hermann, W.A., & Kocher, C. (1997). N-Heterocyclic carbenes *Angew Chem Int Ed Engl 36*, 2162-2187.
117. Matyjaszewski, K.D., T.P. (eds). (2002). Handbook of radical polymerization. *Wiley*.
118. Wang, J., S. & Matyjaszewski, K. . (1995). Controlled/'living' radical polymerization. Atom transfer radical polymerization in the presence of transition-metal complexes. *J Am Chem Soc 117*, 5614-5615.
119. Matyjaszewski, K.X., J. (2001). Atom transfer radical polymerzation. *Chem Rev 101*, 2921-2990.
120. Matyjaszewski, K. (2012). Atom transfer radical polymerization (ATPR): Current status and future perspectives. *Macromolecules 45*, 4015-4039.
121. Ladmiral, V., Mantovani, G., Clarkson, G.J., Cauet, S., Irwin, J.L. and Haddleton, D.M. (2006). Synthesis of neoglycopolymers by a combination of "click chemistry" and living radical polymerization. *J Am Chem Soc 128*, 4823-30.
122. Sumerlin, B.S., Tsarevsky, N. V., Louche, G, Lee, R. Y. , and Matyjaszewski, K. (2005). Highly efficient "click" functionalization of poly(3-azidopropyl methacrylate prepared by ATRP. *Macromolecules 38*, 7540-7545.
123. Moad, G., Rizzardo, E., Thang, S.H. (2005). Living radical polymerization by the RAFT process. *Aust J Chem 58*, 379-410.
124. McCormick, C.L. and Lowe, A.B. (2004). Aqueous RAFT polymerization: recent developments in synthesis of functional water-soluble (co)polymers with controlled structures. *ACC Chem Res 37*, 312-25.
125. Liu, J.Q., Bulmus, V., Herlambang, D.L., Barner-Kowollik, C., Stenzel, M.H. and Davis, T.P. (2007). In situ formation of protein-polymer conjugates through reversible addition fragmentation chain transfer polymerization. *Angew Chem Int Edit 46*, 3099-3103.
126. Heredia, K.L., Grover, G.N., Tao, L. and Maynard, H.D. (2009). Synthesis of Heterotelechelic Polymers for Conjugation of Two Different Proteins. *Macromolecules 42*, 2360-2367.

127. Boyer, C., Bulmus, V., Davis, T.P., Ladmiral, V., Liu, J.Q. and Perrier, S. (2009). Bioapplications of RAFT Polymerization. *Chem Rev 109*, 5402-5436.
128. Heredia, K.L., Nguyen, T.H., Chang, C.W., Bulmus, V., Davis, T.P. and Maynard, H.D. (2008). Reversible siRNA-polymer conjugates by RAFT polymerization. *Chem Commun*3245-3247.
129. Le Droumaguet, B. and Velonia, K. (2008). Click chemistry: A powerful tool to create polymer-based macromolecular chimeras. *Macromol Rapid Comm 29*, 1073-1089.
130. Li, M., De, P., Gondi, S.R. and Sumerlin, B.S. (2008). Responsive polymer-protein bioconjugates prepared by RAFT polymerization and copper-catalyzed azide-alkyne click chemistry. *Macromol Rapid Comm 29*, 1172-1176.
131. Hong, V., Presolski, S.I., Ma, C. and Finn, M.G. (2009). Analysis and optimization of copper-catalyzed azide-alkyne cycloaddition for bioconjugation. *Angew Chem Int Ed Engl 48*, 9879-83.
132. Sivakumar, K., Xie, F., Cash, B.M., Long, S., Barnhill, H.N. and Wang, Q. (2004). A fluorogenic 1,3-dipolar cycloaddition reaction of 3-azidocoumarins and acetylenes. *Org Lett 6*, 4603-4606.
133. Sivakumar, K., Xie, F., Cash, B.M., Long, S., Barnhill, H.N. and Wang, Q. (2004). A fluorogenic 1,3-dipolar cycloaddition reaction of 3-azidocoumarins and acetylenes. *Org Lett 6*, 4603-6.
134. Elia, G. (2008). Biotinylation reagents for the study of cell surface proteins. *Proteomics 8*, 4012-4024.
135. Szychowski, J., Mahdavi, A., Hodas, J.J.L., Bagert, J.D., Ngo, J.T., Landgraf, P., Dieterich, D.C., Schuman, E.M. and Tirrell, D.A. (2010). Cleavable Biotin Probes for Labeling of Biomolecules via Azide-Alkyne Cycloaddition. *J. Am. Chem. Soc. 132*, 18351-18360.
136. Geurink, P.P., Florea, B.I., Li, N., Witte, M.D., Verasdonck, J., Kuo, C.L., van der Marel, G.A. and Overkleeft, H.S. (2010). A cleavable linker based on the levulinoyl ester for activity-based protein profiling. *Angew. Chem. Int. Ed. Engl. 49*, 6802-5.
137. Yokoshima, S., Abe, Y., Watanabe, N., Kita, Y., Kan, T., Iwatsubo, T., Tomita, T. and Fukuyama, T. (2009). Development of photoaffinity probes for gamma-secretase equipped with a nitrobenzenesulfonamide-type cleavable linker. *Bioorg. Med. Chem. Lett. 19*, 6869-71.
138. Rudolf, G.C., Heydenreuter, W. and Sieber, S.A. (2013). Chemical proteomics: ligation and cleavage of protein modifications. *Curr. Opin. Chem. Biol. 17*, 110-7.
139. Leriche, G., Chisholm, L. and Wagner, A. (2012). Cleavable linkers in chemical biology. *Bioorg. Med. Chem. 20*, 571-82.
140. Gillies, E.R., Goodwin, A.P. and Frechet, J.M. (2004). Acetals as pH-sensitive linkages for drug delivery. *Bioconjug Chem 15*, 1254-63.
141. Mahal, L.K., Yarema, K.J. and Bertozzi, C.R. (1997). Engineering chemical reactivity on cell surfaces through oligosaccharide biosynthesis. *Science 276*, 1125-8.
142. Wu, P., Shui, W., Carlson, B.L., Hu, N., Rabuka, D., Lee, J. and Bertozzi, C.R. (2009). Site-specific chemical modification of recombinant proteins produced in mammalian cells by using the genetically encoded aldehyde tag. *Proc Natl Acad Sci U S A 106*, 3000-5.
143. Hang, H.C. and Bertozzi, C.R. (2001). Ketone isosteres of 2-N-acetamidosugars as substrates for metabolic cell surface engineering. *J Am Chem Soc 123*, 1242-3.

144. Grant, D.S., Tashiro, K., Segui-Real, B., Yamada, Y., Martin, G.R. and Kleinman, H.K. (1989). Two different laminin domains mediate the differentiation of human endothelial cells into capillary-like structures in vitro. *Cell 58*, 933-43.
145. Pytela, R., Pierschbacher, M.D., Ginsberg, M.H., Plow, E.F. and Ruoslahti, E. (1986). Platelet membrane glycoprotein IIb/IIIa: member of a family of Arg-Gly-Asp--specific adhesion receptors. *Science 231*, 1559-62.
146. Pytela, R. (1988). Amino acid sequence of the murine Mac-1 alpha chain reveals homology with the integrin family and an additional domain related to von Willebrand factor. *EMBO J 7*, 1371-8.
147. David Robinette, N.N., Kenneth B Tomer, and Christoph H Borchers. (2006). Photoaffinity labeling combined with mass spectrometric approaches as a tool for structural proteomics. *Expert Rev of Proteomics 3*, 399-408.
148. Vu Hong, S.I.P., Celia Ma, and M.G. Finn. (2009). Analysis and Optimization of Copper-Catalyzed Azide-Alkyne Cycloaddition for Bioconjugation. *Angew Chem Int Ed Engl*5.
149. Bitan, G., Scheibler, L., Greenberg, Z., Rosenblatt, M. and Chorev, M. (1999). Mapping the integrin alpha V beta 3-ligand interface by photoaffinity cross-linking. *Biochemistry 38*, 3414-20.
150. Santoro, S.A. and Lawing, W.J., Jr. (1987). Competition for related but nonidentical binding sites on the glycoprotein IIb-IIIa complex by peptides derived from platelet adhesive proteins. *Cell 48*, 867-73.
151. Calvete, J.J., McLane, M.A., Stewart, G.J. and Niewiarowski, S. (1994). Characterization of the cross-linking site of disintegrins albolabrin, bitistatin, echistatin, and eristostatin on isolated human platelet integrin GPIIb/IIIa. *Biochem Biophys Res Commun 202*, 135-40.
152. D'Souza, S.E., Ginsberg, M.H., Burke, T.A. and Plow, E.F. (1990). The ligand binding site of the platelet integrin receptor GPIIb-IIIa is proximal to the second calcium binding domain of its alpha subunit. *J Biol Chem 265*, 3440-6.
153. Yahalom, D., Wittelsberger, A., Mierke, D.F., Rosenblatt, M., Alexander, J.M. and Chorev, M. (2002). Identification of the principal binding site for RGD-containing ligands in the alpha(V)beta(3) integrin: a photoaffinity cross-linking study. *Biochemistry 41*, 8321-31.
154. Pellinen, T. and Ivaska, J. (2006). Integrin traffic. *J Cell Sci 119*, 3723-31.
155. Pizarro-Cerda, J. and Cossart, P. (2006). Bacterial adhesion and entry into host cells. *Cell 124*, 715-27.
156. Hanahan, D. and Weinberg, R.A. (2000). The hallmarks of cancer. *Cell 100*, 57-70.
157. Kinzler, K.W. and Vogelstein, B. (1997). Cancer-susceptibility genes. Gatekeepers and caretakers. *Nature 386*, 761, 763.
158. Johnstone, R.W. (2002). Histone-deacetylase inhibitors: novel drugs for the treatment of cancer. *Nat Rev Drug Discov 1*, 287-99.
159. Gronbaek, K., Hother, C. and Jones, P.A. (2007). Epigenetic changes in cancer. *APMIS 115*, 1039-59.
160. Lund, A.H. and van Lohuizen, M. (2004). Epigenetics and cancer. *Genes Dev 18*, 2315-35.
161. Nightingale, K.P., O'Neill, L.P. and Turner, B.M. (2006). Histone modifications: signalling receptors and potential elements of a heritable epigenetic code. *Curr Opin Genet Dev 16*, 125-36.

162. Jacobson, S. and Pillus, L. (1999). Modifying chromatin and concepts of cancer. *Curr Opin Genet Dev 9*, 175-84.
163. Luger, K., Mader, A.W., Richmond, R.K., Sargent, D.F. and Richmond, T.J. (1997). Crystal structure of the nucleosome core particle at 2.8 A resolution. *Nature 389*, 251-60.
164. Jenuwein, T. and Allis, C.D. (2001). Translating the histone code. *Science 293*, 1074-80.
165. Haberland, M., Montgomery, R.L. and Olson, E.N. (2009). The many roles of histone deacetylases in development and physiology: implications for disease and therapy. *Nat Rev Genet 10*, 32-42.
166. Segre, C.V. and Chiocca, S. (2011). Regulating the regulators: the post-translational code of class I HDAC1 and HDAC2. *J Biomed Biotechnol 2011*, 690848.
167. Reichert, N., Choukrallah, M.A. and Matthias, P. (2012). Multiple roles of class I HDACs in proliferation, differentiation, and development. *Cell Mol Life Sci 69*, 2173-87.
168. Waltregny, D., Glenisson, W., Tran, S.L., North, B.J., Verdin, E., Colige, A. and Castronovo, V. (2005). Histone deacetylase HDAC8 associates with smooth muscle alpha-actin and is essential for smooth muscle cell contractility. *FASEB J 19*, 966-8.
169. Barneda-Zahonero, B. and Parra, M. (2012). Histone deacetylases and cancer. *Mol Oncol 6*, 579-589.
170. Bosch-Presegue, L. and Vaquero, A. (2011). The dual role of sirtuins in cancer. *Genes Cancer 2*, 648-62.
171. Saunders, L.R. and Verdin, E. (2007). Sirtuins: critical regulators at the crossroads between cancer and aging. *Oncogene 26*, 5489-504.
172. Liu, H., Hu, Q., D'Ercole A, J. and Ye, P. (2009). Histone deacetylase 11 regulates oligodendrocyte-specific gene expression and cell development in OL-1 oligodendroglia cells. *Glia 57*, 1-12.
173. Villagra, A., Cheng, F., Wang, H.W., Suarez, I., Glozak, M., Maurin, M., Nguyen, D., Wright, K.L., Atadja, P.W., Bhalla, K., Pinilla-Ibarz, J., Seto, E. and Sotomayor, E.M. (2009). The histone deacetylase HDAC11 regulates the expression of interleukin 10 and immune tolerance. *Nat Immunol 10*, 92-100.
174. Lin, R.J., Sternsdorf, T., Tini, M. and Evans, R.M. (2001). Transcriptional regulation in acute promyelocytic leukemia. *Oncogene 20*, 7204-15.
175. Zelent, A., Guidez, F., Melnick, A., Waxman, S. and Licht, J.D. (2001). Translocations of the RARalpha gene in acute promyelocytic leukemia. *Oncogene 20*, 7186-203.
176. Minucci, S., Nervi, C., Lo Coco, F. and Pelicci, P.G. (2001). Histone deacetylases: a common molecular target for differentiation treatment of acute myeloid leukemias? *Oncogene 20*, 3110-5.
177. Lin, R.J., Egan, D.A. and Evans, R.M. (1999). Molecular genetics of acute promyelocytic leukemia. *Trends Genet 15*, 179-84.
178. Lin, R.J. and Evans, R.M. (2000). Acquisition of oncogenic potential by RAR chimeras in acute promyelocytic leukemia through formation of homodimers. *Mol Cell 5*, 821-30.
179. Minucci, S., Maccarana, M., Cioce, M., De Luca, P., Gelmetti, V., Segalla, S., Di Croce, L., Giavara, S., Matteucci, C., Gobbi, A., Bianchini, A., Colombo, E., Schiavoni, I., Badaracco, G., Hu, X., Lazar, M.A., Landsberger, N., Nervi, C. and Pelicci, P.G. (2000). Oligomerization of RAR and AML1 transcription factors as a novel mechanism of oncogenic activation. *Mol Cell 5*, 811-20.

180. Halkidou, K., Gaughan, L., Cook, S., Leung, H.Y., Neal, D.E. and Robson, C.N. (2004). Upregulation and nuclear recruitment of HDAC1 in hormone refractory prostate cancer. *Prostate 59*, 177-89.
181. Choi, J.H., Kwon, H.J., Yoon, B.I., Kim, J.H., Han, S.U., Joo, H.J. and Kim, D.Y. (2001). Expression profile of histone deacetylase 1 in gastric cancer tissues. *Jpn J Cancer Res 92*, 1300-4.
182. Wilson, A.J., Byun, D.S., Popova, N., Murray, L.B., L'Italien, K., Sowa, Y., Arango, D., Velcich, A., Augenlicht, L.H. and Mariadason, J.M. (2006). Histone deacetylase 3 (HDAC3) and other class I HDACs regulate colon cell maturation and p21 expression and are deregulated in human colon cancer. *J Biol Chem 281*, 13548-58.
183. Zhang, Z., Yamashita, H., Toyama, T., Sugiura, H., Ando, Y., Mita, K., Hamaguchi, M., Hara, Y., Kobayashi, S. and Iwase, H. (2005). Quantitation of HDAC1 mRNA expression in invasive carcinoma of the breast*. *Breast Cancer Res Treat 94*, 11-6.
184. Zhu, P., Martin, E., Mengwasser, J., Schlag, P., Janssen, K.P. and Gottlicher, M. (2004). Induction of HDAC2 expression upon loss of APC in colorectal tumorigenesis. *Cancer Cell 5*, 455-63.
185. Huang, B.H., Laban, M., Leung, C.H., Lee, L., Lee, C.K., Salto-Tellez, M., Raju, G.C. and Hooi, S.C. (2005). Inhibition of histone deacetylase 2 increases apoptosis and p21Cip1/WAF1 expression, independent of histone deacetylase 1. *Cell Death Differ 12*, 395-404.
186. Song, J., Noh, J.H., Lee, J.H., Eun, J.W., Ahn, Y.M., Kim, S.Y., Lee, S.H., Park, W.S., Yoo, N.J., Lee, J.Y. and Nam, S.W. (2005). Increased expression of histone deacetylase 2 is found in human gastric cancer. *APMIS 113*, 264-8.
187. Zhang, Z., Yamashita, H., Toyama, T., Sugiura, H., Omoto, Y., Ando, Y., Mita, K., Hamaguchi, M., Hayashi, S. and Iwase, H. (2004). HDAC6 expression is correlated with better survival in breast cancer. *Clin Cancer Res 10*, 6962-8.
188. Glaser, K.B., Li, J., Staver, M.J., Wei, R.Q., Albert, D.H. and Davidsen, S.K. (2003). Role of class I and class II histone deacetylases in carcinoma cells using siRNA. *Biochem Biophys Res Commun 310*, 529-36.
189. Bolden, J.E., Peart, M.J. and Johnstone, R.W. (2006). Anticancer activities of histone deacetylase inhibitors. *Nat Rev Drug Discov 5*, 769-84.
190. Miller, T.A., Witter, D.J. and Belvedere, S. (2003). Histone deacetylase inhibitors. *J Med Chem 46*, 5097-5116.
191. Mai, A., Massa, S., Rotili, D., Cerbara, I., Valente, S., Pezzi, R., Simeoni, S. and Ragno, R. (2005). Histone deacetylation in epigenetics: An attractive target for anticancer therapy. *Med Res Rev 25*, 261-309.
192. Furumai, R., Matsuyama, A., Kobashi, N., Lee, K.H., Nishiyama, M., Nakajima, H., Tanaka, A., Komatsu, Y., Nishino, N., Yoshida, M. and Horinouchi, S. (2002). FK228 (depsipeptide) as a natural prodrug that inhibits class I histone deacetylases. *Cancer Res 62*, 4916-21.
193. Hu, E., Dul, E., Sung, C.M., Chen, Z., Kirkpatrick, R., Zhang, G.F., Johanson, K., Liu, R., Lago, A., Hofmann, G., Macarron, R., de los Frailes, M., Perez, P., Krawiec, J., Winkler, J. and Jaye, M. (2003). Identification of novel isoform-selective inhibitors within class I histone deacetylases. *J Pharmacol Exp Ther 307*, 720-8.
194. Minucci, S. and Pelicci, P.G. (2006). Histone deacetylase inhibitors and the promise of epigenetic (and more) treatments for cancer. *Nat Rev Cancer 6*, 38-51.

195. Marks, P.A., Richon, V.M., Breslow, R. and Rifkind, R.A. (2001). Histone deacetylase inhibitors as new cancer drugs. *Curr Opin Oncol 13*, 477-83.
196. Weidle, U.H. and Grossmann, A. (2000). Inhibition of histone deacetylases: a new strategy to target epigenetic modifications for anticancer treatment. *Anticancer Res 20*, 1471-85.
197. Maeda, T., Towatari, M., Kosugi, H. and Saito, H. (2000). Up-regulation of costimulatory/adhesion molecules by histone deacetylase inhibitors in acute myeloid leukemia cells. *Blood 96*, 3847-56.
198. Magner, W.J., Kazim, A.L., Stewart, C., Romano, M.A., Catalano, G., Grande, C., Keiser, N., Santaniello, F. and Tomasi, T.B. (2000). Activation of MHC class I, II, and CD40 gene expression by histone deacetylase inhibitors. *J Immunol 165*, 7017-24.
199. Mishra, N., Brown, D.R., Olorenshaw, I.M. and Kammer, G.M. (2001). Trichostatin A reverses skewed expression of CD154, interleukin-10, and interferon-gamma gene and protein expression in lupus T cells. *Proc Natl Acad Sci U S A 98*, 2628-33.
200. Shestakova, E., Bandu, M.T., Doly, J. and Bonnefoy, E. (2001). Inhibition of histone deacetylation induces constitutive derepression of the beta interferon promoter and confers antiviral activity. *J Virol 75*, 3444-52.
201. Kim, M.S., Kwon, H.J., Lee, Y.M., Baek, J.H., Jang, J.E., Lee, S.W., Moon, E.J., Kim, H.S., Lee, S.K., Chung, H.Y., Kim, C.W. and Kim, K.W. (2001). Histone deacetylases induce angiogenesis by negative regulation of tumor suppressor genes. *Nat Med 7*, 437-43.
202. Marks, P.A., Richon, V.M. and Rifkind, R.A. (2000). Histone deacetylase inhibitors: inducers of differentiation or apoptosis of transformed cells. *J Natl Cancer Inst 92*, 1210-6.
203. Gabrielli, B.G., Johnstone, R.W. and Saunders, N.A. (2002). Identifying molecular targets mediating the anticancer activity of histone deacetylase inhibitors: a work in progress. *Curr Cancer Drug Targets 2*, 337-53.
204. Vrana, J.A., Decker, R.H., Johnson, C.R., Wang, Z., Jarvis, W.D., Richon, V.M., Ehinger, M., Fisher, P.B. and Grant, S. (1999). Induction of apoptosis in U937 human leukemia cells by suberoylanilide hydroxamic acid (SAHA) proceeds through pathways that are regulated by Bcl-2/Bcl-XL, c-Jun, and p21CIP1, but independent of p53. *Oncogene 18*, 7016-25.
205. Richon, V.M., Sandhoff, T.W., Rifkind, R.A. and Marks, P.A. (2000). Histone deacetylase inhibitor selectively induces p21WAF1 expression and gene-associated histone acetylation. *Proc Natl Acad Sci U S A 97*, 10014-9.
206. Glaser, K.B., Staver, M.J., Waring, J.F., Stender, J., Ulrich, R.G. and Davidsen, S.K. (2003). Gene expression profiling of multiple histone deacetylase (HDAC) inhibitors: defining a common gene set produced by HDAC inhibition in T24 and MDA carcinoma cell lines. *Mol Cancer Ther 2*, 151-63.
207. Johnstone, R.W., Ruefli, A.A. and Lowe, S.W. (2002). Apoptosis: a link between cancer genetics and chemotherapy. *Cell 108*, 153-64.
208. Frew, A.J., Johnstone, R.W. and Bolden, J.E. (2009). Enhancing the apoptotic and therapeutic effects of HDAC inhibitors. *Cancer Lett 280*, 125-33.
209. Lindemann, R.K., Newbold, A., Whitecross, K.F., Cluse, L.A., Frew, A.J., Ellis, L., Williams, S., Wiegmans, A.P., Dear, A.E., Scott, C.L., Pellegrini, M., Wei, A., Richon, V.M., Marks, P.A., Lowe, S.W., Smyth, M.J. and Johnstone, R.W. (2007). Analysis of

the apoptotic and therapeutic activities of histone deacetylase inhibitors by using a mouse model of B cell lymphoma. *Proc Natl Acad Sci U S A 104*, 8071-6.
210. Newbold, A., Lindemann, R.K., Cluse, L.A., Whitecross, K.F., Dear, A.E. and Johnstone, R.W. (2008). Characterisation of the novel apoptotic and therapeutic activities of the histone deacetylase inhibitor romidepsin. *Mol Cancer Ther 7*, 1066-79.
211. Willis, S.N. and Adams, J.M. (2005). Life in the balance: how BH3-only proteins induce apoptosis. *Curr Opin Cell Biol 17*, 617-25.
212. Rosato, R.R., Almenara, J.A. and Grant, S. (2003). The histone deacetylase inhibitor MS-275 promotes differentiation or apoptosis in human leukemia cells through a process regulated by generation of reactive oxygen species and induction of p21CIP1/WAF1 1. *Cancer Res 63*, 3637-45.
213. Emanuele, S., Lauricella, M., Carlisi, D., Vassallo, B., D'Anneo, A., Di Fazio, P., Vento, R. and Tesoriere, G. (2007). SAHA induces apoptosis in hepatoma cells and synergistically interacts with the proteasome inhibitor Bortezomib. *Apoptosis 12*, 1327-38.
214. Insinga, A., Monestiroli, S., Ronzoni, S., Gelmetti, V., Marchesi, F., Viale, A., Altucci, L., Nervi, C., Minucci, S. and Pelicci, P.G. (2005). Inhibitors of histone deacetylases induce tumor-selective apoptosis through activation of the death receptor pathway. *Nat Med 11*, 71-6.
215. Sutheesophon, K., Nishimura, N., Kobayashi, Y., Furukawa, Y., Kawano, M., Itoh, K., Kano, Y., Ishii, H. and Furukawa, Y. (2005). Involvement of the tumor necrosis factor (TNF)/TNF receptor system in leukemic cell apoptosis induced by histone deacetylase inhibitor depsipeptide (FK228). *J Cell Physiol 203*, 387-97.
216. Wagner, J.M., Hackanson, B., Lubbert, M. and Jung, M. (2010). Histone deacetylase (HDAC) inhibitors in recent clinical trials for cancer therapy. *Clin Epigenetics 1*, 117-136.
217. Kim, H.J. and Bae, S.C. (2011). Histone deacetylase inhibitors: molecular mechanisms of action and clinical trials as anti-cancer drugs. *Am J Transl Res 3*, 166-79.
218. Mohamed, M.M. and Sloane, B.F. (2006). Cysteine cathepsins: multifunctional enzymes in cancer. *Nat Rev Cancer 6*, 764-75.
219. Jedeszko, C. and Sloane, B.F. (2004). Cysteine cathepsins in human cancer. *Biol Chem 385*, 1017-27.
220. Turk, V., Turk, B. and Turk, D. (2001). Lysosomal cysteine proteases: facts and opportunities. *EMBO J 20*, 4629-33.
221. Reinheckel, T., Deussing, J., Roth, W. and Peters, C. (2001). Towards specific functions of lysosomal cysteine peptidases: phenotypes of mice deficient for cathepsin B or cathepsin L. *Biol Chem 382*, 735-41.
222. Saftig, P., Hunziker, E., Wehmeyer, O., Jones, S., Boyde, A., Rommerskirch, W., Moritz, J.D., Schu, P. and von Figura, K. (1998). Impaired osteoclastic bone resorption leads to osteopetrosis in cathepsin-K-deficient mice. *Proc Natl Acad Sci U S A 95*, 13453-8.
223. Yasuda, Y., Kaleta, J. and Bromme, D. (2005). The role of cathepsins in osteoporosis and arthritis: rationale for the design of new therapeutics. *Adv Drug Deliv Rev 57*, 973-93.
224. Joyce, J.A., Baruch, A., Chehade, K., Meyer-Morse, N., Giraudo, E., Tsai, F.Y., Greenbaum, D.C., Hager, J.H., Bogyo, M. and Hanahan, D. (2004). Cathepsin cysteine proteases are effectors of invasive growth and angiogenesis during multistage tumorigenesis. *Cancer Cell 5*, 443-53.

225. Rao, J.S. (2003). Molecular mechanisms of glioma invasiveness: the role of proteases. *Nat Rev Cancer 3*, 489-501.
226. Krueger, S., Haeckel, C., Buehling, F. and Roessner, A. (1999). Inhibitory effects of antisense cathepsin B cDNA transfection on invasion and motility in a human osteosarcoma cell line. *Cancer Res 59*, 6010-4.
227. Mohanam, S., Jasti, S.L., Kondraganti, S.R., Chandrasekar, N., Lakka, S.S., Kin, Y., Fuller, G.N., Yung, A.W., Kyritsis, A.P., Dinh, D.H., Olivero, W.C., Gujrati, M., Ali-Osman, F. and Rao, J.S. (2001). Down-regulation of cathepsin B expression impairs the invasive and tumorigenic potential of human glioblastoma cells. *Oncogene 20*, 3665-73.
228. Krueger, S., Kellner, U., Buehling, F. and Roessner, A. (2001). Cathepsin L antisense oligonucleotides in a human osteosarcoma cell line: effects on the invasive phenotype. *Cancer Gene Ther 8*, 522-8.
229. Gocheva, V., Zeng, W., Ke, D., Klimstra, D., Reinheckel, T., Peters, C., Hanahan, D. and Joyce, J.A. (2006). Distinct roles for cysteine cathepsin genes in multistage tumorigenesis. *Genes Dev 20*, 543-56.
230. Lankelma, J.M., Voorend, D.M., Barwari, T., Koetsveld, J., Van der Spek, A.H., De Porto, A.P., Van Rooijen, G. and Van Noorden, C.J. (2010). Cathepsin L, target in cancer treatment? *Life Sci 86*, 225-33.
231. Ueki, N., Lee, S., Sampson, N.S. and Hayman, M.J. (2013). Selective cancer targeting with prodrugs activated by histone deacetylases and a tumour-associated protease. *Nat Commun 4*, 2735.
232. (2013). Cancer facts & figures.
233. Siegel, R., Ward, E., Brawley, O. and Jemal, A. (2011). Cancer statistics, 2011: the impact of eliminating socioeconomic and racial disparities on premature cancer deaths. *CA Cancer J Clin 61*, 212-36.
234. Christofori, G. (2006). New signals from the invasive front. *Nature 441*, 444-50.
235. Nguyen, D.X., Bos, P.D. and Massague, J. (2009). Metastasis: from dissemination to organ-specific colonization. *Nat Rev Cancer 9*, 274-84.
236. Duffy, M.J. (1996). Proteases as prognostic markers in cancer. *Clin Cancer Res 2*, 613-8.
237. Egeblad, M. and Werb, Z. (2002). New functions for the matrix metalloproteinases in cancer progression. *Nat Rev Cancer 2*, 161-74.
238. Lynch, C.C. and Matrisian, L.M. (2002). Matrix metalloproteinases in tumor-host cell communication. *Differentiation 70*, 561-73.
239. Gocheva, V. and Joyce, J.A. (2007). Cysteine cathepsins and the cutting edge of cancer invasion. *Cell Cycle 6*, 60-4.
240. Laufs, S., Schumacher, J. and Allgayer, H. (2006). Urokinase-receptor (u-PAR): an essential player in multiple games of cancer: a review on its role in tumor progression, invasion, metastasis, proliferation/dormancy, clinical outcome and minimal residual disease. *Cell Cycle 5*, 1760-71.
241. Masterson, J. and O'Dea, S. (2007). Posttranslational truncation of E-cadherin and significance for tumour progression. *Cells Tissues Organs 185*, 175-9.
242. Van Damme, J., Struyf, S. and Opdenakker, G. (2004). Chemokine-protease interactions in cancer. *Semin Cancer Biol 14*, 201-8.
243. Joyce, J.A. and Pollard, J.W. (2009). Microenvironmental regulation of metastasis. *Nat Rev Cancer 9*, 239-52.

244. Nagase, H., Visse, R. and Murphy, G. (2006). Structure and function of matrix metalloproteinases and TIMPs. *Cardiovasc Res 69*, 562-73.
245. Overall, C.M. and Lopez-Otin, C. (2002). Strategies for MMP inhibition in cancer: innovations for the post-trial era. *Nat Rev Cancer 2*, 657-72.
246. Parks, W.C., Wilson, C.L. and Lopez-Boado, Y.S. (2004). Matrix metalloproteinases as modulators of inflammation and innate immunity. *Nat Rev Immunol 4*, 617-29.
247. Birkedal-Hansen, H., Moore, W.G., Bodden, M.K., Windsor, L.J., Birkedal-Hansen, B., DeCarlo, A. and Engler, J.A. (1993). Matrix metalloproteinases: a review. *Crit Rev Oral Biol Med 4*, 197-250.
248. Somerville, R.P., Oblander, S.A. and Apte, S.S. (2003). Matrix metalloproteinases: old dogs with new tricks. *Genome Biol 4*, 216.
249. Morgunova, E., Tuuttila, A., Bergmann, U. and Tryggvason, K. (2002). Structural insight into the complex formation of latent matrix metalloproteinase 2 with tissue inhibitor of metalloproteinase 2. *Proc Natl Acad Sci U S A 99*, 7414-9.
250. Okada, A., Tomasetto, C., Lutz, Y., Bellocq, J.P., Rio, M.C. and Basset, P. (1997). Expression of matrix metalloproteinases during rat skin wound healing: evidence that membrane type-1 matrix metalloproteinase is a stromal activator of pro-gelatinase A. *J Cell Biol 137*, 67-77.
251. Hiraoka, N., Allen, E., Apel, I.J., Gyetko, M.R. and Weiss, S.J. (1998). Matrix metalloproteinases regulate neovascularization by acting as pericellular fibrinolysins. *Cell 95*, 365-77.
252. Sato, H., Takino, T., Okada, Y., Cao, J., Shinagawa, A., Yamamoto, E. and Seiki, M. (1994). A matrix metalloproteinase expressed on the surface of invasive tumour cells. *Nature 370*, 61-5.
253. Seiki, M. (1999). Membrane-type matrix metalloproteinases. *APMIS 107*, 137-43.
254. Belkin, A.M., Akimov, S.S., Zaritskaya, L.S., Ratnikov, B.I., Deryugina, E.I. and Strongin, A.Y. (2001). Matrix-dependent proteolysis of surface transglutaminase by membrane-type metalloproteinase regulates cancer cell adhesion and locomotion. *J Biol Chem 276*, 18415-22.
255. Kajita, M., Itoh, Y., Chiba, T., Mori, H., Okada, A., Kinoh, H. and Seiki, M. (2001). Membrane-type 1 matrix metalloproteinase cleaves CD44 and promotes cell migration. *J Cell Biol 153*, 893-904.
256. Endo, K., Takino, T., Miyamori, H., Kinsen, H., Yoshizaki, T., Furukawa, M. and Sato, H. (2003). Cleavage of syndecan-1 by membrane type matrix metalloproteinase-1 stimulates cell migration. *J Biol Chem 278*, 40764-70.
257. Knauper, V., Osthues, A., DeClerck, Y.A., Langley, K.E., Blaser, J. and Tschesche, H. (1993). Fragmentation of human polymorphonuclear-leucocyte collagenase. *Biochem J 291 (Pt 3)*, 847-54.
258. Itoh, Y., Takamura, A., Ito, N., Maru, Y., Sato, H., Suenaga, N., Aoki, T. and Seiki, M. (2001). Homophilic complex formation of MT1-MMP facilitates proMMP-2 activation on the cell surface and promotes tumor cell invasion. *EMBO J 20*, 4782-93.
259. Seiki, M., Koshikawa, N. and Yana, I. (2003). Role of pericellular proteolysis by membrane-type 1 matrix metalloproteinase in cancer invasion and angiogenesis. *Cancer Metastasis Rev 22*, 129-43.

260. Strongin, A.Y., Collier, I., Bannikov, G., Marmer, B.L., Grant, G.A. and Goldberg, G.I. (1995). Mechanism of cell surface activation of 72-kDa type IV collagenase. Isolation of the activated form of the membrane metalloprotease. *J Biol Chem 270*, 5331-8.
261. Wang, Z., Juttermann, R. and Soloway, P.D. (2000). TIMP-2 is required for efficient activation of proMMP-2 in vivo. *J Biol Chem 275*, 26411-5.
262. Mori, H., Tomari, T., Koshikawa, N., Kajita, M., Itoh, Y., Sato, H., Tojo, H., Yana, I. and Seiki, M. (2002). CD44 directs membrane-type 1 matrix metalloproteinase to lamellipodia by associating with its hemopexin-like domain. *EMBO J 21*, 3949-59.
263. Zarrabi, K., Dufour, A., Li, J., Kuscu, C., Pulkoski-Gross, A., Zhi, J., Hu, Y., Sampson, N.S., Zucker, S. and Cao, J. (2011). Inhibition of matrix metalloproteinase 14 (MMP-14)-mediated cancer cell migration. *J Biol Chem 286*, 33167-77.
264. Nikki A. Evensen, J.L., Jie Yang, Xiaojun Yu, Nicole S. Sampson, Stanley Zucker, Jian Cao. (2013). Development of a High-Throughput Three-Dimensional Invasion Assay for Anti-Cancer Drug Discovery. *PLoS ONE 8*, e82811.
265. Alford, R., Ogawa, M., Choyke, P.L. and Kobayashi, H. (2009). Molecular probes for the in vivo imaging of cancer. *Mol Biosyst 5*, 1279-91.
266. Kelloff, G.J., Krohn, K.A., Larson, S.M., Weissleder, R., Mankoff, D.A., Hoffman, J.M., Link, J.M., Guyton, K.Z., Eckelman, W.C., Scher, H.I., O'Shaughnessy, J., Cheson, B.D., Sigman, C.C., Tatum, J.L., Mills, G.Q., Sullivan, D.C. and Woodcock, J. (2005). The progress and promise of molecular imaging probes in oncologic drug development. *Clin Cancer Res 11*, 7967-85.
267. Sandhu, G.S., Solorio, L., Broome, A.M., Salem, N., Kolthammer, J., Shah, T., Flask, C. and Duerk, J.L. (2010). Whole animal imaging. *Wiley Interdiscip Rev Syst Biol Med 2*, 398-421.
268. Miller, P.W., Long, N.J., Vilar, R. and Gee, A.D. (2008). Synthesis of 11C, 18F, 15O, and 13N radiolabels for positron emission tomography. *Angew Chem Int Ed Engl 47*, 8998-9033.
269. Okarvi, S.M. (2001). Recent progress in fluorine-18 labelled peptide radiopharmaceuticals. *Eur J Nucl Med 28*, 929-38.
270. Wester, H.J., Hamacher, K. and Stocklin, G. (1996). A comparative study of N.C.A. fluorine-18 labeling of proteins via acylation and photochemical conjugation. *Nucl Med Biol 23*, 365-72.
271. Poethko, T., Schottelius, M., Thumshirn, G., Hersel, U., Herz, M., Henriksen, G., Kessler, H., Schwaiger, M. and Wester, H.J. (2004). Two-step methodology for high-yield routine radiohalogenation of peptides: (18)F-labeled RGD and octreotide analogs. *J Nucl Med 45*, 892-902.
272. Polt, R., Porreca, F., Szabo, L.Z., Bilsky, E.J., Davis, P., Abbruscato, T.J., Davis, T.P., Harvath, R., Yamamura, H.I. and Hruby, V.J. (1994). Glycopeptide enkephalin analogues produce analgesia in mice: evidence for penetration of the blood-brain barrier. *Proc Natl Acad Sci U S A 91*, 7114-8.
273. Namavari, M., Cheng, Z., Zhang, R., De, A., Levi, J., Hoerner, J.K., Yaghoubi, S.S., Syud, F.A. and Gambhir, S.S. (2009). A novel method for direct site-specific radiolabeling of peptides using [18F]FDG. *Bioconjug Chem 20*, 432-6.
274. Prante, O., Einsiedel, J., Haubner, R., Gmeiner, P., Wester, H.J., Kuwert, T. and Maschauer, S. (2007). 3,4,6-Tri-O-acetyl-2-deoxy-2-[18F]fluoroglucopyranosyl

phenylthiosulfonate: a thiol-reactive agent for the chemoselective 18F-glycosylation of peptides. *Bioconjug Chem 18*, 254-62.
275. Chambers, A.F., Groom, A.C. and MacDonald, I.C. (2002). Dissemination and growth of cancer cells in metastatic sites. *Nat Rev Cancer 2*, 563-72.
276. Watkins, G.A., Jones, E.F., Scott Shell, M., VanBrocklin, H.F., Pan, M.H., Hanrahan, S.M., Feng, J.J., He, J., Sounni, N.E., Dill, K.A., Contag, C.H., Coussens, L.M. and Franc, B.L. (2009). Development of an optimized activatable MMP-14 targeted SPECT imaging probe. *Bioorg Med Chem 17*, 653-9.
277. Temma, T., Sano, K., Kuge, Y., Kamihashi, J., Takai, N., Ogawa, Y. and Saji, H. (2009). Development of a radiolabeled probe for detecting membrane type-1 matrix metalloproteinase on malignant tumors. *Biol Pharm Bull 32*, 1272-7.
278. Kanie, Y., Enomoto, A., Goto, S. and Kanie, O. (2008). Comparative RP-HPLC for rapid identification of glycopeptides and application in off-line LC-MALDI-MS analysis. *Carbohydr Res 343*, 758-68.
279. Roberts, S.L., Furlan, R.L.E., Otto, S. and Sanders, J.K.M. (2003). Metal-ion induced amplification of three receptors from dynamic combinatorial libraries of peptide-hydrazones. *Org Biomol Chem 1*, 1625-1633.

Appendix

Checklist for compounds

Compound #	Ref.	^{1}H NMR	^{13}C NMR	Other
3	33, 34			
4		O		ESI-MS
5		O		ESI-MS
6	8, 33			
7a	8, 33	O		
7b	8, 33	O		
8a	8, 33	O		
8b	8, 33	O		
9a	8, 33	O		
9b	8, 33	O		
10a	8, 33	O		
10b	8, 33	O		
14	10	O		ESI-MS
16	11	O		ESI-MS
17		O	O	ESI-MS
18		O	O	ESI-MS
19		O		ESI-MS
20		O		ESI-MS
21a		O	O	ESI-MS
21b		O	O	ESI-MS
22a		O	O	ESI-MS
22b		O	O	ESI-MS
23a		O	O	ESI-MS
23b		O	O	ESI-MS

23c		O	O	HRMS
4-1		O	O	HRMS

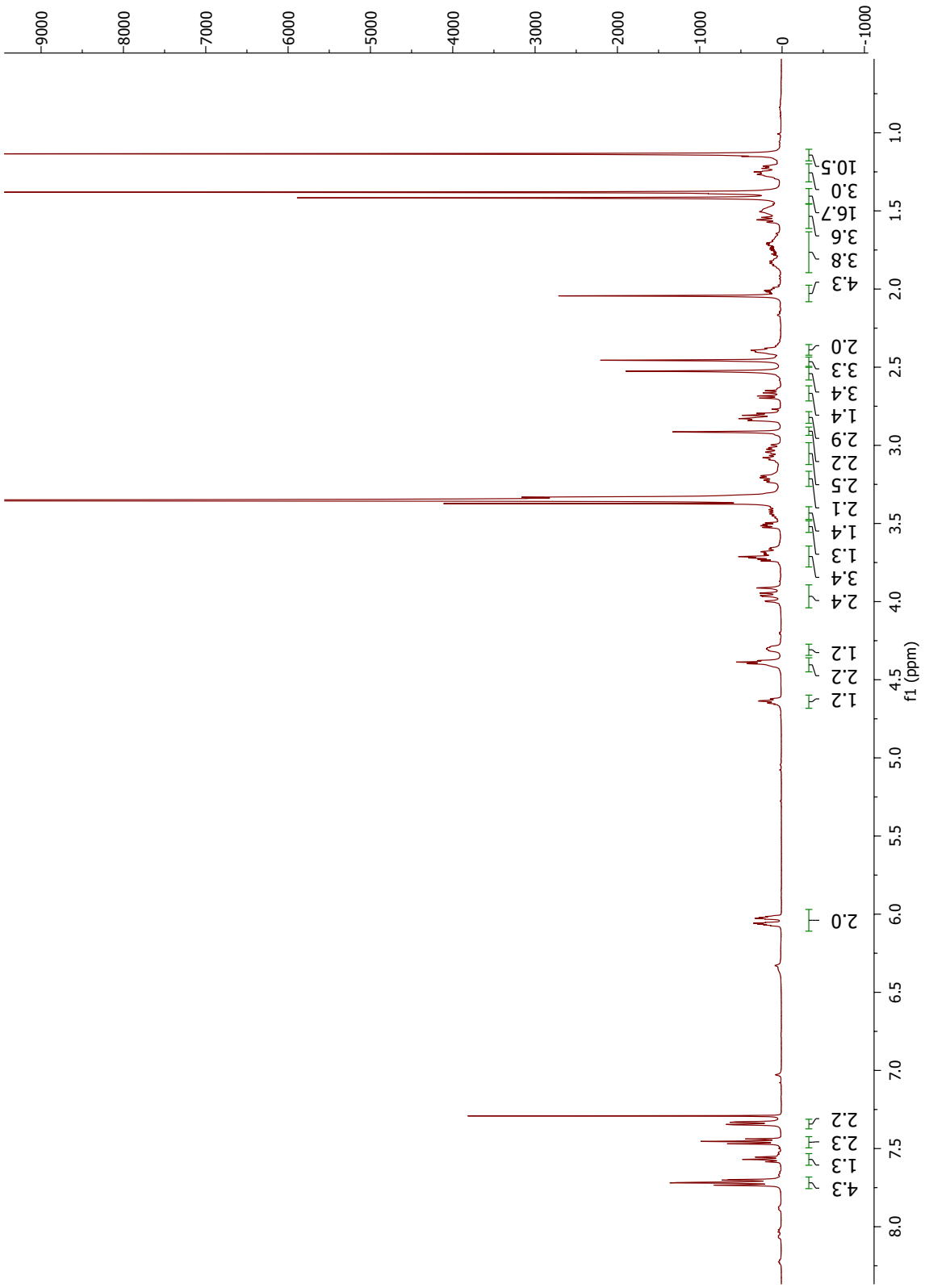

^{1}H NMR Spectrum of peptide **4**

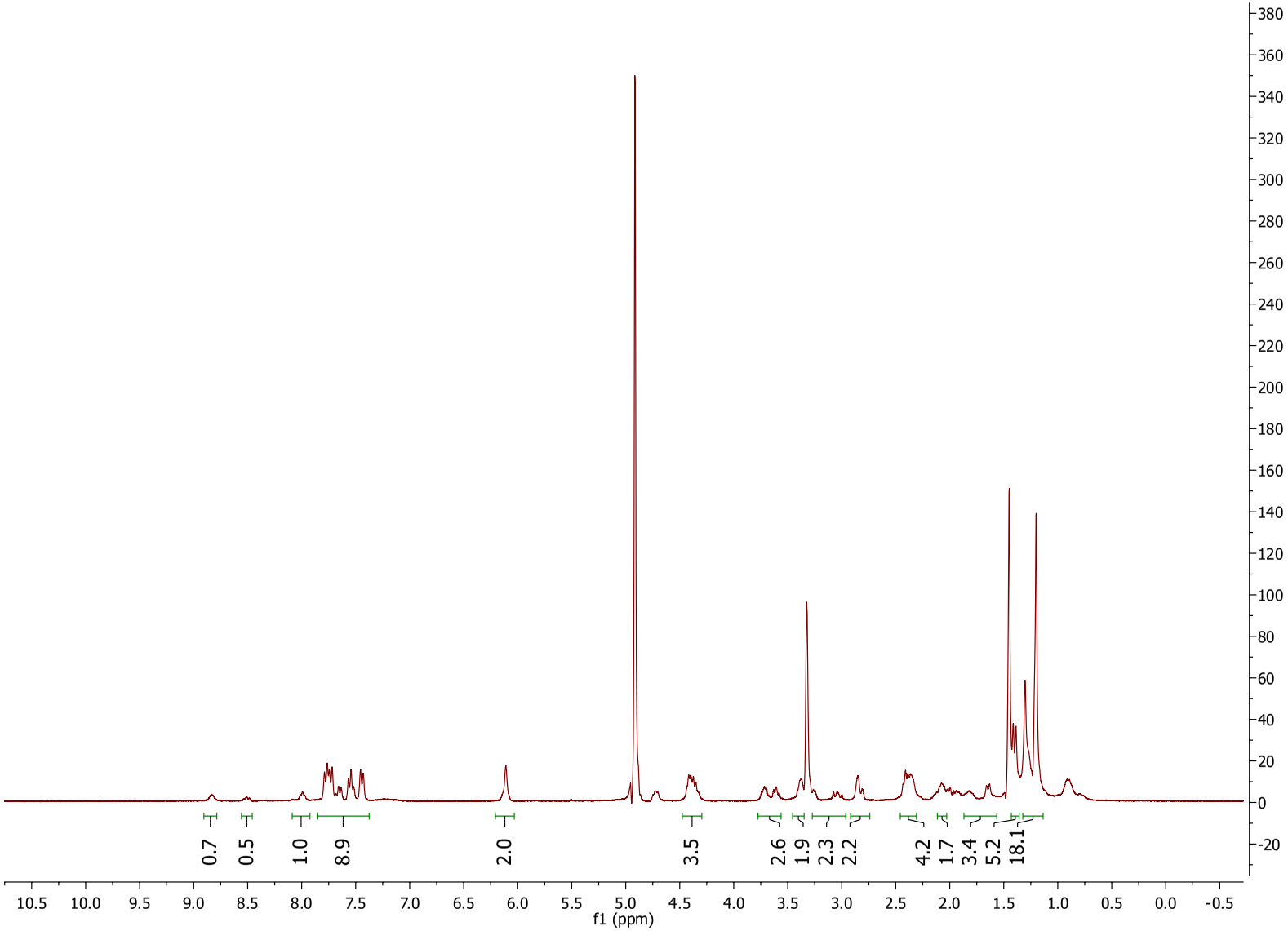

^{1}H NMR Spectrum of peptide **5**

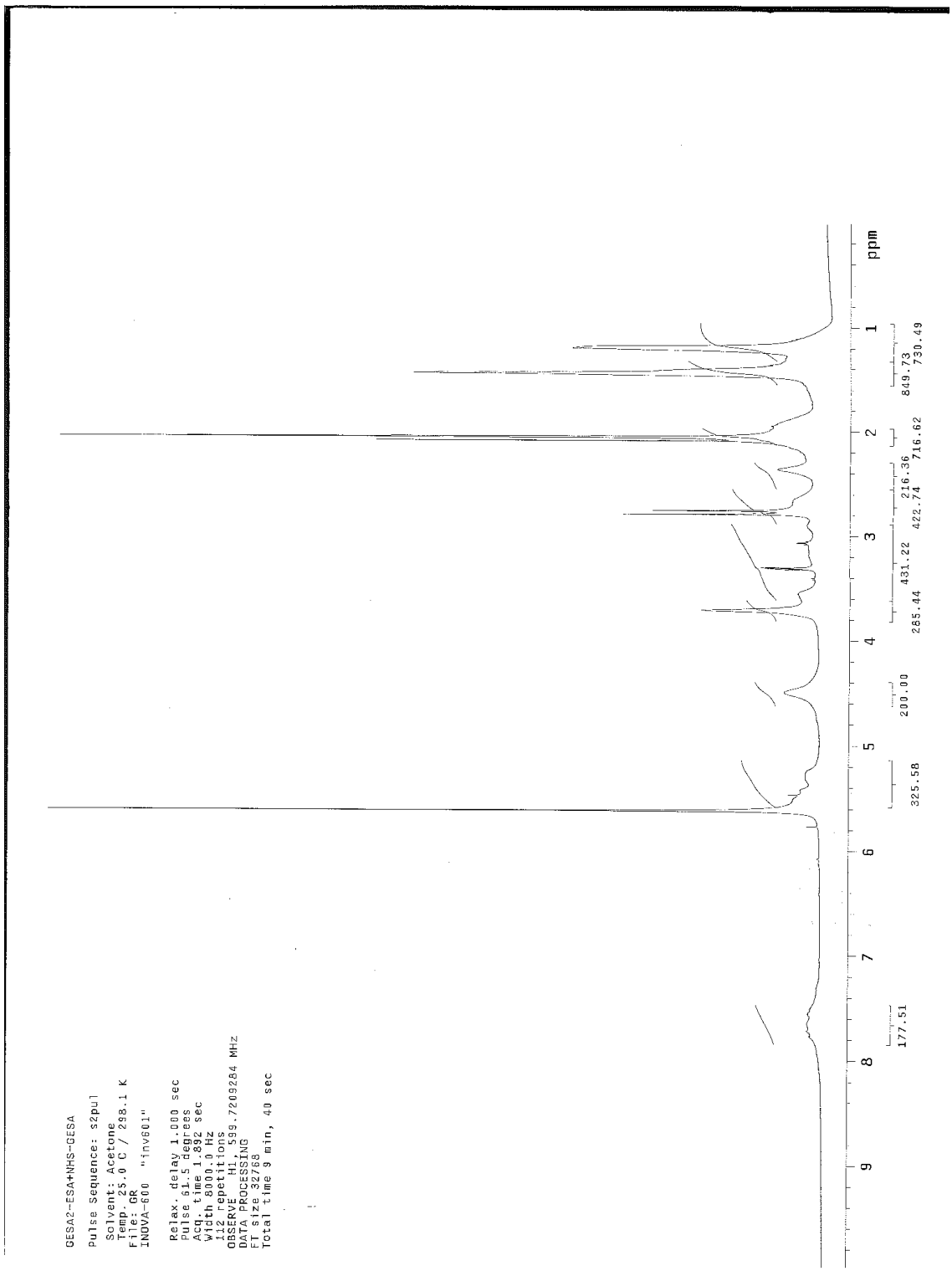

^{1}H NMR Spectrum of polymer **7b**

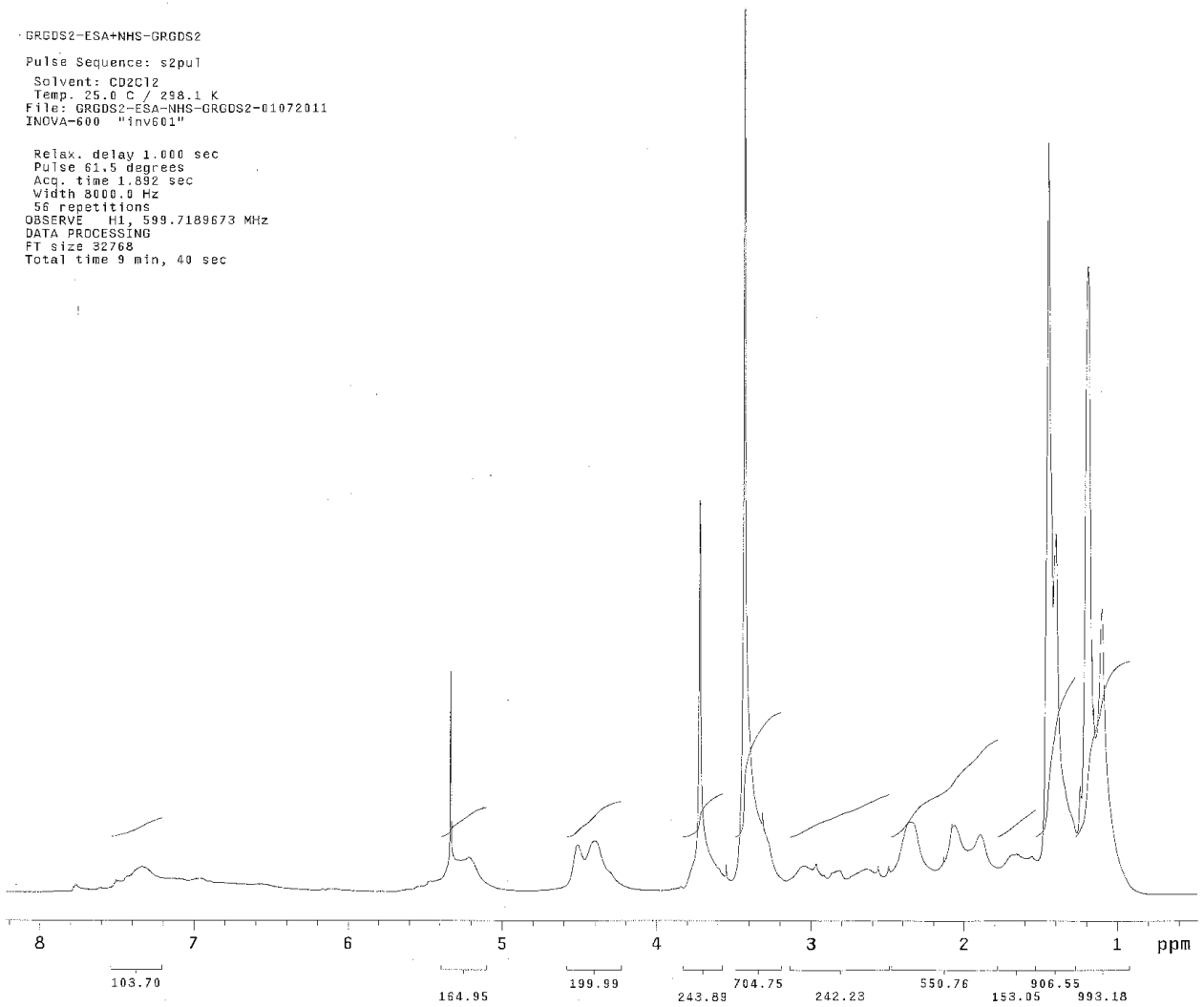

^{1}H NMR Spectrum of polymer **7a**

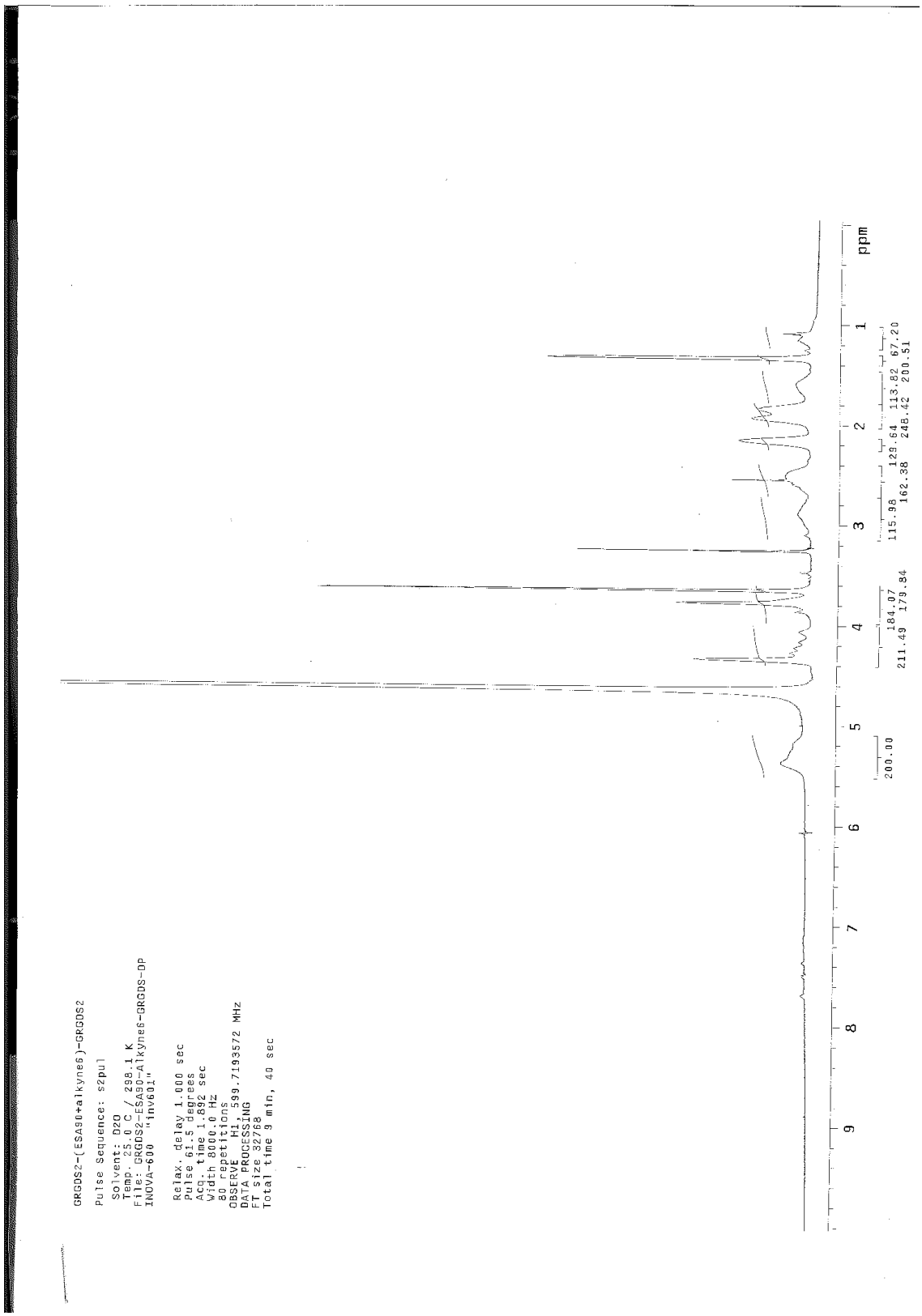

^{1}H NMR Spectrum of polymer **9a**

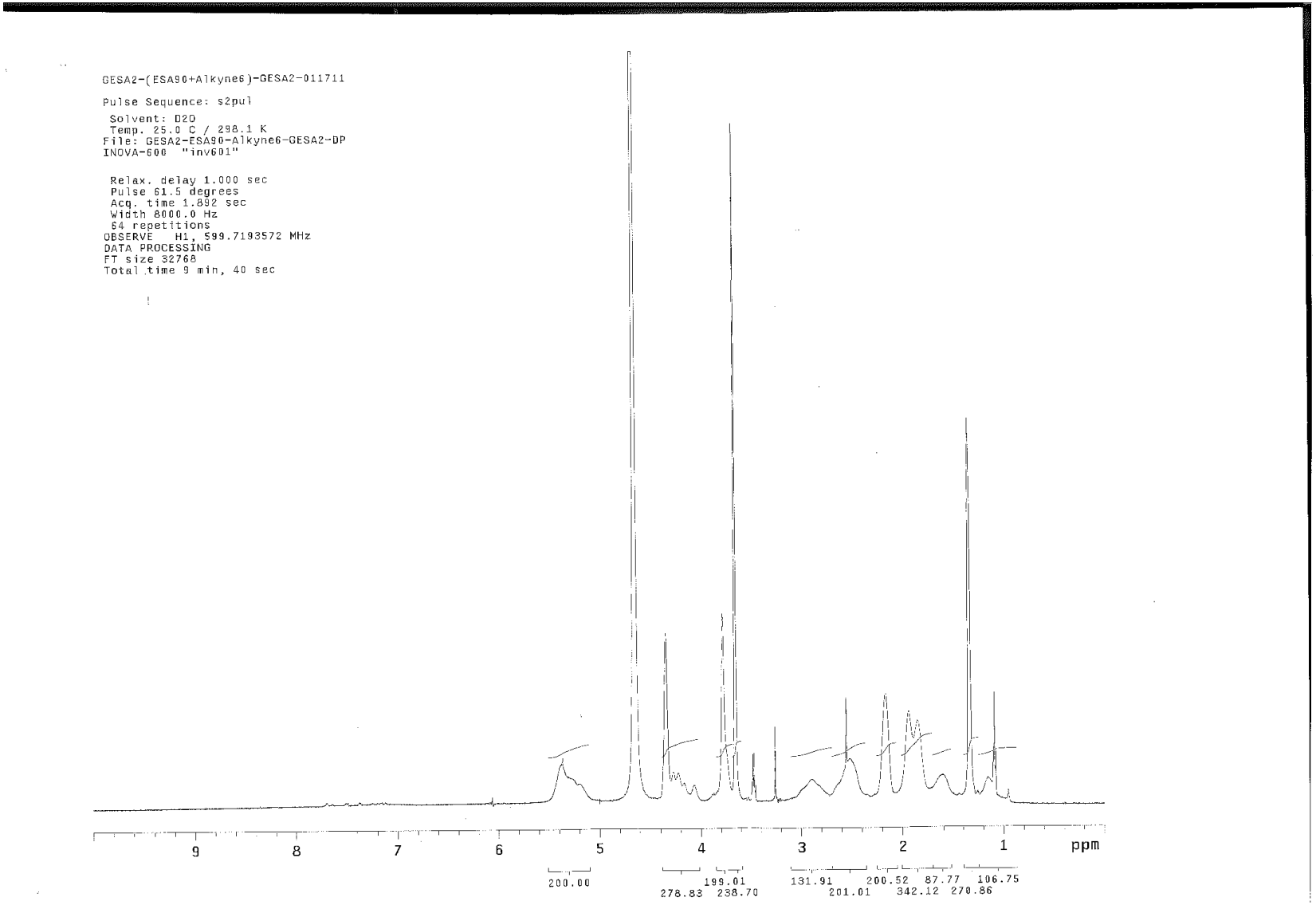

^{1}H NMR Spectrum of polymer **9b**

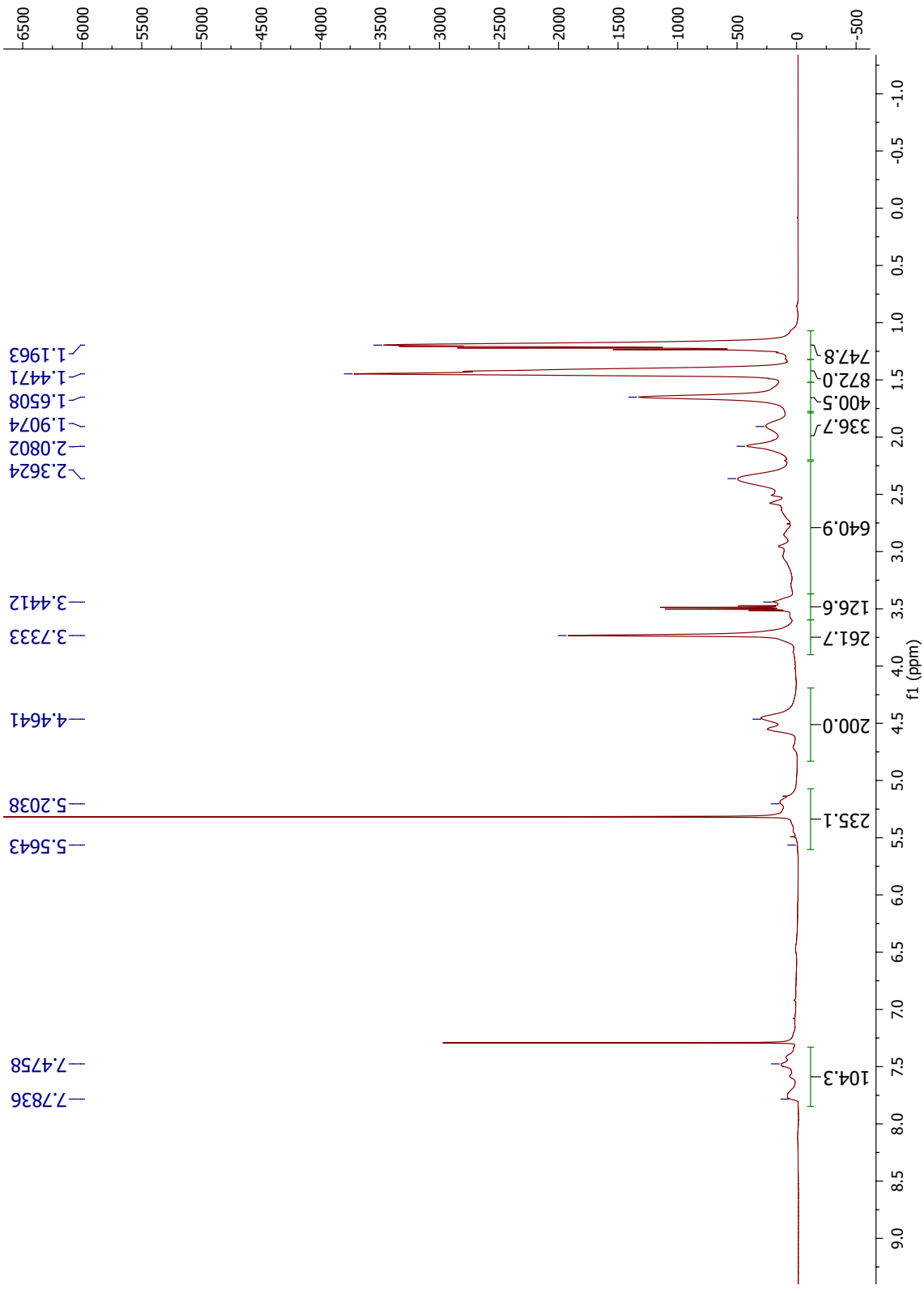

^{1}H NMR Spectrum of polymer **8a**

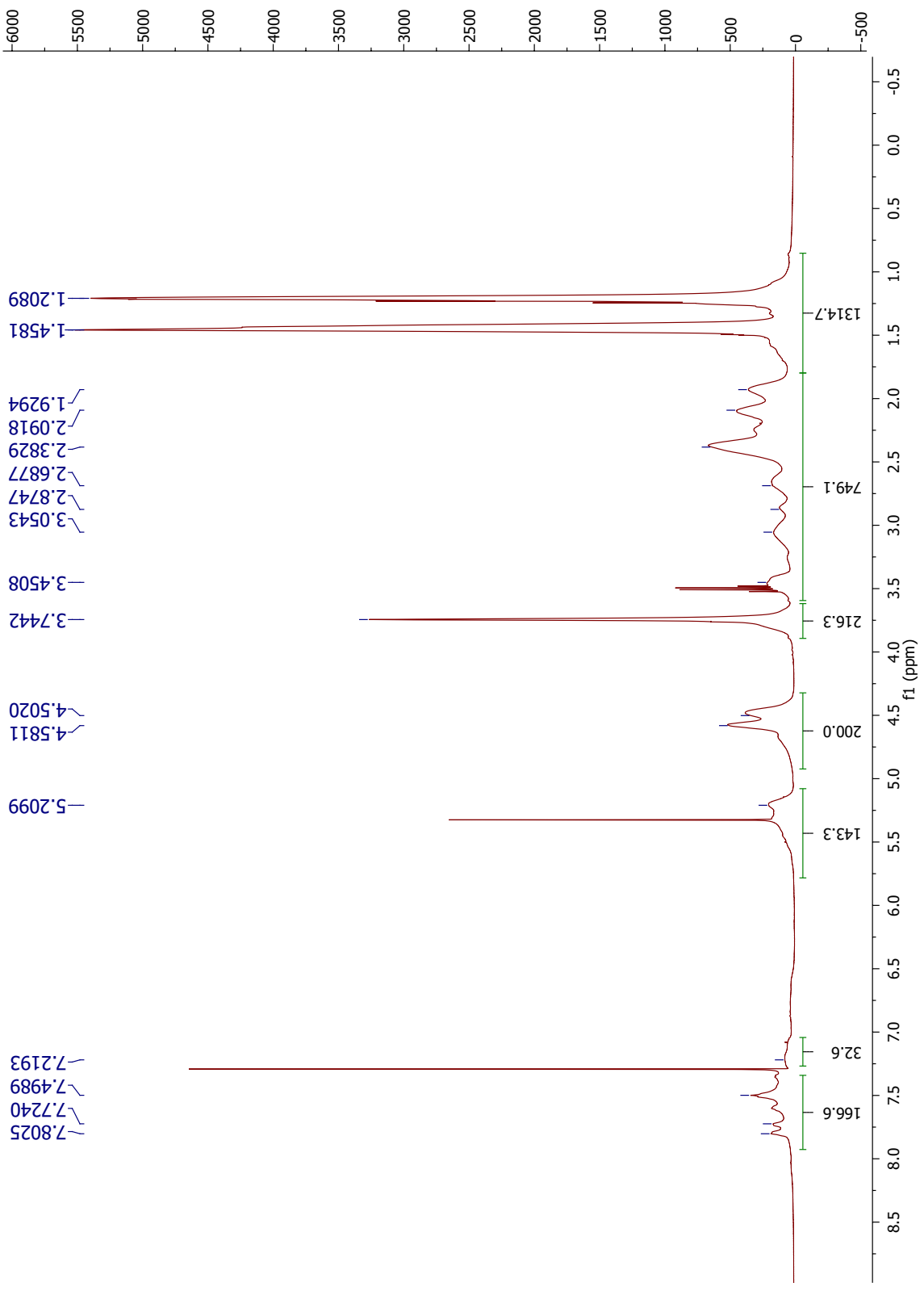

^{1}H NMR Spectrum of polymer **8b**

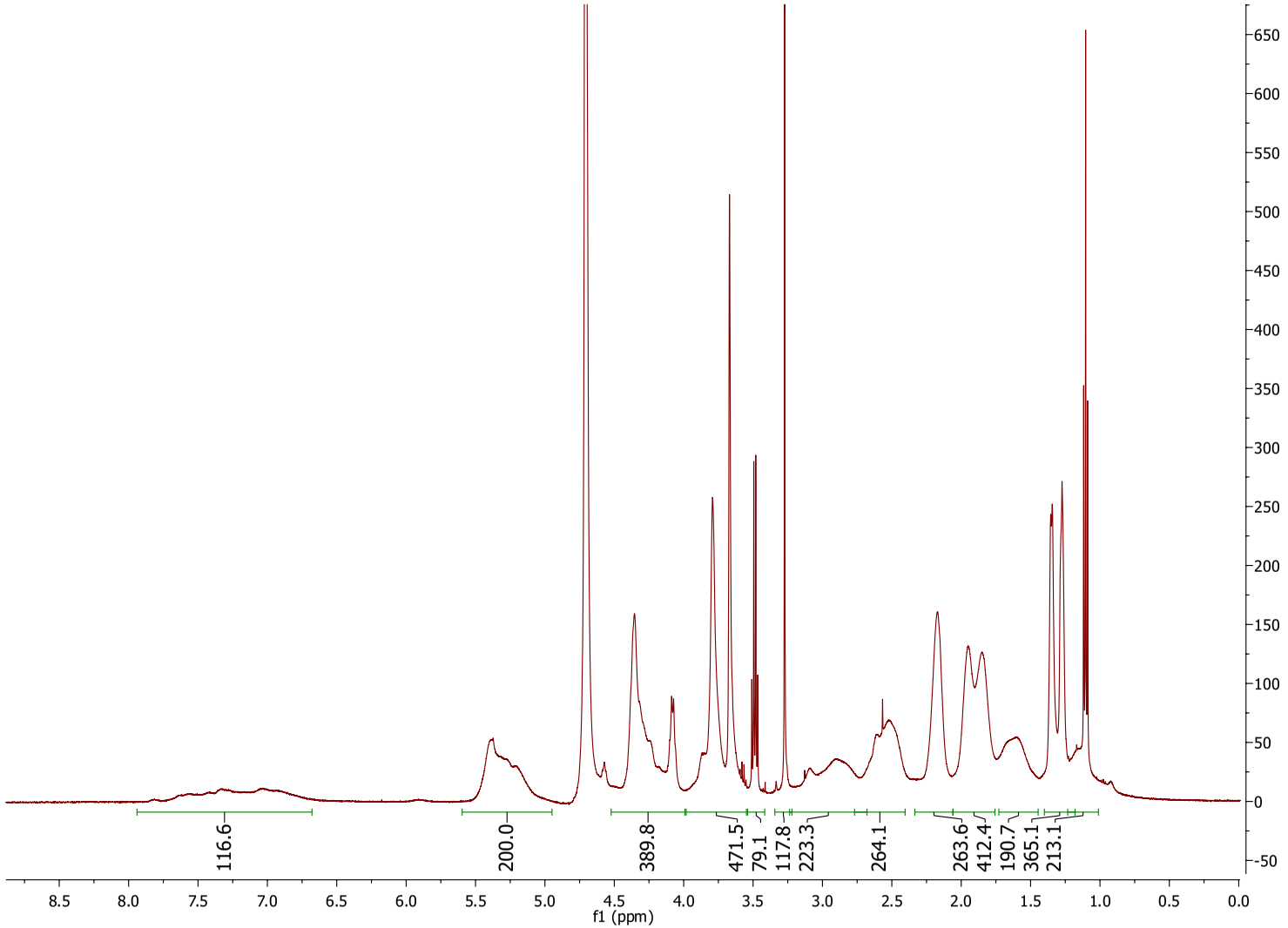

^{1}H NMR Spectrum of polymer **10a**

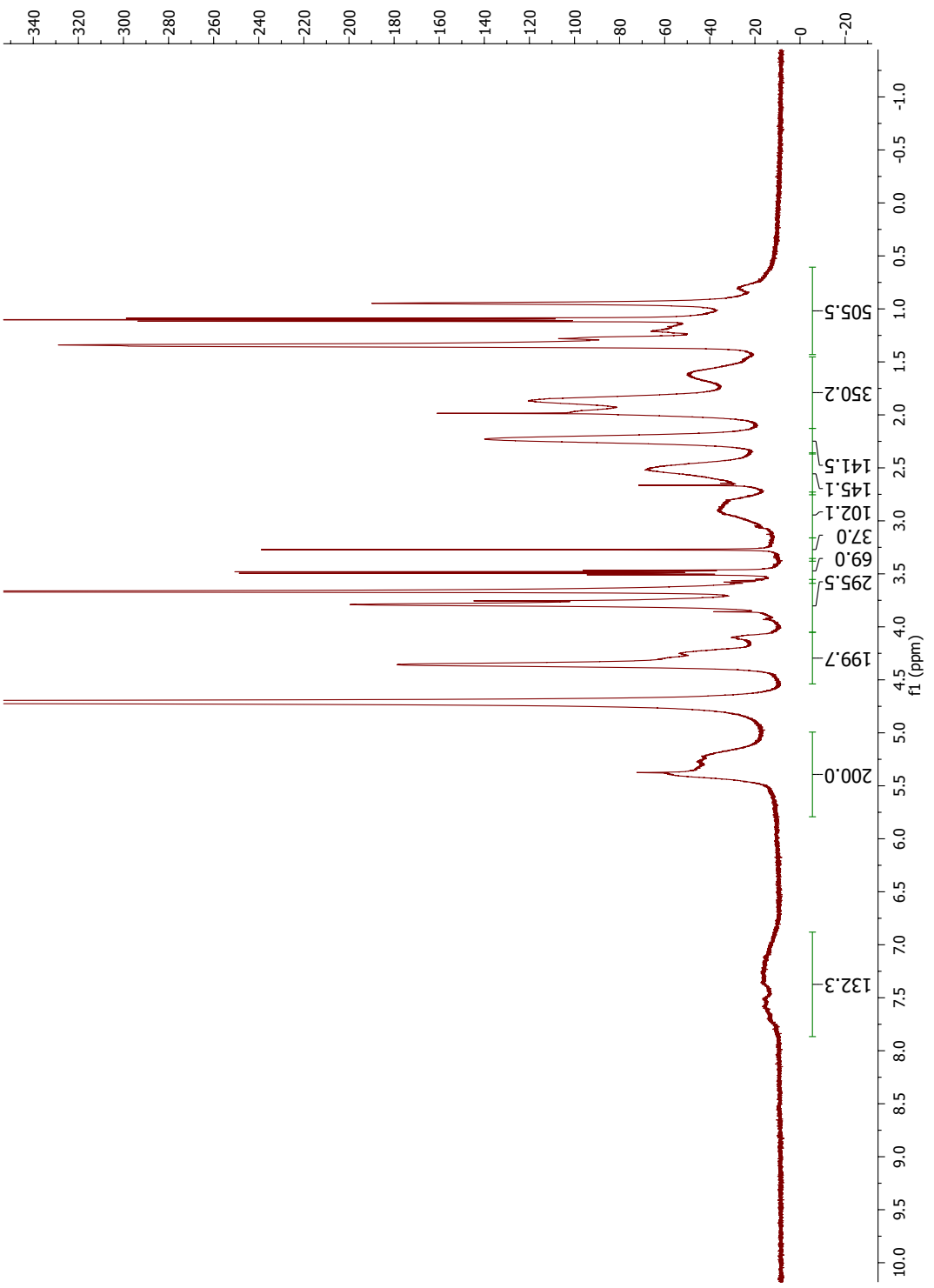

^{1}H NMR Spectrum of polymer **10b**

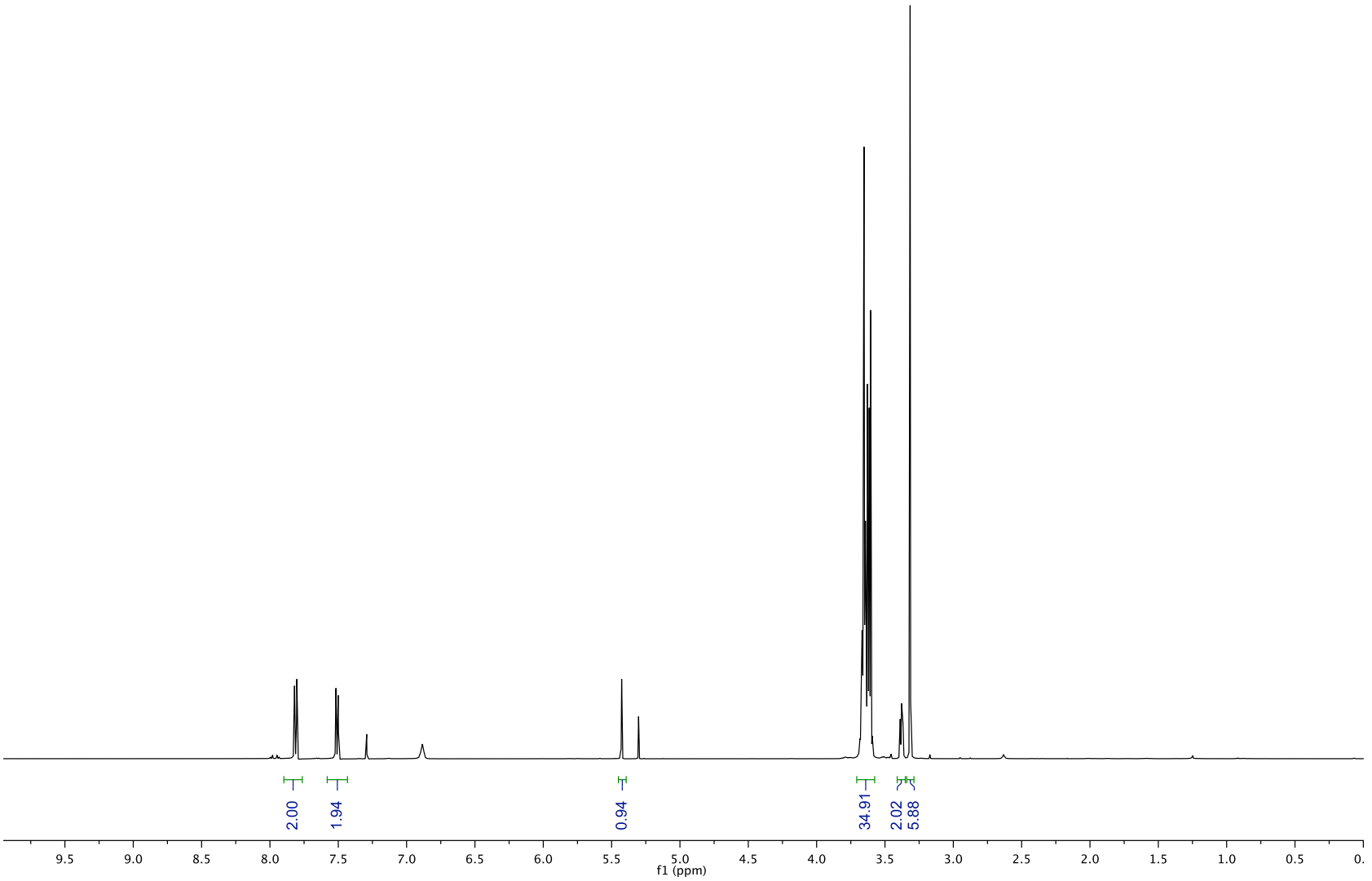

^{1}H NMR Spectrum of **acetal 18**

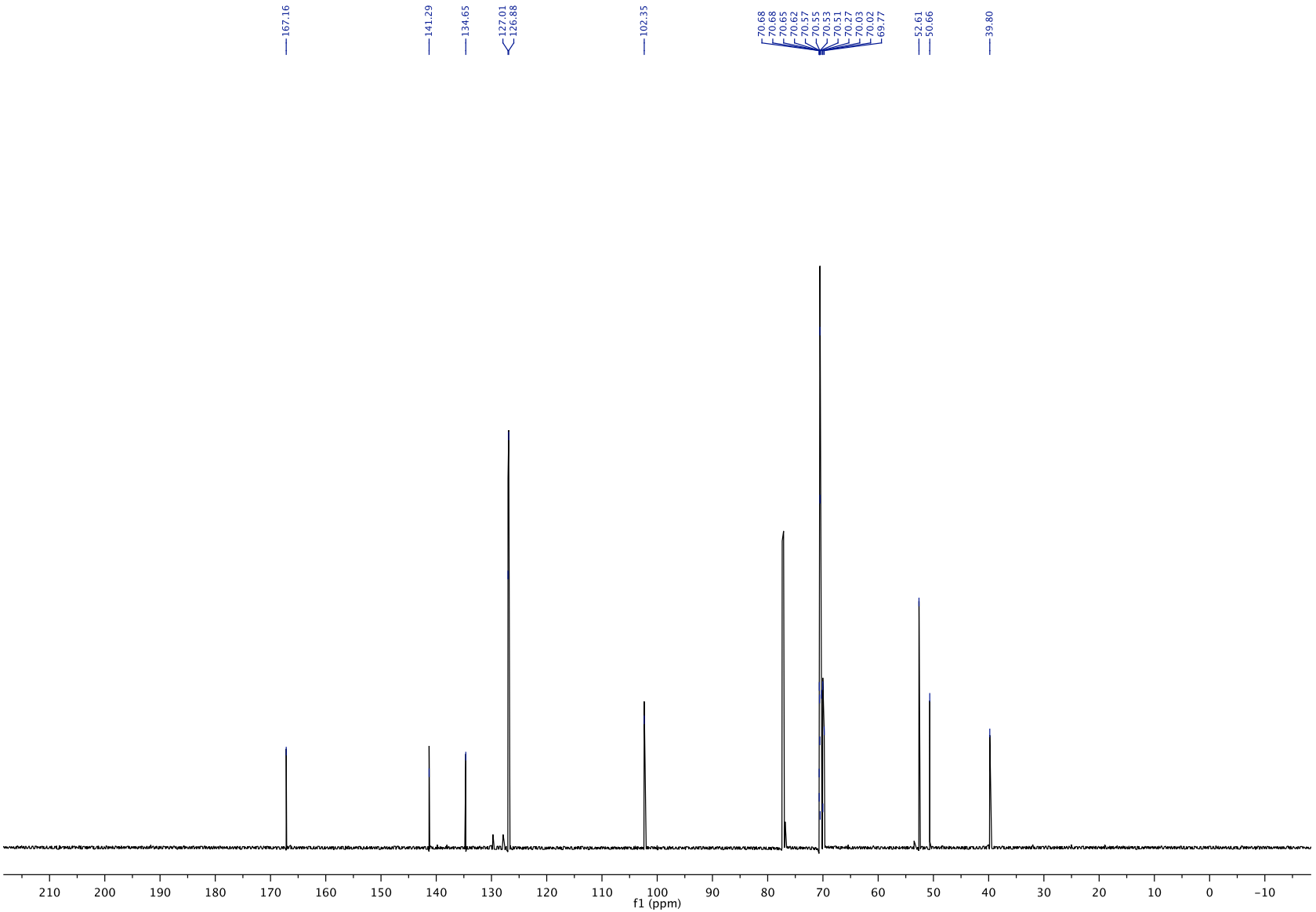

^{13}C NMR Spectrum of **acetal 18**

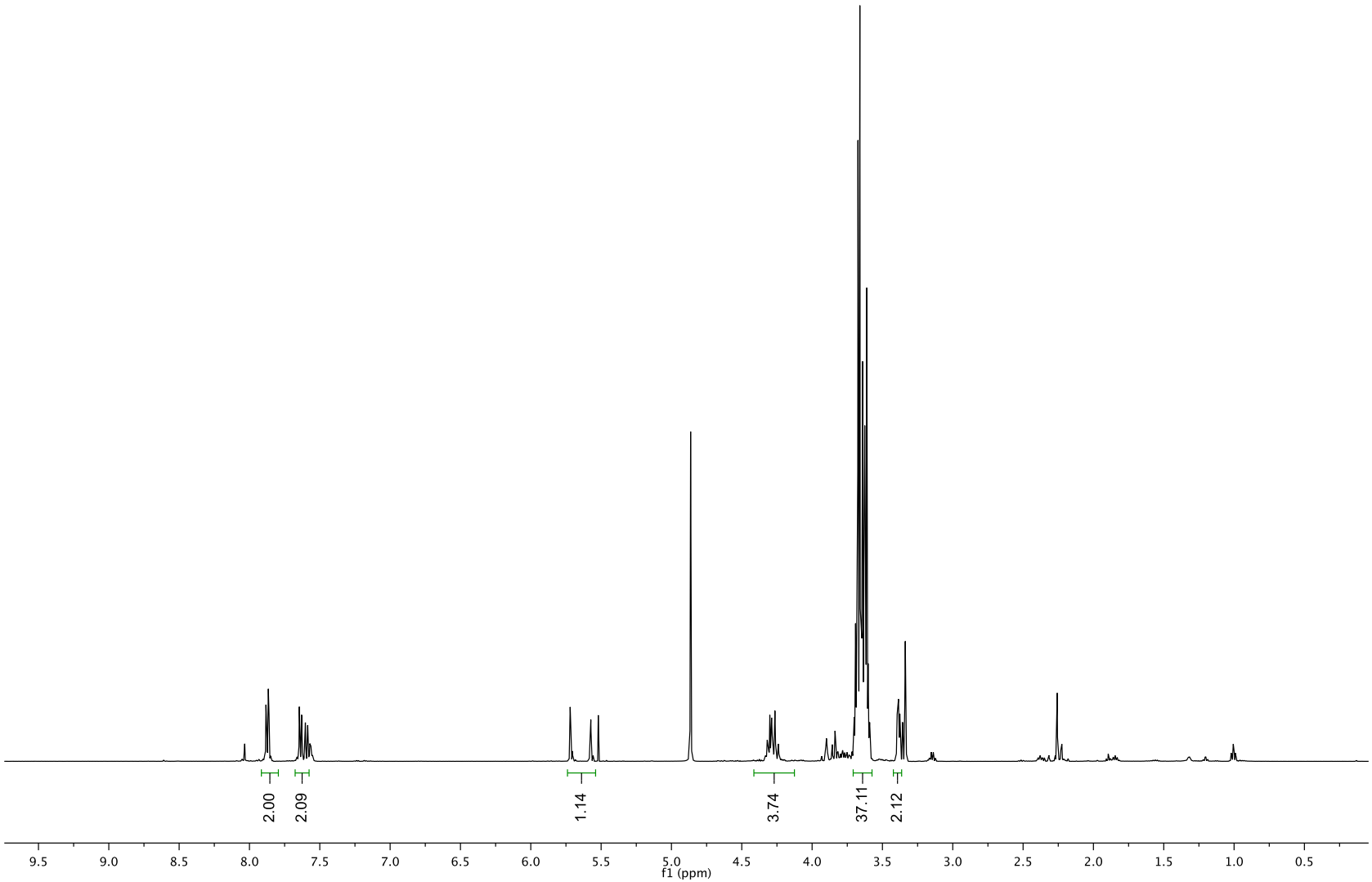

^{1}H NMR Spectrum of trifluoroacetamide **21a**

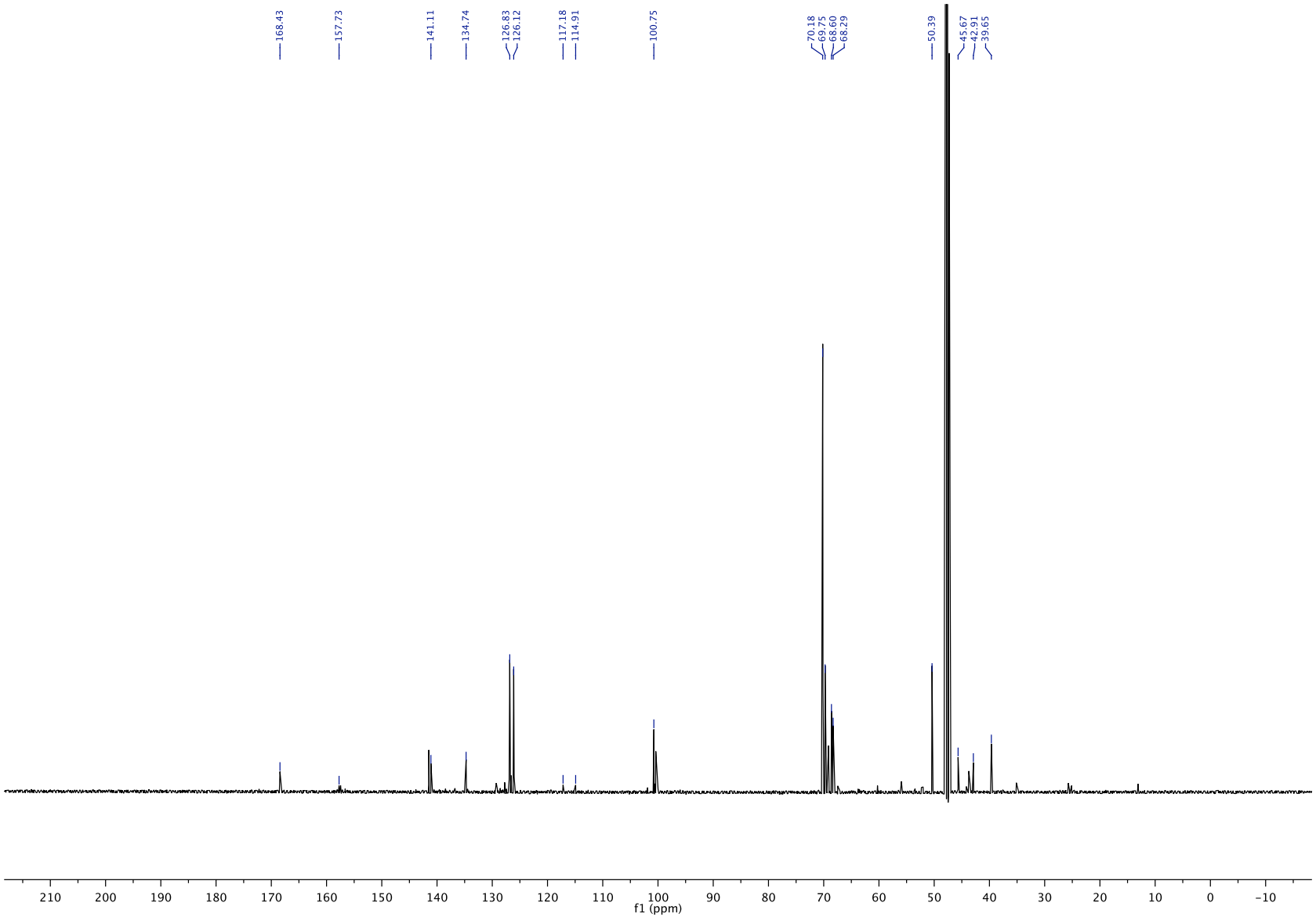

^{13}C NMR Spectrum of trifluoroacetamide **21a**

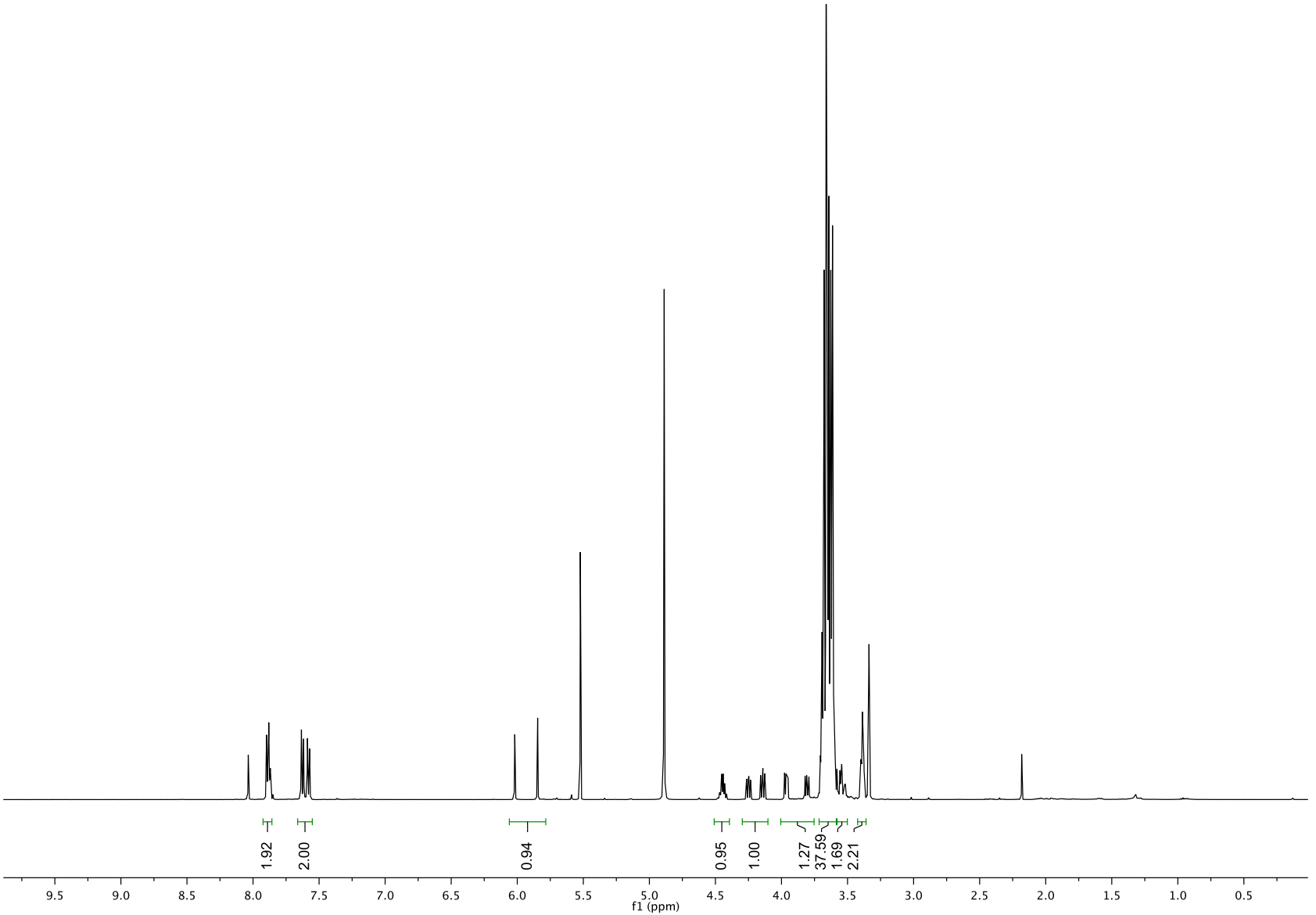

^{1}H NMR Spectrum of trifluoroacetamide **21b**

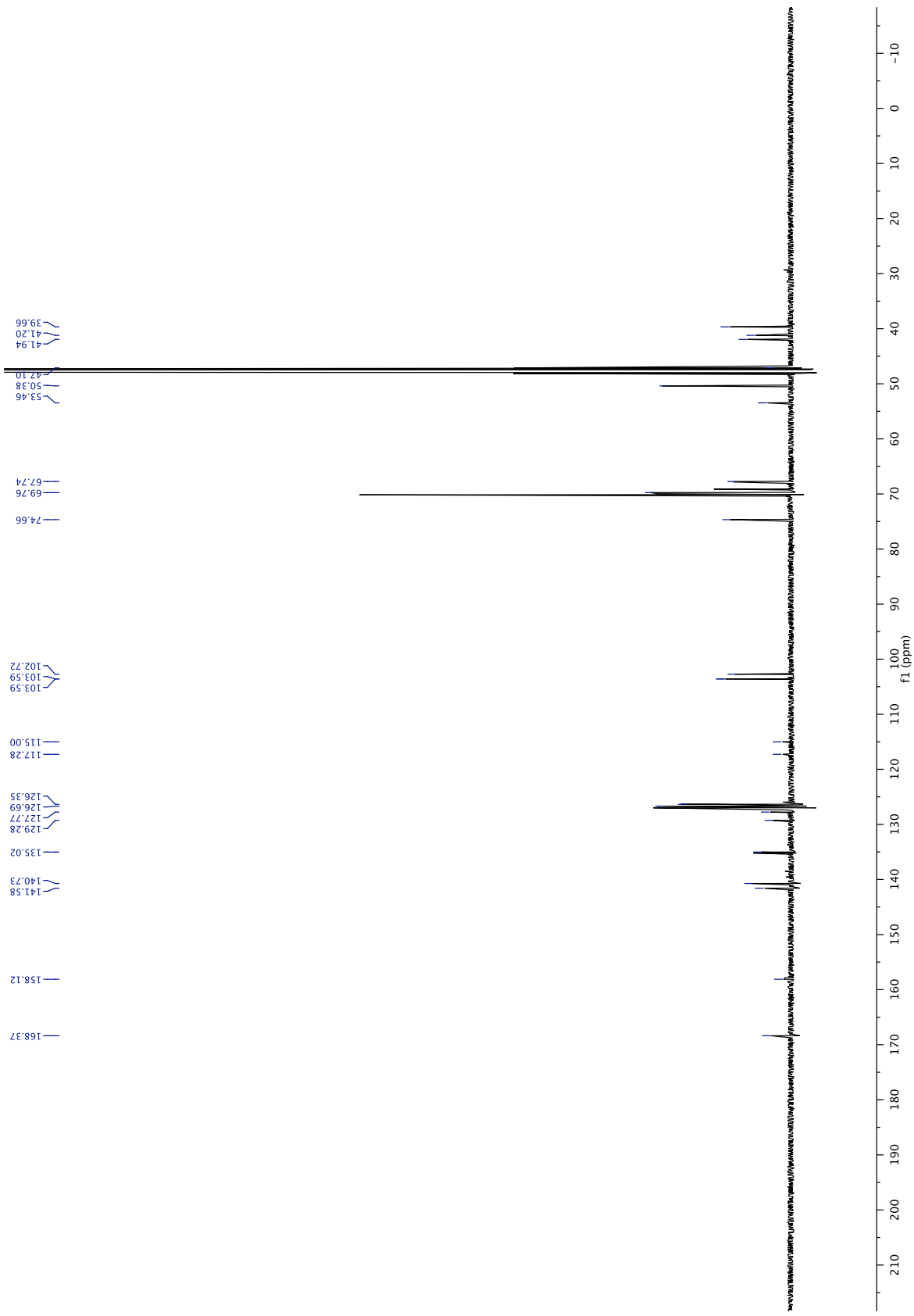

^{13}C NMR Spectrum of trifluoroacetamide **21b**

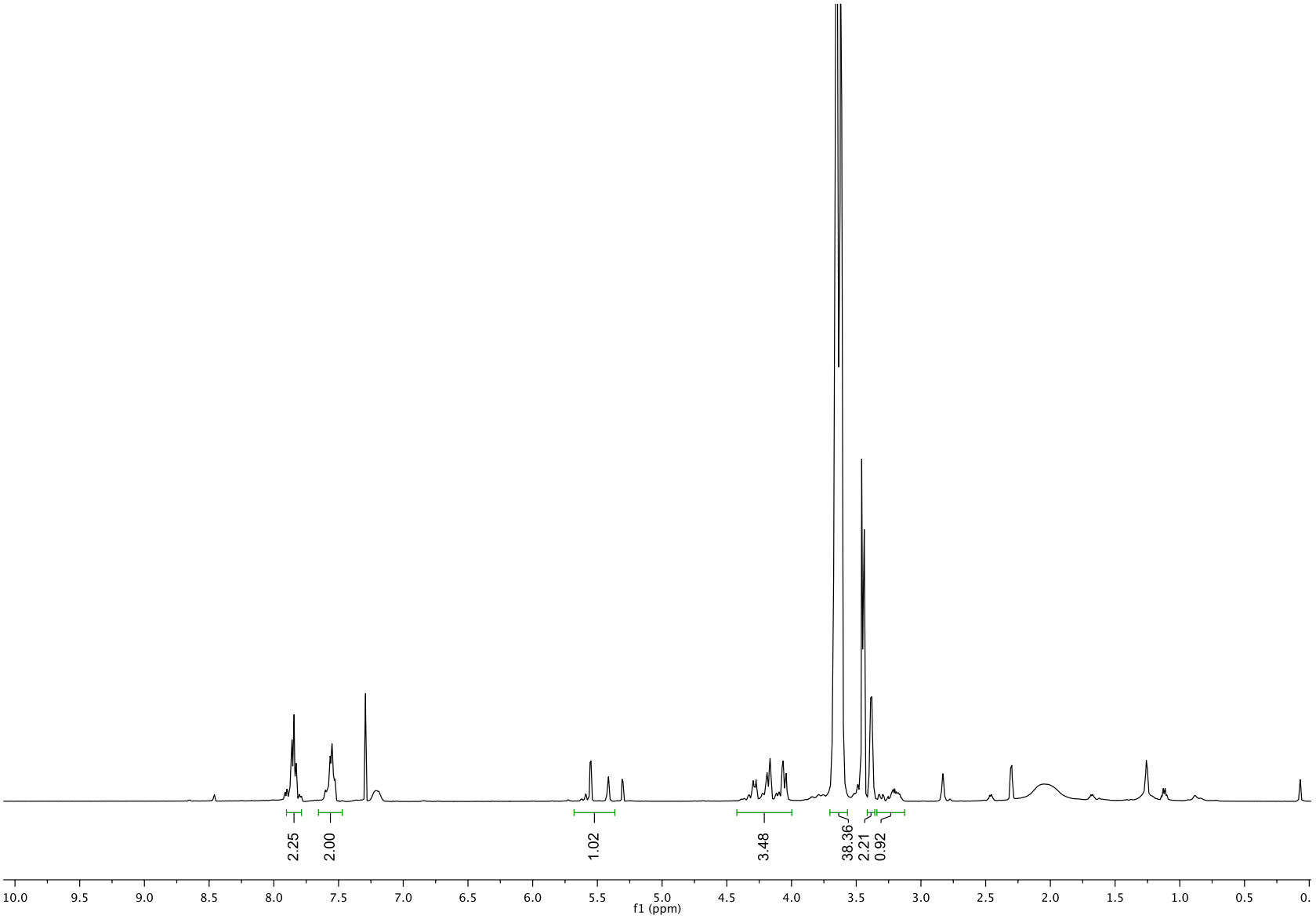

^{1}H NMR Spectrum of amine **22a**

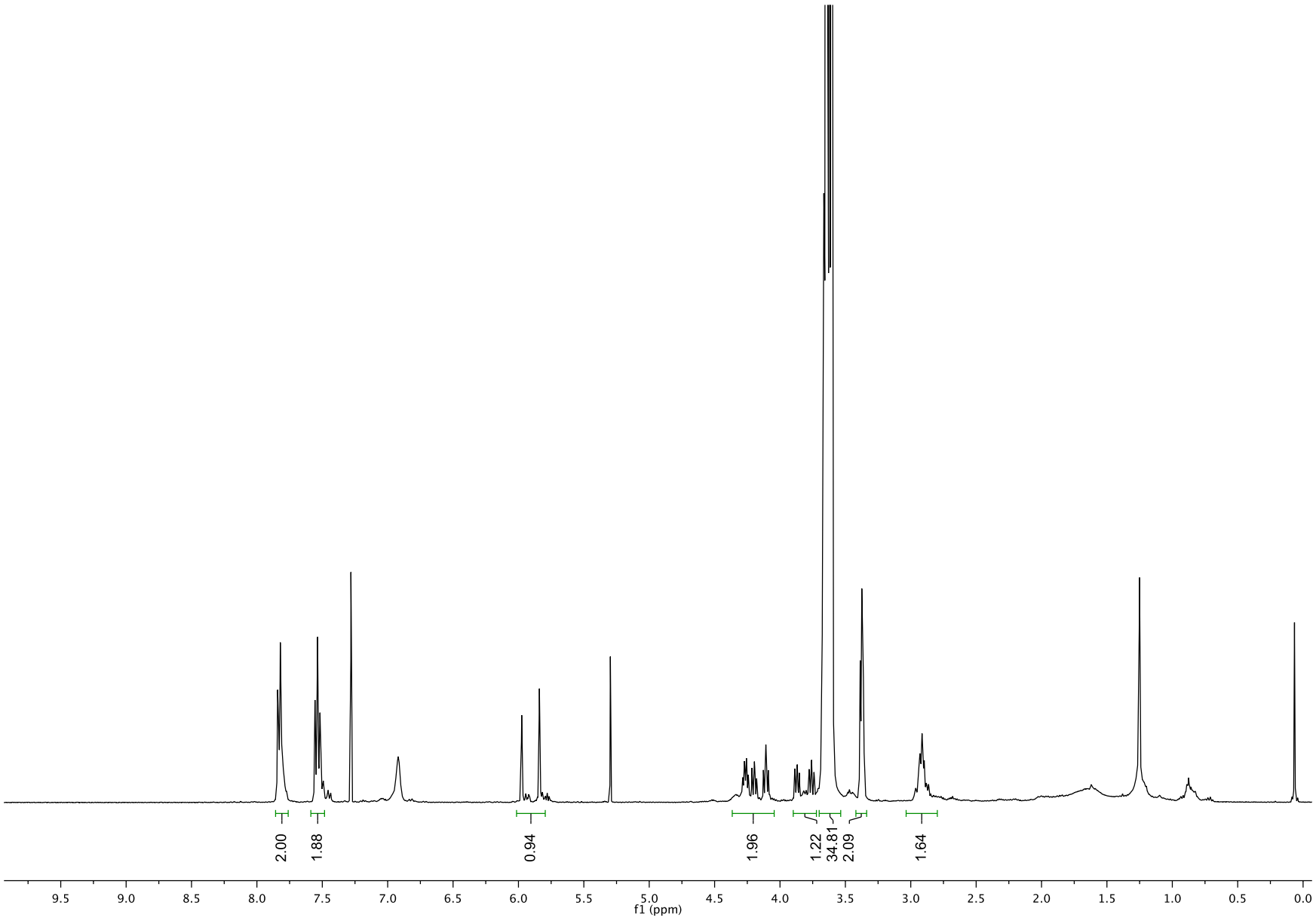

^{1}H NMR Spectrum of amine **22b**

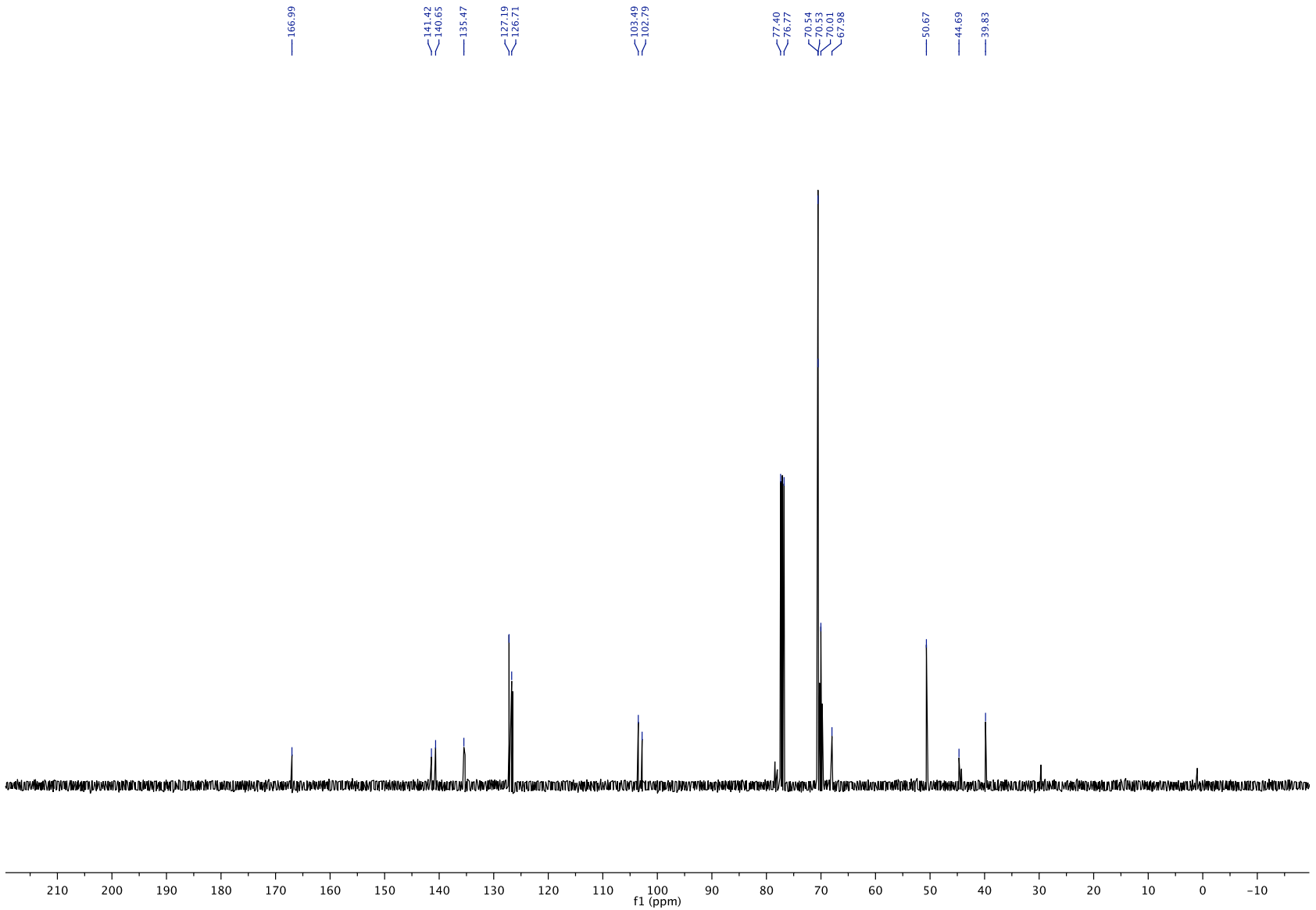

^{13}C NMR Spectrum of amine **22b**

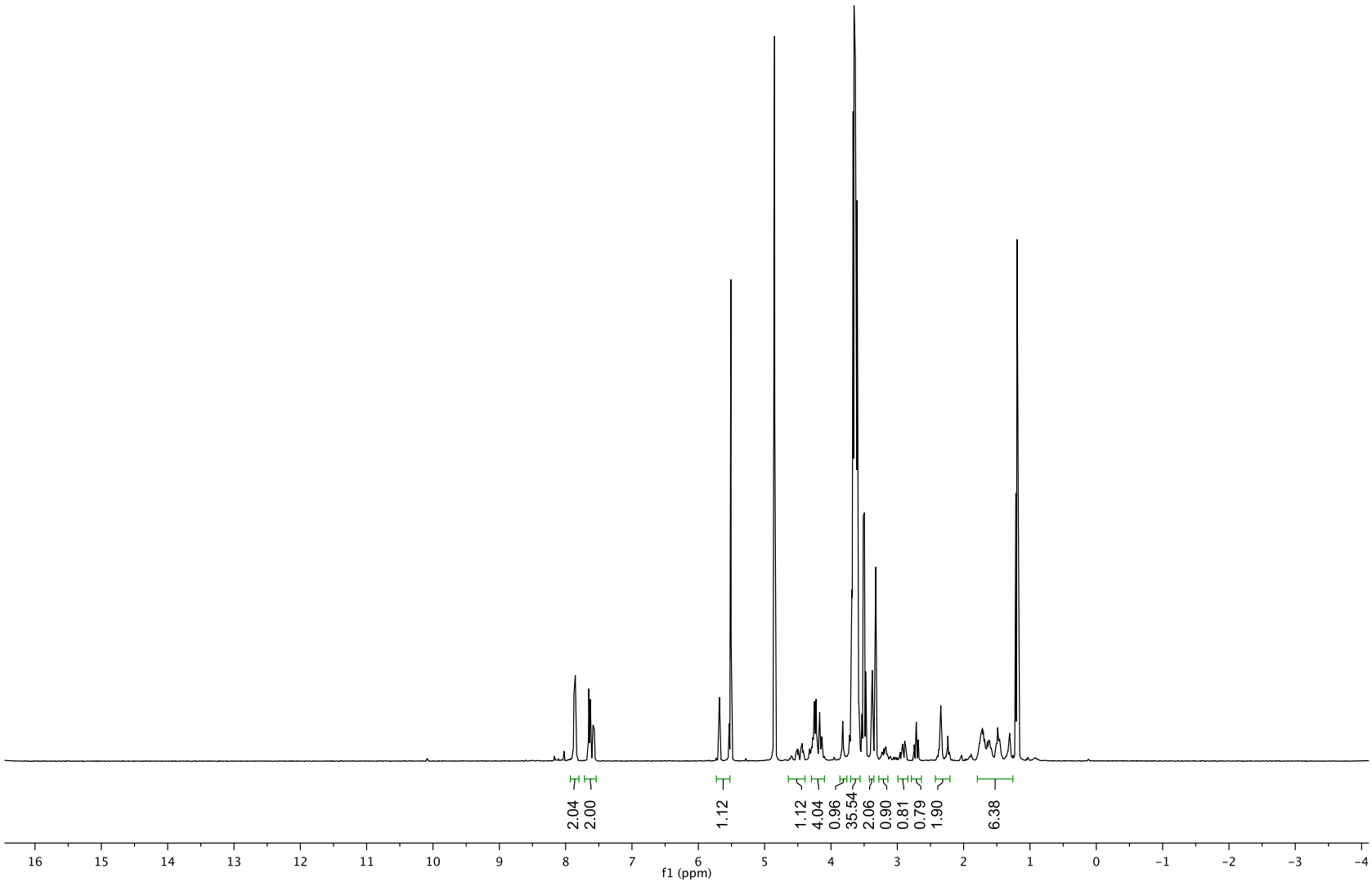

^{1}H NMR Spectrum of amide **23a**

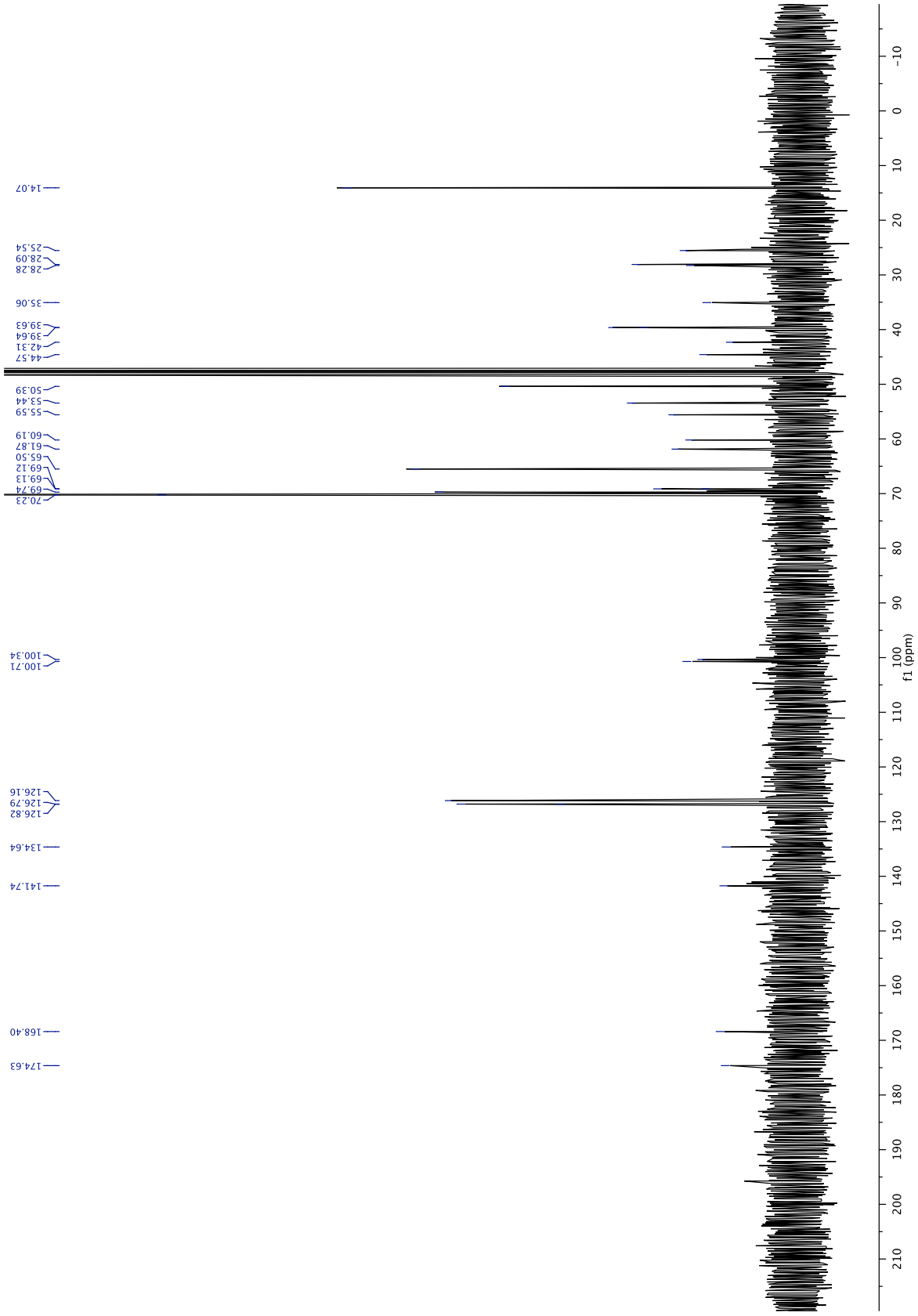

^{13}C NMR Spectrum of amide **23a**

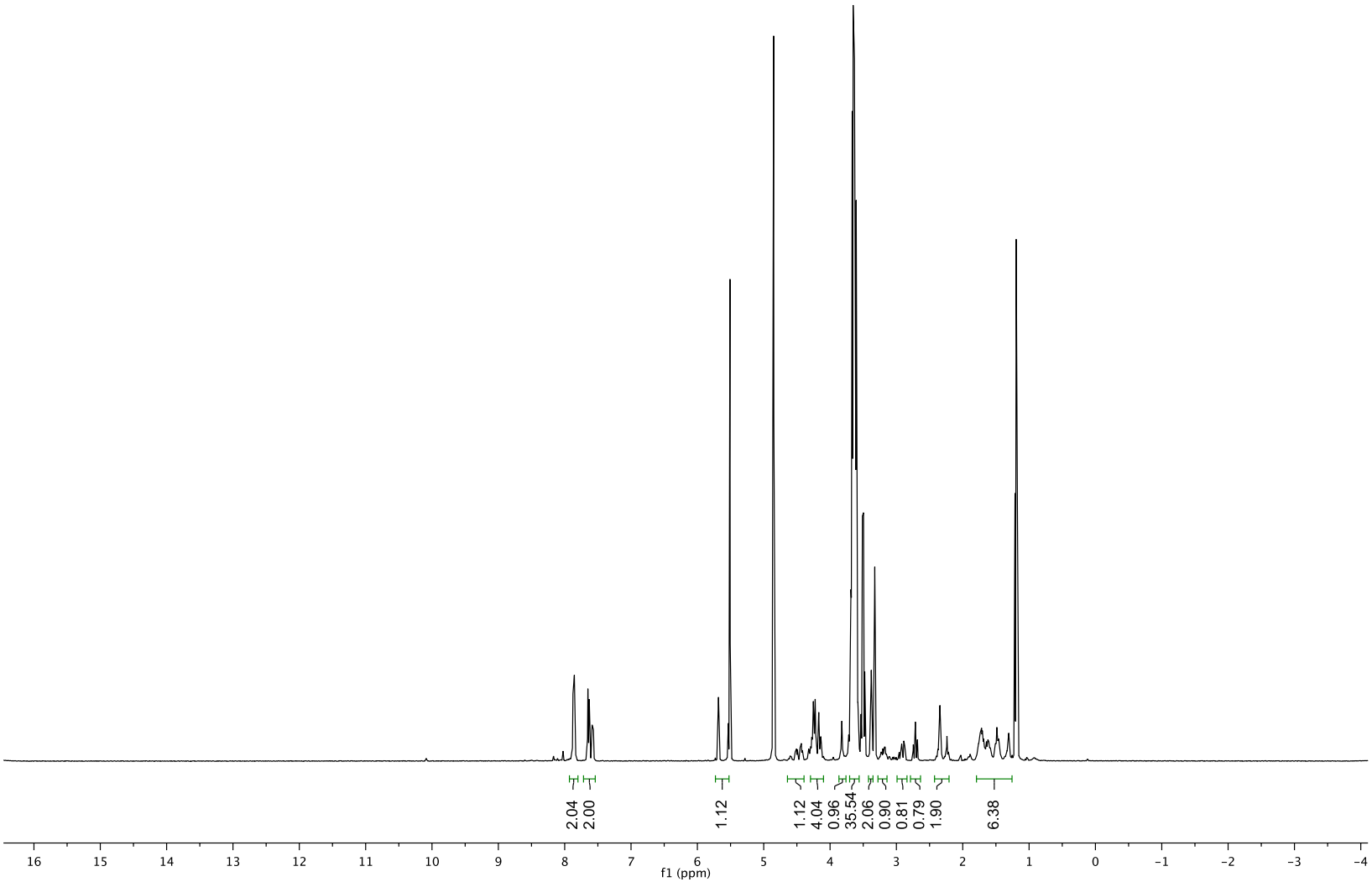

^{1}H NMR Spectrum of amide **23b**

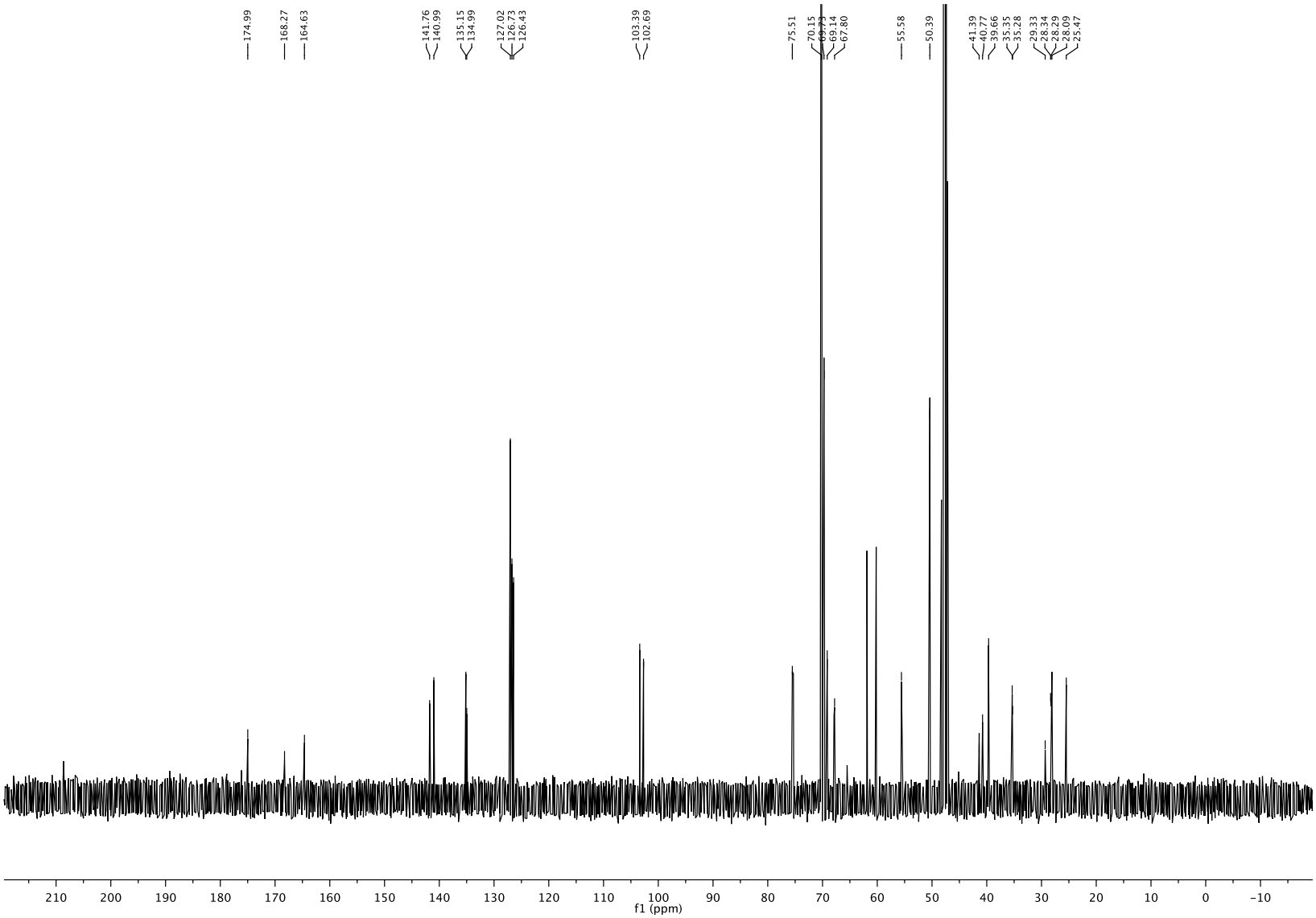

^{13}C NMR Spectrum of amide **23a**

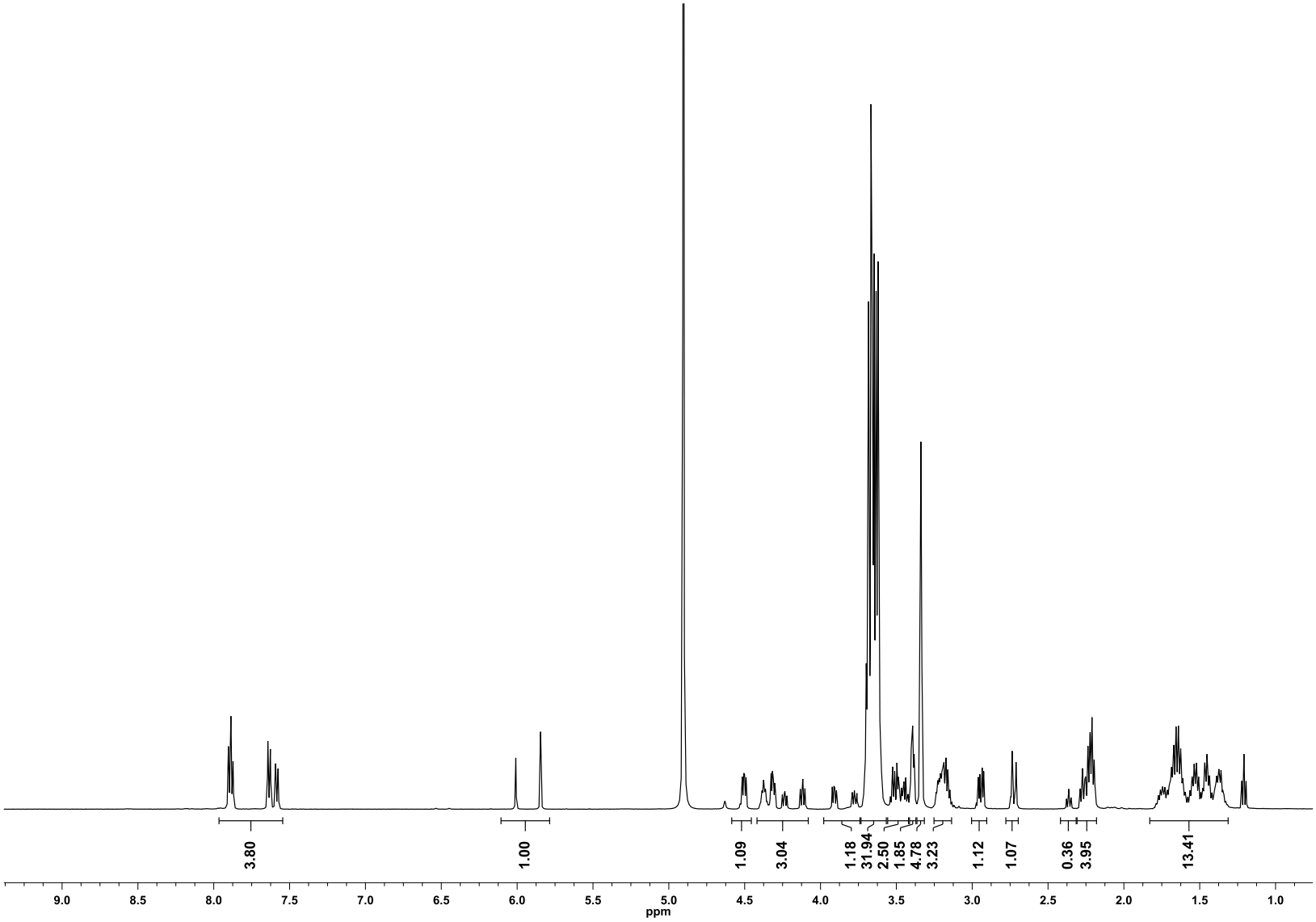

^{1}H NMR Spectrum of amide **23c**

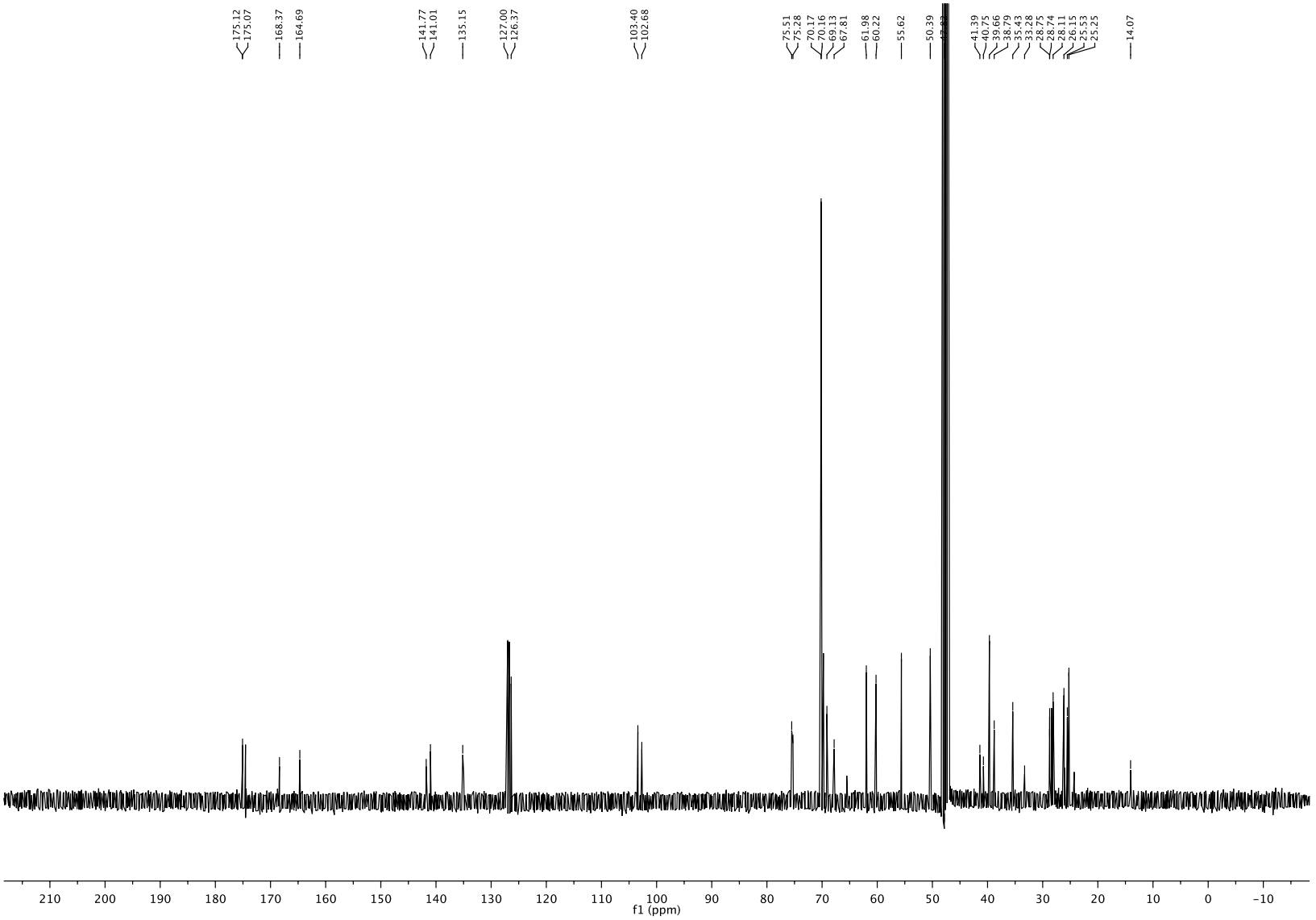

^{13}C NMR Spectrum of amide **23c**

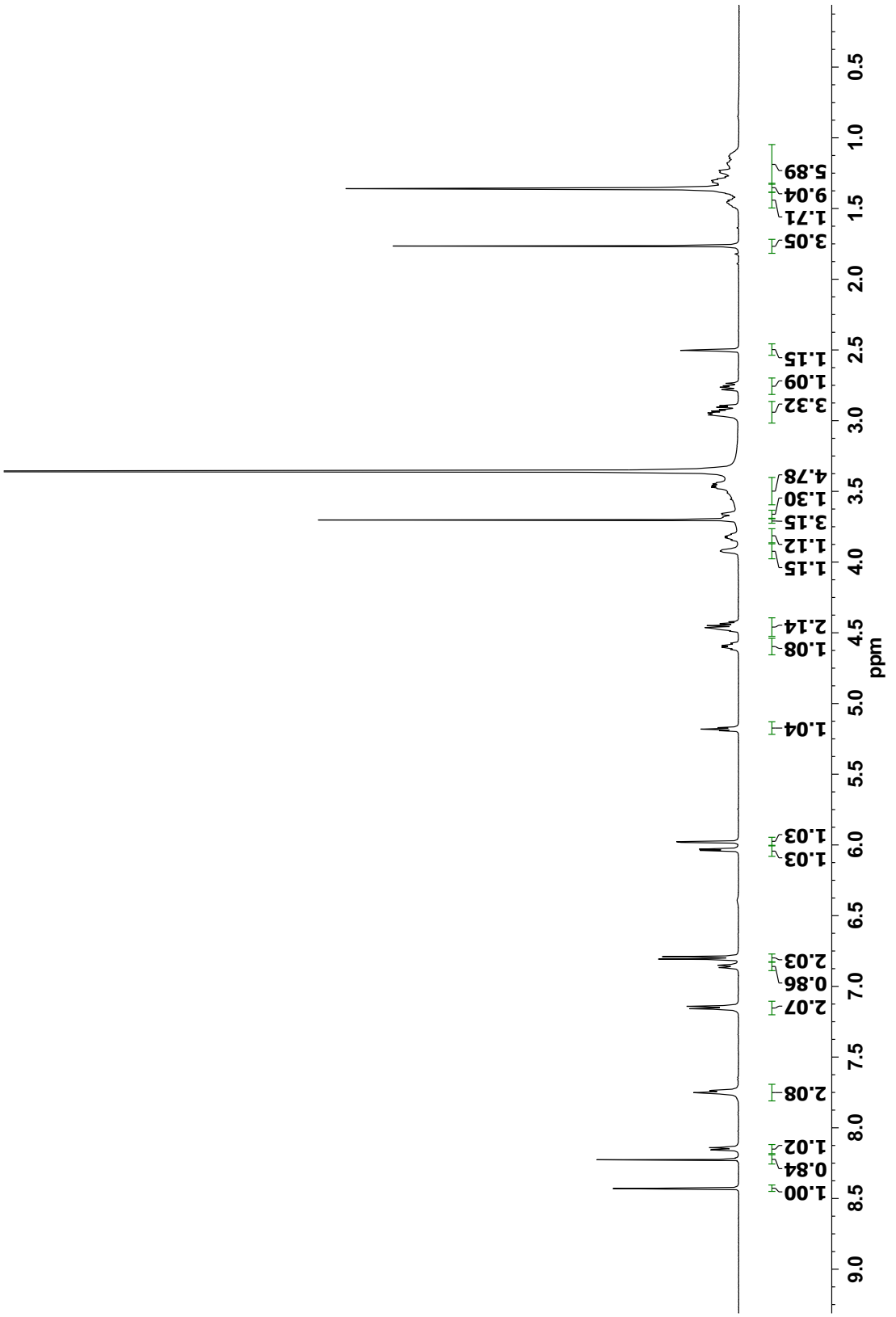

^{1}H NMR Spectrum of compound **4-1**

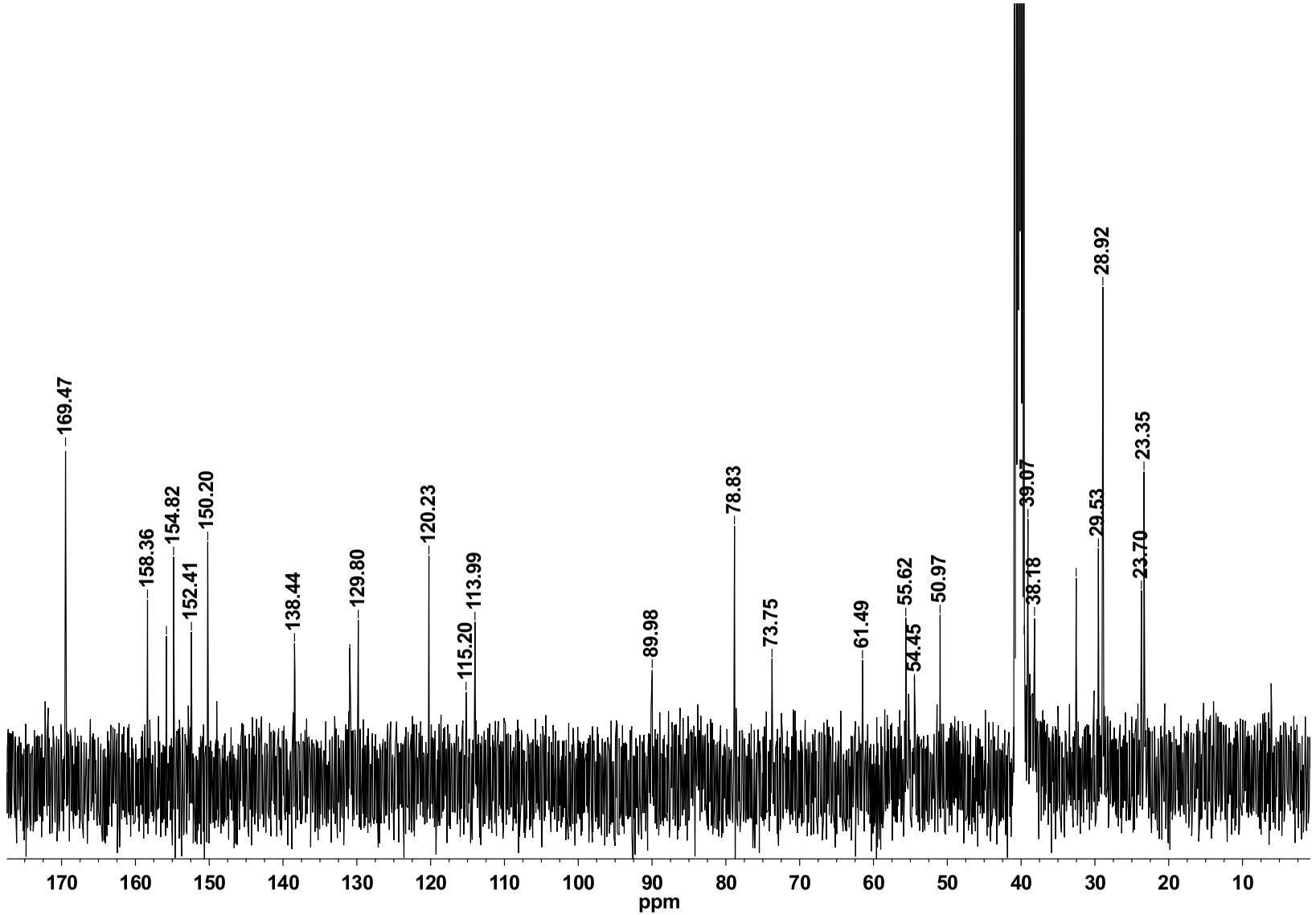

^{13}C NMR Spectrum of compound **4-1**